# DFT Studies on Ground and Excited State Properties of Linear Polyacene Analogues and Polycyclic Aromatic Hydrocarbons

**Thesis Submitted to AcSIR for the Award of the Degree of**
**DOCTOR OF PHILOSOPHY**
**in Chemical Sciences**


By
**Rakhi R.**
**Registration No: 10CC12J39001**


**Under the Guidance of**
**Dr. C. H. Suresh**


**Chemical Sciences and Technology Division**
**CSIR-National Institute for Interdisciplinary Science and Technology**
**Thiruvananthapuram-695019, Kerala, India**

**July, 2018**

# DECLARATION

I hereby declare that the Ph. D. thesis entitled "**DFT Studies on Ground and Excited State Properties of Linear Polyacene Analogues and Polycyclic Aromatic Hydrocarbons**" is an original work carried out by me at Chemical Sciences and Technology Division (CSTD) at CSIR-National Institute for Interdisciplinary Science and Technology (CSIR-NIIST), Thiruvananthapuram under the supervision of Dr. C. H. Suresh, Principal Scientist, CSTD, CSIR-NIIST. The work has not been submitted anywhere else for any degree or diploma.

Thiruvananthapuram Rakhi R

30/07/2018

**Council of Scientific & Industrial Research**
**National Institute for Interdisciplinary Science and Technology**
**Thiruvananthapuram-695019, Kerala, India**

**Dr. C. H. Suresh**
Principal Scientist
Chemical Sciences & Technology Division
*Tel: +91- 4712515472*
*E-mail: sureshch@gmail.com*
*sureshch@niist.res.in*

30th July 2018

# CERTIFICATE

This is to certify that the work incorporated in this Ph. D. thesis entitled "**DFT Studies on Ground and Excited State Properties of Linear Polyacene Analogues and Polycyclic Aromatic Hydrocarbons**" submitted by Ms. Rakhi R to Academy of Scientific and Innovative Research (AcSIR) in fulfillment of the requirements for the award of the Degree of Doctor of Philosophy, embodies original research work done under my supervision. I further certify that this work has not been submitted to any other University or Institution in part or full for the award of any degree or diploma. Research material obtained from other sources has been duly acknowledged in the thesis. Any text, illustration, table, *etc*. used in the thesis from other sources, have been duly cited and acknowledged.

Rakhi R
(Student)

Dr. C. H. Suresh
(Thesis Supervisor)

# ACKNOWLEDGMENT

*The journey was long, exciting, demanding and fully worth travelling. At this juncture of accomplishment, I would like to pay gratitude to all the people who contributed to the successful completion of the Ph. D. Words fell short to contain the sense of deep gratitude I have for every person, things and places which made this journey a beautiful one.*

*I would like to express my sincere gratitude to Dr. C. H. Suresh, my Ph. D. supervisor and mentor for his inspiration, advice, continuous support, and excellent guidance throughout my Ph. D. work. The foundation of thesis stands on the colossal knowledge he has in every field of the research.*

*I place my heartfelt gratitude to Dr. A. Ajayaghosh, Director, CSIR-NIIST, and former directors, Dr. Suresh Das and Dr. Gangan Pratap for the academic support and for providing me the necessary facilities for carrying out the research in this institution.*

*I am thankful to Dr. R. Luxmi Varma, Head, Chemical Sciences and Technology Division and AcSIR coordinator for her timely advice and support for the conduct of academic procedures. I also extend my sincere thanks to former HODs Dr. D. Ramaiah and Dr. K. R. Gopidas, and former AcSIR coordinator Dr. Mangalam S. Nair for all their support and guidelines.*

*I sincerely thank my Doctoral Advisory Committee members Dr. M. L. P. Reddy, Dr. K. R. Gopidas, and Dr. S. Savithri, for their insightful suggestions and support throughout my AcSIR coursework and Ph. D programme. I would also like to thank all the Scientists who took the task of teaching AcSIR coursework, very efficiently. I would also like to extend my gratitude to Dr. B. Krishnakumar, Senior Scientist, Environmental Technology Division, CSIR-NIIST for the necessary scientific help in the completion of CSIR-800 programme.*

*I wish to express thanks to the former and current members of our research group Dr. Ajitha, Dr. Sajith, Dr. Fareed, Dr. Sandhya, Dr. Neetha, Dr. Remya K., Dr. Remya P. R.., Dr. Renjith, Della, Anjali, Remya G. S., Bijina, Divya, and Anila for the support, fruitful discussions, the warm friendship and the pleasant working environment in our lab.*

*I deeply express my thanks to my friends at CSIR-NIIST for the companionship during my stay in Scholar's hostel. I will always cherish the pleasant moments we had together.*

*The administration section and technical staff members in CSIR-NIIST are duly acknowledged for their help during my tenure as a research scholar.*

*I would like to acknowledge the University Grants Commission (UGC), for the financial support.*

*High-performance computational facilities at CSIR-NCL, Pune, and CSIR-4PI, Bangalore is highly acknowledged.*

*I express my deep sense of gratitude to all my beloved teachers in the past for teaching me the fundamentals of chemistry and their inspiration, especially my high school chemistry teacher Brinda and all the Professors in Department of Applied Chemistry, CUSAT.*

*I cherish the phone calls, talks, and chats with all my friends in BIRDS, which made this and every journey beautiful. I owe my deepest gratitude to my family for their love, care, understanding, support, and concern. Words could not express how grateful I am towards both my mother and mother in law, for their support and sacrifice, especially during the last part of this quest. I am thankful to my husband, Renjith for the constant motivation. My baby Rigved, I would like to thank you for wiping away the tensions, pressure, and worries of everything with that smile in your face.*

*Above all, I owe to God Almighty and the whole universe for granting me all the blessings without which, this accomplishment would not have been possible.*

*Rakhi R*

## TABLE OF CONTENTS

**Chapter 3. 1,4-dihydro-1,4-azaborinine Annulated Linear Polyacenes**



**Chapter 4: Polycyclic Aromatic Hydrocarbons of Various Size and Shapes**

# LIST OF FIGURES

# LIST OF SCHEMES



# LIST OF TABLES

# LIST OF ABBREVIATIONS

| | |
|---|---|
| AIMD | *Ab initio* Molecular Dynamics |
| ASE | Atomic/Aromatic Stabilization Energy |
| BOMD | Born-Oppenheimer Molecular Dynamics |

| | |
|---|---|
| CC | Coupled Cluster |
| CCD | Coupled Cluster with Double excitation |
| CCSD | Coupled Cluster with Single and Double excitation |
| CI | Configuration Interaction |
| CIS | Configuration interaction single-excitation |
| CISD | Configuration interaction single and double excitation |
| CISDT | Configuration interaction triple excitation |
| CISDTQ | Configuration interaction quadruple excitation |
| DFT | Density Functional Theory |
| DI | Delocalisation Index |
| DZ | Double Zeta |
| DZP | Double Zeta plus Polarisation |
| EA | Electron Affinity |
| $E_{dh}$ | Dehydrogenation Energy |
| EES | Electronically Excited State |
| ELF | Electron Localisation Function |
| ESP | Electrostatic Potential |
| FET | Field Effect Transistor |
| FLU | Aromatic Fluctuation Index |
| G | Gibb's Free energy |
| G09 | Gaussian 09 |
| G16 | Gaussian 16 |
| GEO | Geometric part of HOMA |
| GGA | Generalised Gradient Approximation |
| GIAO | Gauge Independent Atomic Orbital |
| GS | Ground State |
| GTO | Gaussian Type Orbitals |
| H | Enthalpy |
| HF | Hartree-Fock |
| HK | Hohenberg- Kohn |
| HOMA | Harmonic Oscillator Model for Aromaticity |
| HOMO | Highest Occupied Molecular Orbital |
| IE | Ionisation Energy |

| | |
|---|---|
| ISC | Intersystem Crossing |
| IUPAC | International Union for Pure and Applied Chemistry |
| KS | Kohn-Sham |
| LCD | Liquid Crystal Display |
| LDA | Local Density Approximation |
| LED | Light Emitting Diode |
| LHE | Light Harvesting Efficiency |
| LPA | Linear Polyacene |
| LSDA | Local Spin Density Approximation |
| LUMO | Lowest Unoccupied Molecular Orbital |
| MC | Monte-Carlo |
| MCI | Multicenter Index |
| MD | Molecular Dynamics |
| MESP | Molecular Electrostatic Potential |
| MM | Molecular Mechanics |
| MP | Møller-Plesset |
| NBO | Natural Bond Order |
| NDDO | Neglect of Diatomic Differential Overlap |
| NICS | Nucleus Independent Chemical Shift |
| NMR | Nuclear Magnetic Resonance |
| PAH | Polycyclic Aromatic Hydrocarbon |
| PDI | Para-delocalisation Index |
| PES | Potential Energy Surface |
| PZ/5Z | Pentuple Zeta |
| QM | Quantum Mechanics |
| QTAIM | Quantum Theory of Atoms in Molecule |
| QZ | Quadruple Zeta |
| RE | Resonance Energy |
| STO | Slater Type Orbitals |
| TD-DFT | Time-dependent Density Functional Theory |
| TEM | Transmission Electron Microscopy |

# PREFACE

Linear polyacene (LPA) analogues and polycyclic aromatic hydrocarbons (PAH) are materials having wide application possibilities in the field of optoelectronics. LPAs beyond pentacene are highly unstable and incorporation of heteroatom in their structural skeleton enhances the stability without much change in other properties. Remarkable optical properties like hot luminescence, saturable absorption, and broadband applicability render PAHs an ideal photonic and optoelectronic material. Theoretical investigations are most beneficial for the effective tuning of optoelectronic properties of benzenoid systems and the understanding of the phenomenon of aromaticity. The main focus of the thesis entitled "**DFT Studies on Ground and Excited State Properties of Linear Polyacene Analogues and Polycyclic Aromatic Hydrocarbons**" is to analyze the structure-property relationships of these systems in both ground and excited states which are beneficial for the optoelectronic applications using computational methods. The thesis is divided into four chapters.

The introductory Chapter 1 is divided into two parts, A and B. Part A gives an introduction about optoelectronic uses of linear polyacene analogues and polycyclic aromatic hydrocarbons, the ground and excited states properties that are under the focus of this thesis. Particular emphasis is given to the theoretical aspects and methods for the understanding of these properties. Computational chemistry is a rapidly growing field of chemistry when used in synergy with experimental chemistry act as the most powerful tool in the chemical field. Part B of Chapter 1 encompasses a brief account of computational chemistry and all the theoretical methodologies that are being used in the thesis.

Chapter 2 deals with the design and study of dihydropyrazine annulated linear polyacene systems at M06L/6-311++G(d,p) level density functional theory (DFT) using Gaussian 09 suite of programs. The study is conducted for LPA mimics containing up to six dihydropyrazine units annulated to benzene ($pB_1$ – $pB_6$), naphthalene ($pN_1$ – $pN_6$), anthracene ($pA_1$ – $pA_6$) and tetracene ($pT_1$ – $pT_6$) cores. The multidimensional nature of aromaticity of all these systems is quantified and analyzed using geometric, magnetic and electronic criteria. In $pB_1$, $pN_1$, $pA_1$ and $pT_1$ systems, the sum of dehydrogenation energy ($\sum E_{dh}$) values are 23.8, 38.8, 46.3, and

50.3 kcal/mol, respectively, showing a strong linear correlation with the ratio of the number of π-electrons to number of bonds ($n_\pi$) of the respective systems suggesting that lone pair donation from nitrogen to the π-system increases with decrease in the $n_\pi$ value and that enhances the overall π-bonding strength and aromaticity of the system. The molecular electrostatic potential (MESP) analysis shows that for pB series, the N-heterocycles show that the $V_{min}$ for the N-lone pair region in the range of -25.73 to -34.51 kcal/mol, wherein the innermost N-heterocycle shows the most negative character while the outermost one shows the least negative character. However, compared to $V_{min}$ of dihydrophenazine (-46.25 kcal/mol), the N-lone pairs of the heterocycles are significantly less negative. This showed improvements in the electron-rich character of the core hydrocarbon units at the expense of the N-lone pairs. The absorption spectra of the studied systems show the possibility of tuning the $\lambda_{max}$ values which are an advantage to the optoelectronic industry. From the analysis of the absorption spectra of all the systems in pB series, it is clear that the $\lambda_{max}$ varies from 242 nm for $pB_1$ to 464 nm for $pB_6$. The theoretically calculated light harvesting efficiency of this designed pN, pA and pT series of systems are very high in the range of 0.9, while for pB series the efficiency is not much prominent. The excited state properties of the LPA mimics were also conducted including the singlet-triplet energy gap, geometries. The tuning of electronic properties is evident from these calculations.

Chapter 3 includes the design and studies on LPA mimics containing multiple heterocycles designed by annulating 1,4-dihydro-1,4-azaborinine moieties to benzene ($aB_1$ - $aB_5$), naphthalene ($aN_1$ - $aN_5$), anthracene ($aA_1$ - $aA_5$) and tetracene ($aT_1$ - $aT_5$) cores. The DFT studies using M06L/6-311++G(d,p) method reveal a perfectly planar structure for them, reinforcing the electronic equivalence of CC to BN. The dehydrogenation of a heterocycle is highly endothermic in nature with the lowest value $E_{dh}$ of 74.2 kcal/mol observed for $aB_1$. The average $E_{dh}$ 81.2 kcal/mol is very high meaning that the 1,4-dihydro-1,4-azaborinine based LPA mimics are more stable than the dihydropyrazine based systems. The multidimensional criteria for aromaticity and MESP features are systematically analyzed for all the systems. For aB series, the geometrical aromaticity descriptor harmonic oscillator model of aromaticity (HOMA) index is in the range 0.91 - 0.75, the maximum being 0.91 for the peripheral hydrocarbon ring of $aB_1$ and the lowest 0.75 for the most interior

azaborinine ring of $aB_5$, indicating aromatic character on the hydrocarbon rings as HOMA value close to 1 indicates the overall aromatic nature of molecular system. The nucleus independent chemical shift (NICS) which is the magnetic criteria of aromaticity shows the most negative value of -31.20 for second hydrocarbon ring in $aT_1$ and the least negative value -20.21 for the interior rings of $aT_5$. For molecules showing the same number of rings, $\lambda_{max}$ show similar values. For example, $aB_5$ and $aN_3$ have 11 rings and their respective $\lambda_{max}$ are 371 and 370 nm. Similarly, $aB_3$ and $aA_1$ have seven rings and their $\lambda_{max}$ are 332 and 330 nm, respectively. Studying the nature of aromaticity, thermodynamic stability, HOMO-LUMO energy gap, singlet-triplet energy gap along with the molecular electrostatic potential characteristics is useful for assessing their application potential as structural components in optoelectronic devices.

Chapter 4 deals with the design and studies on differently shaped PAHs using Gaussian 16 suite of programs at M06L/6-31+G(d) level of theory. A prototype of carbon only donor-acceptor system by the connection of two different-shaped PAH via a conjugated diene and a modified version of the same with an electron accepting and electron donating groups attached are also designed and studied. The structure, geometrical features, electronic features and frontier orbitals are analyzed systematically. The desirable localization of MESP electron cloud and frontier orbitals on different parts of the system are observed in many of the systems. For systems having the armchair type of periphery, the Clar's aromatic sextet retention is easily visualized, for the zigzag edged ones this electron localization on Clar's structure was absent. Instead of that, the electron cloud is localized on the outermost rings only. Rectangular shaped PAH systems are electron dense in nature and show very low HOMO-LUMO gaps and most red-shifted absorption features. *$P_z1$* (pyrene) system has an experimental absorption maximum around 250 nm, for which the theoretical value obtained is 235 nm, and it absorbs weakly in the wavelengths 352 nm and 279 nm. The optical data including the absorption maxima values shed light upon the possible tuning and design of suitable candidates in the optoelectronics field.

The analysis of structure-property relationship for optoelectronically promising materials is done in the thesis. We hope that the DFT studies and theoretical predictions provided in this thesis may inspire the exploration of the rich

possibilities of higher LPA mimics and differently shaped PAH for the development of energy efficient devices.

It is mentioned that each chapter in this thesis is considered as an independent unit so that the numbering of all the figures, schemes and tables are done chapter wise.

# Chapter 1

# Introduction

# Part A- Optoelectronic Applications of Polycyclic Aromatic Hydrocarbons, Ground and Excited State properties

# &

# Part B - Computational Chemistry and Theoretical Methodologies

# Part A. Optoelectronic Peculiarities of Polycyclic Aromatic Hydrocarbons, Ground and Excited State Properties

## 1.1.1. Optoelectronic Peculiarities of Polycyclic Aromatic Hydrocarbons

Polycyclic aromatic hydrocarbons (PAHs) are a set of conjugated molecules that are entirely composed aromatic rings without any substituents or heteroatoms.[1] Naturally PAH can be obtained from crude oil , coal and even from outer space.[2, 3] Some of these PAHs are environmental pollutants and carcinogens. By International Union of Pure and Applied Chemistry (IUPAC) definition the simplest PAHs are phenanthrene and anthracene. PAHs can be made up of four-, five-, six and seven- membered rings, of which most common is the six membered ring containing systems. PAHs exclusively made of six membered rings are called as alternant or benzenoid PAHs. Fully benzenoid PAHs which can be drawn without isolated double bonds are highly stable unreactive substances.[4] A representative set of commonly found PAHs are given in Figure 1.1.

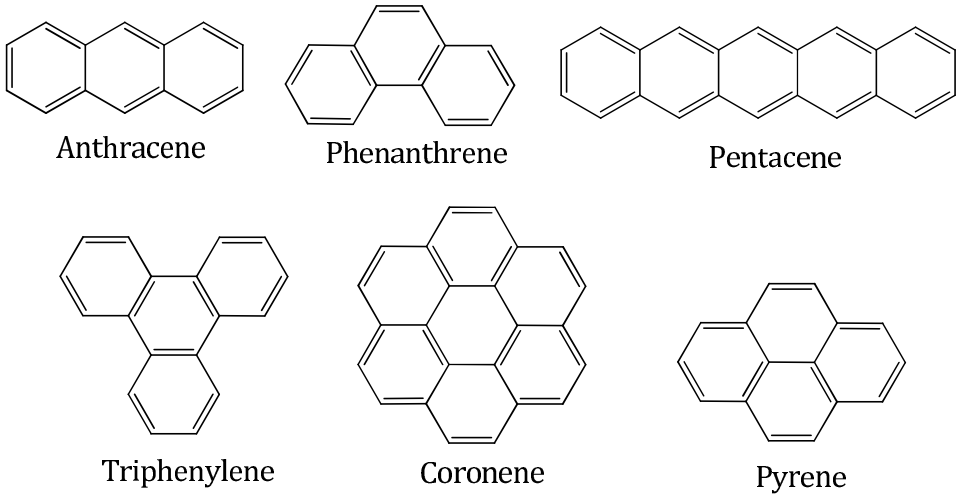


**Figure 1.1**. Examples for commonly found PAHs

The pioneers in the synthesis of PAHs are E. Clar and R. Scholl.[5-10] Most of the structural properties of PAHs are studied by quantum chemical calculations and are in

reasonable accordance with the experimental values.[11-14] PAHs are graphene segments having extensive π-conjugation and thereby considered as promising materials in the construction of organic semiconducting devices.[15-19] Strong intermolecular π-π interactions in such materials add to the value of its use as an electronic material. Hexa-peri-hexabenzocoronene is one of the mostly used PAH which exhibits exceptionally properties as liquid crystal material. Large PAH can be made solution processable via hydrogen termination, alkyl substitution and addition of functional groups. Such processed molecules finds applications as better candidates for organic electronics like light emitting diodes (LEDs), field effect transistors (FETs) and photo-voltaic cells. PAHs have special electronic and self-assembling properties which are highly beneficial in optoelectronic device manufacturing.[20] The formation, transport and the recombination of electrical charges are the key physical features that make PAHs highly desirable for these applications. Carrier mobility, the ability of movement of charges in bulk material is one of determining factor for device performance which is quite high for PAH systems.[21-26]

PAHs find applications in many fields, ranging from as a support to study samples in transmission electron microscope (TEM)[27-29], in solar cells, liquid crystal displays (LCD),[30, 31] as FETs,[32, 33] and as composite materials.[34] Graphene because of the zero band gap faces difficulty in FETs, where PAH having low band gap finds wide applications in the field.

Linear polyacenes (LPAs) are a class of PAH molecules in which benzene rings are laterally fused. Unique properties and their optoelectronic applications are widely and intensively researched upon. [35-38] These are the narrowest PAHs with zigzag ends and because of this structural peculiarity finds applications in spintronics and plasmonics.[39, 40] With the increase in number of benzene rings the difference between the highest occupied molecular orbital (HOMO) and the lowest unoccupied molecular orbital (LUMO) goes on decreasing to make the material more conducting.[41] An infinitely long LPA can be considered as a metal and superconductor at low temperature.[42, 43] Since the properties of polyacenes are largely dependent on their length or the number of rings constituting it, the largest members is expected to show higher reactivity, high carrier motilities, lowest reorganizational energy in addition to the above mentioned low

HOMO-LUMO gap.[44-46] But the synthesis and purification of such longer polyacenes are highly difficult because of the innate instability arising from the higher reactivity.

To circumvent this, substitution on aromatic rings can be done to synthesize substituted LPA.[47, 48] This strategy is efficiently utilized for the synthesis of substituted higher acenes like nonacene.[49-51] The synthetic steps are difficult and isolation is further difficult for higher acenes until recently.[52, 53] Photoreaction followed by matrix isolation yielded higher acenes including heptacene, octacene and nonacene.[49, 54-57] The longest acene synthesized very recently in its unsubstituted form is undecacene having 11 benzene rings fused laterally.[58] As the length of LPA increases the linearity may also get distorted. Introducing heteroatoms like nitrogen,[59-65] boron,[66, 67] sulfur[68] etc in the structural skeletons of LPA is a better strategy for attaining higher LPA like systems. The selection of hetero atoms is to be done in such a way that the electronic and structural features are not varied much. Nitrogen containing oligocenes are demonstrated as n-channel organic semiconductor,[69, 70] with quite high motilities. Easy control of stability, structure, electronic properties and increased electron affinity can be attained by replacement of CH by N.[71] The position of hetero atoms and thereby polarity manipulation can improve the solution processability of such LPA mimics. Vacant $p_z$ orbitals in boron enhances the optoelectronic application potential of boron containing acene molecules.[72] The electronic and steric equivalence of B-N with C=C, makes boron and nitrogen a very good candidate for making a heteroacenes.[73, 74] These molecules show different electronic properties together with characteristic self-assembly behavior.[75, 76] The phosphorescence quantum yield of BN heteroacenes are higher than their acene counterparts.[77] BN containing heteroacenes are demonstrated as excellent materials for OLEDs and luminogen for fluoride ion detection.[78, 79]

Efficiency of photovoltaic cells has direct relationship with the electronic properties as well as the excited state properties. Prediction of these properties beforehand the synthesis will minimize the trial-and-error synthetic steps which is of great use.[80, 81] For the understanding about the stability of the molecules, thorough knowledge about the phenomenon of aromaticity is highly beneficial. The concepts of aromaticity and various methods useful for its quantification are given in Section 1.1.2. The excited state properties are briefly introduced in Section 1.1.3.

## 1.1.2. Aromaticity

Aromaticity is one of the most important phenomena in chemistry,[82-87] the idea of which was proposed 153 years ago by German chemist Friedrich August Kekulé.[88] Even though this phenomenon has a fuzzy nature and lacked exact definition; it has become a central concept to interpret the molecular structure, stability, reactivity and magnetic properties of chemical systems.[82-84, 86, 89-92] [11] The IUPAC definition of aromaticity is as follows, "*the concept of spacial and electronic structure of cyclic molecular systems displaying the effects of cyclic electron delocalization which provide for their enhanced thermodynamic stability (relative to acyclic structural analogues) and tendency to retain the structural type in the course of chemical transformations".*[93] The characteristics that distinguishes aromatic molecules from non-aromatic ones can be listed as[94] (i) the molecule should be a cyclic one with large resonance energy, (ii) substitution is preferred reaction mode instead of addition, (iii) should posses aromatic sextet of electrons, (iv) satisfies the Hückel's 4n+2 π-electrons criterion of aromaticity, (v) should be able to sustain the diamagnetic ring current. Local aromaticity is the aromaticity of a particular ring in a molecule whereas the global aromaticity represents the total aromatic character of a molecule having several fused rings.

Hückel's 4n+2 rule for aromaticity, one of the most used criteria for aromaticity is limited to monocyclic conjugated systems. This rule relates the number of π-electron count to the stability and reactivity of the molecules.[95, 96] For aromatic molecules, the cyclic delocalization of electrons results in extra stabilization while for antiaromatic compounds, the same will result in the destabilization of the molecule. Aromaticity for cyclic π-conjugated systems are defined by reduced bond length compared with acyclic counterparts, enhanced stability, retention of π-electron structure in reactions and diatropic ring current generation by an external magnetic field.[86, 97-100] Clar's sextet rule uses the simple topological features for the assessment of aromaticity, and states that the maximum number of disjoint aromatic benzene units and minimum number of localized double bonds represents the most aromatic structure.[7] For the quantification of aromaticity of PAH a multitude of methods have been developed and is in wide use.[98, 101-107] In the modern view, aromaticity is considered as a multidimensional

phenomenon which has to be analyzed and quantified in terms of energetic, structural, magnetic and electronic (reactivity based) criteria.[87, 94] The various methods that are adopted for this purpose is briefly discussed below.

### 1.1.2.1. Energetic Criteria of Aromaticity

The basic idea behind the use of energy as a criteria for aromaticity measurement is conjugated cyclic π-electron compounds higher stability compared to their chain analogues.[12, 84] Quantitative measurement of aromatic stabilization energy (ASE), influencing the reactivity and behavior of species, gives an idea about the total aromaticity of the molecule.[84, 86, 108-111] Uses of isodesmic, homodesmic and hyperhomodesmic reactions are being relied upon for the treatment of thermo dynamical data for aromatic measurement. The term isodesmic was first introduced in 1970,[112] to predict thermochemistry using primitive electronic structure theory.[113, 114] Isodesmic reactions are a subclass of isogyric reactions, which are the reactions in which there is same number of electron pairs in the reactant and product side.[115] An example for the isogyric reaction is given in Eq. 1.1. An isodesmic reaction is a hypothetical chemical reaction in which the number of formal bonds remains equal for reactants side and product side.[116] Some representative examples are given below.

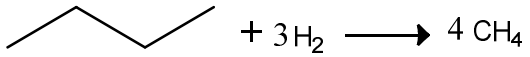


Eq. 1.1

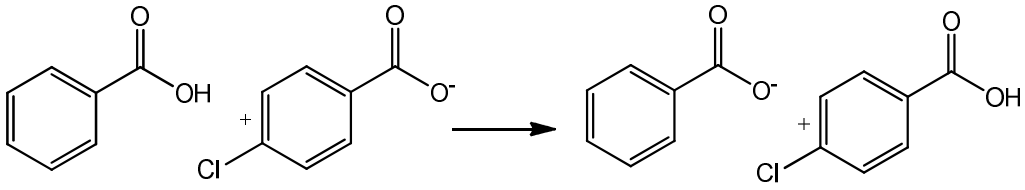


Eq. 1.2

Such reactions are useful in the quantification of structure-stability relationships. For instance, in the case of benzene, isodesmic reaction 1.3 suggests a 23.9 kcal/mol higher stabilization for benzene which could be mainly accounted to the aromatization energy.[117, 118] For practical applications, heat of formation of all the molecules on both sides of the isodesmic equation has to be obtained to measure the aromatization energy. Homodesmotic reactions are a subclass of isodesmic reactions in which the number of carbon atoms in a particular hybridization and number of hydrogen atoms attached to each carbon atoms for reactants and products are the same.[119-123] Example

for homodesmotic reaction for assessment of benzene aromatic stabilization is given in Eq. 1.3.[118] Hyperhomodesmotic reactions differ from homodesmotic ones because it has same number of C-H bonds at identically hybridized fragments (example given in Eq. 1.4).[124] In such reactions the number, type and hybridization of C-C and C-H bonds are preserved.

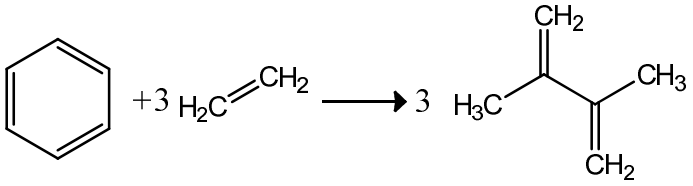


Eq. 1.3

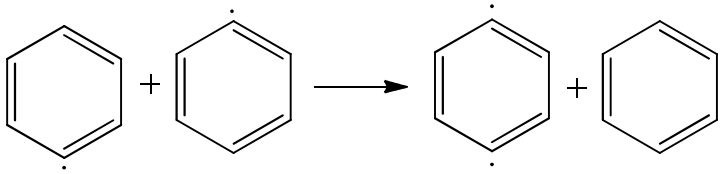

Eq. 1.4

The aromatization energy estimated using homodesmotic reactions are more accurate than that using isodesmic reaction because as seen in equation (1.3), the bonding scenario at the LHS and RHS of the equation is almost identical except for the cyclic delocalization of the π-electrons in the LHS. Hence, the energy change in the reaction can be exclusively accounted for the extra stabilization due to the cyclic delocalization of π-electrons or aromaticity. Following the concept of homodesmotic reactions, a series of reaction classes have been generated like hyperhomodesmotic, semihomodesmotic, etc which have been used by many scientific groups.[125-134]

Heat of combustion and heat of hydrogenation data have been useful in calculation of the empirical resonance energy by the direct measurement of change in enthalpy (ΔH) value[135].[94, 136] These calculations are based on assuming the additive nature of thermo chemical bond energy and neglecting other energetic contribution such as ring strain. The heat of dehydration[137] data is also useful for the resonance energy calculation. Equilibria based approaches are also used for the quantification of heterocycle aromaticity on the energetic scale.[94] The equilibria based aromaticity measurements uses Gibbs free energy change (ΔG) while enthalpy parameter ΔH is used in combustion, hydrogenation and dehydrogenation techniques. [138], [139]

### 1.1.2.2. Geometric Criteria of Aromaticity

Quantification of aromaticity based on structural parameters relies on π-delocalization, planar geometry, equalization of bond lengths, and other geometry parameters.[94] One of the major method that is useful for aromaticity quantification for individual cyclic parts of organic compounds is Harmonic Oscillator Model for Aromaticity (HOMA) index developed by Krygowski et al.[140]. HOMA is calculated using the following equation.

$$HOMA = 1 - \frac{\alpha}{n}\sum_{i}^{n}(R_{opt} - R_i)^2 \qquad \text{Eq. 1.5}$$

Here $\alpha$ is an empirical normalization constant, which is selected in such a way that HOMA is zero for non-aromatic and one for aromatic systems. $n$ is total number of bonds; $R_{opt}$ and $R_i$ are optimal aromatic bond length and computed bond length, respectively. For a perfect aromatic system, HOMA is 1 and a HOMA value close to zero indicates non-aromatic character. Aromatic molecules tend to show bond length equalization and HOMA value close to 1. The CC bond length of benzene is considered as the most optimum for an aromatic hydrocarbon. HOMA is considered as one of the best structure based aromaticity indices which is well correlated with other aromaticity indices, and useful in measuring the effect of distortion from planarity and substitution on the aromaticity, local aromaticity on single rings in condensed systems and the influence of hydrogen bonding in crystal lattice. [82, 99, 141-143]

Bird aromaticity index is a measure of aromaticity for heterocycles. Its value for five member and six member rings is expressed as follows

$$I_{5(6)} = 100[1 - (V/V_k)] \qquad \text{Eq. 1.6}$$

$$V = (100/N_0)\sqrt{[\sum(N - N_0)^2]/n} \qquad \text{Eq. 1.7}$$

$V_k$ = 35 for five membered heterocycle, and $V_k$ = 33.3 for six membered heterocycle,

$$N_0 = (\sum_{n} N)/n \qquad \text{Eq. 1.8}$$

where $N$ is bond order and $n$ is number of bonds. Birds aromaticity indices gives satisfactory correlation with other aromatic criteria like absolute hardness and magnetic criteria.[144-146]

Bond length equalization is used as a measure of aromaticity as the aromatic molecules tends to show resonance and resulting unified bond length. When bond order is used instead of bond length for aromaticity measurement, the geometric criteria is satisfied.[147] Average fluctuation in the bond order is also a measure of aromaticity based on geometric criteria put forward by Pozharskii.[148] Fringuellli *et al.* proposed the use of bond order for the quantification of aromaticity.[149] The bond order is calculated using the Gordy equation[150] which is as follows,

$$N = a.R^{-2} - b \qquad \text{Eq. 1.9}$$

The constants $a$ and $b$ has different values based on the atoms forming the bonds and $R$ is the bond length. The smaller the sum of bond order differences in a ring, the more is the aromaticity of the ring. For benzene the value of it is zero.

### 1.1.2.3. Magnetic Criteria of Aromaticity

Magnetism based aromaticity indices are based on the ring current generation under the influence of an external magnetic field. Experimentally, aromatic character of a molecule is assessed based on proton nuclear magnetic resonance ($^1$H NMR) chemical shifts which are characteristics of respective molecules and the exaltation of magnetic susceptibility.[11, 94, 99]

One of the defining characteristics of aromatic molecules having cyclic electron delocalisation is the ability to sustain a diatropic ring current, [83, 84, 109, 151-155] whereas antiaromatic molecules made of localised destabilised structures sustain a paratropic ring current.[154] Ring current effects can be demonstrated by means of the abnormal proton chemical shifts of the aromatic molecules. In rings, the chemical shift on the bridging hydrogen has been already used as a measure of aromaticity and antiaromaticity.[156, 157] These methods paved the way to the use of absolute magnetic shielding at the ring centre called Nucleus Independent Chemical Shift (NICS) by Schleyer *et al*. as a measure of aromaticity and antiaromaticity.[158] The values are reported with a reversed sign to make them compatible with the chemical shift

conventions of NMR spectroscopy, which is more familiar. In this method, negative NICS values indicate aromaticity and positive values antiaromaticity.

NICS is used as a measure of aromaticity for rings,[159-163] clusters,[164-168] metal complexes[169] and even in transition states.[170-175] There are contradiction in the case of cyclic trimer of hydrogen bonded HF molecule which exhibits negative NICS value, which is proved to be non-aromatic.[176] This proved that the NICS value is valid in the molecules which have an important $p_z$-orbital which produces π-electron cloud. NICS values exhibit good correlations with aromatic stabilisation energies[109] and magnetic susceptibility exaltations, which are aromaticity parameters making it a reliable tool for the calculation of the same. Also, unlike exaltations, the ring size dependence in the values is nil in NICS calculations. As moving away from the ring centres maximum chemical shifts are observed. NICS is greatly influenced by the coupling between the induced magnetic fields of adjacent rings in the case of acene molecules.[97, 177-181] Accuracy of which is validated by Mills *et al*. by demonstrating an excellent correlation between experimental shifts and $^{13}C$ NMR shifts calculated with DFT calculations.[182] Experimental measures of aromaticity on pyrene derivatives also supported the validity of NICS.[183] NICS values of [n]annulenes show only a modest dependence on size of the rings. 10 π systems have comparatively high NICS values than that of 6 π systems. Antiaromatic 4n π systems like cyclobutadiene, pentalene, heptalene, planar cuyclooctatetraene have NICS(0) values 27.6, 18.1, 22.7 and 30.1 respectively, which are highly positive values.[158] Spherical aromaticity[184], which is also called as three dimensional aromaticity can be also demonstrated by NICS in the case of closo-$B_{12}H_{12}^{-2}$ and other polyhedral borane compounds. NICS calculation is also employed successfully on inorganic ring compounds analogous to polyacenes.[185] Summation of $NICS_{zz}(1)$ values for ring system serves as a measure of global aromaticity since there is excellent correlation between the former and the magnetic susceptibility exaltation.[182] But for π-stalked systems for the quantification of aromaticity NICS should be used with caution according to the studies on polyflourenes.[186]

Ring currents in an aromatic system cause a shift in proton resonances in NMR spectrum, and magnetic susceptibility exaltation and a change in NICS. [13, 111, 187-189]

Pauling in 1936 suggested diamagnetic anisotropy of aromatic molecules are due to $2p_z$ electrons of carbon atom, which are free to move from one atom to the adjacent ones under the influence of an electric field.[190] This is the basis of application of ring currents as a measure of aromaticity. Aromatic molecules support ring currents which effects in deshielding on the outer and shielding in the inner electrons of the ring. For monocyclic heteroaromatics homodesmotic reaction energy measurement shows that proton shielding can be a measure of cyclic stabilizing and destabilizing effects which is directly linked to the quantification of aromaticity or antiaromaticity.[191]

o-Benzylic coupling constant and bond order have a direct correlation, thus making it a good experimental means to measure the degree of aromaticity for heterocyclics.[192] Other C-C coupling constants are also very effective in aromaticity assessment of five membered heterocycles.[193] Magnitude of strong chemical shift in $^1$H NMR spectra of dipolar molecules induced by aromatic solvents is a direct measure of molecular magnetic isotropies.[194] Solvent shift parameter($S$) is a quantitative aromaticity parameter, which is expressed as the difference in proton chemical shift between acetonitrile and cyclohexane in solvent X and the same in solvent neat cyclohexane.[94] The $S$ value for benzene is 1.00 ppm and that for olefins is near to zero.

The exaltation which is the difference between the observed molar magnetic succeptibility $\chi_M$ and calculated one $\chi_{M'}$is useful in aromaticity assessment,[187, 195-197] which is highly dependent on ring size, the calibration of standards are done for the calculations.[153, 189, 198-201] For aromatic molecules, exaltations are negative indicating diamagnetic nature, and for paramagnetic antiaromatic compounds the exaltations are positive.[142] Magnetic susceptibility exaltation shows excellent linear correlation with $NICS_{zz}(1)$ values for neutral, cationic and monoanionic species.[182]

### 1.1.2.4. Electronic Criteria of Aromaticity

The measurement of aromaticity by electronic criteria can be realized by the molecular electrostatic potential (MESP), HOMO-LUMO gap, absolute and relative hardness and polarizability.[11, 202]

Aromaticity can be understood by knowing the extent of electron delocalization in a molecule. But finding out electron delocalization extent from the experimentally

measurable electron density[203] is difficult. Aromaticity and π-electron distribution has close association as per the theoretical calculations done by various groups.[204, 205] MESP is an electronic property that quantifies the electron cloud and delocalization of it in a particular molecule beneficial in understanding the molecular structure and reactivity.[206-214] Electron density has a direct correlation with MESP, and the topology of it can gives pictorial information about the charge distribution in the molecule. Identifying the most negative valued MESP ($V_{min}$) positions in a molecule is useful for understanding the electron localization/delocalization character of π-regions in molecules.[215, 216] Electrostatic potential is used as a probe to measure electron delocalization by Politzer *et al*. by taking the minimum value along the C=C and comparing with the same at ethylene.[217]. $V_{min}$ analysis has been previously used for studying the Clar's aromatic sextet theory[6, 7] of PAHs and related systems.[210, 218-222] Illustration of aromaticity by Clar's theory using MESP topography for triphenylene molecule using B3LYP and MP2 theory with 6-31+G(d,p) basis set is given in Figure 1.1, where the MESP clearly projects the aromatic core.[218]

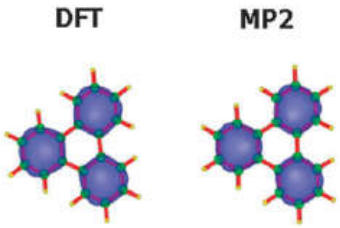


Figure 1.2. MESP topography of triphenylene molecule illustrating the Clar's sextet position. Figure adapted from Suresh et. al.[223]

Characterization of π-region in the PAHs has direct correlation with aromaticity has been shown by Suresh and Gadre by the mapping of MESP topography.[224] Hammet constants, a measure of quantifies the electronic perturbation on the benzene nucleus when substituents are attached is directly correlated to MESP topography.[225] Politzer *et al*. also reinforced the use of MESP as a tool for the theoretical assessment of π-regions in the molecules.[226-229] Electron withdrawing and donating power of substituents on arene ring can be quantified and the location of electron rich centers can be exactly pinpointed using the $V_{min}$ values.[212] Electrostatic potential at nuclei is considered as the

best descriptor for local properties which include the aromaticity and surface properties.[230, 231]

HOMO and LUMO which are called as the frontier molecular orbitals hugely influences the reactivity and stability of molecules. The difference between the energy of these two is termed as HOMO-LUMO gap, which is closely related to the number of aromatic sextets in the molecule.[232] Addition of electrons to the high lying LUMO and extraction of the electrons from the low lying HOMO is energetically unfavorable. Thus large HOMO-LUMO gap infers high kinetic energy as well as low reactivity.[233-238] In the case of [4n+2] annulenes, the direct relationship between resonance energies (REs) and HOMO-LUMO gap has been shown by Haddon and Fukunaga, thereby correlating thermodynamic and kinetic criteria for aromaticity measurement.[239] This finding is written in the form of an equation as given below,

$$RE = -\frac{(\pi\rho_{rs})^2(\varepsilon_{LUMO} - \varepsilon_{HOMO})}{24} \qquad \text{Eq. 1.10}$$

where $RE$ is the resonance energy and $\rho_{rs}$ is the bond order of the r-s bond. Also resonance energies and reduced ring currents have similar relationship for the same set of systems.[240] A small HOMO-LUMO gap is associated with antiaromaticity, based on some studies conducted in late 1970s and early 1980s.[241-249] Linear relationships between paratropic $^1$H NMR shifts ($\Delta\delta$) and HOMO-LUMO energy gap is observed for doubly charged fused benzenoid polycyclic compounds.[246] The relationship for diacation and dianion are respectively given below, where $\Delta_{HL}$ is the HOMO-LUMO gap in eV.

$$\Delta\delta(ppm) = -1.23\Delta_{HL} + 4.31$$

$$\Delta\delta(ppm) = -2.50\Delta_{HL} + 6.40 \qquad \text{Eq. 1.11}$$

HOMO-LUMO bonding type is considered as an indicator of aromaticity according to studies by Sinanoğlu et al.[250, 251] Hückel π electron energy, number of Kekule structures and the HOMO-LUMO gap can be related.[252] For benzenoid hydrocarbons HOMO-LUMO gap can be calculated using the following equation,

$$\Delta_{HL} = 2[-2.90611(2n_{CC}/n_C)^{1/2} + 3.91744K^{2/N}] \qquad \text{Eq. 1.12}$$

where $n_{CC}$ and $n_C$ are the numbers of C-C bonds and carbon rings respectively and $K$ is number of Kekúle structures. Using HOMO-LUMO separation multiplied by the number of conjugated atoms, an aromaticity index is demonstrated by Aihara *et al*. in the case of kinetic stability of PAHs and fullerenes.[233-235] This index is termed as T-index, which is useful in the spotting of chemical reactivity at the most reactive site for a number of fullerene molecules containing isolated pentagons.[235]

In a chemical system the resistance of the electronic chemical potential, μ to a change in number of electrons is termed as the absolute hardenss (η), which is measured by the plot curvature of energy versus number of electrons.[93] Absolute hardness ($\eta$) can be used as a measure of aromaticity according to Zhou, Parr and Gharst based on the fact that both aromaticity and hardness are measure of high stability and low reactivity.[237] High value of absolute hardness implies high stability as well as aromaticity. The difference between the electron affinity (*EA)* and the ionization energy (*IE*) is the negative of the hardness of the species.

$$EA - IE = -\eta \qquad \text{Eq. 1.13}$$

Hardness can be reformulated using the terms of molar refractivity as $19.6/R_D^3$, where $R_D$ is the molar refractivity.[253, 254] In Molecular orbital (MO) theory, absolute hardness is defined as the energy gap between the LUMO and HOMO.

$$\eta = (\varepsilon_{\mathrm{LUMO}} - \varepsilon_{\mathrm{HOMO}})/2 \qquad \text{Eq. 1.14}$$

For a series of aromatic and heteroromatic rings good correlations are observed between resonance energies and Birds $I_A$ index.[255-258]

Charge density derived electronic parameters can also be used as a measure of aromaticity.[202] Charge density descriptors based on the bond order and density at the ring critical point have also been developed and used for the aromaticity quantification.[259, 260] Natural bond order (NBO) analysis of charge densities have been demonstrated as a source of delocalization effects which is used in aromaticity measurement.[261, 262] Electron localization function (ELF) analysis yields degree of π-electron delocalization, which is a good indicator of aromaticity, but quantification of the same is not feasible.[263-267]

The electron delocalization measures that have been derived from second order density have been successfully employed as a local aromaticity descriptor.[268, 269] Delocalization index, *δ(A,B)* is an aromaticity index that have been derived from Quantum Theory of Atoms In Molecule (QTAIM) theory. Para-delocalization index (PDI) is a local aromaticity descriptor that have been developed by Solá et al.[142] The average of all the delocalization indices (DIs) of para-related carbon atoms in a six membered ring is termed as PDI. The basis of PDI is the concept of the aromaticity is related to cyclic delocalization of π-electrons. This quantity gives an idea about the amount of electrons shared or delocalized among atoms. DI of single C-C bond and the atomic stabilization energy (ASE) are in good correlation according to a density functional theory study by Chesnut and Bartolotti.[270] Bader and coworkers in 1990s found out that in the case of benzene, the delocalization of density in para-related carbons is greater than that between meta-related carbons ($\delta(C,C')_p$=0.10 electrons > $\delta(C,C')_m$=0.07electrons).[269, 271]

Aromatic fluctuation index which is abbreviated as *FLU* is another method which uses charge density descriptors for the aromaticity quantification.[202] This method have been introduced to account for the limitations in PDI within the framework of AIM theory by Bader.[272-274] The value should be close to zero for aromatic molecule. The amount and similarity of electron sharing between adjacent atoms are taken in account in this method.[202] Multicenter indices $I_{ring}$ , $I_{NG}$, $I_{NB}$ and *MCI* have been employed in the quantification of aromaticity. The multicentre index $I_{ring}$ which is proposed by Giambiagi *et al*.[275] is given as,

$$I_{ring}(A) = \sum_{i_1,i_2,..,i_N} n_{i_1}..n_{i_N} S_{i_1 i_2}(A_1) S_{i_2 i_3}(A_2) \dots S_{i_N i_1}(A_N) \qquad \text{Eq. 1.15}$$

where $S_{ij}(A)$ is the overlap integral of natural orbitals *i* and *j* of the atom *A*, $n_{ij}$ are their occupancies. A normalized version of $I_{ring}$ index is has been proposed by Solá *et al*. in the year 2007 which is called as $I_{NG}$ which is less dependent on the ring size than other homologues.[276] it is expressed as follows.

$$I_{NG}(A) = \frac{\pi^2}{4NN_\pi} I_{ring}^{1/N} \qquad \text{Eq. 1.16}$$

where $N$ is total number of atoms in the molecule and $N_\pi$ is the total number of π-electrons. Summing up all the $I_{ri/ng}$ values arising from all the permutations of the indices defines another index called as Multicenter index (*MCI*) as proposed by Butlinck *et al*.[277] given as,

$$MCI(A) = \frac{1}{2N}\sum_{P(A)} I_{ring}(A) \qquad \text{Eq.1.17}$$

where *P(A)* stands for the permutation operator. Normalized version of *MCI* for aromatic rings is called $I_{NB}$ and is given as given below, where C ≈ 1.5155.

$$I_{NB}(A) = \frac{C}{NN_\pi}[2NMCI(A)]^{1/N} \qquad \text{Eq. 1.18}$$

Applications of Multicenter indices are general and can be used in the scenarios in which PDI, FLU or HOMA are unsuccessful. Higher the values of multicenter indices infers higher the aromatic character of molecules.

## 1.1.3. Excited State Properties

When a molecule absorbs highly energetic electromagnetic radiation (when the energy of the photon matches with the energy difference between the orbitals), electrons gets promoted from lower energy orbitals to the vacant higher energy orbitals resulting in the generation of an excited state. Excited states are stable high energy electronic configurations of molecular systems, which are relevant to many areas of chemistry like photochemistry and electronic spectroscopy. Excited states can participate in chemical reaction which is the basis of photochemistry. Only a few of the many orbitals are involved in the excitation process, called the frontier orbitals. Electronically occupied highest energy orbitals and lowest energy vacant orbitals are termed frontier orbitals. Transition due to lowest energy photon is between Highest Occupied Molecular Orbital (HOMO) and Lowest Unoccupied Molecular Orbital (LUMO). HOMO-LUMO gap is closely related to number of resonant sextets in the molecule.[232] High kinetic stability is a direct consequence of large HOMO-LUMO gap, since the addition of electrons to high lying LUMO and extraction of electrons from high lying HOMO is energetically unfavourable.[233-238]

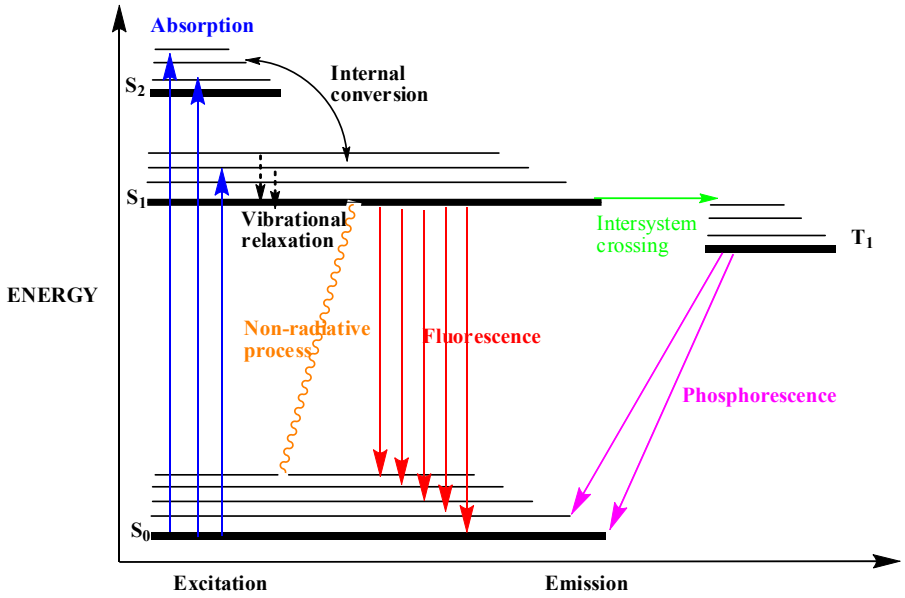


Figure 1.3. Jablonski diagram

Electronic states of a molecule and the transitions are illustrated using Jablonski diagram (Figure 1.3) named after Polish physicist Aleksander Jablonski.[278] The possible transitions and the names of resulting phenomena are listed below. $S_0 \rightarrow S_n$, where n=1,2,3…. are termed absorption which results in a excited state molecule. When the energy of the impeding photon matches with the energy difference between the orbitals absorption occurs. $S_1 \rightarrow S_0$, fluorescence, the spontaneous emission of radiation from higher energy orbitals to the ground state of the molecule. $T_1 \rightarrow S_0$, phosphorescence which is the delayed emission from the triplet excited state to the ground state of the molecule. The exchange of electrons between different excited states are termed internal conversion (IC). The relaxation of electrons from the higher excited levels to the lowest excited level is called as vibrational relaxation. Non-radiative processes are the relaxation from the excited level to the ground state without any emission of radiation. When electron exchange occurs between the excited states of different multiplicity intersystem crossing (ISC) occurs, which is the cause of phosphorescence indirectly.

Electronic excited states have wide applications ranging from spectroscopy to photochemistry. Structure and dynamics of excited states are necessary for modeling the photochemical reactions. Time-dependent density functional theory (TD-DFT) is a powerful tool for the analysis and evaluation of electronically excited states (EES).[80, 279-

[283] Evaluation of low lying triplet excited states is also feasible theoretically which helps in the calculation of vertical and adiabatic energy difference with respect to the ground state, geometrical peculiarities associated with excitation and singlet-triplet exchange energies.[284-289] The triplet states can give direct information about energy loss pathways of solar cell engineering.[290-292] For solar energy trapping new molecules with optimized properties does not depend merely on the HOMO-LUMO gap, but also on the triplet energies.[287] The spacial separation between the electron-hole pair minimizes the exchange interaction between singly occupied excited states and bring about a reduced singlet-triplet energy gap.[293]

Theoretically excited states can be calculated using various methods like coupled cluster (CC), Moller-Plesset perturbation (MP) theory, multi-configurational self consistent field, configuration interaction (CI) and time-dependent density functional theory (TD-DFT) etc.[294-299] TD-DFT is most commonly used in the dye designing research, since the error in the relative data is minimum when a set of structurally similar molecules are being considered.[300] Examples of excited state properties are light absorption, light emission and excited state reactions like electron transfer, energy transfer and bond breaking. Structure and dynamics of excited states are necessary for modeling the photochemical reactions. Efficiency of photovoltaic cells has direct relationship with the electronic properties as well as the excited state properties. Prediction of these properties beforehand the synthesis will minimize the trial-and-error synthetic steps which is of great use.[80, 81] Prediction and rationalization of absorption spectra of several systems have been done using TD-DFT.[301-305] The nature of the geometry of the excited states and the simulation of fluorescence spectrum of the concerned geometry have been extensively studied by TD-DFT.[306, 307]

### 1.1.3.1. Absorption, Emission and Adiabatic Energies

Absorption, emission and adiabatic energies can be calculated using various theoretical methods. The energy difference between the electronically excited state (*EES*) and ground state (*GS*) determined at *GS* geometry corresponds to idealized absorption, whereas the same calculated on *EES* geometry corresponds to the

fluorescence when *EES* is singlet state, and phosphorescence when *EES* is a triplet state.[300]

$$E^{vert-abso} = E^{EES}(R^{GS}) - E^{GS}(R^{GS}) \quad \text{Eq. 1.19}$$

$$E^{vert-fluo} = E^{EES}(R^{EES}) - E^{GS}(R^{EES}) \quad \text{Eq. 1.20}$$

Absorption is the most widely computed data using TD-DFT, since there is no need of *EES* density or energy. Fluorescence measurement needs access to the TD-DFT forces in order to optimize the *EES* geometry. But the experimental results cannot be considered as purely vertical, the comparison of the vertical absorption and measured absorption maxima ($\lambda_{max}$) will not give exact results. An adiabatic contribution is the difference of energies of two states in their respective minimum.

$$E^{adia} = E^{EES}(R^{EES}) - E^{GS}(R^{GS}) \quad \text{Eq. 1.21}$$

An absorption spectra or a UV-Visible spectrum is a plot between absorbance vs. wavelength which displays a series of absorption bands. The wavelength maximum ($\lambda_{max}$) is the wavelength at which the absorbance is maximum, which is useful in the approximation of the energy difference (ΔE) the orbitals involved in the transition.

Consider a widely used light absorbing compound, anthracene having 14 π molecular orbitals having 14 electrons, since all the carbon atoms involves in the π-bonding. MO(7) is HOMO and MO(8) is LUMO. As an example, the experimental absorption spectrum of naphthalene displays an absorption band in the 300-400 nm range and the longest wavelength maximum is observed at around 370nm. Higher energy absorption bands having $\lambda_{max}$ lesser than 250 nm are due to $\pi \rightarrow \pi^*$ transitions.

## 1.1.3.2. Geometries and Vibrational Frequencies

Finding out the optimal geometries of *EESs* using theoretical methods is useful in the analysis of fluorescence, since the experimental determination of *EES* bond lengths and valance angles are very difficult.[300] Stokes shifts are the difference between emission and absorption energies, which is prominent when there is large difference between *EES* and *GS* energies. Conformational changes can be predicted by this method, which in many ways is beneficial for complex reaction situations. The vibrational frequencies of the *GS* and *EES* will be different, the modification of the

characteristic vibrational modes happens when the molecules gets excited to their corresponding *EES*. TD-DFT second derivatives are needed for determining the vibrational signatures of EES. From known vibrational signatures vibrationally resolved optical spectra is computed which provide the shape of absorption and emission bands.

### 1.1.3.3. Singlet-triplet Energy Gap

Singlet-triplet splitting are much more sensitive to the exact mathematical form of the function than the transition energies.[300] The energy difference corresponding to first triplet state (T1) and ground state (S0) corresponds to the phosphorescence phenomena, and is directly related to the phosphorescence lifetime of the molecule, which has a direct relation with the photo-stability of the molecule. Whereas the energy gap between T1 and first singlet excited state (S1) ($\Delta E_{T1\text{-}S1}$) corresponds to the (ISC) phenomena, which is a nonradiative slowest form of relaxation. The efficiency of ISC can be improved by reducing the energy gap between the singlet and triplet excited states.[308] Spin-orbit coupling is directly related to the ISC, the rate of which largely affects the conversion efficiency of a solar cell.[290, 307] Phosphorescence is a manifestation of ISC where the relaxation from the excited triplet state to the singlet ground state occurs. Experimental determination of triplet states properties are very difficult to access, and their theoretical evaluation is very useful.[287, 306] The emission process is the vertical S1→S0 transition; thereby the energy gap ($\Delta E_{S1\text{-}S0}$) is a direct measure of the emission lifetime. Delayed S1 to S0 de-excitation accounts for the fluorescence and the energy difference can be directly related to the fluorescence lifetime also. Optical gap of a system is predicted by the energy of lowest singlet excited state, and energy ordering of T1 with respect to S1 is very important factor that determines the reverse intersystem crossing (RISC) which is a determining factor of efficiency of electroluminescence.[309]

### 1.1.3.4. Spectral Features

The entire spectral phenomena are marked in the Figure 1. 3 of Jablonski diagram. The absorption and relaxation processes involving the electronically excited states are normally associated with the change in energy resulting in the specific spectral features

corresponding to the processes that the systems are undergoing. The absorption involves the excitation of electrons into the EES from the electronically ground state. The emission involves the de-excitation of the same. The triplet and singlet states of the excited states determine whether the process is fluorescence or phosphorescence. In principle all the information regarding the excited states can be accurately obtained computationally. In the first approximation the vertical excitation energy is the difference in potential energy curve between the excited state and ground state. The prediction and visualization of absorption, fluorescence, emission and phosphorescence spectra of molecules are possible. The characterization of chiral light and thereby circular dichroism spectra is possible with a greater effort. These kind of spectral calculations are of great use to chemists in the spectral and structural elucidation field.

The vibronic fine-structure of electronic spectra gives information about vibrational modes frequencies and excited state geometry of the molecule. These properties are otherwise very difficult to obtain experimentally. The spectral features give a direct picture of the wavelengths and the range corresponding various phenomena which are of prime interest in the energy absorption, emission, the prior understanding of which can enhance the device manufacturing efficiency quite high.

### 1.1.3.5. Other Parameters

Vibrational coupling, dipole moments and atomic point charges are some of the measurable quantities which are observable and can be found out by theoretical methods such as TD-DFT. Color, charge transfer, potential energy surfaces(PES), non-Frank-Condon transitions etc are some of the other excited state properties of molecule. The absorption of a photon in the visible region of the electromagnetic spectrum excite the GS to an EES, other than that it also modifies the wavelengths of reflected and transmitted light, the phenomena of chemical colors thus originates. From the shape of the absorption spectra the color of the molecule can be described using TD-DFT method relatively easily.[311, 312]

# Part B: Computational Chemistry and Theoretical Methodologies

## 1.2. Introduction to Computational Chemistry

The term theoretical chemistry is mathematical description of chemistry which is generally used when a mathematical method is automated for implementation on a computer.[313] Computational chemistry includes quantum mechanics, molecular mechanics, simulations and other methods which use computers in understanding the nature of molecular systems. Molecular mechanics makes use of Newtonian force field where molecules are represented by ball and spring model. Analysis of very big systems like biomolecules (e. g. DNA) containing thousands of atoms can be effectively analyzed by this method. Quantum mechanics uses wavefunction obtained by solving the Schrödinger wave equation for representing a molecular system. All the properties associated with a system can be obtained from the wavefunction using appropriate operators with the aid of suitable approximations applied in the systems when the size of the system increases. Computational chemistry is very useful in the fields ranging from designing of drugs, dyes which are useful in solar industries, prediction of reactions and mechanisms, to design of functional materials.

Different computational methods are available which ranges from highly accurate to highly approximate ones. Highly accurate methods are feasible only for very small molecular systems whereas for larger systems approximate ones are only beneficial. It is clear that the computational cost can be improved only at the expense of the size of the system. Depending upon the formalism these methods are classified into (a) *ab initio* quantum chemical methods, (b) semi-empirical quantum chemical methods, (c) density functional methods, (d) molecular dynamics and Monte-Carlo simulations (e) hybrid quantum mechanics/molecular mechanics (QM/MM) methods, and (f) molecular mechanics. For systems having very big size like protein, DNA etc, *ab initio* studies are not used since it will take time eternity for solving such systems accurately.

### 1.2.1. *Ab initio* Methods

The literal meaning of the Latin word *ab initio* is 'from the beginning'. As the name suggests *ab initio* methods involves calculations that are derived directly using the theoretical principles, where the information from the experiments are not at all involved. Time-independent Schrödinger equation[314] for a system composed of *N* electrons and *M* nuclei has the form

$$H\Psi = E\Psi \qquad \text{Eq. 1.23}$$

Where *H* is the Hamiltonian operator, $\Psi$ is the N-body wavefunction and *E* is the energy eigen value of the system. A Hamiltonian operator is composed of kinetic and potential energy operators, corresponding to nucleus-nucleus, nucleus-electron and electron-electron interactions and the same for *N* electrons and *M* nucleus is written in the form as given below.

$$H = -\sum_{i=1}^{N}\frac{1}{2}\nabla_i^2 - \sum_{A=1}^{M}\frac{1}{2M_A}\nabla_A^2 - \sum_{i=1}^{N}\sum_{A=1}^{M}\frac{Z_A}{\boldsymbol{r}_{iA}} + \sum_{i=1}^{N}\sum_{j>i}^{N}\frac{1}{\boldsymbol{r}_{ij}} + \sum_{A=1}^{M}\sum_{B>1}^{M}\frac{Z_A Z_B}{\boldsymbol{R}_{AB}} \qquad \text{Eq. 1.24}$$

Position vector of nuclei and electrons are represented as $R_A$ and $\boldsymbol{r_i}$. The distance between $i^{th}$ electron and $A^{th}$ nucleus is $\boldsymbol{r}_{iA}$ , between $i^{th}$ and $j^{th}$ electrons is $\boldsymbol{r}_{ij}$ and between $A^{th}$ and $B^{th}$ nucleus is given as $\boldsymbol{R}_{AB}$. $M_A$ is the ratio of mass of the nucleus to the mass of the electron and $Z_A$ is the atomic number. The first two terms are the kinetic energies of *N* electrons with masses *m* and *M,* and nuclei with mass $M_A$, third term is the Coulombic attraction between electrons and nuclei, while the fourth and fifth terms are the electrostatic repulsion terms between electrons and nuclei respectively.

The simplest *ab initio* approach is Hartree-Fock (HF) method, in which total molecular wavefunction $\Psi$ is approximated as a Slater determinant composed of occupied spin orbitals. The exact solving of the Schrödinger wave equation is impossible, solving of which can be realized using approximations. The most common and primary approximation used is the Born-Oppenheimer approximation[315] based on the fact that the nuclear velocity is much smaller compared to velocity of electrons, since nuclear mass is very high compared to mass of electron. The molecular nucleus is therefore considered stationary and the separation of the nuclear and electronic

motions is done by applying the Born-Oppenheimer approximations. For a molecule having stationary nucleus the Hamiltonian can be written as

$$H_{elec} = -\sum_{i=1}^{N}\frac{1}{2}\nabla_i^2 - \sum_{i=1}^{N}\sum_{A=1}^{M}\frac{Z_A}{\boldsymbol{r}_{iA}} + \sum_{i=1}^{N}\sum_{j>i}^{N}\frac{1}{\boldsymbol{r}_{ij}} \qquad \text{Eq. 1.25}$$

Electron-electron interactions which are specified in the third term in the equation, is the most challenging to deal with. We have to consider a scheme in which the corresponding terms should be zero implying that the *N* electrons are moving completely independent of each other. In such an ideal situation the total wavefunction can be considered as a product of *N* one electron wavefunctions.

$$\Psi = \psi_1(\boldsymbol{r_1})\,\psi_2(\boldsymbol{r_2})\,\ldots.\psi_N(\boldsymbol{r_N}) \qquad \text{Eq. 1.26}$$

Once wavefunction is obtained the complete information about a system can be understood, by taking the expectation value of the concerned operator for the property we need to measure. An exact solution of the Schrödinger wave equation is possible only for the most primitive systems. For obtaining the correct solutions of many body Schrödinger equation, several approximations are necessary to be made. Four sources of errors in *ab initio* calculations are the Born-Oppenheimer approximation, the use of an incomplete basis set, incomplete correlation and the omission of relativistic effects.

To answer the electron-electron interaction issue in the Hamiltonian, Hartree approximation is employed. Under it each electron is considered as moving in a field that has been created by all other electrons. Thus the interactions between electrons are depending only on the position of electron under consideration. By applying this approximation, the electron-electron interaction term is approximated as sum of one-electron potentials $v_i$ where $\psi_i$ is orbital for the $i^{th}$ electron.

$$\sum_{i\neq j}^{N}\frac{1}{\boldsymbol{r}_{ij}} \approx \sum_{i=1}^{N}\vartheta_i(\boldsymbol{r}_i) = \sum_{i=1}^{N}\frac{\rho(\boldsymbol{r_j}) - |\psi_i(\boldsymbol{r}_j)|^2}{|\boldsymbol{r_i} - \boldsymbol{r_j}|}\,d\boldsymbol{r}_j \qquad \text{Eq. 1.27}$$

The eigen value equation including the electronic Hamiltonian is written as

$$\mathrm{H_{elec}}\phi_{\mathrm{elec}}(\{\mathbf{r_i}\};\{\mathbf{R}_\mathrm{A}\}) = \mathrm{E_{elec}}\phi_{\mathrm{elec}}(\{\mathbf{r_i}\};\{\mathbf{R}_\mathrm{A}\}) \qquad \text{Eq. 1.28}$$

where the position of electron and nuclei is represented by $\{\boldsymbol{r_i}\}$ and $\{\boldsymbol{R}_A\}$ respectively. By solving the above equation the electronic wavefunction is obtained which has

exclusive dependence on electronic co-ordinates and parametrical dependence on the nuclear co-ordinates. The expression for the electronic wavefunction is given as

$$\phi(\{\mathbf{r}_i\};\{\mathbf{R}_A\}) = \phi_{elec}(\{\mathbf{r}_i\};\{\mathbf{R}_A\})\phi_{nucl}(\{\mathbf{R}_A\}) \quad \text{Eq. 1.29}$$

By solving the electronic wavefunction equations using appropriate operators, all the properties of molecular systems can be found out. Since the exact solution of Schrödinger equation is feasible only for the most trivial systems like hydrogen atom and helium ion, the need of approximations arises for solving many body Schrödinger equation.

### 1.2.1.1. Hartree- Fock (HF) Method

Hartree-Fock theory is an approximate method for solving the Schrödinger wave equation stating that every electronic motion in a molecule can be described by a single particle function (orbital) which does not depend on the motion of other electrons in the system.[316-318] In HF approach the *N* electron wavefunction for a given state is written as a Slater determinant, an antisymmetrized product of spin orbitals.

$$\Psi(\boldsymbol{x}_1, \boldsymbol{x}_2, \dots, \boldsymbol{x}_N) = \frac{1}{\sqrt{N!}} \begin{vmatrix} \chi_i(\boldsymbol{x}_1)\, \chi_j(\boldsymbol{x}_1) \cdots \chi_N(\boldsymbol{x}_1) \\ \chi_i(\boldsymbol{x}_2)\, \chi_j(\boldsymbol{x}_2) \cdots \chi_N(\boldsymbol{x}_2) \\ \dots\dots\dots\dots\dots\dots\dots\dots\dots\dots \\ \chi_i(\boldsymbol{x}_N)\, \chi_j(\boldsymbol{x}_N) \cdots \chi_N(\boldsymbol{x}_N) \end{vmatrix} \quad \text{Eq. 1.30}$$

In the equation $1/\sqrt{N!}$ is a normalization constant, $\chi$ represents the spin orbitals and $\boldsymbol{x_1}$,$\boldsymbol{x_2}$ etc represents the combined spacial and spin coordinates of the respective electrons. The normalized Slater determinant in short notation, where the electrons 1,2…etc sequentially occupy the spin orbitals is given as below.

$$\Psi(\boldsymbol{x}_1, \boldsymbol{x}_2, \dots, \boldsymbol{x}_N) = |\chi_i \chi_j \dots . \chi_k\rangle \quad \text{Eq. 1.31}$$

In HF approximation the orthonormal spin orbitals that minimize the total energy is given by,

$$E[\Psi] = \frac{\langle \Psi | H | \Psi \rangle}{\langle \Psi | \Psi \rangle} \quad \text{Eq. 1.32}$$

In Hartree-Fock theory, the Hartree-Fock potential $V_{HF}(i)$ is defined as the average potential experienced by the $i^{th}$ electron due to the other electrons which is given as,

$$V_{HF}(i) = \sum_{i=1}^{N} \sum_{i,j=1}^{N} (J_{ij} - K_{ij}) \qquad \text{Eq. 1.33}$$

where,

$$J_{ij} = \iint \psi_i(x_1)\psi_i^*(x_1)\frac{1}{r_{12}}\psi_j^*(x_2)\psi_j(x_2)dx_1dx_2 \qquad \text{Eq. 1.34}$$

$$K_{ij} = \iint \psi_i(x_1)\psi_j^*(x_1)\frac{1}{r_{12}}\psi_i(x_2)\psi_j^*(x_2)dx_1dx_2 \qquad \text{Eq. 1.35}$$

$J_{ij}$ and $K_{ij}$ are called Coulomb and exchange integrals respectively.

The Fock operator, the one electron operator in HF theory has the form

$$F = -\frac{1}{2}\nabla_i^2 - \sum_{A=1}^{M}\frac{Z_A}{\boldsymbol{r}_{iA}} + V_{HF}(i) \qquad \text{Eq. 1.36}$$

Therefore,

$$F\psi_i(x) = \sum_{j=1}^{N} \varepsilon_{ij}\psi_j(x) \qquad \text{Eq. 1.37}$$

The equation for HF energy when subjected to orthogonalization condition gives HF differential equations.

In HF approximation electro-electron repulsion is treated as an average quantity and it replaces the complicated many body problem by one electron problem. The HF equations are solved by self-consistent field (SCF) method in which iterative solving is done by guessing a trial set of spin orbitals which are used to construct the Fock operator. A revised Fock operator is obtained from the spin orbitals from the solution and this cycle continues until the convergence criterion is satisfied.

Roothaan and Hall proposed the derivation of HF equations for closed shell systems,[319, 320] where HF equation is rewritten considering the spin orbitals as linear combinations of basis functions expressed as shown here.

$$\psi_i = \sum_{\mu=1}^{K} C_{\mu i}\phi_\mu \qquad i = 1, 2, \ldots\ldots, K \qquad \text{Eq. 1.38}$$

$\phi_\mu$, $C_{\mu i}$ and $K$ are basis functions corresponding to atomic orbitals, its coefficients and the total number of basis functions respectively. Roothaan Hall equation is written in the form of a single matrix equation given as,

$$\mathbf{FC=SC\varepsilon} \qquad \text{Eq. 1.39}$$

where F, S and ε are Fock matrix, overlap matrix and orbital energies respectively. For the determination of eigen values for Roothaan Hall equation the diagonalisation of Fock matrix is to be done for finding out the unknown MO coefficients.

HF equations can be solved correctly, yet the method itself turns to be theoretically incomplete. Examples for the limitations are prediction of qualitatively incorrect results in the ordering of the ionization potentials of $N_2$, inability to describe the dissociation of molecules into open-shell fragments by restricted HF method and inaccurate potential energy curves when unrestricted HF method is used for the same.[321] Even though within HF theory the electronic exchange is correctly treated, the electronic correlation is missing. Therefore for the inclusion of correlation energy in calculations needs to go beyond the HF theory. Self consistent derivation is needed for the solution of the Hartree approximation, however not antisymmetric with respect to electron exchange, thereby doesn't obey Pauli's exclusion principle. Total wavefunction is still expressed in terms of Hartree product. For the inclusion of the Pauli's exclusion principle going beyond Hartree method is needed.

### 1.2.1.2. Post Hartree-Fock Methods

HF methods have many problems, one of the prominent among them is the complete neglect of the correlation between electrons of same spin.[321] To improve HF approximation correlation energy ($E_{corr}$) which is the difference between the exact nonrelativistic energy ($E_{exact}$) of the system and the Hartree-Fock energy ($E_{HF}$) obtained in the limit that the basis set approaches completeness. $E_{HF}$ being always greater than $E_{exact}$ , the correlation energy will be always negative.

$$E_{corr} = E_{exact} - E_{HF} \qquad \text{Eq. 1.40}$$

The instances where correlation effects are taken into account in the calculations are Møller-Plesset (MP) perturbation theory[322], configuration interaction (CI)[323] and coupled cluster (CC)[324]. In perturbation theory the difference between the exact Hamiltonian and sum of one electron operators is introduced as a perturbation to the unperturbed HF solution, so that electron repulsion term is involved in calculations. Second order perturbation corrections when included leads to the MP2 method.[325, 326]

Third and fourth order Møller-Plesset calculations (MP3 and MP4) are also available. The size-independent nature of MP theory is one of the main advantages of the method, whereas drawbacks includes the non-variational nature which results in the yielding of lower energy than the true value, and the computational expensiveness. The basis of CI method is that instead of single Slater determinant used for the approximation of wavefunction, a linear combination of Slater determinants is used for writing the wavefunction.[299, 327] For describing the electronic state, within the HF determinant one or more occupied orbitals are replaced with a virtual orbital creating an excited state. The classification of CI calculations are done by the number of excitations used for the construction of each determinant, and are classified as Configuration interaction single-excitation (CIS), Configuration interaction single and double excitation (CISD), Configuration interaction triple excitation (CISDT) and Configuration interaction quadruple excitation (CISDTQ). The latter two are done only when high accuracy results are needed. Like CI, in CC method also multi-determinant wavefunction is used instead of single determinant wavefunction. In CC method, taking the basic HF molecular orbital method, multi-electron wavefunctions are constructed using the exponential cluster operator accounting for the electron correlation. Coupled cluster with only double excitation operator is termed CCD, when single excitations are also added its termed CC singles-doubles (CCSD) model, CCSDT implies when connected triple excitations are also included in the later case and if the singles/triplets coupling term is included it is termed CCSD(T). CC calculations are not variational, but its size extensive and also it is computationally very expensive than HF methods.

### 1.2.2. Semi-empirical Methods

For larger molecular systems the use of *ab initio* methods are computationally very expensive. Semi-empirical methods which are based on Schrödinger wave equations are used in such calculations. This method uses approximations extensively and considers only the outermost electrons during calculations while neglecting the core ones.[328, 329] Approximations are employed extensively in the construction of Fock matrix and complicated integrals in the Hartree-Fock calculations are omitted. The limitations due to all these factors are tried to solve by parametrizing using

experimental data or *ab initio* calculations. Neglect of Diatomic Differential Overlap (NDDO) method uses unit matrix instead of overlap matrix *S.* This method is used in most popular semi-empirical methods like MNDO, AM1 and PM3. RM1 and PM6 are extensions of AM1 and PM3 which are more accurate than other semi-empirical ones. These methods are useful as a tool for scanning a problem before going for the higher level more accurate treatments, which will help to lessen the computational cost even though in less quantity. Semi-empirical methods are faster than *ab initio* methods, but they are less accurate and the errors are difficult to rectify because of its less systematic nature.

### 1.2.3. Density Functional Theory (DFT)

Density functional theory approximates the energy of molecular systems based on electron density $\rho(\boldsymbol{r})$. The foundation stones of density functional theory were laid as early as 1920s where major contributions are from Thomas and Fermi.[330-332] Full fledged applications of DFT was realized in 1960s only with the work of Hohenberg, Kohn and Sham.[333, 334] Electron density which is also known as the probability density function is the probability of finding an electron at a position '$\boldsymbol{r}$' with co-ordinates *(x,y,z)* per unit volume, *dxdydz.* It is defined as the integral over the spin co-ordinates of all electrons and over all but one of the special variables $(\vec{x} \equiv \vec{r}, s)$.

$$\rho(\boldsymbol{r}) = N \int d^3\boldsymbol{r_2} \int d^3\boldsymbol{r_3} \dots \int d^3\boldsymbol{r_N}\, \psi^*(\boldsymbol{r}_1, \boldsymbol{r}_2, \dots, \boldsymbol{r}_N)\psi(\boldsymbol{r}_1, \boldsymbol{r}_2, \dots, \boldsymbol{r}_N) \qquad \text{Eq. 1.41}$$

Here $\boldsymbol{r}_i$ represents position co-ordinates, $\rho(\boldsymbol{r})$ determines the probability of finding any of the *N* electrons within the volume element $d\boldsymbol{r}$ or the total number of electrons *N* is obtained by integrating electron density over all space. i.e.,

$$N = \int \rho(\boldsymbol{r}) d\boldsymbol{r} \qquad \text{Eq. 1.42}$$

Electron density is three dimensional irrespective of the number of electrons present, whereas wavefunction for an N-electron system is a function of 3N spacial co-ordinates. Therefore DFT can be applied to much larger systems with hundreds and thousands of atoms. Electron probability density $\rho$ is a function $\rho(\boldsymbol{r})$ of a point in space located by radius vector $\boldsymbol{r}$ measured from an origin and the energy E is a function of its

electron density,. $E = f(\rho)$. Thereby energy $E$ is a functional of $\boldsymbol{r}$, $E = [\rho(\boldsymbol{r})]$. Electronic energy is a functional of electron density and one-to-one correspondence exists between them.

### 1.2.3.1. Thomas Fermi Density Model

In 1920s the work of Thomas and Fermi paved the foundations of the density functional theory, which introduced the idea of expressing the energy of the system as a function of electron density. This method forms the conceptual basis for the density functional theory. In Thomas-Fermi model[330-332] the kinetic energy is derived from quantum statistical theory based on uniform electron gas model and the nucleus-electron and electron-electron interactions are treated classically.

Kinetic energy ($T_{TF}$) of an electron gas is expressed as,

$$T_{TF}[\rho(\boldsymbol{r})] = \frac{3}{10}(3\pi^2)^{2/3}\int \rho^{5/3}(\boldsymbol{r})\, d\boldsymbol{r} \qquad \text{Eq. 1.43}$$

The equation implies to the approximation that the kinetic energy of electrons depends on the electron density only. To this adding the nucleus-electron and electron-electron interaction energy we can obtain the total energy in terms of electron density as,

$$E[\rho(\boldsymbol{r})] = \frac{3}{10}(3\pi^2)^{2/3}\int \rho^{5/3}(\boldsymbol{r})d\boldsymbol{r} + Z\int \frac{1}{2}\rho(\boldsymbol{r})d\boldsymbol{r} + \frac{\mathbf{1}}{\mathbf{2}}\int \frac{\rho(\boldsymbol{r}_1)\rho(\boldsymbol{r}_2)}{|\boldsymbol{r}_1 - \boldsymbol{r}_2|}d\boldsymbol{r}_1 d\boldsymbol{r}_2 \qquad \text{Eq. 1.44}$$

The second term in the equation is the nucleus-electron interaction whereas the third term is the electron-electron interaction. Even though chemically unusable because of inaccuracy, Thomas-Fermi model is the first time in history where it has been shown that energy can be expressed solely using electron density.

### 1.2.3.2. Hohenberg-Kohn Existence Theorem

The theory is originated with Hohenberg and Kohn theorem which stated that the ground state electronic energy of a molecule can be determined from the electron density instead of wavefunction. Electron density is expressed as a linear combination of basis functions which are mathematically similar to HF orbitals used for construction of determinants which acts as Kohn-Sham orbitals. From this determinant of orbitals the electron density calculated is used in computation of energy. In DFT integrals for

coulomb repulsion need to be done only over electron density a three dimensional function.

Thomas and Fermi theorem were further enforced by Hohenberg and Kohn in the year 1964 by formulating and proving a theorem which has strong mathematical foundation.[335] It stated (i) there is one to one correspondence between the external potential and the electron density; (ii) the ground state energy can be obtained variationally. This implies that the density that minimizes the exact energy is the ground state energy of the system. That means ground state energy is directly related to ground state electron density. Energy functional can be expressed as sum of terms arising from electron interaction with the external potential field and the term that represents the sum of kinetic energy of electrons and interelectronic interaction contributions.

$$E[\rho(\boldsymbol{r})] = \int V_{ext}(\boldsymbol{r})\rho(\boldsymbol{r})d\boldsymbol{r} + F[\rho(\boldsymbol{r})] \qquad \text{Eq. 1.45}$$

The equivalent Schrodinger equation in DFT can be written as,

$$\left[\frac{\delta E[\rho(\boldsymbol{r})]}{\delta\rho(\boldsymbol{r})}\right]_{V_{ext}} = \mu \qquad \text{Eq. 1.46}$$

In the equation $\mu$ is a Lagrangian multiplier with specific chemical potential for the electron for its nuclei. For a set of interacting electrons a practical way to solve the Hohenberg-Kohn theorem is suggested by Kohn and Sham.[334] Kohn and Sham wrote the electron density of the system as the sum of the square moduli of a set of one-electron orbitals.

$$\rho(\boldsymbol{r}) = \sum_{i=1}^{N} |\psi_i(\boldsymbol{r})|^2 \qquad \text{Eq. 1.47}$$

$F[\rho(\boldsymbol{r})]$ is expressed as a sum of three terms, viz. kinetic energy $E_{KE}[\rho(\boldsymbol{r})]$, the electron-electron Coloumbic interaction $E_H[\rho(\boldsymbol{r})]$ and exchange and correlation contributions $E_{XC}[\rho(\boldsymbol{r})]$.

$$F[\rho(\boldsymbol{r})] = E_{KE}[\rho(\boldsymbol{r})] + E_H[\rho(\boldsymbol{r})] + E_{XC}[\rho(\boldsymbol{r})] \qquad \text{Eq. 1.48}$$

These terms can be expressed mathematically as follows, the kinetic energy of a system of non-interacting electrons,

$$E_{KE}[\rho(\boldsymbol{r})] = \sum_{i=1}^{N} \int \psi_i(\boldsymbol{r}) \left(-\frac{\nabla^2}{2}\right) \psi_i(\boldsymbol{r}) d\boldsymbol{r} \qquad \text{Eq. 1.49}$$

Hartree electrostatic energy between electrons,

$$E_H[\rho(\boldsymbol{r})] = \frac{1}{2} \iint \frac{\rho(\boldsymbol{r}_1)\rho(\boldsymbol{r}_2)}{|\boldsymbol{r}_1 - \boldsymbol{r}_2|} d\boldsymbol{r}_1 d\boldsymbol{r}_2 \qquad \text{Eq. 1.50}$$

Therefore within Kohn-Sham scheme, the full expression for energy of an N-electron system can be written as,

$$E[\rho(\boldsymbol{r})] = \sum_{i=1}^{N} \int \psi_i(\boldsymbol{r}) \left(-\frac{\nabla^2}{2}\right) \psi_i(\boldsymbol{r}) d\boldsymbol{r} + \frac{1}{2} \iint \frac{\rho(\boldsymbol{r}_1)\rho(\boldsymbol{r}_2)}{|\boldsymbol{r}_1 - \boldsymbol{r}_2|} d\boldsymbol{r}_1 d\boldsymbol{r}_2 + E_{XC}[\rho(\boldsymbol{r})] - \sum_{\alpha} \frac{Z_\alpha}{|\boldsymbol{r} - R_\alpha|} \rho(\boldsymbol{r}) d\boldsymbol{r} \qquad \text{Eq. 1.51}$$

$E_{XC}[\rho(\boldsymbol{r})]$ is the error made in the use of the non-interacting kinetic energy and the same in treatment of the electron-electron interaction. Applying suitable variational condition and introduction of the term for electron density, we get the one electron Kohn-Sham equation where $\varepsilon_i$ is the orbital energies.

$$\left\{-\frac{\nabla^2}{2} - \left(\sum_{\alpha=1}^{M} \frac{Z_\alpha}{\boldsymbol{r}_{1\alpha}}\right) + \frac{\rho(\boldsymbol{r}_2)}{\boldsymbol{r}_{12}} d\boldsymbol{r}_2 + V_{XC}[(\boldsymbol{r}_1)]\right\} \psi_i(\boldsymbol{r}_i) = \varepsilon_i \psi_i(\boldsymbol{r}_i) \qquad \text{Eq. 1.51}$$

In the equation, $V_{XC}$ is called the exchange-correlation potential which is exchange correlation energy per electron density.

$$V_{XC}[\boldsymbol{r}] = \frac{\delta E_{XC}[\rho(\boldsymbol{r})]}{\delta \rho(\boldsymbol{r})} \qquad \text{Eq. 1.53}$$

### 1.2.3.3. Exchange-correlation Functionals

The exchange correlation energy is divided into two terms; an exchange term $E_x$ corresponding to the electron interactions of same spin electrons and a correlation $E_c$ corresponding to the electron interaction of opposite spin.

$$E_{XC}[\rho(\boldsymbol{r})] = E_X[\rho(\boldsymbol{r})] + E_C[\rho(\boldsymbol{r})] \qquad \text{Eq. 1.54}$$

Xu and Goddard in 2004 made a statement in which the inability of Kohn-Sham DFT for the generation of the exact form of exchange-correlation functional, $V_{xc}$.[336] For practical purposes, the modification of the electron-correlation potential have been

done by several methods viz. (i) local density approximation (LDA) (ii) generalized gradient approximation (GGA) (iii) meta-GGA (iv) hybrid functional.

The simplest approach for the modification of correlation correction functional is the local density approximation.[332, 337, 338] In this method, the exchange-correlation energy at any point in space is a function of electron density at that point and is given by the electron density of a homogenous gas of the same density. The exchange functional is given as

$$E_X^{LDA}[\rho(\boldsymbol{r}) = -\frac{3}{4}\left(\frac{3}{\pi}\right)^{1/3}\int \rho^{4/3}(\boldsymbol{r})d\boldsymbol{r} \qquad \text{Eq. 1.55}$$

LDA is expected to work for systems with slowly varying electron densities, but failed in the cases of even semiconductors and insulators due to the large cancellations in the exchange part. Example for LDA functional is S-VWN. A more generalized application of LDA proposed by Slater *et al.* is called the local spin density approximation (LSDA).[339] In this spin densities are included in the functional so that the many conceptual problems in LDA is solved. The exchange functional in LSDA is given by,

$$E_X^{LDA}[\rho(\boldsymbol{r})] = 2^{1/3}\left(-\frac{3}{4}\left(\frac{3}{\pi}\right)^{1/3}\right)\int\left(\rho_\alpha^{4/3}(\boldsymbol{r}) + \rho_\beta^{4/3}(\boldsymbol{r})\right)d\boldsymbol{r} \qquad \text{Eq. 1.56}$$

$\alpha$ and $\beta$ represents the spin up and spin down respectively.

Separately obtaining the correlation energy $E_c$ from exchange energy is difficult in the LDA. By incorporating the Monte Carlo results Vosco et al have developed different formulations of this functional, termed as Vosco-Wilk-Nusair or VWN functionals.[340]

The generalized gradient approximation methods (GGAs) make the assumption that the exchange correlation energies depends on the gradient of the density, $\nabla\rho(\boldsymbol{r})$ in addition to the electron density. In the molecules the electron density varies rapidly over a small region of space, this leads to the formulation of GGA. The exchange correlation corresponding is given as,

$$E_{XC}[\rho_\alpha(\boldsymbol{r}), \rho_\beta(\boldsymbol{r})] \equiv \int \varepsilon_{XC}(\rho_\alpha(\boldsymbol{r}), \rho_\beta(\boldsymbol{r}), \nabla\rho_\alpha(\boldsymbol{r})\rho_\beta(\boldsymbol{r}))d^3\boldsymbol{r} \qquad \text{Eq. 1.57}$$

The exchange part of $E_{XC}$ was proposed by Perdew and Wang (PW86)[341] and correction part was proposed by Becke in 1988 (B88).[342] The gradient correction to the

correlation part was proposed by Perdew (P86)[343], Perdew and Wang in 1991 (PW91)[344], by Lee, Yong and Parr (LYP)[345] and in 1996 by Perdew, Burke and Ernzerhof (PBE)[346].

Meta-GGA functionals which depends on density, its gradient and higher order density gradients have significant improvement over GGA methods. They involve the derivatives of the occupied Kohn-Sham orbitals. Example for meta-CGA is M06-L method, a Minnesota functional.

A hybrid density functional (H-GGA) method which was introduced in 1993, combines the exchange correlation of a GGA method with a percentage of HF exchange.[347] The exact HF exchange amount is semiemperically fitted from experimental aromatization energies, ionization potentials, proton affinities, total atomic energies and other data. Example for hybrid GGA is B3LYP and for hybrid meta-GGA are M05-2X and M06-2X. Formulation of hybrid DFT was a turning point in the history of computational chemistry, which made the DFT an accepted everyday tool globally.

### 1.2.3.3.1. Minnesota Functionals

A suite of approximate exchange-correlation functionals termed as Minnesota functional was presented and parameterized by Zhao and Truhlar.[348-355] The first family of functionals is termed M05 family, which is composed of M05, global hybrid functional with 28% HF exchange and M05-2X, a global hybrid functional with 56 % HF exchange. These were constructed using the strategies of constrain satisfaction, empirical fits and mixing Hartree-Fock and approximate DFT exchange.[356, 357] The second family of functional is termed M06 family which is more improved than the M05 family consisting of M06-L[352], revM06-L[358], M06[354], M06-2X[354] and M06-HF[353]. M06-L is the local functional with 0% HF exchange and is constructed using the strategies of constraint satisfaction, modeling the exchange-correlation hole and empirical fits. A modified version for smooth potential curves and accuracy called revM06-L is constructed recently. M06 is a global hybrid functional with 27% HF exchange, useful for thermo chemistry, non-covalent interactions and organometalics. Global hybrid functional with 54% HF exchange is termed M06-2X which can be useful in the kinetics

calculations also other than those described for earlier cases. Global hybrid functional with 100% HF exchange is termed M06-HF and is useful in charge-transfer TD-DFT and other processes. M08, M011, M012 and M015 families of electron correlation methods are also in use, which has different groups under each of them based on the percentage of HF exchange. M08 family is improvement of M06-2X functional, whereas M011 family introduces range-separation in functionals, M012 family uses a non-separable functional form and M015 family is also based on non-separable form of functionals without the range separation.[349, 355, 359-363]

### 1.2.3.4. Time-Dependent Density Functional Theory (TD-DFT)

Ground-state DFT is concerned with systems when the all external potential are stationary, which can be described by time-independent Schrödinger wave equation. During the situations like an atom or a molecule is under the influence of external electromagnetic field, electron or proton scattering and the excited state of molecules etc, this ground state DFT fails. For the treatment of electronically excited states (EESs), DFT should be modified to account for the time-dependent (TD) nature of electromagnetic waves, since EESs are generated as a result of light-matter interactions.[300] This leads to the exact solution of Schrodinger wave equation named Time-dependent density functional theory (TD-DFT).[279] Thereby, TDDFT is a tool which is used for the computation of electronically excited state signatures, like optical spectra of molecules, non-linear optics, photochemistry etc. Prediction and rationalization of absorption spectra of several systems have been done using TD-DFT.[301-305] The nature of the geometry of the excited states and the simulation of fluorescence spectrum of the concerned geometry have been extensively studied by TD-DFT.[306, 307]

Earlier excited states were treated by methods like ΔSCF approach. In 1999 it has been reviewed that excited states can be treated within the DFT framework.[280, 364] The basic ideas of ground state density functional theory (DFT) are extended to time-dependent DFT for treatment of excitations and other general time dependent phenomena. DFT relies on wave functions and many body Schrödinger equation, whereas TD-DFT depends on one body electron density, $n(\mathbf{r},t)$.

A system of $N$ electrons with coordinates $\boldsymbol{r} = (\boldsymbol{r}_1 \ldots \boldsymbol{r}_N)$ obeys the time-dependent Schrodinger equation which is given below,

$$i\frac{\partial}{\partial t}\psi(\boldsymbol{r},t) = \widehat{H}(\boldsymbol{r},t)\psi(\boldsymbol{r},t) \qquad \text{Eq. 1.58}$$

The wavefunction at a time $t$ is a functional of the wavefunction at time $t_0$, $\psi[\psi_0](t)$. The absolute square of the electronic wavefunction, $|\psi(\boldsymbol{r},t)|^2$ is interpreted as the probability of finding the electrons at position $\boldsymbol{r}$. $N$-electron TD-Schrodinger equation is solved typically using approximations like Frenkel-Dirac stationary action principle[365-367] when the action,

$$A[\psi;\psi_0](t,t_0) = \int_{t_0}^{t} \left( \langle \psi[\psi_0](t') \left| i\frac{\partial}{\partial t'} \right| \psi[\psi_0](t') \rangle - E[\psi_0](t') \right) dt' \qquad \text{Eq. 1.59}$$

is made stationary with respect to variations of $\psi[\psi_0]t'$ on the interval $t'$ and subjected to the constraints

$$\delta\psi[\psi_0](t_0) = \delta\psi[\psi_0](t) = 0 \qquad \text{Eq. 1.60}$$

Therefore here

$$E[\psi_0](t) = \langle \psi[\psi_0](t)|\widehat{H}|\psi[\psi_0](t)\rangle \qquad \text{Eq. 1.61}$$

is instantaneous energy which contains system dynamics from previous times. The approximate equation of motion is developed from any approximate instantaneous energy expression. Setting $\delta\psi[\psi_0](t)$ as zero is not accurate, since the boundary condition $\psi_0$ also determines $\delta\psi[\psi_0](t)$. Taking this into account Frenkel-Dirac-Vignale stationary action principle[368] becomes

$$\delta A[\psi[\psi_0](t,t_0) = i\langle \psi[\psi_0](t)|\delta\psi[\psi_0](t)\rangle \qquad \text{Eq. 1.62}$$

And the only constraint that the above equation is subjected to is $\delta\psi[\psi_0](t_0) = 0$ implying the equation to be satisfied over the time interval ($t_0$,t). Also $i\langle \psi[\psi_0](t)|\delta\psi[\psi_0](t)\rangle$ is set to zero in the Frenkel-Dirac formulation. Replacing the instantaneous energy in Frenkel-Dirac equation with the Kohn-Sham energy and the wavefunction with Kohn-Sham determinant, Frenkel-Dirac stationary condition leads to the TD Kohn-Sham equation which was used in calculation of photo-absorption cross sections of rare gas atoms[369] without the formal justification.

$$\left[-\frac{1}{2}\nabla^2 + \vartheta_{ext}(t) + \vartheta_H[\rho(t)] + \vartheta_{XC}\left[\rho_\alpha(t), \rho_\beta(t)\right]\right]\psi_i(t) = i\frac{\partial\psi_i(t)}{\partial t} \quad \text{Eq. 1.63}$$

The Hamiltonian can be written in the form

$$\widehat{H} = \hat{T}(\boldsymbol{r}) + \widehat{W}(\boldsymbol{r}) + \hat{V}_{ext}(\boldsymbol{r}, t) \quad \text{Eq. 1.64}$$

In the equation, the first term represents the kinetic energy of electrons, while $\widehat{W}$ represents the Coulomb repulsion between the electrons and $\hat{V}_{ext}(\boldsymbol{r}, t)$ is time-dependent external potential.

$$\hat{T}(\boldsymbol{r}) = -\frac{1}{2}\sum_{i=1}^{N}\nabla_i^2 \quad \text{Eq. 1.65}$$

$$\widehat{W}(\boldsymbol{r}) = -\frac{1}{2}\sum_{\substack{i.j=1 \\ I\neq j}}^{N}\frac{1}{|\boldsymbol{r}_i - \boldsymbol{r}_j|} \quad \text{Eq. 1.66}$$

The theoretical foundations of TD-DFT is laid by the pioneering work of Runge and Goss[279] in which the time-dependent analogue of HK theorem[335] is proved and developed a KS scheme[334] for time dependent instances. Runge and Gross incorporated the description of time-dependent phenomena into the DFT formulism by generalizing the Hohenberg-Kohn theorem into time dependent densities and potential. According to Runge-Gross theorem, there is one to one correspondence between the time-dependent external potential, $\vartheta_{ext}(\boldsymbol{r}t)$ and the time-dependent electron density, $\rho(\boldsymbol{r}t)$ for a fixed initial state. This can be treated as generalized Hohenberg-Kohn theorem. The density of the interacting system can be written as follows

$$\rho(\boldsymbol{r}, t) = \sum_{i}^{occ}|\phi_i(\boldsymbol{r}, t)|^2 \quad \text{Eq. 1.67}$$

The orbitals $\phi_i(\boldsymbol{r}, t)$ can be used to satisfy the time-dependent Kohn-Sham equations,

$$i\frac{\partial\phi_i(\boldsymbol{r}, t)}{\partial t} = \left(-\frac{\nabla^2}{2} + \vartheta_S[\rho](\boldsymbol{r}, t)\right)\phi_i(\boldsymbol{r}, t) \quad \text{Eq. 1.68}$$

The exchange correlation potential can be defined by,

$$\vartheta_S[\rho](\boldsymbol{r}, t) = \vartheta_{ext}(\boldsymbol{r}, t) + \int d\boldsymbol{r}'\frac{\rho(\boldsymbol{r}', t)}{|\boldsymbol{r} - \boldsymbol{r}'|} + \vartheta_{XC}(\boldsymbol{r}, t) \quad \text{Eq. 1.69}$$

Runge-Gross theorem is the time-dependent extension of the ordinary Hohenberg-Kohn theorem. In static quantum mechanics, the ground state of the system

can be determined through the minimization of the total energy functional, i.e., there exists a one-to-one correspondence between the time dependent external potential and the time-dependent electron density. This implies that the wavefunction is determined up to an arbitrary phase factor,

$$\psi(t) = e^{-i\varphi(t)}\psi[\rho,\psi] \qquad \text{Eq. 1.70}$$

Runge-Gross formulation of TD-DFT is limited to the applied electric field only. Magnetic field effects being significantly feeble in case of molecular property studies, this appears satisfactory in such cases. By introduction of a current density dependence and exchange correlation vector potential, TD magnetic fields can also be included in TD-DFT.

$$E[\phi] = \langle\phi|\widehat{H}|\phi\rangle \qquad \text{Eq. 1.71}$$

In time-dependent systems, there is no variational principle on the basis of the total energy since it's not a conserved energy, but on the quantity analogous to energy, the quantum mechanical action.

$$A[\phi] = \int_{t_0}^{t_1} dt\, \langle\phi(t)\left|i\frac{\partial}{\partial t} - \widehat{H}(t)\right|\phi(t)\rangle \qquad \text{Eq. 1.72}$$

Electronic absorption spectra using the LR theory is calculated using TD-DFT which is one of the major applications of the method. Calculation of induced dipole moment, $\mu_{ind}(t)$ which is the difference between the TD and permanent dipole moments of the system, after propagating the Kohn-Sham orbitals in presence of a small dynamic perturbation $\vartheta_{appl}(\boldsymbol{r},t) = \varepsilon(t)$ is involved in the calculation of absorption spectra. The dynamic polarizability α is defined by the linear term given below.

$$\mu_{ind}(t) = \int \alpha\left(t-t'\right)\varepsilon\left(t'\right)d\,t' \qquad \text{Eq. 1.73}$$

Applying Fourier transform, we can get it as α(ω)=μ(ω)/Ɛ(ω), also having sum-over-states form, we can write as

$$\alpha(\omega) = \sum_{I=0} \frac{f_I}{\omega_I^2 - \omega^2} \qquad \text{Eq. 1.74}$$

where $\omega_I$ and $f_I$ are vertical excitation energies and the corresponding oscillator strength respectively. The Laurentian broadened stick spectrum is obtained as

$$S(\omega) = \frac{2\omega}{\pi}\zeta m\alpha(\omega + i\eta) \quad \text{Eq. 1.75}$$

The modelling of absorption spectra itself is an indication of use of TD-DFT for the excited state phenomena like fluorescence, intersystem crossing, phosphorescence etc. TD-DFT providing only the excitation energy makes it necessary to calculate the excited state PESs by addition of excited state energy obtained from TD-DFT to the ground state energy obtained by static ground state DFT.

$$E_I^{TD-DFT} \equiv E_0^{DFT} + \omega_I^{TD-DFT} \quad \text{Eq. 1.76}$$

where $\omega_I$ is the excitation energy. The TD-DFT fluorescence energy is a TD-DFT singlet excitation energy which is calculated at the optimized geometry of the singlet excited state. The Stokes shift corresponding to this phenomenon is the difference between the absorption and fluorescence energies.

$$\omega_{STOKES} = \omega_{ABS} - \omega_{FLUO} \quad \text{Eq. 1.77}$$

The vertical absorption and fluorescence energies can be written as a function of energy and the geometry of the system at electronically excited state (EES) and ground state (GS), which is shown in the equations 1.74 and 1.75.

$$E^{vert-abso} = E^{EES}R^{GS} - E^{GS}R^{GS} \quad \text{Eq. 1.78}$$

$$E^{vert-fluo} = E^{EES}R^{EES} - E^{GS}R^{EES} \quad \text{Eq. 1.79}$$

Comparison of TD-DFT results with accurate spectroscopic information shows that the excited state structures , dipole moments, vibrational frequencies for small systems have equivalent accuracy as that of ground state DFT methods.[306] this stands as a validation of TD-DFT as a tool for understanding the excited state properties. These findings are confirmed by studies on other systems and correlated *ab initio* results.[370-372] KS reference has enhanced stability compared to HF reference which is an advantage that makes TD-DFT reasonable method. TD-DFT is very effective and widely used in the analysis of condensed PAHs.[373-377]

## 1.2.4. Hybrid Quantum Mechanics/Molecular Mechanics (QM/MM) Methods

Quantum mechanical methods (QM) can compute the ground state and excited state properties of molecular systems pretty accurately and can model chemical

reactions; but for larger systems it's computationally expensive. Molecular mechanics (MM) is able to model very large models quickly but compromising on the accuracy level. The hybrid QM/MM method includes the strength of both quantum mechanics and molecular mechanics, which are accuracy and speed respectively. The method is generally applied to properties like molecular energies and structures, energy and structure of transition states, atomic charges and reaction pathways etc.[378] In this method a system is treated separately where the active site will be treated by accurate QM method, whereas the rest of the molecule will be treated with the help of molecular mechanics or other computationally inexpensive techniques.[379-381] The most used method is ONIOM (Our N-layered Integrated molecular Orbital + molecular Mechanics) method developed by Morokuma and co-workers, which applies different levels of theory to different parts of a system yielding reliable results.[382-384]

### 1.2.5. Molecular Dynamics (MD) and Monte-Carlo (MC) Simulations

Molecular properties are very sensitive to the temperature and the environment, the effects of which can be incorporated by statistical mechanics means. Two major techniques used for the generation of an ensemble are molecular dynamics (MD) and Monte-Carlo (MC) simulation. Time dependent behavior such as vibrational or Brownian motion of molecular systems are simulated using molecular dynamics.[385, 386] The Newtonian classical laws of motion are used for calculating the energy of the system. Thermodynamic quantities, diffusion constants, correlations functions etc can be calculated using MD simulations. This method generates a series of time-correlated points in the phase space or a trajectory by the propagation of a starting set of coordinates and velocities according to the Newton's second law by a series of finite steps. There are three types of MD technique viz. classical MD, ab-initio MD (AIMD) and Born-Oppenheimer MD (BOMD).

In classical MD the force on atoms are derived from classical potential such as Leonard-Jones, Buckingham etc, which do not describe electronic motion making the method computationally cheap. In MD the state of a system at any future time is predicted from its current state.[387] The local atomic properties like chemical bonding are difficult to account for in classical MD and dynamics of large molecular systems

nuclear motion is computationally expensive. *Ab initio* MD succeeds in this areas where classical MD fails. In this method of ab-initio MD the atomic motion is simulated using quantum mechanically calculated forces, whereas the heavier nucleus movement is considered classical using Newton's equation of motion.[388, 389] Car and Parrinello in 1985 demonstrated the field of AIMD as a combination of MD technique with DFT and termed it as CPMD.[390] A set of techniques which are based on the minimization of the electronic orbitals to the ground state at every step are termed Born-Oppenheimer molecular dynamics (BOMD). In this method time-independent Schrodinger wave equation is solved when the nuclei is propagating through classical molecular dynamics.

Techniques in which solutions are made by approximating through statistical sampling are termed Monte Carlo simulations.[391] The sampling is possible by applying the probability theory on the mathematical expression. Main positive about MC simulation is the ability of easy parallelization, enabling for ideal method that can be used in large CPU clusters. These are free from the restrictions of Newton's equations of motion solutions therefore no dynamical information can be obtained from the traditional Monte Carlo simulations. Another drawback is the difficulty in simulation of protein where large scale movements are happening in an explicit solvent.

### 1.2.6. Molecular Mechanics

When the size of the molecule is very big, ab-initio and semi-empirical methods cannot be used for modeling such systems. In such situations, another way for modeling is used which completely avoids quantum mechanics, but uses molecular mechanics also called force field method. It uses classical Newtonian methods in description of structure as well as properties of molecules.[392, 393] Bio-molecules like protein, DNA, RNA etc are examples for such systems which are modeled using molecular mechanics. This method is generally most useful as the primary tool of computational biochemists. The wave function or the electron density use is nil in such calculations.

Predictions of transition states and equilibrium geometries as well as the relative energy between two conformers or molecules is done considerably well by this method. In molecular mechanics, the energy is represented as a simple equation of the energy of the compound. Such set of equations and associated constants are termed a force field.

The main assumption that we make in MM method is that the energy change associated with a particular molecular motion will be same in all molecules, for example the stretching energy of C-C bond will be of equal magnitude in all the systems in the universe, this is termed as transferability of parameters. Also the molecules are considered as the collection of atoms which are connected via elastic forces. The potential energy associated with structural features of molecules like bond lengths, bond angles, etc are the sources of these forces.

$$E^{tot} = E^{str} + E^{ang} + E^{tor} + E^{nb} + E^{col} \quad \text{Eq. 1.80}$$

$E^{str}$ represents the energy associated with stretching of bonds, $E^{ang}$ is energy associated with the angular distortion that is associated with the distortion of bond angles from the equilibrium position, $E^{tor}$ is associated energy change with respect to the change in torsional angle, $E^{nb}$ is energy associated with non-bonded interaction while $E^{col}$ represents the Coulombic force arising energy. The functional form of the force field can be given as equation,

$$E^{total} = \sum_{bonds} K_r\left(r - r_{eq}\right)^2 + \sum_{angles} K_\theta\left(\theta - \theta_{eq}\right)^2 + \sum_{dihedrals} \frac{V_n}{2}[1 + \cos(n\phi - \gamma)] + \sum_{i<j}\left[\frac{A_{ij}}{r_{ij}^{12}} - \frac{B_{ij}}{r_{ij}^{6}} + \frac{q_i q_j}{\varepsilon r_{ij}}\right] \quad \text{Eq. 1.81}$$

In the equation $K_r$ is the force constant for the bond when it's stretched, and r, and $r_{eq}$ represents bond lengths when stretched and at relaxed state respectively. For the second term that represents angular energy, the force constant due to angular distortion and the distorted angle as well as equilibrium angle is given. For the third term $V_i$ is Fourier coefficients and $\gamma$ is the torsional angle. Non bonded interactions are approximated using Leonard-Jones potential, where $r_{ij}$ is distances between centers of non-bonded atoms, which is used in calculating the Coulombic energy of non-bonded atoms having charge $q_i$ and $q_j$.

## 1.2.7. Basis Sets

A set of mathematical functions using which the wavefunction can be effectively constructed are termed basis set. The linear combinations of predefined set of non-orthogonal one electron wave functions which are used to build molecular orbitals are

termed basis sets. The weights or the coefficients of these combinations are to be determined. The basis sets are majorly of two types viz. Slater type orbitals(STO)[394] and Gaussian type orbitals (GTO)[395, 396] The very first basis sets that were used for calculations were STO's which area set of functions which decays exponentially with the distance from the nuclei. That implies STOs have exponential dependence in the form of $e^{-\xi r}$ and is given by the following mathematical expression,

$$\chi_{\zeta,n,l,m}(r,\theta,\varphi) = NY_{l,m}(\theta,\varphi)r^{n-1}e^{-\xi r} \quad \text{Eq. 1.82}$$

Where $N$ is the normalization constant, $Y_{l,m}$ is spherical harmonic functions. STOs are mainly used for atomic and diatomic systems where high accuracy is needed. These are also used with density functional methods that do not include exact exchange and Coulomb energy calculation is done by fitting the density into a set of auxiliary functions.

Gaussian type orbitals[395] are written in terms of polar and Cartesian coordinates systems as given in equation 1.83 and 1.84 below.

$$\chi_{\zeta,n,l,m}(r,\theta,\varphi) = NY_{l,m}(\theta,\varphi)r^{2n-2-l}e^{-\xi r^2} \quad \text{Eq. 1.83}$$

$$\chi_{\zeta,n,l,m}(x,y,z) = Nx^{l_x}y^{l_y}z^{l_z}e^{-\xi r^2} \quad \text{Eq. 1.84}$$

The sum of $l_x$, $l_y$ and $l_z$ determines the type of the orbital, when all these indices are zero, the GTO has a spherical symmetry and is called an s-type GTO. $\xi$ represents the width or spread of the orbital and x,y,z are the Cartesian coordinates. GTOs have $r^2$ dependence in exponential unlike STOs where the dependence is r in exponential, which makes GTOs inferior to STOs. GTOs yield poor ability in the representation of the proper behaviour near the nucleus, and falls off too rapidly far from the nucleus when compared with an STO.

The type of the function (STO/GTO), the location (nuclei) and the number of functions are the most important aspects of the generation of basis sets. The smallest number of functions possible is termed minimal basis set, in which only the necessary functions are used to contain all the electrons of neutral atom. The minimal basis set for H and He is single s-function, for first row elements two s-functions and one set of p-functions and for second row elements, three s-functions and two sets of p-functions. The next improvement to minimum basis set is the doubling of all basis functions,

which results in double zeta (DZ) type basis. Doubling the number of basis functions gives a better description of the phenomena of different electron distribution in different directions. Doubling the number of valance orbitals only produces split valence basis which is widely used than DZ. Further improvement in basis set size is called triple zeta, which contains three times the functions as that of minimum basis set. Quadruple zeta (QZ) and Quintuple/Pentuple Zeta (PZ or 5Z) are also used. Higher angular momentum functions also known as polarization functions are another important function to account for the difference in electron distribution along and perpendicular to the bond. In this p-orbitals introduces a polarization of s-orbitals, d-orbitals are used for polarizing p-orbitals, f-orbitals for d-orbital polarization, etc. polarization functions are mandatory in methods using electron correlation. Single set of polarization means p-functions on hydrogen and d-functions on heavy atoms, adding which to the DZ basis forms double zeta plus polarization (DZP) type basis

STOs are not amenable in calculations involving molecular orbitals, since some of the integrals are difficult to evaluate when AOs are centered on different nuclei. Up to four centered integrals are feasible in STOs if they are centered on single atom, but if atomic orbitals are centered on two or more atoms evaluation of even three centered integrals also become difficult if not impossible. Thereby GTOs are mostly used in computational calculations. There are varieties of Gaussian basis sets available which are continuously improved over the years. The simplest GTOs are the single-zeta Gaussian basis set which is commonly called as minimal basis set. The most popular single-zeta basis set is STO-3G consists of three primitive GTOs. Inner shell orbitals being inactive participants in calculations, they are described with single Slater orbital and double or triple zeta are used for the valance electrons. This is Called split-valance basis set. 3-21G and 6-31G are examples for such basis sets. 3-21G shows a single basis set consisting of 3 Gaussian functions for inner electrons and the valance electrons are represented by two separate basis functions, one consisting of two Gaussian functions and the other one Gaussian function. In 6-31 the number of Gaussian functions are six and are increased. Polarization functions or diffuse functions are used in elaborating the basis sets. The electron cloud deformality which arises due to the interaction between atoms is called polarization which is denoted using * or **describing the use of

extra set of d-orbitals for heavy atoms and p-orbitals for hydrogen. This can also be done adding (d) or (d,p) after G in basis set. The spreading of electron density over the molecules are added using the diffuse functions which is denoted by + or aug in the name of basis set and when diffuse functions are added to hydrogen atoms also we use the notation of ++.

## 1.2.8. Molecular Electrostatic Potential (MESP)

The most fundamental quantitative law in electrostatic is given by Charles Augustin de Coulomb in 1784, describing the force of attraction or repulsion between two point charges as directly proportional to the product of the quantity of charge and inversely proportional to the square of the distance between the charges. This law can be mathematically expressed as

$$F = \frac{q_1 q_2 \hat{\boldsymbol{r}}}{4\pi\varepsilon_0 \boldsymbol{r}^2} \qquad \text{Eq. 1.85}$$

where $q_1$ and $q_2$ are point charges separated by a distance of $r$ in vacuum, $\hat{r}$ is a unit vector that joins the position vectors $q_1$ and $q_2$ and $4\pi\varepsilon_0$ is the constant of proportionality in SI units. In a medium $\varepsilon_0$ is replaced by an appropriate constant $\varepsilon$, called permittivity of the medium. $E_0$ value equals to 8.854 x $10^{-12}C^2N^{-1}m^{-2}$.

Intensity of an electric field ($E$) is defined as force acting on unit test charge placed at a reference point in the field. Therefore, the field due to a fixed point charge q present at a position r is given by

$$E = \frac{\boldsymbol{qr}}{4\pi\varepsilon_0 |\boldsymbol{r}|^3} \qquad \text{Eq. 1.86}$$

The unit of which is Newton per Coulomb.

Now considering the principle of superposition involving a system of two or more charges ($q_\alpha$) , the electric field is given as the vector sum of all the fields $E_\alpha$ produced by individual charges.

$$E(\boldsymbol{r}) = \sum_\alpha E_\alpha(\boldsymbol{r}) = \frac{1}{4\pi\varepsilon_0} \sum_\alpha \frac{q_\alpha(\boldsymbol{r} - \boldsymbol{r_\alpha})}{|\boldsymbol{r} - \boldsymbol{r_\alpha}|^3} \qquad \text{Eq. 1.87}$$

Coloumbic electrostatic potential, $V(\boldsymbol{r})$ at a point is similar to the electrostatic potential (ESP) at a point due to a collection of discrete charges $q_\alpha$ located at $r_\alpha$.

$$V(\boldsymbol{r}) = \frac{1}{4\pi\varepsilon_0}\sum_{\alpha}\frac{q_\alpha}{|\boldsymbol{r}-\boldsymbol{r_\alpha}|} \qquad \text{Eq. 1.88}$$

Considering a continuous distribution of charge over space is responsible for the ESP, instead of discrete charges, potential generated at a reference point *r* is $\rho(r')d^3r'/|r-r'|$. The potential generated by entire charge distribution is obtained by integrating it over the entire space.

$$V(\boldsymbol{r}) = \frac{1}{4\pi\varepsilon_0}\int\frac{\rho(\boldsymbol{r}')d^3\boldsymbol{r}'}{|\boldsymbol{r}-\boldsymbol{r}'|} \qquad \text{Eq. 1.89}$$

Combining equation 1.88 and 1.89, the electrostatic potential for the combination of discrete charges $q_\alpha$ placed at $r_\alpha$ and distribution ρ(**r**) is obtained as given below.

$$V(\boldsymbol{r}) = \frac{1}{4\pi\varepsilon_0}\left\{\sum_{\alpha}\frac{q_\alpha}{|\boldsymbol{r}-\boldsymbol{r_\alpha}|} + \int\frac{\rho(\boldsymbol{r}')d^3\boldsymbol{r}'}{|\boldsymbol{r}-\boldsymbol{r}'|}\right\} \qquad \text{Eq. 1.90}$$

The molecular electrostatic potential[206, 397] at a given point near a molecule is the force acting on a positive test charge located at that position through the electrical charge cloud generated through the molecules electron and nuclei. It can be regarded as the potential of a molecule to interact with an electric charge located at a position r. The π-electron cloud of the molecules is seen in the MESP isosurface lobes and the most negative valued MESP ($V_{\text{min}}$) is useful for comparing the relative electron rich character of the π-regions in different molecules.[398, 399] A positive charge is attracted to the regions in molecule where *V(r)* is negative and is repelled from the regions where the value is positive. MESP is calculated from the electron density *ρ(r)* using the equation 1.91:[400]

$$V(r) = \sum_{\alpha}^{N}\frac{Z_\alpha}{|\boldsymbol{r}-\boldsymbol{R}_\alpha|} - \int\frac{\rho(\boldsymbol{r}')d^3\boldsymbol{r}'}{|\boldsymbol{r}-\boldsymbol{r}'|} \qquad \text{Eq. 1.91}$$

where $Z_\alpha$ is the charge of the nucleus α located at $R_\alpha$ and *r'* is an arbitrary integration variable. *V(r)* is expressed as a sum of two terms, the bare nuclear potential and the electronic contributions respectively. Molecular geometry is the deciding factor in the measurement of electrostatic potential according to the above equation. And the value of *V(r)* is positive in the regions which are close to the nuclei and is negative in electron

rich regions. Electron densities can have non-negative values only, yet the quantity *V(r)* which is derived from electron density can have positive, zero and negative values.

MESP topography provides an excellent picture of molecular reactivity, intermolecular interactions and a variety of chemical phenomena. Identifying the most negative valued MESP ($V_{min}$) positions in a molecule is useful for understanding the electron localization/delocalization character of π-regions in molecules.[215, 216] for a typical polycyclic aromatic hydrocarbon coronene, the MESP isosurface with highlighted regions of $V_{min}$ is shown in Figure 1.5. $V_{min}$ analysis has been previously used for studying the Clar's aromatic sextet theory of polycyclic aromatic hydrocarbons and related systems.[210, 218, 219] In the thesis MESP analysis is mainly used for quantification of aromaticity as well as the tool for electron delocalization visualization.

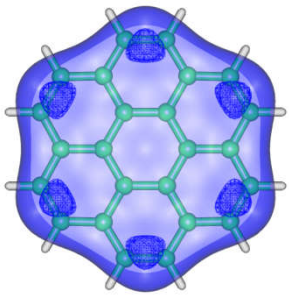

Figure 1.4. MESP isosurface of coronene molecule with the location of $V_{min}$ highlighted.

## 1.2.9. Harmonic Oscillator Model of Aromaticity (HOMA)

Harmonic oscillator model of aromaticity (HOMA) is a geometry based aromaticity measurement that has been widely used for the quantification of planar individual rings. Julg et al[401] in 1967 constructed a normalized function of the CC-bond lengths variance in the case of carbocyclic π-electron systems given by the equation,

$$A_j = 1 - \frac{255}{n}\sum_{i=1}^{n}\left(1 - \frac{R_i}{R_{av}}\right) \qquad \text{Eq. 1.92}$$

where $n$ is the number of peripheral bonds of length $R_i$ and $R_{av}$ is the mean value of all the bond lengths. Normalization constant 255 is chosen so that in the case of a perfect aromatic system of Kekúle's benzene, the $A_j$ value assumes zero. When all the bond lengths are same the value becomes equal to 1. Julg's idea was modified in the year

1972 by replacing the mean bond length with the theoretical quantity the optimal bond length, $R_{opt}$ . $R_{opt}$ is the bond length which will be realized only on a fully aromatic system.[141]

The assumption which is the foundation of HOMA model is that the harmonic oscillator energy of extension or compression of a bond depends on the force constants, which are in turn depends on the bond lengths. The length of a bond for which the energy requirement is same for the extension into a single bond and compression into a double bond is termed optimal bond length. The basis of HOMA is the assumption that the change in C-C bondlengths causes the energy changes in hydrocarbon ring systems. According to harmonic oscillator model the energy change ($\Delta E_r$) corresponding to bond *r* is proportional to the square of the bond length change.

$$\Delta E = \frac{1}{2}k_s(R - R_s)^2 + \frac{1}{2}k_d(R - R_d)^2 \qquad \text{Eq.1.93}$$

In the equation *s* and *d* refers to single and double bonds respectively and *k* is their respective force constants. The reference values take are the CC bond length in ethane ($R_{C\text{-}C}$=1.524 Å) as single bond and that in ethene ($R_{C=C}$=1.334 Å) for double bond, considering the relation between the force constants for double and single bonds as 2:1. Then the formula for $R_{opt}$ is given as

$$R_{opt} = \frac{(R_{C-C} + 2R_{C=C})}{3} = 1.397 \qquad \text{Eq. 1.94}$$

Optimal bond length is calculated by normalization of total energy change over all bonds and is given as

$$R_{opt} = (k_s R_s + k_d R_d)/(k_s + k_d) \qquad \text{Eq. 1.95}$$

The experimental value of benzene bond length obtained by the X-ray measurement at 10 K is 1.398Å[402], which is in good agreement with calculated value by this method. The formula for *HOMA* is given as follows:

$$HOMA = 1 - \frac{\alpha}{n}\sum_{i}^{n}(R_{opt} - R_i)^2 \qquad \text{Eq. 1.96}$$

where α=98.89 is an empirical normalization constant, chosen in such a way that *HOMA*=0 for a model nonaromatic system and *HOMA*=1 for a system where all bonds are equal to the $R_{opt}$=1.397 Å, *n* is the number of CC bonds taken into consideration, $R_{opt}$

is the optimal aromatic bond length and $R_i$ is the experimental or computed bond length. The values for $\alpha$ and $R_{opt}$ major bonds that have been used in this thesis is given in Table 1. For a perfect aromatic system the *HOMA* value is 1 and for non-aromatic ones the value approaches zero.

Table 1.1. α and $R_{opt}$ values of typical bonds.[98]

| Type of bond | $\alpha$ | $R_{opt}$(Å) |
|---|---|---|
| CC | 257.70 | 1.388 |
| CN | 93.52 | 1.334 |
| CB | 138.06 | 1.564 |
| CO | 157.38 | 1.265 |

HOMA is split into energetic (EN) and geometric (GEO) contributions by Krygowski et al in 1996,[403, 404] according to the relation HOMA=1-EN-GEO. The splitting lead to the discovery that the HOMA index can be greater than 1 for systems in which $R_{av}$ is lesser than $R_{opt}$. The bond length alternation is measured by the GEO part, while EN term indicates the bond elongation in the ring.[405] The equation for both these terms are given below.

$$GEO = \frac{\alpha}{n}\sum_{i=1}^{n}(R_{av} - R_i)^2 \qquad \text{Eq. 1.97}$$

$$EN = \alpha(R_{opt} - R_{av})^2 \qquad \text{for } R_{opt} < R_{av} \qquad \text{Eq. 1.98}$$

$$EN = -\alpha(R_{opt} - R_{av})^2 \qquad \text{for } R_{av} < R_{opt} \qquad \text{Eq. 1.99}$$

For systems having larger $R_{opt}$ values when compared to $R_{av}$ value, the HOMA value can be greater than 1.

## 1.2.10. Nucleus Independent Chemical Shift (NICS)

Magnetic criteria of aromaticity is popularly described in terms of Nucleus independent chemical shift (NICS) index as portrayed by Schleyer and co-workers.[111] This method is the most popular method for the determination of the magnetic properties of molecule. The aromaticity and non-aromaticity of single ring systems and

individual rings in polycyclic aromatic rings can be quantified using NICS analysis. The negative value of absolute shielding computed at ring centre or any other position of interest is termed NICS index. NICS uses a ghost atom with no electrons, neutrons or protons placed at desired location in a molecular system, which acts as a sensor for the magnetic environment at that location.[102] We are using GIAO (Gauge-independent atomic orbital) method[406-408] for the interpretation of the signal that has been sent by the ghost atom. The diatropic magnetic field at the point is indicated by a negative NICS value and paratropic magnetic field is indicated by a positive NICS value.

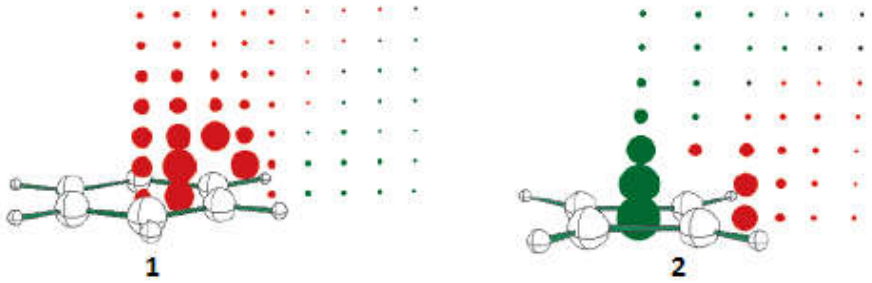


Figure 1.6. NICS grid plot of (**1**) benzene and (**2**) cyclobutadiene. Figure adapted from Schleyer *et. al.* 2001[409]

When an aromatic or antiaromatic molecule is placed in an external magnetic field, induced ring currents are generated in the molecule which generates an induced magnetic field. The chemical shift of the nuclei of the molecule is influenced by this field which is used as a probe for the direction and magnitude of the induced magnetic field and thereby the phenomenon of aromaticity or antiaromaticity. NICS grid plot of aromatic benzene ring and antiaromatic cyclobutadiene is illustrated in Figure1.6. the red and green colour represents the diatropic (negative NICS) and paratropic (positive NCIS) ring current, respectively.

We have analyzed three popular NICS indices, viz. the NICS at the center of each six-membered ring (NICS(0)), at 1 Å above every ring center (NICS(1)) and also the z-component of NICS at 1 Å above the ring center ($NICS_{zz}(1)$). The position of ghost atoms in calculation of NICS (0) and NICS(1) is illustrated in the Figure 1.7. Among these indices, $NICS_{zz}(1)$ is considered to be more reliable than others. And therefore $NICS_{zz}(1)$ values are being reported in the thesis.

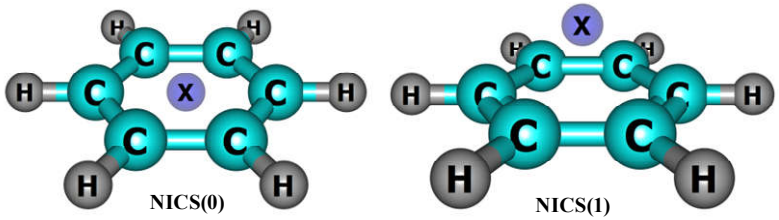


Figure 1.7. Picture showing the position of ghost atom for the calculation of NICS(0) and NICS(1) for benzene ring

## 1.3. Conclusions

Polycyclic aromatic hydrocarbons and linear polyacene analogues makes an excellent electronic material for the organic electronics industry since these class of molecules have tunable electronic and structural properties LPAs beyond pentacene are highly unstable and Remarkable optical properties like hot luminescence, saturable absorption and broadband applicability render PAHs an ideal photonic and optoelectronic material. Accessing of the stability of such systems is done with the understanding of aromaticity. In part A of chapter 1, the peculiarities of PAHs the multidimensionality of aromaticity is briefly discussed with examples for energetic, geometric, magnetic and electronic criteria. The excited state properties which are beneficial in the assessment of optoelectronic features of systems are given special emphasis and is discussed in the part A of Chapter 1. Theoretical investigations are most beneficial for the effective tuning of optoelectronic properties of benzenoid systems and the understanding of the phenomenon of aromaticity. The main focus of the thesis is to analyze the structure-property relationships of these systems in both ground and excited states using computational methods.

Prediction and calculation of molecular structure and properties can be done using computational chemistry methods, which involves the laws and equations that are applicable to the atomic and subatomic systems. Commonly used methods in computational chemistry and their theoretical sides are elaborated in the Chapter 1. An account of DFT methods which is the theoretical method we have adopted in calculations in this thesis is given in details. TD-DFT methods and its formulation is also detailed in part B of Chapter 1, which is used in the excited state calculations in the

thesis. Various methods and their principles adopted in quantification of aromaticity like HOMA, NICS and MESP analysis are also outlined.

## 1.4. Scope of the Thesis

The present thesis focuses on the designing and structure-property relationships of linear polyacenes (LPAs) analogues and polycyclic aromatic hydrocarbons (PAHs). Aromaticity and stability of the designed molecules are analysed using various methods, like structural (HOMA), energetic (dehydrogenation energy), magnetic (NICS) and electronic (MESP) criteria. The design and study of long chain linear polyacene analogues containing hetero-atoms in the acene structural skeleton (LPA mimics) are important due to potential applications of such molecules in optoelectronic devices. To reveal their stability, aromaticity, electronic character, HOMO-LUMO energy gap and singlet-triplet energy gap of LPA mimics, theoretical DFT calculations are carried out on them. In short, by adjusting the length of LPA unit as well as by choosing the appropriate number of heterocyclic rings for annulations, an LPA mimic showing the desired band gap and $\Delta E_{ST}$ gap can be designed for potential applications in the fabrication of efficient optoelectronic devices. The absorption maxima values can also be tuned, and made absorb or emit radiation of specific wavelength by the adjustment of length of LPA and number of heterorings as in the case of band gap. The molecular orbital representation gives the idea about the structure and orientation of the frontier molecular orbitals which is helpful in the prediction of the transitions and interactions in the molecule as a whole. The fourth chapter deals with the electronic and optical tuning of the polycyclic aromatic hydrocarbons. The electrostatic potential analysis enables the pictorial representation of the electron cloud around the molecule, which indirectly gives an idea about the stability of the molecule. Alternation of the size and shape of PAHs can give different properties especially absorption spectra. The effect of geometry on such phenomena can be analysed theoretically which will be helpful in the application of such materials in various fields such as optics industry. The thesis casts light upon the effect of morphology, either the number or the overall shape of the systems on the stability, frontier orbitals, excited state properties like absorption spectra and singlet-triplet bandgap and HOMO-LUMO gap etc.

## 1.5. References


1. J. C. Fetzer., *The Chemistry and Analysis of the Large Polycyclic Aromatic Hydrocarbons*, John Wiley, New York, 2000.
2. F. J. Lovas, R. J. McMahon, J.-U. Grabow, M. Schnell, J. Mack, L. T. Scott and R. L. Kuczkowski, *J. Am. Chem. Soc.*, **2005**, 127, 4345-4349.
3. R. G. Harvey, Q. Dai, C. Ran, K. Lim, I. Blair and T. M. Penning, *Polycycl. Aromat. Compd.*, **2005**, 25, 371-391.
4. M. Kastler, J. Schmidt, W. Pisula, D. Sebastiani and K. Müllen, *J. Am. Chem. Soc.*, **2006**, 128, 9526-9534.
5. E. Clar, in *Polycyclic Hydrocarbons*, Academic Press, London, 1964, vol. 1, pp. 126-129.
6. E. Clar, *Polycyclic hydrocarbons Vol. 1&2*, Academic Press, London, 1964.
7. E. Clar, *The Aromatic Sextet*, Wiley, New York, 1972.
8. R. Scholl, C. Seer and R. Weitzenböck, *Chem. Ber.*, **1910**, 43, 2202-2209.
9. R. Scholl and C. Seer, *Liebigs Ann. Chem.*, **1912**, 394, 111-177.
10. E. Clar and D. G. Stewart, *J. Am. Chem. Soc.*, **1953**, 75, 2667-2672.
11. F. De Proft and P. Geerlings, *Chem. Rev.*, **2001**, 101, 1451-1464.
12. S. W. Slayden and J. F. Liebman, *Chem. Rev.*, **2001**, 101, 1541-1566.
13. R. H. Mitchell, *Chem. Rev.*, **2001**, 101, 1301-1316.
14. R. Goddard, M. W. Haenel, W. C. Herndon, C. Krueger and M. Zander, *J. Am. Chem. Soc.*, **1995**, 117, 30-41.
15. Q. Meng, H. Dong, W. Hu and D. Zhu, *J. Mater. Chem.*, **2011**, 21, 11708-11721.
16. W. Pisula, X. Feng and K. Müllen, *Chem. Mater.*, **2011**, 23, 554-567.
17. M. D. Watson, A. Fechtenkötter and K. Müllen, *Chem. Rev.*, **2001**, 101, 1267-1300.
18. C. D. Simpson, J. Wu, M. D. Watson and K. Müllen, *J. Mater. Chem.*, **2004**, 14, 494-504.
19. R. J. Bushby and O. R. Lozman, *Curr. Opin. Solid State Mater. Sci.*, **2002**, 6, 569-578.
20. J. Wu, W. Pisula and K. Müllen, *Chem. Rev.*, **2007**, 107, 718-747.

21. Z. H. Wang, C. Li, E. M. Scherr, A. G. MacDiarmid and A. J. Epstein, *Phys. Rev. Lett.*, **1991**, 66, 1745-1748.
22. A. Aleshin, R. Kiebooms, R. Menon, F. Wudl and A. J. Heeger, *Phys. Rev. B*, **1997**, 56, 3659-3663.
23. A. J. Heeger, *J. Phys. Chem. B*, **2001**, 105, 8475-8491.
24. H. Sirringhaus, N. Tessler and R. H. Friend, *Science*, **1998**, 280, 1741.
25. H. Sirringhaus, P. J. Brown, R. H. Friend, M. M. Nielsen, K. Bechgaard, B. M. W. Langeveld-Voss, A. J. H. Spiering, R. A. J. Janssen, E. W. Meijer, P. Herwig and D. M. de Leeuw, *Nature*, **1999**, 401, 685.
26. A. Narita, X.-Y. Wang, X. Feng and K. Mullen, *Chem. Soc. Rev.*, **2015**, 44, 6616-6643.
27. R. S. Pantelic, J. C. Meyer, U. Kaiser, W. Baumeister and J. M. Plitzko, *J. Struct. Biol.*, **2010**, 170, 152-156.
28. N. R. Wilson, P. A. Pandey, R. Beanland, R. J. Young, I. A. Kinloch, L. Gong, Z. Liu, K. Suenaga, J. P. Rourke, S. J. York and J. Sloan, *ACS Nano*, **2009**, 3, 2547-2556.
29. R. R. Nair, P. Blake, J. R. Blake, R. Zan, S. Anissimova, U. Bangert, A. P. Golovanov, S. V. Morozov, A. K. Geim, K. S. Novoselov and T. Latychevskaia, *Appl. Phys. Lett.*, **2010**, 97, 153102.
30. P. Blake, P. D. Brimicombe, R. R. Nair, T. J. Booth, D. Jiang, F. Schedin, L. A. Ponomarenko, S. V. Morozov, H. F. Gleeson, E. W. Hill, A. K. Geim and K. S. Novoselov, *Nano Lett.*, **2008**, 8, 1704-1708.
31. X. Wang, L. Zhi and K. Müllen, *Nano Lett.*, **2008**, 8, 323-327.
32. J. S. Moon, D. Curtis, M. Hu, D. Wong, C. McGuire, P. M. Campbell, G. Jernigan, J. L. Tedesco, B. VanMil, R. Myers-Ward, C. Eddy and D. K. Gaskill, *IEEE Electron Device Lett.*, **2009**, 30, 650-652.
33. Y.-M. Lin, K. A. Jenkins, A. Valdes-Garcia, J. P. Small, D. B. Farmer and P. Avouris, *Nano Lett.*, **2009**, 9, 422-426.
34. L. Gong, I. A. Kinloch, R. J. Young, I. Riaz, R. Jalil and K. S. Novoselov, *Adv. Mater.*, **2010**, 22, 2694-2697.
35. S. F. Nelson, Y. Y. Lin, D. J. Gundlach and T. N. Jackson, *Appl. Phys. Lett.*, **1998**, 72, 1854-1856.

36. D. J. Gundlach, Y. Y. Lin, T. N. Jackson, S. F. Nelson and D. G. Schlom, *IEEE Electron Device Lett.*, **1997**, 18, 87-89.
37. J. E. Anthony, *Angew. Chem. Int. Ed.*, **2008**, 47, 452-483.
38. M. Watanabe, K.-Y. Chen, Y. J. Chang and T. J. Chow, *Acc. Chem. Res.*, **2013**, 46, 1606-1615.
39. W. Han, R. K. Kawakami, M. Gmitra and J. Fabian, *Nature Nanotechnology*, **2014**, 9, 794.
40. L. Bursi, A. Calzolari, S. Corni and E. Molinari, *ACS Photonics*, **2014**, 1, 1049-1058.
41. P. Sony and A. Shukla, *Phys. Rev. B*, **2007**, 75, 155208.
42. T. Minakata and M. Ozaki, *J. Appl. Phys.*, **1993**, 73, 1819-1825.
43. S. Kivelson and O. L. Chapman, *Phys. Rev. B*, **1983**, 28, 7236-7243.
44. K. N. Houk, P. S. Lee and M. Nendel, *J. Org. Chem.*, **2001**, 66, 5517-5521.
45. C. Wang, H. Dong, W. Hu, Y. Liu and D. Zhu, *Chem. Rev.*, **2012**, 112, 2208-2267.
46. Z. Sun, Q. Ye, C. Chi and J. Wu, *Chem. Soc. Rev.*, **2012**, 41, 7857-7889.
47. J. Thorley Karl and E. Anthony John, *Isr. J. Chem.*, **2014**, 54, 642-649.
48. X. Shi and C. Chi, *Chem. Rec.*, **2016**, 16, 1690-1700.
49. S. Zade Sanjio and M. Bendikov, *angew. Chem. Int. Ed.*, **2010**, 49, 4012-4015.
50. I. Kaur, M. Jazdzyk, N. N. Stein, P. Prusevich and G. P. Miller, *J. Am. Chem. Soc.*, **2010**, 132, 1261-1263.
51. B. Purushothaman, M. Bruzek, R. Parkin Sean, A.-F. Miller and E. Anthony John, *Angew. Chem. Int. Ed.*, **2011**, 50, 7013-7017.
52. F. Bettinger Holger and C. Tönshoff, *Chem. Rec.*, **2014**, 15, 364-369.
53. R. Dorel and M. Echavarren Antonio, *Eur. J. Org. Chem.*, **2016**, 2017, 14-24.
54. M. Watanabe, Y. J. Chang, S.-W. Liu, T.-H. Chao, K. Goto, M. M. Islam, C.-H. Yuan, Y.-T. Tao, T. Shinmyozu and T. J. Chow, *Nat. Chem.*, **2012**, 4, 574.
55. R. Mondal, C. Tönshoff, D. Khon, D. C. Neckers and H. F. Bettinger, *Journal of the American Chemical Society*, **2009**, 131, 14281-14289.
56. R. Einholz, T. Fang, R. Berger, P. Grüninger, A. Früh, T. Chassé, R. F. Fink and H. F. Bettinger, *J. Am. Chem. Soc.*, **2017**, 139, 4435-4442.
57. C. Tönshoff and H. F. Bettinger, *Angew. Chem. Int. Ed.*, **2010**, 49, 4125-4128.

58. R. Zuzak, R. Dorel, M. Kolmer, M. Szymonski, S. Godlewski and M. Echavarren Antonio, *Angew. Chem. Int. Ed.*, **2018**, 0.
59. J. Fan, L. Zhang, A. L. Briseno and F. Wudl, *Org. Lett.*, **2012**, 14, 1024-1026.
60. J. E. Frey, G. M. Marchand and R. S. Bolton, *Inorganic Chemistry*, **1982**, 21, 3239-3241.
61. G. Li, Y. Wu, J. Gao, C. Wang, J. Li, H. Zhang, Y. Zhao, Y. Zhao and Q. Zhang, *J. Am. Chem. Soc.*, **2012**, 134, 20298-20301.
62. U. H. F. Bunz, J. U. Engelhart, B. D. Lindner and M. Schaffroth, *Angew. Chem. Int. Ed.*, **2013**, 52, 3810-3821.
63. Q. Miao, *Adv. Mater.*, **2014**, 26, 5541-5549.
64. J. U. Engelhart, F. Paulus, M. Schaffroth, V. Vasilenko, O. Tverskoy, F. Rominger and U. H. F. Bunz, *J. Org. Chem.*, **2016**, 81, 1198-1205.
65. J. U. Engelhart, B. D. Lindner, O. Tverskoy, F. Rominger and U. H. F. Bunz, *Org. Lett.*, **2012**, 14, 1008-1011.
66. C. Dou, S. Saito, K. Matsuo, I. Hisaki and S. Yamaguchi, *Angew. Chem. Int. Ed.*, **2012**, 51, 12206-12210.
67. K. Matsuo, S. Saito and S. Yamaguchi, *J. Am. Chem. Soc.*, **2014**, 136, 12580-12583.
68. W. Jiang, Y. Zhou, H. Geng, S. Jiang, S. Yan, W. Hu, Z. Wang, Z. Shuai and J. Pei, *J. Am. Chem. Soc.*, **2011**, 133, 1-3.
69. C. J. Tonzola, M. M. Alam, W. Kaminsky and S. A. Jenekhe, *J. Am. Chem. Soc.*, **2003**, 125, 13548-13558.
70. J.-i. Nishida, Naraso, S. Murai, E. Fujiwara, H. Tada, M. Tomura and Y. Yamashita, *Org. Lett.*, **2004**, 6, 2007-2010.
71. M. Winkler and K. N. Houk, *J. Am. Chem. Soc.*, **2007**, 129, 1805-1815.
72. Z. M. Hudson and S. Wang, *Dalton Trans.*, **2011**, 40, 7805-7816.
73. Z. Liu and T. B. Marder, *Angew. Chem. Int. Ed.*, **2008**, 47, 242-244.
74. M. J. D. Bosdet and W. E. Piers, *Can. J. Chem.*, **2009**, 87, 8-29.
75. X.-Y. Wang, F.-D. Zhuang, R.-B. Wang, X.-C. Wang, X.-Y. Cao, J.-Y. Wang and J. Pei, *J. Am. Chem. Soc.*, **2014**, 136, 3764-3767.
76. G. Li, W.-W. Xiong, P.-Y. Gu, J. Cao, J. Zhu, R. Ganguly, Y. Li, A. C. Grimsdale and Q. Zhang, *Org. Lett.*, **2015**, 17, 560-563.

77. J. S. A. Ishibashi, A. Dargelos, C. Darrigan, A. Chrostowska and S.-Y. Liu, *Organometallics*, **2017**, 36, 2494-2497.
78. X. Wang, F. Zhang, J. Liu, R. Tang, Y. Fu, D. Wu, Q. Xu, X. Zhuang, G. He and X. Feng, *Org. Lett.*, **2013**, 15, 5714-5717.
79. J. Zhou, R. Z. Tang, X. Y. Wang, W. Z. Zhang, X. D. Zhuang and F. Zhang, *J. Mater. Chem. C*, **2016**, 4, 1159-1164.
80. J. Ku, Y. Lansac and Y. H. Jang, *J. Phys. Chem. C*, **2011**, 115, 21508-21516.
81. J.-M. Ku, D.-K. Kim, T.-H. Ryu, E.-H. Jung, Y. Lansac and Y.-H. Jang, *Bull Korean Chem. Soc.*, **2012**, 33, 1029-1036.
82. P. v. R. Schleyer, *Chem. Rev.*, **2001**, 101, 1115-1118.
83. P. J. Garrat, *Aromaticity*, Wiley, New York, 1986.
84. V. I. Minkin, M. N. Glukhovtsev and B. Y. Simkin, *Aromaticity and Antiaromaticity: Electronic and Structural Aspects*, Wiley, New York, 1994.
85. P. v. R. Schleyer and H. Jiao, *Pure Appl. Chem.*, **1996**, 68, 209.
86. T. M. Krygowski, M. K. Cyrañski, Z. Czarnocki, G. Häfelinger and A. R. Katritzky, *Tetrahedron*, **2000**, 56, 1783-1796.
87. L. T. Scott and J. S. Seigel, *Tetrahedron*, **2002**, 57, 9.
88. Kekulé, *Bull. Soc. Chim. Fr. (Paris)*, **1865**, 3, 98.
89. P. v. R. Schleyer, *Chem. Rev.*, **2005**, 105, 3433-3435.
90. A. T. Balaban, *Pure Appl. Chem.*, **1980**, 52, 1409.
91. K. K. Baldridge and J. S. Siegel, *J. Phys. Org. Chem.*, **2004**, 17, 740-742.
92. D. Lloyd, *J. Chem. Inf. Comput. Sci.*, **1996**, 36, 442-447.
93. V. I. Minkin, *Pure Appl. Chem.*, **1999**, 71, 1919-1981.
94. A. R. Katritzky, K. Jug and D. C. Oniciu, *Chem. Rev.*, **2001**, 101, 1421-1450.
95. E. Z. Hückel, *Eur. Phys. J. A*, **1932**, 76, 628-628.
96. E. Z. Hückel, *Grundzüge. der Theorie ungesättiger und aromatischer Verbindungen*, Verlag Chemie, Berlin, 1938.
97. Z. Chen, C. S. Wannere, C. Corminboeuf, R. Puchta and P. v. R. Schleyer, *Chem. Rev.*, **2005**, 105, 3842-3888.
98. T. M. Krygowski, H. Szatylowicz, O. A. Stasyuk, J. Dominikowska and M. Palusiak, *Chem. Rev.*, **2014**, 114, 6383-6422.

99. T. M. Krygowski and M. K. Cyrański, *Chem. Rev.*, **2001**, 101, 1385-1420.
100. M. J. S. Dewar, *Angew. Chem. Int. Ed. Engl.*, **1971**, 10, 761-776.
101. F. Feixas, E. Matito, J. Poater and M. Sola, *Chem. Soc. Rev.*, **2015**, 44, 6434-6451.
102. R. Gershoni-Poranne and A. Stanger, *Chem. Soc. Rev.*, **2015**, 44, 6597-6615.
103. K. Cocq, C. Lepetit, V. Maraval and R. Chauvin, *Chem. Soc. Rev.*, **2015**, 44, 6535-6559.
104. H. Szatylowicz, O. A. Stasyuk and T. M. Krygowski, in *Advances in Heterocyclic Chemistry*, eds. E. F. V. Scriven and C. A. Ramsden, Academic Press, 2016, vol. 120, pp. 301-327.
105. I. Fernandez, G. Frenking and G. Merino, *Chem. Soc. Rev.*, **2015**, 44, 6452-6463.
106. D. Ranjita, C. Arindam, P. Sudip and K. C. Pratim, *Curr. Org. Chem.*, **2013**, 17, 2831-2844.
107. S. Paul, T. Goswami and A. Misra, *AIP Adv.*, **2015**, 5, 107211.
108. M. K. Cyrañski, T. M. Krygowski, A. R. Katritzky and P. v. R. Schleyer, *J. Org. Chem.*, **2002**, 67, 1333-1338.
109. v. Paul, Ragué, Schleyer., H. Jiao, B. Goldfuss and K. Freeman Peter, *Angew. Chem. Int. Ed. Engl.*, **1995**, 34, 337-340.
110. A. R. Katritzky, M. Karelson, S. Sild, T. M. Krygowski and K. Jug, *J. Org. Chem.*, **1998**, 63, 5228-5231.
111. P. v. R. Schleyer, C. Maerker, A. Dransfeld, H. Jiao and N. J. R. v. E. Hommes, *J. Am. Chem. Soc.*, **1996**, 118, 6317-6318.
112. W. J. Hehre, R. Ditchfield, L. Radom and J. A. Pople, *J. Am. Chem. Soc.*, **1970**, 92, 4796-4801.
113. J. A. Pople, L. Radom and W. J. Hehre, *J. Am. Chem. Soc.*, **1971**, 93, 289-300.
114. W. J. Hehre, L. Radom, P. v. R. Schleyer and J. A. Pople, *Ab Initio Molecular Orbital Theory*, Wiley-Interscience, New York, 1986.
115. S. E. Wheeler, K. N. Houk, P. v. R. Schleyer and W. D. Allen, *J. Am. Chem. Soc.*, **2009**, 131, 2547-2560.
116. D. A. Ponomarev and V. V. Takhistov, *J. Chem. Educ.*, **1997**, 74, 201.
117. M. N. Glukhovtsev and P. von Ragué Schleyer, *Chem. Phys. Lett.*, **1992**, 198, 547-554.

118. C. H. Suresh and N. Koga, *J. Org. Chem.*, **2002**, 67, 1965-1968.
119. W. J. Hehre, R. T. McIver, J. A. Pople and P. v. R. Schleyer, *J. Am. Chem. Soc.*, **1974**, 96, 7162-7163.
120. L. Radom, *J. Chem. Soc. Chem. Commun.*, **1974**, 403-404.
121. P. George, M. Trachtman, C. W. Bock and A. M. Brett, *Theo. Chim. Acta*, **1975**, 38, 121-129.
122. P. George, M. Trachtman, A. M. Brett and C. W. Bock, *J. Chem. Soc., Perkin Trans. 2*, **1977**, 1036-1047.
123. P. George, M. Trachtman, C. W. Bock and A. M. Brett, *Tetrahedron*, **1976**, 32, 317-323.
124. S. Wheeler, E., *WIREs Comput. Mol. Sci.*, **2012**, 2, 204-220.
125. J. B. Hess and L. Schaad, *J. Am. Chem. Soc.*, **1983**, 105, 7500-7505.
126. L. Nyulászi, P. Várnai and T. Veszprémi, *J. Mol. Struct. (Theochem)*, **1995**, 358, 55-61.
127. R. Vianello, F. Liebman Joel and B. Maksić Zvonimir, *Chem. Eur. J.*, **2004**, 10, 5751-5760.
128. D. Barić, B. Kovačević, Z. B. Maksić and T. Müller, *J. Phys. Chem. A*, **2005**, 109, 10594-10606.
129. D. B. Chesnut and K. M. Davis, *J. Comput. Chem.*, **1998**, 18, 584-593.
130. A. M. El-Nahas, J. W. Bozzelli, J. M. Simmie, M. V. Navarro, G. Black and H. J. Curran, *J. Phys. Chem. A*, **2006**, 110, 13618-13623.
131. P. George, C. W. Bock and M. Trachtman, *Theo. Chim. Acta*, **1987**, 71, 289-298.
132. B. M. Gimarc and M. Zhao, *J. Phys. Chem.*, **1994**, 98, 1596-1600.
133. M. Zhao and B. M. Gimarc, *J. Phys. Chem.* , **1993**, 97, 4023-4030.
134. D. S. Warren and B. M. Gimarc, *J. Phys. Chem.*, **1993**, 97, 4031-4035.
135. N. C. Baird, *J. Chem. Educ.*, **1971**, 48, 509.
136. D. Lewis and D. Peters, *Facts and Theories of Aromaticity*, The Macmillan Press Ltd., London, 1975.
137. A. V. Chapman, M. J. Cook, A. R. Katritzky, M. H. Aabraham, A. F. Danil De Namor, L. Dumont and J. Reisse, *Tetrahedron*, **1978**, 34, 1571-1575.
138. N. C. Baird, *J. Chem. Educ.*, **1971**, 48, 509.

139. A. V. Chapman, M. J. Cook, A. R. Katritzky, M. H. Abraham, A. F. Danil de Namor, L. Dumont and J. Reisse, *Tetrahedron*, **1978**, 34, 1571.
140. J. Kruszewski and T. M. Krygowski, *Tetrahedron Lett.*, **1972**, 13, 3839-3842.
141. J. Kruszewski and T. M. Krygowski, *Tetrahedron Lett.*, **1972**, 13, 3839-3842.
142. J. Poater, X. Fradera, M. Duran and M. Sola, *Chem. Eur. J.*, **2003**, 9, 400.
143. J. Poater, X. Fradera, M. Duran and M. Sola, *Chem. Eur. J.*, **2003**, 9, 1113.
144. C. W. Bird, *Tetrahedron*, **1997**, 53, 3319.
145. C. W. Bird, *Tetrahedron*, **1998**, 54, 4641.
146. M. K. Cyrañski, T. M. Krygowski and C. W. Bird, *Tetrahedron*, **1998**, 54.
147. R. Daudel, R. Lefebvre and C. Moser, *Quantum Chemistry*, Interscience, New York, 1959.
148. A. F. Pozharskii, *Chem. Heterocycl. Compd.*, **1985**, 21, 717.
149. F. Fringuelli, G. Marino, A. Taticchi and G. Grandolini, *J. Chem. Soc., Perkin Trans.*, **1974**, 2, 332.
150. W. Gordy, *J. Chem. Phys.*, **1947**, 15, 305.
151. J. A. Elvidge and L. M. Jackman, *J. Chem. Soc.*, **1961**, 859-866.
152. P. v. R. Schleyer, C. Maerker, A. Dransfeld, H. Jiao and N. J. R. van Eikema Hommes, *J. Am. Chem. Soc.*, **1996**, 118, 6317-6318.
153. P. R. Schleyer and H. Jiao, *Pure Appl. Chem.*, **1996**, 68, 209-218.
154. J. A. Pople and K. G. Untch, *J. Am. Chem. Soc.*, **1966**, 88, 4811-4815.
155. U. Fleischer, W. Kutzelnigg, P. Lazzeretti and V. Muehlenkamp, *J. Am. Chem. Soc.*, **1994**, 116, 5298-5306.
156. R. J. Hunadi, *J. Am. Chem. Soc.*, **1983**, 105, 6889-6895.
157. R. A. Pascal, C. G. Winans and D. Van Engen, *J. Am. Chem. Soc.*, **1989**, 111, 3007-3010.
158. P. v. R. Schleyer, C. Maerker, A. Dransfeld, H. Jiao and N. J. R. v. E. Hommes, *J. Am. Chem. Soc.*, **1996**, 118, 6317-6318.
159. G. Subramanian, P. von Ragué Schleyer and H. Jiao, *Angew. Chem. int. Ed. Engl.*, **2003**, 35, 2638-2641.
160. H. Jiao, R. Schleyer Paul von, R. Warmuth, N. Houk Kendall and R. Beno Brett, *Angew. Chem. int. Ed. Engl.*, **1997**, 36, 2761-2764.

161. A. A. Fokin, H. Jiao and P. v. R. Schleyer, *J. Am. Chem. Soc.*, **1998**, 120, 9364-9365.
162. T. K. Zywietz, H. Jiao, P. v. R. Schleyer and A. de Meijere, *J. Org. Chem.*, **1998**, 63, 3417-3422.
163. S. Patchkovskii and W. Thiel, *J. Mol. Model.*, **2000**, 6, 67-75.
164. M. Bühl, *Chem. Eur. J.*, **1998**, 4, 734-739.
165. M. Ferrer Santiago and M. Molina Jose, *J. Comput. Chem.*, **1999**, 20, 1412-1421.
166. M. L. McKee, Z.-X. Wang and P. v. R. Schleyer, *J. Am. Chem. Soc.*, **2000**, 122, 4781-4793.
167. A. Hirsch, Z. Chen and H. Jiao, *Angew. Chem. Int. Ed.*, **2000**, 39, 3915-3917.
168. M. Bühl and A. Hirsch, *Chem. Rev.*, **2001**, 101, 1153-1184.
169. P. v. R. Schleyer, B. Kiran, D. V. Simion and T. S. Sorensen, *J. Am. Chem. Soc.*, **2000**, 122, 510-513.
170. H. Jiao and R. Schleyer Paul von, *J. Phys. Org. Chem.*, **1998**, 11, 655-662.
171. F. P. Cossío, I. Morao, H. Jiao and P. v. R. Schleyer, *J. Am. Chem. Soc.*, **1999**, 121, 6737-6746.
172. D. Sawicka, S. Wilsey and K. N. Houk, *J. Am. Chem. Soc.*, **1999**, 121, 864-865.
173. M. Manoharan, F. De Proft and P. Geerlings, *J. Org. Chem.*, **2000**, 65, 7971-7976.
174. R. de Lera Angel, R. Alvarez, B. Lecea, A. Torrado and P. Cossío Fernando, *angew. Chem. Int. Ed.*, **2001**, 40, 557-561.
175. S. P. Verevkin, H.-D. Beckhaus, C. Rüchardt, R. Haag, S. I. Kozhushkov, T. Zywietz, A. de Meijere, H. Jiao and P. v. R. Schleyer, *J. Am. Chem. Soc.*, **1998**, 120, 11130-11135.
176. R. Islas, G. Martínez-Guajardo, J. O. C. Jiménez-Halla, M. Solà and G. Merino, *J. Chem. Theory Comput.*, **2010**, 6, 1131-1135.
177. J. I. Wu, I. Fernández and P. v. R. Schleyer, *J. Am. Chem. Soc.*, **2013**, 135, 315-321.
178. P. Lazzeretti, *Phys. Chem. Chem. Phys.*, **2004**, 6, 217-223.
179. J. Poater, M. Solà, R. G. Viglione and R. Zanasi, *J. Org. Chem.*, **2004**, 69, 7537-7542.
180. H. Fallah-Bagher-Shaidaei, C. S. Wannere, C. Corminboeuf, R. Puchta and P. v. R. Schleyer, *Org. Lett.*, **2006**, 8, 863-866.
181. C. Corminboeuf, T. Heine, G. Seifert, P. v. R. Schleyer and J. Weber, *Phys. Chem. Chem. Phys.*, **2004**, 6, 273-276.

182. N. S. Mills and K. B. Llagostera, *J. Org. Chem.*, **2007**, 72, 9163-9169.
183. R. V. Williams, J. R. Armantrout, B. Twamley, R. H. Mitchell, T. R. Ward and S. Bandyopadhyay, *J. Am. Chem. Soc.*, **2002**, 124, 13495-13505.
184. J. Aihara, *J. Am. Chem. Soc.*, **1978**, 100, 3339-3342.
185. P. K. Chattaraj and D. R. Roy, *J. Phys. Chem. A*, **2007**, 111, 4684-4696.
186. S. Osuna, J. Poater, J. M. Bofill, P. Alemany and M. Solà, *Chem. Phys. Lett.*, **2006**, 428, 191-195.
187. H. J. Dauben, J. D. Wilson and J. L. Laity, *J. Am. Chem. Soc.*, **1968**, 90, 811.
188. W. Haberditzl, *Angew. Chem. int. Ed. Engl.*, **2003**, 5, 288-298.
189. T. G. Schmalz, C. L. Norris and W. H. Flygare, *J. Am. Chem. Soc.*, **1973**, 95, 7961-7967.
190. L. Pauling, *J. Chem. Phys.*, **1936**, 4, 673.
191. D. B. Chesnut, *Chem. Phys.*, **1998**, 231, 1.
192. J. E. Gready, P. M. Hatton and S. Sternhell, *J. Heterocycl. Chem.*, **1992**, 29, 935.
193. M. Witanowski and Z. Biedrzyka, *Magn. Res. Chem.*, **1994**, 32, 62.
194. F. A. L. Anet and G. E. Schenck, *J. Am. Chem. Soc.*, **1971**, 93, 556-557.
195. H. J. Dauben, J. D. Wilson and J. L. Laity, *J. Am. Chem. Soc.*, **1969**, 91, 1991.
196. D. P. Craig, *Non-Benzenoid Aromatic Compounds*, Interscience, New York, 1956.
197. D. P. Craig, *Theoretical Organic Chemistry*, Kekule Symp. Butterworth, London, 1959.
198. H. J. Dauben, D. J. D. Wilson and J. L. Laity, *Non-Benzenoid Aromatics*, Academic Press, 1971.
199. J. A. Pople, *J. Chem. Phys.*, **1956**, 24, 1111-1111.
200. D. W. Davies, *The theory of electric and magnetic properties of molecules*, Wiley, London, 1967.
201. W. H. Flygare and R. C. Benson, *J. Am. Chem. Soc.*, **1970**, 92, 7523-7529.
202. E. Matito, M. Duran and M. Solà, *J. Chem. Phys.*, **2005**, 122, 014109.
203. M. A. Spackman and R. F. Stewart, *Chemical Applications of Atomic and Molecular Electrostatic Potentials*, Plenum, New York, 1981.
204. Y. Jiang and H. Zhang, *Theor. Chim. Acta.*, **1989**, 75, 279-297.
205. Z. Zhou and R. G. Parr, *J. Am. Chem. Soc.*, **1989**, 111, 7371-7379.

206. E. Scrocco and J. Tomasi, *Adv. Quantum Chem.*, **1978**, 11, 116.
207. T. Brinck, S. Murray Jane and P. Politzer, *Int. J. Quantum Chem.*, **1993**, 48, 73-88.
208. P. Politzer, S. Murray Jane and C. Concha Monica, *Int. J. Quantum Chem.*, **2002**, 88, 19-27.
209. P. Politzer and J. S. Murray, *Theor. Chem. Acc.*, **2002**, 108, 134.
210. C. H. Suresh and S. R. Gadre, *J. Org. Chem.*, **1999**, 64, 2505-2512.
211. S. R. Gadre and S. S. Pundlik, *J. Am. Chem. Soc.*, **1995**, 117, 9559-9563.
212. C. H. Suresh and S. R. Gadre, *J. Phys. Chem. A*, **2007**, 111, 710-714.
213. C. H. Suresh, N. Koga and S. R. Gadre, *Organometallics*, **2000**, 19, 3008-3015.
214. C. H. Suresh, N. Koga and S. R. Gadre, *J. Org. Chem.*, **2001**, 66, 6883-6890.
215. S. R. Gadre, S. V. Bapat, K. Sundararajan and I. H. Shrivastava, *Chem. Phys. Lett.*, **1990**, 175, 307-312.
216. S. R. Gadre, S. A. Kulkarni and I. H. Shrivastava, *J. Chem. Phys.*, **1992**, 96, 5253-5260.
217. J. S. Murray, J. M. Seminario and P. Politzer, *Int. J. Quantum Chem.*, **1994**, 94, 575.
218. K. P. Vijayalakshmi and C. H. Suresh, *New J. Chem.*, **2010**, 34, 2132-2138.
219. C. H. Suresh and M. J. Ajitha, *J. Org. Chem.*, **2013**, 78, 3918-3924.
220. C. H. Suresh, P. Alexander, K. P. Vijayalakshmi, P. Sajith and S. R. Gadre, *Physical Chemistry Chemical Physics*, **2008**, 10, 6492-6499.
221. K. P. Vijayalakshmi and C. H. Suresh, *Org. Biomol. Chem.*, **2008**, 6, 4384-4390.
222. K. P. Vijayalakshmi and H. Suresh Cherumuttathu, *J. Comput. Chem.*, **2008**, 29, 1808-1817.
223. K. P. Vijayalakshmi and C. H. Suresh, *New Journal of Chemistry*, **2010**, 34, 2132-2138.
224. C. H. Suresh and S. R. Gadre, *Journal of Organic Chemistry*, **1999**, 64, 2505-2512.
225. S. R. Gadre and C. H. Suresh, *J. Org. Chem.*, **1997**, 62, 2625-2627.
226. M. Haeberlein, J. S. Murray, T. Brinck and P. Politzer, *Can. J. Chem.*, **1992**, 70, 2209-2214.
227. J. S. Murray, T. Brinck and P. Politzer, *J. Mol. Struct. (Theochem)*, **1992**, 255, 271-281.
228. P. Politzer, L. Abrahmsen and P. Sjoberg, *J. Am. Chem. Soc.*, **1984**, 106, 855-860.

229. T. Brinck, J. S. Murray and P. Politzer, *Mol. Phys.*, **1992**, 76, 609-617.
230. B. Galabov, V. Nikolova and S. Ilieva, *Chem. Eur. J.*, **2013**, 19, 5149-5155.
231. Y. Zhao and D. G. Truhlar, *J. Am. Chem. Soc.*, **2007**, 129, 8440-8442.
232. Y. Ruiz-Morales, *J. Phys. Chem. A*, **2002**, 106, 11283-11308.
233. J.-i. Aihara, *J. Phys. Chem. A*, **1999**, 103, 7487-7495.
234. J.-i. Aihara, *Theor. Chem. Acc.*, **1999**, 102, 134-138.
235. M. Yoshida and J.-i. Aihara, *Phys. Chem. Chem. Phys.*, **1999**, 1, 227-230.
236. R. G. Parr and Z. Zhou, *Acc. Chem. Res.*, **1993**, 26, 256-258.
237. Z. Zhou, R. G. Parr and J. F. Garst, *Tetrahedron Lett.*, **1988**, 29, 4843-4846.
238. D. E. Manolopoulos, J. C. May and S. E. Down, *Chem. Phys. Lett.*, **1991**, 181, 105-111.
239. R. C. Haddon and T. Fukunaga, *Tetrahedron Lett.*, **1980**, 21, 1191-1192.
240. R. C. Haddon, *J. Am. Chem. Soc.*, **1979**, 101, 1722.
241. M. P. Cava and M. J. Mitchell, *Cyclobutadiene and Related Compounds*, Academic, New York, 1967.
242. M. J. S. Dewar, *Angew. Chem. Int. Ed.*, **1971**, 10, 761.
243. M. J. S. Dewar, *Angew. Chem.*, **1971**, 83, 859.
244. K. P. C. Vollhardt and L. S. Yee, *J. Am. Chem. Soc.*, **1977**, 99, 2010.
245. I. Willner and M. Rabinovitz, *J. Org. Chem.*, **1980**, 45, 1628.
246. A. Minsky, A. Y. Meyer and M. Rabinovitz, *Tetrahedron*, **1985**, 41, 785.
247. Y. Cohen, J. Klein and M. Rabinovitz, *J. Chem. Soc.; Chem. Commun.*, **1986**.
248. Y. Cohen, N. H. Roelofs, G. Reinhardt, L. T. Scott and M. Rabinovitz, *J. Org. Chem.*, **1987**, 52, 4207.
249. P. H. M. Budzelaar, D. Cremer, M. Wallasch, E. U. Wurthwein and P. v. R. Schleyer, *J. Am. Chem. Soc.*, **1987**, 109, 6290.
250. O. Sinanoğlu, *Int. J. Quantum Chem. Symp.*, **1988**, 22, 143.
251. O. Sinanoğlu, *Tetrahedron Lett.*, **1988**, 889.
252. J. Cioslowski, *Int. J. Quantum Chem.*, **1987**, 31, 581.
253. L. Komorowski, *Chem. Phys.*, **1987**, 114, 55.
254. L. Komorowski, in *Structure and Bonding*, ed. K. D. Sen, Springer-Verlag., Berlin, Heidelberg., 1993, vol. 80, p. 45.

255. C. W. Bird, *Tetrahedron*, **1985**, 41, 1409.
256. C. W. Bird, *Tetrahedron*, **1986**, 42, 89.
257. C. W. Bird, *Tetrahedron*, **1992** 48, 335.
258. C. W. Bird, *Tetrahedron*, **1996**, 52, 9945.
259. K. Jug, *J. Org. Chem.*, **1983**, 48, 1344.
260. S. T. Howard and T. M. Krygowski, *Can. J. Chem.*, **1997**, 75, 1174.
261. G. P. Bean, *J. Org. Chem.*, **1998**, 63, 2497.
262. N. Sadlej-Sosnowska, *ibid*, **2001**, 66, 8737.
263. A. Savin, R. Nesper, S. Wengert and T. F. Fassler, *Angew. Chem. Int. Ed.*, **1997**, 36, 1809.
264. A. D. Becke and K. E. Edgecombe, *J. Chem. Phys.*, **1990**, 92, 5397.
265. D. B. Chesnut and L. J. Bartolotti, *Chem. Phys.*, **2000**, 253, 1.
266. J. C. Santos, W. Tiznado, R. Contreras and P. Fuentealba, *J. Chem. Phys.*, **2004**, 120, 1670.
267. C. Lepetit, M. B. Nielsen, F. Diederich and R. Chauvin, *Chem. Eur. J.*, **2003**, 9, 5056.
268. R. F. W. Bader and M. E. Stephens, *J. Am. Chem. Soc.*, **1975**, 97, 7391.
269. X. Fradera, M. A. Austen and R. F. W. Bader, *J. Phys. Chem. A*, **1999**, 103, 304.
270. D. B. Chesnut and L. J. Bartolotti, *Chem. Phys.*, **2000**, 257, 175-181.
271. R. F. W. Bader, A. Streitwieser, A. Neuhaus, K. E. Laidig and P. Speers, *J. Am. Chem. Soc.*, **1996**, 118, 4959-4965.
272. R. F. W. Bader, *Acc. Chem. Res.*, **1985**, 18, 9.
273. R. F. W. Bader, *Atoms In Molecules: A Quantum Theory*, Clarendon, Oxford, 1990.
274. R. F. W. Bader, *Chem. Rev.*, **1991**, 91, 893.
275. M. Giambiagi, M. S. de Giambiagi, C. D. dos Santos and A. P. de Figueiredo, *Phys. Chem. Chem. Phys.*, **2000**, 2, 3381.
276. J. Cioslowski, E. Matito and M. Sola, *J. Phys. Chem. A*, **2007**, 111, 6521.
277. P. Bultinck, M. Rafat, R. Ponec, B. Van Gheluwe, R. Carbó-Dorca and P. Popelier, *J. Phys. Chem. A*, **2006**, 110, 7642-7648.
278. A. Jablonski, *Nature*, **1933**, 131, 839.
279. E. Runge and E. K. U. Gross, *Phys. Rev. Lett.*, **1984**, 52, 997-1000.

280. M. E. CASIDA, in *Recent Advances in Density Functional Methods*, WORLD SCIENTIFIC, 2011, pp. 155-192.
281. R. E. Stratmann, G. E. Scuseria and M. J. Frisch, *J. Chem. Phys.*, **1998**, 109, 8218-8224.
282. R. Bauernschmitt and R. Ahlrichs, *Chem. Phys. Lett.*, **1996**, 256, 454-464.
283. N. Banerji, E. Gagnon, P.-Y. Morgantini, S. Valouch, A. R. Mohebbi, J.-H. Seo, M. Leclerc and A. J. Heeger, *J. Phys. Chem. C*, **2012**, 116, 11456-11469.
284. J. Cornil, I. Gueli, A. Dkhissi, J. C. Sancho-Garcia, E. Hennebicq, J. P. Calbert, V. Lemaur, D. Beljonne and J. L. Brédas, *J. Chem. Phys.*, **2003**, 118, 6615-6623.
285. J. C. Sancho-García, C. L. Foden, I. Grizzi, G. Greczynski, M. P. de Jong, W. R. Salaneck, J. L. Brédas and J. Cornil, *J. Phys. Chem. B*, **2004**, 108, 5594-5599.
286. B. P. Karsten, L. Viani, J. Gierschner, J. Cornil and R. A. J. Janssen, *J. Am. Chem. Soc.*, **2008**, 112, 10764-10773.
287. B. P. Karsten, J. C. Bijleveld, L. Viani, J. Cornil, J. Gierschner and R. A. J. Janssen, *J. Mater. Chem.* , **2009**, 19, 5343-5350.
288. B. P. Karsten, L. Viani, J. Gierschner, J. Cornil and R. A. J. Janssen, *J. Phys. Chem. A*, **2009**, 113, 10343-10350.
289. A. Köhler and D. Beljonne, *Adv. Funct. Mater.*, **2004**, 14, 11-18.
290. D. Veldman, C. J. Meskers Stefan and A. J. Janssen René, *Adv. Funct. Mater.*, **2009**, 19, 1939-1948.
291. A. Köhler and H. Bässler, *Mater. Sci. Eng. R.*, **2009**, 66, 71-109.
292. R. Schueppel, K. Schmidt, C. Uhrich, K. Schulze, D. Wynands, J. L. Brédas, E. Brier, E. Reinold, H. B. Bu, P. Baeuerle, B. Maennig, M. Pfeiffer and K. Leo, *Phys. Rev. B*, **2008**, 77, 085311.
293. D. Hait, T. Zhu, D. P. McMahon and T. Van Voorhis, *J. Chem. Theory Comput.*, **2016**, 12, 3353-3359.
294. W. J. Hehre, *A Guide to Molecular Mechanics and Quantum Chemical Calculations*, Wavefunction, Inc., Irvine, California, 2003.
295. K. R. Glaesemann, M. S. Gordon and H. Nakano, *Phys. Chem. Chem. Phys.*, **1999**, 1, 967-975.

296. K. R. Glaesemann, N. Govind, S. Krishnamoorthy and K. Kowalski, *J. Phys. Chem. A*, **2010**, 114, 8764-8771.
297. A. Dreuw and M. Head-Gordon, *Chem. Rev.*, **2005**, 105, 4009-4037.
298. P. J. Knowles and H.-J. Werner, *Theor. Chim. Act.*, **1992**, 84, 95-103.
299. J. B. Foresman, M. Head-Gordon, J. A. Pople and M. J. Frisch, *J. Phys. Chem.*, **1992**, 96, 135-149.
300. C. Adamo and D. Jacquemin, *Chem. Soc. Rev.*, **2013**, 42, 845-856.
301. D. Guillaumont and S. Nakamura, *Dyes Pigm.*, **2000**, 46, 85-92.
302. A. Matsuura, H. Sato, W. Sotoyama, A. Takahashi and M. Sakurai, *J. Mol. Struct. (Theochem)*, **2008**, 860, 119-127.
303. D. Jacquemin, E. A. Perpète, I. Ciofini, C. Adamo, R. Valero, Y. Zhao and D. G. Truhlar, *J. Chem. Theory Comput.*, **2010**, 6, 2071-2085.
304. L. L. Walkup, K. C. Weerasinghe, M. Tao, X. Zhou, M. Zhang, D. Liu and L. Wang, *J. Phys. Chem. C*, **2010**, 114, 19521-19528.
305. D. Jacquemin, E. A. Perpète, I. Ciofini and C. Adamo, *Theor. Chem. Accounts*, **2008**, 120, 405-410.
306. F. Furche and R. Ahlrichs, *J. Chem. Phys.*, **2002**, 117, 7433-7447.
307. C. Risko, M. D. McGehee and J.-L. Bredas, *Chem. Sci.*, **2011**, 2, 1200-1218.
308. S. Xu, Y. Yuan, X. Cai, C.-J. Zhang, F. Hu, J. Liang, G. Zhang, D. Zhang and B. Liu, *Chem. Sci.*, **2015**, 6, 5824-5830.
309. S. Naskar and M. Das, *ACS Omega*, **2017**, 2, 1795-1803.
310. G. J. P. Deblonde, A. Moncomble, G. Cote, S. Belair and A. Chagnes, *RSC Advances*, **2015**, 5, 7619-7627.
311. M. E. Beck, *Int. J. Quantum. Chem.*, **2005**, 101, 683-689.
312. D. Jacquemin, E. Brémond, I. Ciofini and C. Adamo, *J. Phys. Chem. Lett.*, **2012**, 3, 468-471.
313. D. C. Young, in *Computational Chemistry*, John Wiley & Sons, Inc., 2002, pp. 1-4.
314. E. Schrödinger, *Ann. Phys.*, **1926**, 79, 361.
315. B. M. Oppenheimer, *Ann. Phys.*, **1927**, 84, 457.
316. R. Hartree, R., *Proc. Cambridge Phil. Soc.*, **1928**, 24.
317. J. C. Slater, *Phys. Rev.*, **1930**, 35, 210.

318. V. Fock, *Z. Phys.*, **1930**, 61, 126.
319. G. G. Hall, *Proc. Roy. Soc. (London) A*, **1951**, 205, 541.
320. C. C. J. Roothaan, *Rev. Mod. Phys.*, **1951**, 23, 69-89.
321. A. Szabo and N. A. Ostlung, *Modern quantum chemistry: Introduction to advanced electronic structure theory*, McGraw-Hill, NewYork, 1989.
322. C. Møller and M. S. Plesset, *Phys. Rev.*, **1934**, 46, 618.
323. C. D. Sherrill and H. F. Schaefer, *Adv. Quantum Chem.*, **1999**, 34, 143.
324. R. J. Bartlett, *J. phys. Chem.*, **1989**, 93, 1697.
325. L. Brillouin, *Actualities Sci. Ind.*, **1934**, 159, 37.
326. H. P. Kelly, *Advances in chemical physics*, John Wiley & Sons, New York, 1969.
327. J. A. Pople, J. S. Binkley and R. Seeger, *Int. J. Quantum Chem. Symp.*, **1976**, 10, 1.
328. J. A. Pople and D. L. Beveridge, *Approximate Molecular Orbital Theory*, McGraw-Hill, New York, 1970.
329. J. J. P. Stewart, *Rev. Comp. Chem.*, **1990**, 1, 45.
330. E. Fermi, *Rend. Accad. Nazl. Lincei*, **1927**, 6, 602.
331. E. Fermi, *Z. Phys.* , **1928**, 48, 73.
332. L. H. Thomas, *Proc. Cambridge Phil. Soc.*, **1927**, 23, 542.
333. P. K. Hohenerg, W., *Phys. Rev. B*, **1964**, 136, 864.
334. W. Kohn and L. J. Sham, *Phys. Rev.*, **1965**, 140, A1133-A1138.
335. P. Hohenberg and W. Kohn, *Phys. Rev.*, **1964**, 136, B864-B871.
336. X. Xu and W. A. Goddard, *J. Phys. Chem. A*, **2004**, 108, 8495.
337. P. A. M. Dirac, *Proc. Cambridge Phil. Roy. Soc.*, **1930**, 26, 376.
338. E. Fermi, *Rend. Accd. Nazl. Lincei*, **1927**, 6, 602.
339. J. C. Slater, *Phys. Rev.*, **1951**, 81, 385.
340. S. H. Vosco, L. Wilk and M. Nusair, *Can. J. Chem.*, **1980**, 58, 1200.
341. J. P. Perdew and Y. Wang, *Phys. Rev. B*, **1986**, 33, 8800.
342. A. D. Becke, *Phys. Rev. A*, **1988**, 38, 3098-3100.
343. J. P. Perdew, *Phys. Rev. B*, **1986**, 33, 8822.
344. J. P. Perdew and Y. Wang, *Phys. Rev. B*, **1992**, 45, 13244.
345. C. Lee, W. Yang and R. G. Parr, *Phys. Rev. B*, **1988**, 37, 785-789.
346. J. P. Perdew, S. Burke and M. Ernzerhof, *Phys. Rev. Lett.*, **1996**, 77, 3865.

347. A. D. Becke, *J. Chem. Phys.*, **1993**, 98, 5648-5652.
348. R. Pevereti and D. G. Truhlar, *J. Phys. Chem. Lett.*, **2011**, 2, 2810.
349. R. Pevereti and D. G. Truhlar, *Phys. Chem. Chem. Phys.*, **2012**, 14, 13171.
350. J. Zhao and D. G. Truhlar, *J. Chem. Theory Comput.*, **2005**, 1, 415.
351. J. Zhao and D. G. Truhlar, *J. Phys. Chem. A*, **2005**, 109, 5656.
352. Y. Zhao and D. G. Truhlar, *J. Chem. Phys.*, **2006**, 125, 194101.
353. J. Zhao and D. G. Truhlar, *J. Phys. Chem. A*, **2006**, 110, 13126.
354. Y. Zhao and D. G. Truhlar, *Theor. Chem. Acc.*, **2008**, 120, 215-247.
355. J. Zhao and D. G. Truhlar, *J. Chem. Theory Comput.*, **2008**, 4, 1849.
356. Y. Zhao, N. E. Schultz and D. G. Truhlar, **2005**.
357. Y. Zhao, N. E. Schultz and D. G. Truhlar, *J. Chem. Theory Comput.*, **2006**, 2, 364-382.
358. Y. Wang, X. Jin, H. S. Yu, D. G. Truhlar and X. He, *Proc. Nat. Acad. Sci. USA*, **2017**, 114, 8487.
359. R. Peverati and D. G. Truhlar, *J. Chem. Theory Comput.*, **2012**, 8, 2310-2319.
360. R. Peverati and D. G. Truhlar, *Phys. Chem. Chem. Phys.*, **2012**, 14, 13171-13174.
361. R. Peverati and D. G. Truhlar, *Phys. Chem. Chem. Phys.*, **2012**, 14, 16187-16191.
362. H. S. Yu, X. He, S. L. Li and D. G. Truhlar, *Chem. Sci.*, **2016**, 7, 5032-5051.
363. H. S. Yu, X. He and D. G. Truhlar, *J. Chem. Theory Comput.*, **2016**, 12, 1280-1293.
364. R. Singh and B. M. Deb, *Phys. Rep.*, **1999**, 311, 50.
365. P. A. M. Dirac, *Math. Proc. Camb. Philos. Soc.*, **1930**, 26, 376-385.
366. J. Frenkel, *Wave mechanics, Advanced General Theory*, Clarendon, Oxford, 1934.
367. P. W. Langhoff, S. T. Epstein and M. Karplus, *Rev. Mod. Phys.*, **1972**, 44, 602-644.
368. G. Vignale, *Phys. Rev. A*, **2008**, 77, 062511.
369. A. Zangwill and P. Soven, *Phys. Rev. A*, **1980**, 21, 1561-1572.
370. R. Burcl, R. D. Amos and N. C. Handy, *Chem. Phys. Lett.*, **2002**, 355, 8-18.
371. M. Odelius, D. Laikov and J. Hutter, *J. Mol. Struct. (THEOCHEM)*, **2003**, 630, 163-175.
372. A. Köhn and C. Hättig, *J. Chem. Phys.*, **2003**, 119, 5021-5036.
373. H. H. Heinze, A. Görling and N. Rösch, *J. Chem. Phys.*, **2000**, 113, 2088-2099.

374. N. Sadlej-Sosnowska, W. P. Ozimiński and A. Krówczyński, *Chem. Phys.*, **2003**, 294, 65-72.
375. D. Delaere, M. T. Nguyen and L. G. Vanquickenborne, *J. Phys. Chem. A*, **2003**, 107, 838-846.
376. K. A. Nguyen, J. Kennel and R. Pachter, *J. Chem. Phys.*, **2002**, 117, 7128-7136.
377. D. Delaere, M. Tho Nguyen and L. G. Vanquickenborne, *Chem. Phys. Lett.*, **2001**, 333, 103-112.
378. H. M. Senn and W. Thiel, *Angew. Chem. Int. Ed.*, **2009**, 48, 1198-1229.
379. A. Warshel and M. Levitt, *J. Mol. Biol.*, **1976**, 103, 227-249.
380. J. Gao, *Rev. Comp. Chem.*, **1996**, 7, 119.
381. T. Z. Mordarsini and W. Thiel, *Chimia*, **1998**, 52, 288.
382. F. Maseras and K. Morokuma, *J. Comput. Chem.*, **1995**, 16, 1170-1179.
383. S. Humbel, S. Sieber and K. Morokuma, *J. Chem. Phys.*, **1996**, 105, 1959-1967.
384. S. Dapprich, I. Komáromi, K. S. Byun, K. Morokuma and M. J. Frisch, *J. Mol. Struct. (Theochem)*, **1999**, 461-462, 1-21.
385. T. Schlick, *Molecular Modeling and Simulation*, Springer-Verlag, New York, 2002.
386. D. C. Rapaport, *The Art of Molecular Dynamics Simulation*, Cambridge University Press, Cambridge, 2004.
387. M. P. Allen and D. J. Tildesley, *Computer simulation of liquids*, Clarendon Press, 1989.
388. M. C. Payne, M. P. Teter, D. C. Allan, T. A. Arias and J. D. Joannopoulos, *Rev. Mod. Phys.*, **1992**, 64, 1045-1097.
389. M. E. Tuckerman, P. J. Ungar, T. von Rosenvinge and M. L. Klein, *J. Phys. Chem.*, **1996**, 100, 12878-12887.
390. R. Car and M. Parrinello, *Phys. Rev. Lett.*, **1985**, 55, 2471-2474.
391. J. Doll and D. L. Freeman, *IEEE Comput. Sci. Eng.*, **1994**, 1, 22.
392. P. K. Weiner and P. A. Kollman, *J. Comput. Chem.*, **1981**, 2, 287-303.
393. D. B. Boyd and K. B. Lipkowitz, *J. Chem. Educ.*, **1982**, 59, 269.
394. L. C. K. Allen, A. M., *Rev. Modern. Phys.*, **1960**, 32.
395. S. F. Boys, *Proc. R. Soc. Lond. A* **1950**, 200, 542.

396. D. D. Feller, E. R., *Basis Sets for Ab Initio Molecular Orbital Calculations and Intermolecular Interactions*, VCH, New York, 1990.
397. B. Pullman, *Int. J. Quantum Biol. Symp.*, **1990**, 17, 609.
398. S. R. Gadre, S. V. Bapat, K. Sundararajan and I. H. Shrivastava, *Chem. Phys. Lett.*, **1990**, 175, 307-312.
399. M. Leboeuf, A. M. Köster, K. Jug and D. R. Salahub, *J. Chem. Phys.*, **1999**, 111, 4893-4905.
400. S. R. Gadre and R. N. Shirsat, *Electrostatics of Atoms and Molecules*, Univesities Press, Hyderabad, 2000.
401. A. Julg and P. Françoise, *Theor. Chim. Acta.*, **1967**, 7, 249.
402. G. A. Jeffrey, J. R. Ruble, R. K. McMullan and J. A. Pople, *Proc. R. Soc. London*, **1987**, 47, A414.
403. T. M. Krygowski and M. Cyrański, *Tetrahedron*, **1996**, 52, 1713-1722.
404. T. M. Krygowski and M. Cyrański, *Tetrahedron*, **1996**, 52, 10255-10264.
405. F. Feixas, E. Matito, J. Poater and M. Solà, *J. Phys. Chem. A*, **2007**, 111, 4513-4521.
406. R. Ditchfield, *Mol. Phys.*, **1974**, 27, 789-807.
407. K. Wolinski, J. F. Hinton and P. Pulay, *J. Am. Chem. Soc.*, **1990**, 112, 8251-8260.
408. J. R. Cheeseman, G. W. Trucks, T. A. Keith and M. J. Frisch, *J. Chem. Phys.*, **1996**, 104, 5497-5509.
409. P. v. R. Schleyer, M. Manoharan, Z.-X. Wang, B. Kiran, H. Jiao, R. Puchta and N. J. R. van Eikema Hommes, *Org. Lett.*, **2001**, 3, 2465-2468.

# Chapter 2

# Dihydropyrazine Annulated Linear Polyacenes

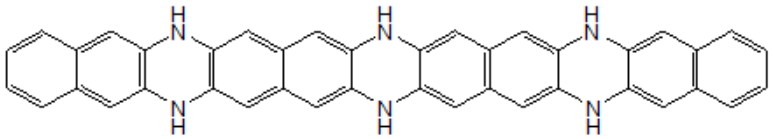

Dihydropyrazine annulated to naphthalene core

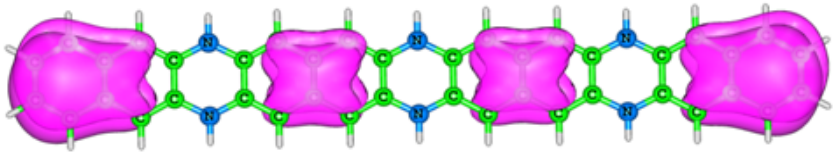

Electrostatic potential reveals electronic features of naphthalene core

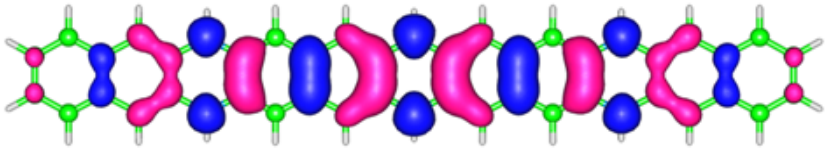

HOMO shows delocalization of N-lone pairs

## *2.1. Abstract*

*Linear polyacenes (LPA) beyond pentacene are highly unstable and their application potential in optoelectronics field is very limited. On the basis of theoretical studies at M06L/6-311++G(d,p) level DFT, we show that annulating dihydropyrazine units to LPA cores can yield large LPA mimics. This strategy enhances the aromaticity of the LPA core and also provides a way to modulate HOMO-LUMO energy gap by choosing appropriate LPA core and extend of dihydropyrazine annulation. The study is conducted for LPA mimics containing up to six dihydropyrazine units annulated to benzene ($pB_1$ – $pB_6$), naphthalene ($pN_1$ – $pN_6$), anthracene ($pA_1$ – $pA_6$) and tetracene ($pT_1$ – $pT_6$) cores. The longest of them $pT_6$ contains 34 linearly connected six-membered rings. Dehydrogenation energy ($E_{dh}$) of the N-heterocycles of the LPA mimics showed endothermic character and indicated their higher stability than the dehydrogenated N-heteroacenes. The total $E_{dh}$ ($\Sigma E_{dh}$) is proportional to the increase in the number of heterocycles and increase in the size of the LPA core. Aromaticity of individual rings of all the LPA mimics is assessed on the basis of harmonic oscillator model of aromaticity (HOMA) and nucleus independent chemical shift (NICS) parameters. Both parameters showed strong linear correlation with $\Sigma E_{dh}$, confirming the geometric, magnetic and energetic criteria of aromaticity. The electronic features of the LPA mimics assessed by analysing molecular electrostatic potential topography and molecular orbitals have shown that LPA cores retain the reactivity of the parent LPA. Further, significant mixing of the N-lone pairs of the heterocycle with the carbon π-orbitals improves aromaticity and decreases HOMO-LUMO energy gap. The excited state properties of the LPA mimics were also analysed, which includes the singlet-triplet energy gap, geometries and absorption spectral properties. The tuning of electronic properties is evident from these calculations. The theoretically calculated light harvesting efficiency of these designed pN, pA and pT series of systems are very high in the range of 0.9, while for pB series the efficiency is not much prominent.*

## 2.2. Introduction

Linear polyacenes (LPAs), aromatic hydrocarbons composed of linearly fused benzene rings,[1] possess attractive optical and electronic properties suitable for nanotechnology applications, organic electronics,[2] lithium ion batteries,[3] ferromagnetic materials,[4] etc. The optoelectronic application potential of these

molecules is linked to their ability to tune the HOMO– LUMO gap with the increase in the oligomer size,[5, 6] strong solid state two dimensional interactions in the electronic level,[5] and charge mobility.[5, 7, 8] Among the LPAs, pentacene is widely studied due to its optical and semiconducting properties suitable for applications in the area of organic field effect transistors. Though LPA systems longer than pentacene such as heptacene, octacene and nonacene have been synthesized on a polymer matrix by photogeneration, the application potential of their p-type semiconducting properties is very limited due to chemical instability.[9-11] According to Clar's theory, a LPA system is inherently more reactive with the increase in its length due to the phenomenon of aromatic dilution.[12, 13] Clar's rule of aromatic sextets is a very powerful tool to describe the properties of $sp^2$ -carbon bonded systems like polycyclic aromatic hydrocarbons (PAH).[14] Clar proposed that in the case of PAH, the structure showing the maximum number of localized sextets and the minimum number of localized double bonds is the most aromatic and most stable.[15, 16] For instance, in the isomeric 4-ring systems given in Scheme 2.1, the aromaticity follows the order tetracene < benzophenanthrene ~ chrysene < triphenylene. In the LPA topology of tetracene, one can draw only one sextet of π-electrons in Clar's formula (Scheme 2.1) whereas more than one sextet is possible for all other topologies.[17] With the increase in the length of LPAs, the aromatic character decreases as only one sextet can be delocalized for the whole system, which leads to significant double bond localization in the molecule and higher reactivity (Scheme 2.2). The arrow emanating from the sextet ring in Scheme 2.2 suggests aromatic dilution.

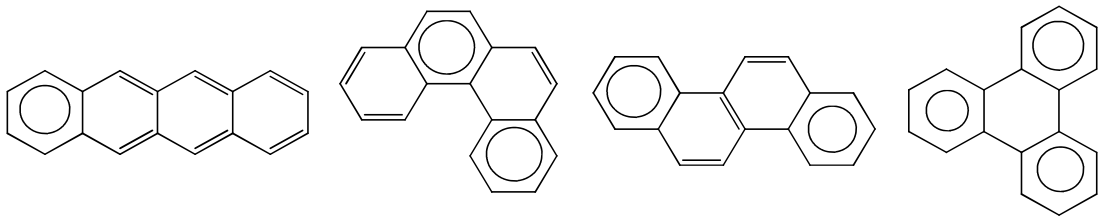

**Scheme 2.1.** Clar's sextet formula for isomeric 4-ring systems, from left tetracene, benzophenanthrene, chrysene, triphenylene.

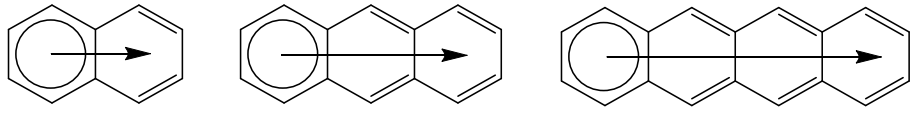

**Scheme 2.2**. Clar's notation to show the aromatic dilution in linear polyacenes.

Bultinck *et al.* derived the atoms-in-molecule based six centre index (SCI-AIM) to study the electron delocalization in a linear polyacene series and showed that

aromaticity decreases on going from outer to inner rings.[18] Aromaticity is currently described as a multidimensional phenomenon, related to the structural, electronic, magnetic and energetic properties of molecules.[19-26] A large volume of literature exists in the case of linear polyacenes dedicated to the understanding of magnetic properties and aromaticity.[27-30]

Since LPAs larger than pentacene are chemically highly unstable, one practical way to introduce more fused hexagonal rings in the chain is by designing suitable LPA mimics. This could be done by doping heteroatoms into the LPA framework.[2, 31] The nitrogen atom, isoelectronic with C–H, is an immediate choice to integrate into the acene skeleton as this could retain the π-conjugation features of the molecule.[32] Synthetic strategies utilizing condensation reactions,[33, 34] coupling reactions,[35-38] Diels-Alder reactions,[39] and oxidative coupling reactions have been utilized for the synthesis of N-heteroacenes.[40-46] Large N-heteroacenes have been known since the beginning of the 20$^{th}$ century[47, 48] and are still being intensively researched.[32, 49-56] Many diazapentacene derivatives have been successfully utilized as electronic materials in thin film transistors.[51, 57-62] Herein we propose that by fusing LPA moieties with two N–H units, large LPA mimics can be designed which could show substantial improvement in the aromatic character of the LPA core. The incorporation of the N–H units proposes the utilization of N-lone pairs to enhance the π-electron conjugation as well as the net electron content within a hexagon in the molecule. This design strategy improves the aromatic sextet distribution in the LPA mimics and suggests the formation of stable oligomeric and even polymeric long chain mimics of LPAs. In such systems, the N-heterocyclic connection between two LPA moieties is fulfilled by a 1,4-dihydropyrazine unit. Even though the existence of 1,4-dihydropyrazine derivatives was known, the successful synthesis of a carboxylic acid ester derivative was performed in the year 1969 only.[63] The structure of these alleged 1,4-dihydropyrazines came into the scene a year after that.[64] The photophysical properties of N,N-dimethyl derivatives of the above mentioned pyrazines were also widely studied.[65] The successful synthesis of the non-substituted system took one more year for completion.[66] Attempts for an easy and economical synthesis of such systems are continuing.[67-70] Linear extensions of dihydropyrazine moieties connected through benzene groups are known and among them three benzene groups interconnected by two dihydropyrazine groups are

termed tetraazapentacenes.[71, 72] Halogen substituted tetraazapentacenes have been successfully synthesized,[72] but not the unsubstituted ones. 6,13-Dihydrodibenzo[b,i]phenazine is successfully synthesised which can be used as a pentacene substitute having superior qualities.[57]

## 2.3. Computational Methods

All the molecules have been optimized using the M06L/6-311++G(d,p) level of density functional theory (DFT) as implemented in the Gaussian09 suite of programs.[73-75] All the optimized structures are confirmed as energy minima by vibrational frequency calculation. The wavefunction generated using M06L/6-311++G(d,p) is used for molecular electrostatic potential (MESP) calculations. For all the molecules, the aromaticity of each ring is quantified by computing the nucleus independent chemical shift (NICS)[76] at the ring center (NICS(0)). Also NICS at 1 Å above the ring center (NICS(1)) and the z-component of NICS at 1 Å above the ring center ($NICS_{zz}(1)$) are calculated. The harmonic oscillator model of the aromaticity (HOMA) index is calculated for all the systems using the procedure of Krygowski et al.[77] Using time-dependent density functional theory (TD-DFT)[78-81] techniques at the same level of theory, the absorption spectra of every set of molecules are calculated. TD-DFT calculation is beneficial in calculating the excited state geometries and energies.[82-85] Therefore, time-dependent optimisation is done to get the structure and energy for first triplet (T1) and first singlet (S1) state of all the molecules analysed, and the energy gap between the singlet and triplet energy were calculated. Frontier molecular orbital analysis is performed for every molecule to understand the bonding characters and HOMO-LUMO gap is measured from the calculation. The selection of the M06L functional (meta-GGA local functional with 0% Hartree–Fock (HF) exchange) is based on a previous benchmark study which showed that this method can yield a reliable geometry and interaction energy close to the CCSD(T) level accuracy for a variety of non-covalent dimers.[86] Furthermore, recent studies conducted using this method on a variety of systems have provided reliable results in agreement with high accuracy ab initio methods and dispersion-corrected DFT methods.[87-89] In order to further substantiate the use of this method to study the present set of molecules for aromaticity, we have done calculations using two more Minnesota functionals, *viz*. M06/6-311++G(d,p) (hybrid meta-GGA method with

27% HF exchange) and M06-2X/6-311++G(d,p) (hybrid meta-GGA method with 54% HF exchange) for a representative series of molecules.

## 2.4. Results and Discussion

### 2.4.1. Design Strategy

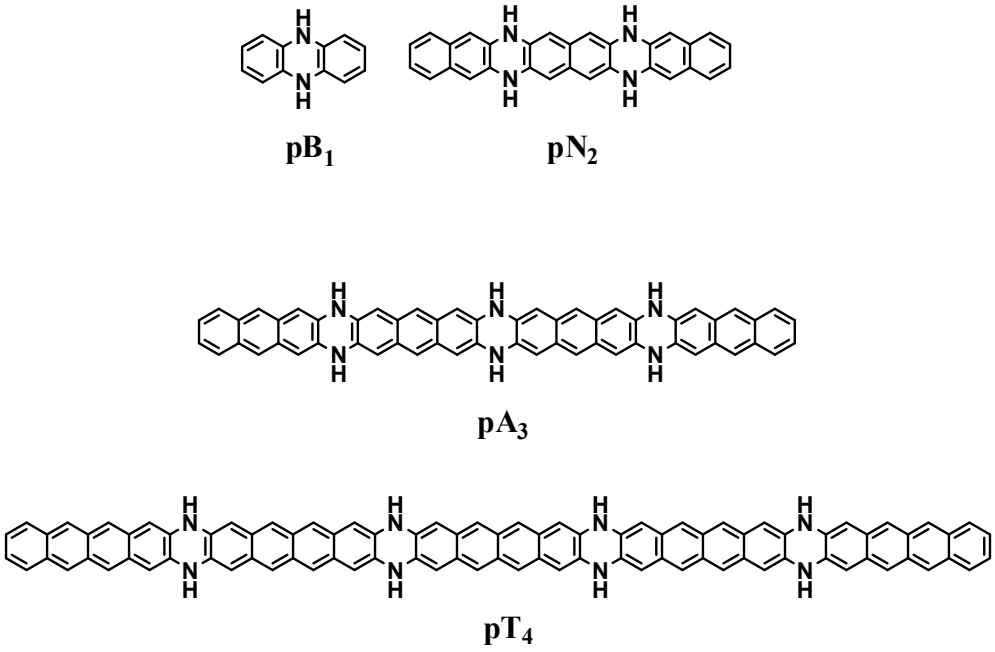


**Figure 2.1.** Representative structures of the molecules under study containing 1,4-dihydropyrazine-type N-heterocycles.

The molecular design strategy is based on improving the Clar's sextet distribution in the LPA mimics. Benzene has the perfect aromatic sextet and its six π-electrons are delocalized over the six CC bonds meaning that the number of π-electrons per CC bond ($n_\pi$) is 1. In all PAH systems, $n_\pi$ is always less than 1 and for LPA series, this value decreases with increase in the acene length. For instance, for naphthalene, anthracene, tetracene, and pentacene, $n_\pi$ is 0.91, 0.88, 0.86 and 0.85, respectively. By fusing two LPA moieties through two -NH- units, a higher LPA mimic can be designed. Every fusion point will represent a 1,4-dihydropyrazine unit. In the LPA mimic, the formal π-electron count of every N-heterocycle is 8 which is Hückel antiaromatic. However, as the $n_\pi$ electron count of the LPA decreases, electron flow from the electron rich N-heterocycle to the hydrocarbon core is expected which could stabilize the system. We use a notation that uses two letters and one number to represent each of the designed systems. The first letter in the notation is p

which represents 1,4-dihydropyrazine-type character of the N-heterocycle while the second letter B, N, A or T represents the core unit made up of benzene, naphthalene, anthracene or tetracene moieties, respectively. Further, the numbers 1, 2, 3, 4, 5 and 6 represent the number of 1,4-dihydropyrazine-type N-heterocycles in the molecule. For a system having 'n' dihydropyrazine moieties, there will be 'n+1' benzene, naphthalene, anthracene or tetracene units present. For example, $pB_1$ made up of one 1,4-dihydropyrazine-type heterocycle and two benzene cores is the dihydrophenazine molecule (Figure 2.1). Similarly $pN_2$ represents an LPA mimic made up of three naphthalene cores and two 1,4-dihydropyrazine-type N-heterocycles. The dihydropyrazine systems selected for this study are $pB_1$ – $pB_6$, $pN_1$ – $pN_6$, $pA_1$ – $pA_6$ and $pT_1$ – $pT_6$.

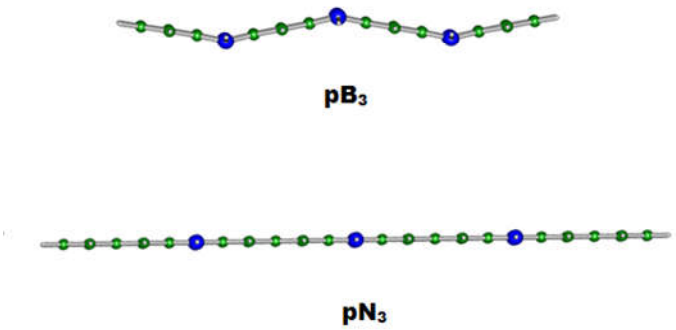


**Figure 2.2**. Representative set of molecules to distinguish zigzag pB and planar all other series.

In Table 2.1, the $n_\pi$ value of all the LPA mimics is depicted along with $n_\pi$ value of the LPA. It is very clear that annulation of an LPA with N-heterocycles improves the net electron content of the LPA mimic. This effect is dominant in pB series as all molecules retain $n_\pi$ value 1 for all benzene cores. In pN, pA and pT series, $n_\pi$ is always higher than the LPA core and it increases with increase in the length of the molecule. Hence, increase in aromatic character is expected with increase in the net electron content of the system. The molecules in pB series show a zigzag structure with respect to the orientation of the six-membered rings as shown in Figure 2.2 while all other systems exhibit a planar structure. In pB series, pyramidalisation at NH group occurs in every ring and leads to zigzag structure. This phenomenon can be attributed to the fact that benzene cores in pB series possess full sextet of

electrons and thus reluctant to accept lone pair electron density from nitrogen. Thus, N-centers adopt pyramidal configuration to avoid destabilization from inherent Hückel antiaromaticity within the N-heterocycle.

**Table 2.1**. The ratio of number of π electrons to total number of bonds ($n_\pi$) in LPAs and LPA-based heterocycles. B, N, A and T represent benzene, naphthalene, anthracene and tetracene, respectively.

| System | $n_\pi$ | System | $n_\pi$ | System | $n_\pi$ | System | $n_\pi$ |
|---|---|---|---|---|---|---|---|
| B | 1.000 | N | 0.909 | A | 0.875 | T | 0.857 |
| $pB_1$ | 1.000 | $pN_1$ | 0.923 | $pA_1$ | 0.889 | $pT_1$ | 0.870 |
| $pB_2$ | 1.000 | $pN_2$ | 0.927 | $pA_2$ | 0.893 | $pT_2$ | 0.873 |
| $pB_3$ | 1.000 | $pN_3$ | 0.929 | $pA_3$ | 0.895 | $pT_3$ | 0.875 |
| $pB_4$ | 1.000 | $pN_4$ | 0.930 | $pA_4$ | 0.896 | $pT_4$ | 0.876 |
| $pB_5$ | 1.000 | $pN_5$ | 0.930 | $pA_5$ | 0.897 | $pT_5$ | 0.877 |
| $pB_6$ | 1.000 | $pN_6$ | 0.931 | $pA_6$ | 0.897 | $pT_6$ | 0.877 |

## 2.4.2. Dehydrogenation Energy

In a recent review on the topic of large heterocyclic acenes, Bünz *et al.* described that hydrogenation of **1** to **2** is exothermic by 49.5 kcal/mol and thermodynamically favourable while hydrogenation of **2** to **3** is endothermic by 2.5 kcal/mol (Figure 2.3).[90]

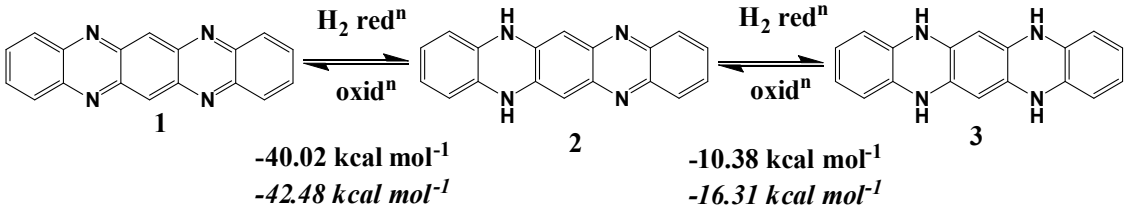


**Figure 2.3**. Calculated heats of hydrogenation for the reduction of **1** to **2** and **2** to **3**. (values in regular font is for M06L/6-311++G(d,p) level and that in italics is for B3LYP/6-31G(d,p) level).

In the present study, **3** is $pB_2$. Bünz also correlated the synthesis of terminal substituted 2 to its thermodynamic stability. However our theoretical calculations using the method used by Bünz (B3LYP/6-31G(d,p)) suggests that hydrogenation of **1** to **2** and **2** to **3** are exothermic by 42.5 and 16.3 kcal/mol, respectively. It indicates

an error in the previous calculation. Further, at M06L/6-311++G(d,p) level too, both hydrogenation reactions are found to be exothermic and the hydrogenation energy values are in agreement with the B3LYP method (hydrogenation of **1** to **2** is and **2** to **3** are exothermic by -40.02 and -10.38 kcal/mol, respectively). In order to assess the thermodynamic stability of the systems ($pB_1$ – $pB_6$, $pN_1$ – $pN_6$, $pA_1$ – $pA_6$ and $pT_1$ – $pT_6$), energy change associated with dehydrogenation of N-centers is calculated.

The dehydrogenation energy ($E_{dh}$) corresponding to the N-heterocycles of all the set of molecules are given in the Table 2.2 at M06L/6-311++G(d,p) level. The notations N1, N2 etc. is used to indicate the number of N-heterocycles dehydrogenated in the molecule, starting from one terminal to the other. All the reactions are endothermic suggesting that the hydrogen-rich states are more stable than the dehydrogenated states. This is very clear from the total $E_{dh}$ given in Table 2.2. The increase in total $E_{dh}$ ($\Sigma E_{dh}$) is proportional to the increase in the number of heterocycles and increase in the size of the PAH moiety. In $pB_1$, $pN_1$, $pA_1$ and $pT_1$ systems, $\Sigma E_{dh}$ values are 23.8, 38.8, 46.3, and 50.3 kcal/mol, respectively. These numbers show a strong linear correlation with the $n_\pi$ values of the respective systems (Figure 2.4). This correlation suggests that lone pair donation from nitrogen to the π-system increases with decrease in the $n_\pi$ value and that enhances the overall π-bonding strength and aromaticity of the system. As a result, the dehydrogenation reaction becomes increasingly more difficult for larger acene mimics. For instance, $E_{dh}$ for the second ring of $pB_2$, $pN_2$, $pA_2$ and $pT_2$, third ring of $pB_3$, $pN_3$, $pA_3$ and $pT_3$, forth ring of $pB_4$, $pN_4$, $pA_4$ and $pT_4$, fifth ring of $pB_5$, $pN_5$, $pA_5$ and $pT_5$ and sixth ring of $pB_6$, $pN_6$, $pA_6$ and $pT_6$ show gradual increase, proportional to the decrease in $n_\pi$ of the system, in all the cases, $n_\pi$ versus $E_{dh}$ correlations show correlation coefficient in the range 0.997 - 0.999.

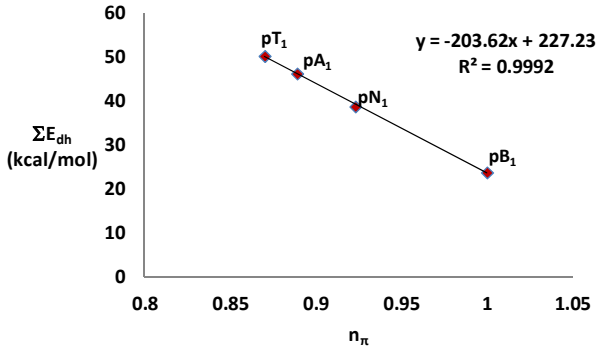


**Figure 2.4**. Correlation between $n_\pi$ and $\Sigma E_{dh}$ of $pB_1$, $pN_1$, $pA_1$ and $pT_1$ systems.

**Table 2.2.** Dehydrogenation energy $E_{dh}$ (kcal/mol) of the N-heterocycles of LPA mimics.

| System | N1 | N2 | N3 | N4 | N5 | N6 | $\Sigma E_{dh}$ |
|---|---|---|---|---|---|---|---|
| $pB_1$ | 23.8 | | | | | | 23.8 |
| $pB_2$ | 40.0 | 12.2 | | | | | 52.2 |
| $pB_3$ | 45.6 | 25.8 | 11.3 | | | | 82.7 |
| $pB_4$ | 47.9 | 30.4 | 24.0 | 11.2 | | | 113.5 |
| $pB_5$ | 48.8 | 32.7 | 27.2 | 24.6 | 11.1 | | 144.4 |
| $pB_6$ | 49.5 | 34.1 | 30.2 | 27.4 | 18.7 | 15.6 | 175.5 |
| $pN_1$ | 38.8 | | | | | | 38.8 |
| $pN_2$ | 48.0 | 32.9 | | | | | 80.9 |
| $pN_3$ | 47.4 | 41.8 | 31.9 | | | | 121.1 |
| $pN_4$ | 39.3 | 44.0 | 40.3 | 31.6 | | | 155.2 |
| $pN_5$ | 34.3 | 44.6 | 24.7 | 57.6 | 31.7 | | 192.9 |
| $pN_6$ | 31.3 | 45.0 | 43.3 | 41.8 | 39.6 | 31.4 | 232.4 |
| $pA_1$ | 46.3 | | | | | | 46.3 |
| $pA_2$ | 51.6 | 43.1 | | | | | 94.7 |
| $pA_3$ | 38.7 | 48.2 | 42.6 | | | | 129.5 |
| $pA_4$ | 32.9 | 49.2 | 47.6 | 42.7 | | | 172.4 |
| $pA_5$ | 49.1 | 43.3 | 35.7 | 47.4 | 42.3 | | 217.8 |
| $pA_6$ | 18.5 | 49.6 | 48.8 | 49.7 | 45.9 | 42.3 | 254.8 |
| $pT_1$ | 50.3 | | | | | | 50.3 |
| $pT_2$ | 41.0 | 48.2 | | | | | 89.2 |
| $pT_3$ | 45.51 | 39.8 | 47.9 | | | | 153 |
| $pT_4$ | 44.2 | 32.5 | 51.0 | 47.9 | | | 175.6 |
| $pT_5$ | 15.9 | 51.8 | 51.4 | 50.9 | 47.7 | | 217.7 |
| $pT_6$ | 33.6 | 49.6 | 47.5 | 32.0 | 50.9 | 47.7 | 261.3 |

To substantiate the results the calculations are done for a representative set of molecules (pN series) including exchange correlation functionals using M06 and M062X methods at the same basis set of 6-311++G(d,p). The results are given in Table 2.3. The $\Sigma E_{dh}$ values obtained using these methods and those using M06L method show very similar trend. In all the cases, a gradual increase in $\Sigma E_{dh}$ value

with increase in the number of heterocycles and increase in the length of the hydrocarbon part is observed. However, the endothermic character of the dehydrogenation process is ~10-20% higher for the M06 method and ~15-35% higher for the M062X method than the M06L level values. The percentage of exchange integral has a direct influence on the dehydrogenation energy values as evident from the above calculations.

**Table 2.3.** Dehydrogenation energy $E_{dh}$ (kcal/mol) of the pN series of LPA mimics at M06/6-311++G(d,p) and M062X/6-311++G(d,p) levels of theory.

| System | N1 | N2 | N3 | N4 | N5 | N6 | $\Sigma E_{dh}$ |
|---|---|---|---|---|---|---|---|
| **M06** | | | | | | | |
| $pN_1$ | 42.4 | | | | | | 42.4 |
| $pN_2$ | 37.4 | 51.9 | | | | | 89.3 |
| $pN_3$ | 36.7 | 46.4 | 61.7 | | | | 144.7 |
| $pN_4$ | 36.5 | 45.9 | 48.5 | 54.2 | | | 185.1 |
| $pN_5$ | 36.4 | 45.3 | 47.7 | 50.0 | 49.6 | | 229.1 |
| $pN_6$ | 36.4 | 45.3 | 57.4 | 39.4 | 44.4 | 52.1 | 275.0 |
| **M062X** | | | | | | | |
| $pN_1$ | 44.8 | | | | | | 44.8 |
| $pN_2$ | 39.8 | 55.2 | | | | | 95.0 |
| $pN_3$ | 39.2 | 49.6 | 75.0 | | | | 163.8 |
| $pN_4$ | 39.1 | 49.0 | 52.2 | 67.3 | | | 207.6 |
| $pN_5$ | 39.0 | 48.9 | 51.5 | 62.9 | 53.8 | | 256.0 |
| $pN_6$ | 39.0 | 48.8 | 51.3 | 52.3 | 58.6 | 55.8 | 305.8 |

## 2.4.3. Bond length Equalisation and Aromatic Character

Geometry based indices have been used for quantifying aromaticity especially in the case of planar systems.[77, 91] The bond length based index of aromaticity, HOMA developed by Krygowski *et al.* is one of the most prominent among this category and is used to compare the aromaticity of a variety of organic molecules. For a perfect aromatic system, HOMA is 1 and a value close to zero indicates non-aromatic character. Aromatic molecules tend to show bond length equalization and HOMA value close to 1. The CC bond

length of benzene (1.4 Å), is considered as the most optimum for an aromatic hydrocarbon.

In the present study, the notations Nring1, Nring2 etc. is used to indicate the most peripheral to the interior symmetrically distinguishable N-heterocycles. Similarly, notations Cring1, Cring2 etc are used to indicate the most peripheral to the interior carbon rings. The HOMA calculated for all the molecules are depicted in Tables 2.4, 2.5, 2.6 and 2.7.

**Table 2.4**. HOMA index of pB series of LPA mimics.

| System | $pB_1$ | $pB_2$ | $pB_3$ | $pB_4$ | $pB_5$ | $pB_6$ |
|---|---|---|---|---|---|---|
| Cring1 | 0.98 | 0.98 | 0.98 | 0.98 | 0.98 | 0.98 |
| Nring1 | 0.69 | 0.68 | 0.68 | 0.67 | 0.67 | 0.67 |
| Cring2 | | 0.99 | 0.99 | 0.99 | 0.99 | 0.99 |
| Nring2 | | | 0.66 | 0.67 | 0.66 | 0.65 |
| Cring3 | | | | 0.99 | 0.99 | 0.99 |
| Nring3 | | | | | 0.66 | 0.66 |
| Cring4 | | | | | | 0.99 |
| ΣHOMA | 1.67 | 2.65 | 3.31 | 4.3 | 4.95 | 5.93 |

**Table 2.5**. HOMA index of pN series of LPA mimics.

| System | $pN_1$ | $pN_2$ | $pN_3$ | $pN_4$ | $pN_5$ | $pN_6$ |
|---|---|---|---|---|---|---|
| Cring1 | 0.85 | 0.85 | 0.85 | 0.85 | 0.86 | 0.86 |
| Cring2 | 0.77 | 0.76 | 0.76 | 0.77 | 0.77 | 0.77 |
| Nring1 | 0.69 | 0.69 | 0.69 | 0.70 | 0.70 | 0.70 |
| Cring3 | | 0.80 | 0.81 | 0.82 | 0.82 | 0.82 |
| Cring4 | | | 0.80 | 0.81 | 0.81 | 0.81 |
| Nring2 | | | 0.70 | 0.68 | 0.71 | 0.71 |
| Cring5 | | | | 0.81 | 0.82 | 0.82 |
| Cring6 | | | | | 0.81 | 0.81 |
| Nring3 | | | | | 0.71 | 0.71 |
| Cring7 | | | | | | 0.81 |
| ΣHOMA | 2.31 | 3.10 | 4.61 | 5.44 | 7.01 | 7.82 |

In pB series, HOMA of every benzene unit is 0.98 or 0.99, showing the perfect aromatic nature of the individual benzene rings. Further, the N-heterocycle has a HOMA in the range 0.65 - 0.69 which indicates substantial aromatic character as only a 30 - 35% reduction in aromaticity is observed compared to the HOMA 1.00 of one of the most aromatic N-heterocycle, pyridine. In the pN series, among the carbon rings, terminal ring is the most aromatic with HOMA 0.85 – 0.86 whereas the ring adjacent to it is the least aromatic (HOMA 0.76 – 0.77). In $pN_3$ – $pN_5$, both rings of the interior naphthalene units show nearly same aromatic character (HOMA 0.80 – 0.82) and the N-heterocycles show slightly higher values (0.68 – 0.71) than pB series.

**Table 2.6**. HOMA index of pA series of LPA mimics.

| System | $pA_1$ | $pA_2$ | $pA_3$ | $pA_4$ | $pA_5$ | $pA_6$ |
|---|---|---|---|---|---|---|
| Cring1 | 0.72 | 0.73 | 0.72 | 0.72 | 0.72 | 0.72 |
| Cring2 | 0.74 | 0.74 | 0.74 | 0.74 | 0.74 | 0.74 |
| Cring3 | 0.65 | 0.65 | 0.65 | 0.65 | 0.65 | 0.65 |
| Nring1 | 0.65 | 0.65 | 0.65 | 0.65 | 0.65 | 0.65 |
| Cring4 | | 0.69 | 0.69 | 0.69 | 0.69 | 0.69 |
| Cring5 | | 0.75 | 0.75 | 0.75 | 0.75 | 0.75 |
| Cring6 | | | 0.68 | 0.68 | 0.68 | 0.68 |
| Nring2 | | | 0.66 | 0.66 | 0.66 | 0.66 |
| Cring7 | | | | 0.69 | 0.69 | 0.69 |
| Cring8 | | | | 0.75 | 0.75 | 0.75 |
| Cring9 | | | | | 0.68 | 0.68 |
| Nring3 | | | | | 0.66 | 0.66 |
| Cring10 | | | | | | 0.68 |
| Cring11 | | | | | | 0.75 |
| ΣHOMA | 2.76 | 4.21 | 5.54 | 6.98 | 8.32 | 9.75 |

In the case of $pA_1$, HOMA of Cring1, Cring2, Cring3 is 0.72, 0.74 and 0.65, respectively. The above mentioned pattern and magnitude of HOMA is retained in $pA_2$ – $pA_5$. Further, HOMA 0.68 – 0.75 is observed for the carbon rings of all other anthracene moieties whereas a slightly lower HOMA 0.65 – 0.68 is observed for all the dihydropyrazine rings. In the case of pT series, all the terminal tetracene

moieties show nearly identical HOMA patterns with terminal, second, third and fourth carbon rings showing values 0.64 – 0.65, 0.67 – 0.68, 0.64 – 0.65, and 0.58, respectively. The inner tetracene moieties show HOMA in the range 0.61 – 0.67 whereas the aromatic character of N-heterocycles is in the range 0.62 – 0.64, the lowest compared to all other systems. The HOMA of benzene (1.00), naphthalene (0.77), anthracene (0.62 for Cring1, 0.70 for Cring2), and tetracene (0.53 for Cring1, 0.60 for Cring2) are almost fully retained or even enhanced in all the respective carbon rings in the LPA-based N-heterocyclic systems.

**Table 2.7**. HOMA index of pT series of LPA mimics.

| System | $pT_1$ | $pT_2$ | $pT_3$ | $pT_4$ | $pT_5$ | $pT_6$ |
|---|---|---|---|---|---|---|
| Cring1 | 0.64 | 0.64 | 0.65 | 0.65 | 0.65 | 0.65 |
| Cring2 | 0.68 | 0.68 | 0.67 | 0.67 | 0.67 | 0.68 |
| Cring3 | 0.65 | 0.65 | 0.65 | 0.65 | 0.64 | 0.65 |
| Cring4 | 0.58 | 0.58 | 0.58 | 0.58 | 0.58 | 0.58 |
| Nring1 | 0.62 | 0.62 | 0.64 | 0.62 | 0.63 | 0.64 |
| Cring5 | | 0.61 | 0.61 | 0.61 | 0.61 | 0.61 |
| Cring6 | | 0.67 | 0.67 | 0.67 | 0.67 | 0.67 |
| Cring7 | | | 0.66 | 0.67 | 0.67 | 0.67 |
| Cring8 | | | 0.61 | 0.61 | 0.61 | 0.61 |
| Nring2 | | | 0.63 | 0.63 | 0.63 | 0.63 |
| Cring9 | | | | 0.61 | 0.61 | 0.61 |
| Cring10 | | | | 0.67 | 0.67 | 0.67 |
| Cring11 | | | | | 0.67 | 0.67 |
| Cring12 | | | | | 0.61 | 0.61 |
| Nring3 | | | | | 0.63 | 0.63 |
| Cring13 | | | | | | 0.61 |
| Cring14 | | | | | | 0.67 |
| ΣHOMA | 3.17 | 4.45 | 6.37 | 7.64 | 9.55 | 10.86 |

Further substantiation of the results is done by including the HF exchange in the method and running the calculation on a representative set of molecules (pN series). The HOMA values of the systems using the methods are given in Table 2.8 and Table 2.9. Even though the trends are similar there is change in the magnitude

of the ∑HOMA when the HF exchange percentage is increasing. Calculations using M06 method yields HOMA values which are approximately 2-4% higher than that of M06L method and M062X method yielded HOMA values which are approximately 1-3% less than the M06L results.

**Table 2.8**. HOMA index of pN series at M06/6-311++G(d,p)) level of theory.

| | $pN_1$ | $pN_2$ | $pN_3$ | $pN_4$ | $pN_5$ | $pN_6$ |
|---|---|---|---|---|---|---|
| Cring1 | 0.88 | 0.88 | 0.88 | 0.88 | 0.88 | 0.88 |
| Cring2 | 0.79 | 0.79 | 0.78 | 0.78 | 0.78 | 0.79 |
| Nring1 | 0.7 | 0.71 | 0.71 | 0.71 | 0.71 | 0.71 |
| Cring3 | | 0.84 | 0.84 | 0.84 | 0.84 | 0.84 |
| Cring4 | | | 0.83 | 0.83 | 0.83 | 0.83 |
| Nring2 | | | 0.72 | 0.73 | 0.72 | 0.72 |
| Cring5 | | | | 0.84 | 0.84 | 0.84 |
| Cring6 | | | | | 0.84 | 0.84 |
| Nring3 | | | | | 0.7 | 0.72 |
| Cring7 | | | | | | 0.84 |
| ΣHOMA | 2.37 | 3.22 | 4.77 | 5.6 | 7.15 | 8.01 |

**Table 2.9**. HOMA index of pN series at M062X/6-311++G(d,p) level of theory.

| | $pN_1$ | $pN_2$ | $pN_3$ | $pN_4$ | $pN_5$ | $pN_6$ |
|---|---|---|---|---|---|---|
| Cring1 | 0.86 | 0.86 | 0.86 | 0.86 | 0.86 | 0.86 |
| Cring2 | 0.75 | 0.74 | 0.73 | 0.74 | 0.74 | 0.74 |
| Nring1 | 0.65 | 0.65 | 0.65 | 0.65 | 0.65 | 0.65 |
| Cring3 | | 0.81 | 0.81 | 0.82 | 0.82 | 0.82 |
| Cring4 | | | 0.8 | 0.8 | 0.8 | 0.8 |
| Nring2 | | | 0.67 | 0.67 | 0.67 | 0.66 |
| Cring5 | | | | 0.81 | 0.81 | 0.81 |
| Cring6 | | | | | 0.8 | 0.81 |
| Nring3 | | | | | 0.67 | 0.67 |
| Cring7 | | | | | | 0.81 |
| ΣHOMA | 2.25 | 3.06 | 4.53 | 5.35 | 6.83 | 7.63 |

The HOMA value represents the local aromaticity of individual rings whereas the sum of the HOMA values of all the rings can be considered as a measure of the

global aromaticity of the molecules. This quantity referred to as ΣHOMA is depicted in Table 2.10. The ΣHOMA of all the different series of compounds show strong linear correlations with the corresponding total dehydrogenation energy $\Sigma E_{dh}$ (Figure 2.5). These correlations strongly suggest that $E_{dh}$ values are intimately connected with the aromatization energy of the molecule. According to Clar, the LPA systems show 'aromatic dilution' with increase in the length of the molecule. This phenomenon is clearly visible in the correlation plots shown in Figure 2.5 in terms of the decrease in slope as we move from pB to pN to pA to pT series of molecules.

**Table 2.10**. ∑HOMA values of all LPA mimics.

| System | ΣHOMA | System | ΣHOMA | System | ΣHOMA | System | ΣHOMA |
|---|---|---|---|---|---|---|---|
| $pB_1$ | 1.67 | $pN_1$ | 2.31 | $pA_1$ | 2.76 | $pT_1$ | 3.17 |
| $pB_2$ | 2.65 | $pN_2$ | 3.10 | $pA_2$ | 4.21 | $pT_2$ | 4.45 |
| $pB_3$ | 3.31 | $pN_3$ | 4.61 | $pA_3$ | 5.54 | $pT_3$ | 6.37 |
| $pB_4$ | 4.30 | $pN_4$ | 5.44 | $pA_4$ | 6.98 | $pT_4$ | 7.64 |
| $pB_5$ | 4.95 | $pN_5$ | 7.01 | $pA_5$ | 8.32 | $pT_5$ | 9.55 |
| $pB_6$ | 5.93 | $pN_6$ | 7.82 | $pA_6$ | 9.75 | $pT_6$ | 10.86 |

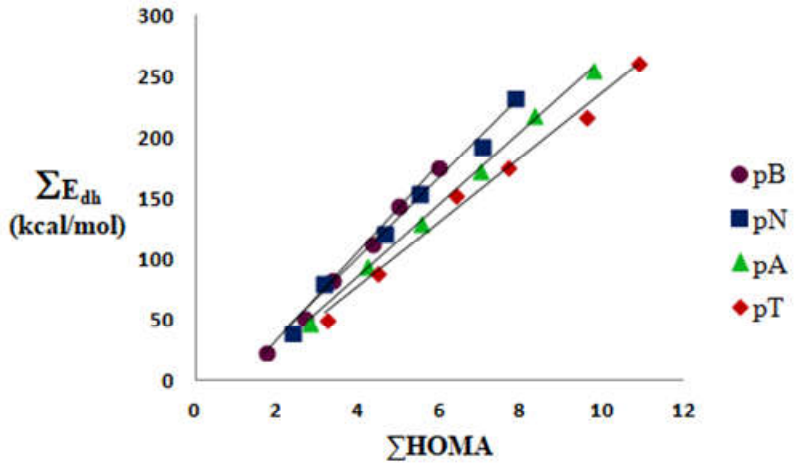


**Figure 2.5.** Correlation between ∑HOMA and $\sum E_{dh}$.

By plotting the total sum of HOMA values in a molecule and the sum of total dehydrogenation energy, a correlation plot (Figure 2.6) is obtained which shows a decrease in slope with the increase in the HF exchange percentage as a result of the progression in the $E_{dh}$ values when the HF exchange is increased.

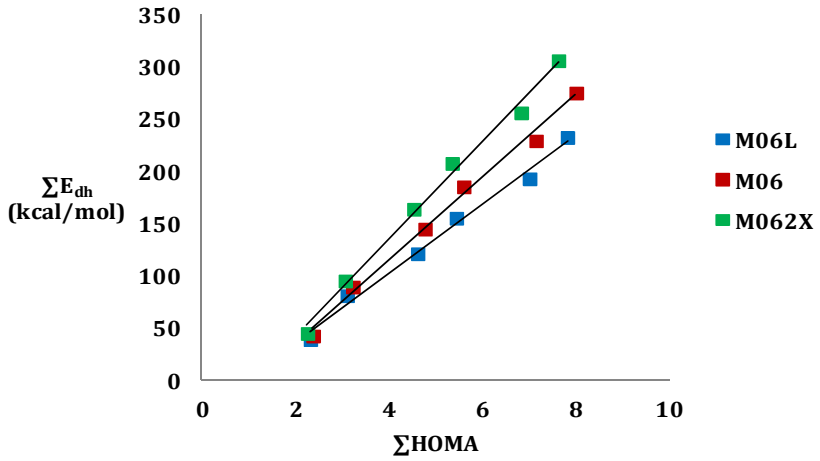


**Figure 2.6**. Correlation between ∑HOMA and $\sum E_{dh}$ of pN series using M06L/M06 and M062X methods.

## 2.4.4. Nucleus Independent Chemical Shift (NICS) and Aromatic Character

Magnetic criteria of aromaticity is popularly described in terms of NICS index as portrayed by Schleyer and co-workers.[76] We have analyzed three popular NICS indices, *viz*. the NICS at the center of each six-membered ring (NICS(0)), at 1 Å above every ring center (NICS(1)) and also the z-component of NICS at 1 Å above the ring center ($NICS_{zz}(1)$). Among these indices, $NICS_{zz}(1)$ is considered to be more reliable than others and for all the discussions, this quantity is used in the text. In fact, the relative ordering of the magnitude of all the three indices are very similar and so the conclusions drawn from any of them are same. The discrepancies of NICS, its size-, shape- and distance dependencies as well as more sophisticated approaches to NICS treatment of aromaticity have been elaborated in the past.[92] The coupling between induced magnetic fields from adjacent rings also affects the NICS measure.[27, 92-94] We do not attempt to directly compare NICS of PAH molecules and LPA mimics because this index varies with respect to the number of heteroatoms, size and symmetry of the molecules. The $NICS_{zz}(1)$ values of benzene, naphthalene, Cring1 of anthracene and Cring1 of tetracene are -17.30, -28.65, -26.32 and -23.95, respectively and that of Cring2 of anthracene and Cring2 of tetracene are -34.11 and -33.85, respectively. These values may give a false impression that benzene is the least aromatic and the most aromatic is Cring2 of anthracene or tetracene. As NICS works best for comparing the aromaticity of a similar set of molecules, we will focus on the relative

ordering of the NICS along the symmetrically unequal rings, starting from one at the terminal to the last in the middle (Tables 2.11 to 2.14).

**Table 2.11.** $NICS_{zz}(1)$ values of pB series of LPA mimics.

| | $pB_1$ | $pB_2$ | $pB_3$ | $pB_4$ | $pB_5$ | $pB_6$ |
|---|---|---|---|---|---|---|
| Cring1 | -15.56 | -17.94 | -18.03 | -18.69 | -19.22 | -19.98 |
| Nring1 | 18.49 | 16.10 | 16.26 | 16.51 | 16.51 | 16.69 |
| Cring2 | | -7.02 | -7.32 | -7.08 | -6.70 | -6.45 |
| Nring2 | | | 13.65 | 13.83 | 14.00 | 14.02 |
| Cring3 | | | | -8.68 | -8.63 | -8.83 |
| Nring3 | | | | | 13.60 | 13.66 |
| Cring4 | | | | | | -8.71 |

**Table 2.12.** $NICS_{zz}(1)$ values of pN series of LPA mimics.

| | $pN_1$ | $pN_2$ | $pN_3$ | $pN_4$ | $pN_5$ | $pN_6$ |
|---|---|---|---|---|---|---|
| Cring1 | -22.65 | -22.39 | -22.46 | -22.17 | -22.12 | -21.86 |
| Cring2 | -14.48 | -14.53 | -14.10 | -14.11 | -14.19 | -14.18 |
| Nring1 | 19.18 | 19.14 | 19.24 | 19.20 | 19.30 | 19.34 |
| Cring3 | | -9.95 | -9.80 | -9.64 | -9.35 | -9.13 |
| Cring4 | | | -10.40 | -10.57 | -10.57 | -10.82 |
| Nring2 | | | 18.27 | 18.21 | 18.47 | 18.51 |
| Cring5 | | | | -10.35 | -10.06 | -9.86 |
| Cring6 | | | | | -10.30 | -10.45 |
| Nring3 | | | | | 18.70 | 18.70 |
| Cring7 | | | | | | -10.10 |

In all the pB, pN, pA, and pT series of molecules, the Crings show significant negative $NICS_{zz}(1)$ indicating aromatic character whereas all the Nrings show positive $NICS_{zz}(1)$ indicating antiaromaticity. In pB series, the negative character of $NICS_{zz}(1)$ increases gradually for Cring1 and reaches the most negative -19.98 for $pB_6$. The inner Crings show significantly lower negative $NICS_{zz}(1)$ (-6.45 to -8.83) than the terminal ones whereas compared to the terminal Nrings (18.49 to 16.51), the inner Nrings appear to be less antiaromatic (13.60 to 14.02).

**Table 2.13**. $NICS_{zz}(1)$ values of pA series of LPA mimics.

| | $pA_1$ | $pA_2$ | $pA_3$ | $pA_4$ | $pA_5$ | $pA_6$ |
|---|---|---|---|---|---|---|
| Cring1 | -23.70 | -23.09 | -22.94 | -22.78 | -22.49 | -22.47 |
| Cring2 | -26.77 | -26.36 | -25.93 | -25.68 | -25.49 | -25.38 |
| Cring3 | -14.68 | -14.82 | -15.32 | -15.68 | -16.02 | -16.41 |
| Nring1 | 14.84 | 15.11 | 15.19 | 15.25 | 15.29 | 15.13 |
| Cring4 | | -12.51 | -11.79 | -11.45 | -11.02 | -10.64 |
| Cring5 | | -21.31 | -21.25 | -21.21 | -21.15 | -21.26 |
| Cring6 | | | -12.82 | -13.04 | -13.32 | -13.74 |
| Nring2 | | | 15.52 | 15.56 | 15.64 | 15.69 |
| Cring7 | | | | -12.36 | -11.93 | -11.60 |
| Cring8 | | | | -21.11 | -20.97 | -21.01 |
| Cring9 | | | | | -12.56 | -13.00 |
| Nring3 | | | | | 15.63 | 15.60 |
| Cring10 | | | | | | -12.21 |

**Table 2.14.** $NICS_{zz}(1)$ values of pT series of LPA mimics.

| | $pT_1$ | $pT_2$ | $pT_3$ | $pT_4$ | $pT_5$ | $pT_6$ |
|---|---|---|---|---|---|---|
| Cring1 | -22.49 | -21.79 | -21.17 | -20.67 | -20.39 | -19.52 |
| Cring2 | -30.10 | -29.59 | -29.34 | -29.05 | -28.72 | -28.46 |
| Cring3 | -27.96 | -27.78 | -27.91 | -28.17 | -28.57 | -28.57 |
| Cring4 | -14.61 | -14.64 | -14.90 | -15.34 | -15.41 | -16.00 |
| Nring1 | 13.75 | 13.45 | 13.09 | 12.89 | 12.76 | 12.45 |
| Cring5 | | -13.18 | -12.67 | -12.03 | -12.08 | -11.27 |
| Cring6 | | -24.82 | -24.71 | -24.54 | -24.48 | -24.71 |
| Cring7 | | | -24.58 | -24.63 | -24.74 | -24.70 |
| Cring8 | | | -13.31 | -13.59 | -13.79 | -14.38 |
| Nring2 | | | 13.69 | 13.67 | 13.60 | 13.77 |
| Cring9 | | | | -12.81 | -12.38 | -11.98 |
| Cring10 | | | | -24.45 | -24.31 | -24.32 |
| Cring11 | | | | | -24.44 | -24.48 |
| Cring12 | | | | | -13.03 | -13.44 |
| Nring3 | | | | | 13.73 | 13.80 |
| Cring13 | | | | | | -12.55 |
| Cring14 | | | | | | -24.26 |

**Table 2.15.** Sum of negative $NICS_{zz}(1)$ of all LPA mimics.

| System | $\Sigma NICS_{zz}(1)$ | System | $\Sigma NICS_{zz}(1)$ | System | $\Sigma NICS_{zz}(1)$ | System | $\Sigma NICS_{zz}(1)$ |
|---|---|---|---|---|---|---|---|
| $pB_1$ | -15.56 | $pN_1$ | -37.13 | $pA_1$ | -65.15 | $pT_1$ | -95.16 |
| $pB_2$ | -24.96 | $pN_2$ | -46.87 | $pA_2$ | -98.09 | $pT_2$ | -131.80 |
| $pB_3$ | -25.35 | $pN_3$ | -56.76 | $pA_3$ | -110.05 | $pT_3$ | -168.59 |
| $pB_4$ | -34.45 | $pN_4$ | -66.84 | $pA_4$ | -143.31 | $pT_4$ | -205.28 |
| $pB_5$ | -34.55 | $pN_5$ | -76.59 | $pA_5$ | -154.95 | $pT_5$ | -242.34 |
| $pB_6$ | -43.97 | $pN_6$ | -86.40 | $pA_6$ | -167.72 | $pT_6$ | -278.64 |

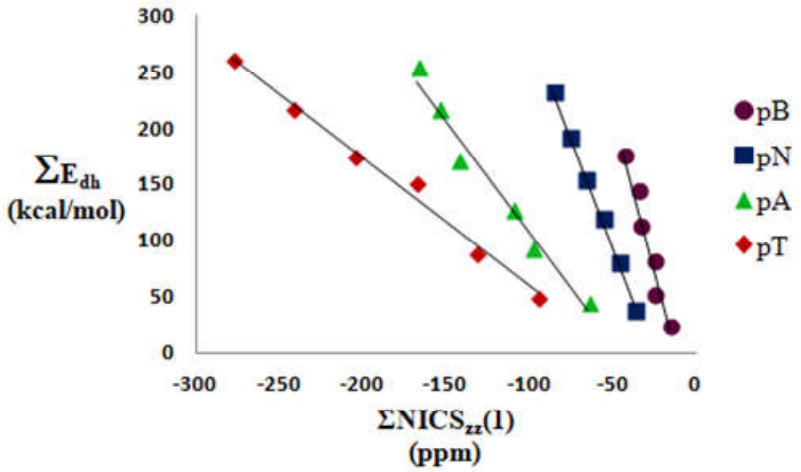


**Figure 2.7**. Correlation between $\sum NICS_{zz}(1)$ and $\sum E_{dh}$ for pB, pN, pA, and pT series of molecules.

The positive $NICS_{zz}(1)$ values of Nrings can be correlated to π-electron count 8 of the N-heterocycle. Like pB series, $NICS_{zz}(1)$ of pN, pA and pT series too indicate significant decrease in aromaticity for LPA moieties from terminal to inner region. Moreover, compared to $NICS_{zz}(1)$ in the range 18.21 to 19.34 observed for N-heterocycles of pN series, $NICS_{zz}(1)$ for pA series shows a decrease by 3.37 to 3.65 units while that of pT series shows a decrease by 5.45 to 5.54 units. The sum of the $NICS_{zz}(1)$ values of all the rings can be considered as a measure of the global aromaticity of the molecules. This quantity referred to as $\Sigma NICS_{zz}(1)$ is also depicted in Table 2.15. A linear correlation between total negative $NICS_{zz}(1)$ value ($\Sigma NICS_{zz}(1)$) that represents the aromatic character of the Crings and the total dehydrogenation energy $\Sigma E_{dh}$ exists for pB, pN, pA and pT series of molecules (Figure 2.8). The magnitude of the slope of the correlation line is the highest for pB series and it decreases along the pN, pA and pT series indicating aromatic dilution.

This correlation as well as the correlation between ΣHOMA and $\Sigma E_{dh}$ in Figure 2.5, clearly brings out the multidimensional character of aromaticity, *viz*. the underlying magnetic, structural and energetic features.

Magnetic measures of aromaticity such as NICS are shown to give better results with the inclusion of HF exchange; thereby M06 and M062X methods are used for the calculation of the same for a set of representative molecules, *i.e*, pN series as that used in the case of HOMA index calculation. The values obtained are given in Table 2.16 and Table 2.17. The trends are similar as that of the M06L method, and the magnitude of $NICS_{zz}(1)$ values increases with the increase in the percentage of HF exchange. For M06 method the change in magnitude is approximately 10-19% and for the M062X calculations the increase in the magnitude is in the range of 14-27%. In addition to it, there is significant decrease in the aromaticity from the outer to the inner rings of the acenes which is clearly visible in the results.

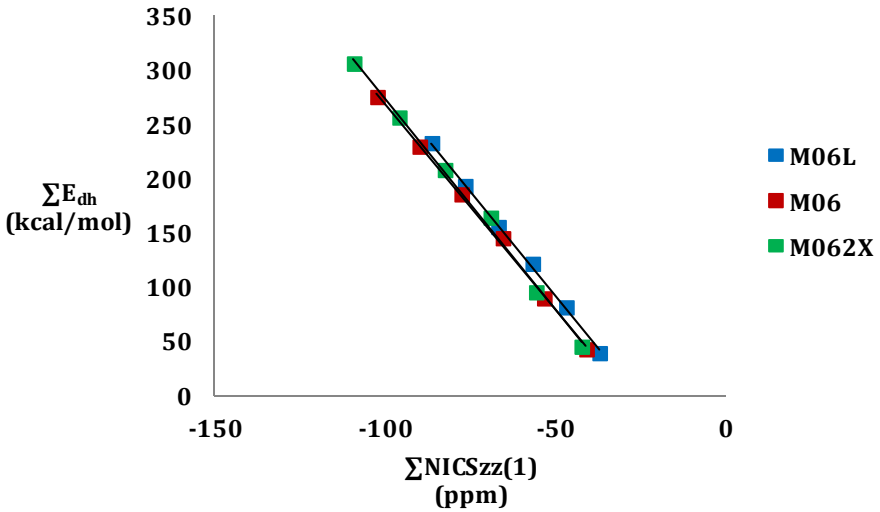


**Figure 2.8** Correlation between sum of negative $NICS_{zz}(1)$ and $\sum E_{dh}$ of pN series of molecules.

The sum of negative NICS values on all the hydrocarbon rings of the system and the sum of dehydrogenation energy for the three different methods, when plotted against each other, a linear correlation is obtained (Figure 2.8). From the figure it is clear that the slope for all the three methods is very similar to each other, indicating that the percentage of HF exchange is not a very good decisive factor in the case of magnetic features of aromaticity.

**Table 2.15.** $NICS_{zz}(1)$ values of pN series at M06/6-311++G(d,p) level of theory.

| | $pN_1$ | $pN_2$ | $pN_3$ | $pN_4$ | $pN_5$ | $pN_6$ |
|---|---|---|---|---|---|---|
| Cring1 | -24.65 | -24.52 | -23.92 | -23.46 | -23.25 | -22.94 |
| Cring2 | -16.34 | -15.95 | -15.51 | -15.13 | -14.95 | -14.69 |
| Nring1 | 19.06 | 19.26 | 19.30 | 19.35 | 19.44 | 19.48 |
| Cring3 | | -12.90 | -12.98 | -12.95 | -12.94 | -12.91 |
| Cring4 | | | -13.12 | -13.07 | -13.04 | -13.13 |
| Nring2 | | | 18.70 | 18.65 | 18.47 | 19.04 |
| Cring5 | | | | -13.06 | -12.96 | -13.02 |
| Cring6 | | | | | -12.85 | -12.88 |
| Nring3 | | | | | 18.15 | 19.23 |
| Cring7 | | | | | | -12.86 |

**Table 2.16.** $NICS_{zz}(1)$ values of pN series at M062X/6-311++G(d,p) level of theory.

| | $pN_1$ | $pN_2$ | $pN_3$ | $pN_4$ | $pN_5$ | $pN_6$ |
|---|---|---|---|---|---|---|
| Cring1 | -25.04 | -24.25 | -23.16 | -22.46 | -21.78 | -21.10 |
| Cring2 | -17.31 | -17.58 | -18.22 | -18.76 | -19.34 | -19.87 |
| Nring1 | 20.65 | 20.33 | 20.49 | 20.49 | 20.44 | 20.40 |
| Cring3 | | -13.92 | -13.39 | -12.68 | -12.03 | -11.36 |
| Cring4 | | | -14.29 | -14.84 | -15.46 | -16.10 |
| Nring2 | | | 20.33 | 20.45 | 20.41 | 20.45 |
| Cring5 | | | | -13.78 | -13.06 | -12.34 |
| Cring6 | | | | | -14.29 | -14.93 |
| Nring3 | | | | | 20.32 | 20.42 |
| Cring7 | | | | | | -13.56 |

## 2.4.5. Molecular Electrostatic Potential and Electron Delocalisation

Figure 2.9 depicts the MESP features of benzene, naphthalene, anthracene and tetracene. The MESP features of the LPA mimics $pB_6$, $pN_6$, $pA_6$ and $pT_6$ are depicted in Figure 2.10 as representative cases. For the rest of the systems also, MESP features show close similarity to the representative cases. The π-electron cloud of the molecules is seen in the MESP isosurface lobes and the most negative valued

MESP ($V_{min}$) is useful for comparing the relative electron rich character of the π-regions in different molecules. [100, 101] For instance, $V_{min}$ analysis has been previously used for studying the Clar's aromatic sextet theory of polycyclic aromatic hydrocarbons and related systems.[16, 100, 101]

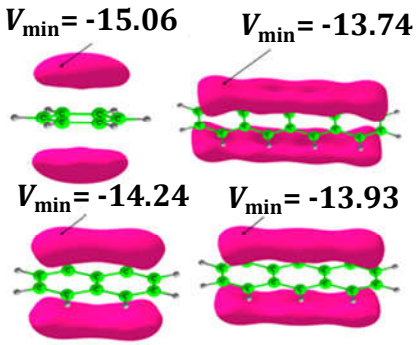


**Figure 2.9**. Plots of MESP isosurface (-9.0 kcal/mol) for benzene, naphthalene, anthracene and tetracene along with MESP minimum in kcal/mol.

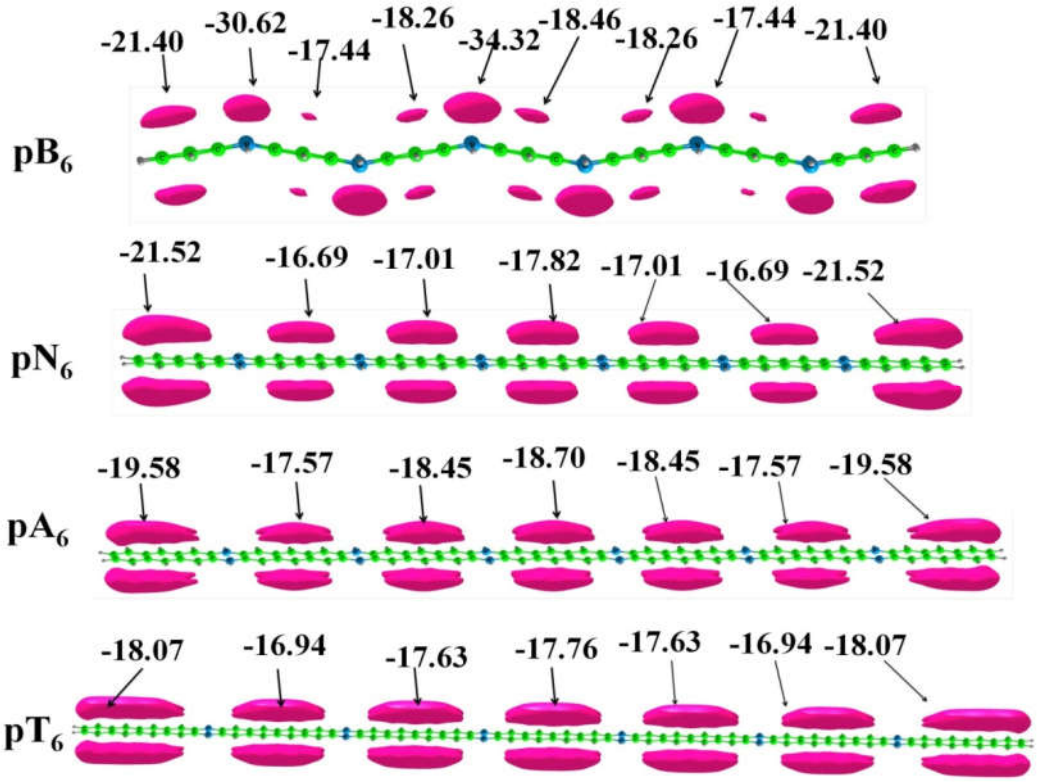


**Figure 2.10**. Plots of MESP isosurface (-9.0 kcal/mol) for $pB_6$, $pN_6$, $pA_6$ and $pT_6$ along with MESP minimum in kcal/mol.

$V_{min}$ values of benzene, naphthalene, anthracene and tetracene are -15.06, -14.24, -13.94 and -13.74 kcal/mol respectively, which indicate the gradual decrease in the electron rich character of the aromatic system with increase in the number of annulated rings. The $V_{min}$ is the most negative for benzene (-15.06 kcal/mol) and

along the LPA series, it gradually decreases with increase in $n_\pi$ value. The $V_{min}$ observed on the LPA unit of every system is depicted in Table 2.17 along with the sum of all $V_{min}$ values referred to as $\Sigma V_{min}$.

**Table 2.18.** MESP minimum (kcal/mol) observed on the LPA units for pB, pN, pA, and pT series of molecules.

| System | $V_{min}$ on the LPA unit from left to right | | | | | | | $\Sigma V_{min}$ |
|---|---|---|---|---|---|---|---|---|
| | 1 | 2 | 3 | 4 | 5 | 6 | 7 | (kcal/mol) |
| $pB_1$ | -19.0 | -19.0 | | | | | | -38.1 |
| $pB_2$ | -20.4 | -15.4 | -20.4 | | | | | -56.1 |
| $pB_3$ | -20.8 | -16.6 | -16.6 | -20.8 | | | | -74.8 |
| $pB_4$ | -21.1 | -17.1 | -17.5 | -17.1 | -21.1 | | | -93.9 |
| $pB_5$ | -21.3 | -17.3 | -18.0 | -18.0 | -17.3 | -21.3 | | -113.2 |
| $pB_6$ | -21.4 | -17.4 | -18.3 | -18.5 | -18.3 | -17.4 | -21.4 | -132.4 |
| $pN_1$ | -18.3 | -18.3 | | | | | | -36.6 |
| $pN_2$ | -20.1 | -14.4 | -20.1 | | | | | -54.6 |
| $pN_3$ | -20.8 | -15.7 | -15.7 | -20.8 | | | | -73.1 |
| $pN_4$ | -21.2 | -16.5 | -16.9 | -16.5 | -21.2 | | | -92.1 |
| $pN_5$ | -21.4 | -16.8 | -17.4 | -17.4 | -16.8 | -21.4 | | -111.2 |
| $pN_6$ | -21.5 | -17.0 | -17.8 | -18.0 | -17.8 | -17.0 | -21.5 | -130.4 |
| $pA_1$ | -17.4 | -17.4 | | | | | | -34.9 |
| $pA_2$ | -18.6 | -15.8 | -18.6 | | | | | -53.1 |
| $pA_3$ | -19.2 | -16.9 | -16.9 | -19.2 | | | | -72.2 |
| $pA_4$ | -19.3 | -17.4 | -17.9 | -17.4 | -19.3 | | | -91.3 |
| $pA_5$ | -19.6 | -17.7 | -18.4 | -18.4 | -17.7 | -19.6 | | -111.3 |
| $pA_6$ | -19.5 | -17.6 | -18.4 | -18.7 | -18.4 | -17.6 | -19.5 | -129.6 |
| $pT_1$ | -16.6 | -16.6 | | | | | | -33.1 |
| $pT_2$ | -17.4 | -15.3 | -17.4 | | | | | -50.1 |
| $pT_3$ | -17.7 | -16.3 | -16.3 | -17.7 | | | | -67.9 |
| $pT_4$ | -18.0 | -16.6 | -17.0 | -16.6 | -18.0 | | | -86.0 |
| $pT_5$ | -18.0 | -16.8 | -17.4 | -17.4 | -16.8 | -18.0 | | -104.4 |
| $pT_6$ | -18.0 | -16.9 | -17.6 | -17.7 | -17.6 | -16.9 | -18.0 | -122.7 |

In pB series, the N-heterocycles show $V_{min}$ for the N-lone pair region in the range -25.73 to -34.51 kcal/mol, wherein the innermost N-heterocycle shows the most negative character while the outermost one shows the least negative character. However, compared to $V_{min}$ of dihydrophenazene (-46.25 kcal/mol), the N-lone pairs of the heterocycles are significantly less negative. This indicates minor delocalization of the N-lone pairs in the LPA mimics which is not surprising considering the pyramidal nature of the N-centers. In the pN series, $V_{min}$ observed for the N-heterocycles is in the range -3.14 to -8.78 kcal/mol while the pA and pT series do not show $V_{min}$ for the N-heterocycles. This indicates that the N-lone pair is strongly delocalized with the LPA units of pN, pA and pT series of molecules and the planar configuration of N-centers substantiate this statement. The $V_{min}$ data in Table 2.18 clearly show that as the size of the LPA mimic increases, the negative character of $V_{min}$ on the outer most LPA unit increases gradually. This pattern is almost repeated in the interior LPA units as well. The enhancement in the negative character of $V_{min}$ with increase in size of the molecule suggests the increasing participation of N-lone pairs in π-electron delocalization. This also means that the aromaticity of the molecule increases with increase in the length of the molecule. In fact, $\Sigma V_{min}$ quantity emerge as a good indicator of the electron delocalization in the molecule and shows a strong linear correlation with the total dehydrogenation energy $\Sigma E_{dh}$ for the different series of molecules (Figure 2.11). The magnitude of the slope of the correlation plot is the highest for the pT series and it decreases along the pA, pN and pB series. This indicates that the N-lone pair donation to enhance the aromaticity of the hydrocarbon portions is the highest for pT series and the lowest for the pB series. The MESP isosurface features also indicate that each of the LPA unit in the LPA mimic almost retains the MESP features of the parent hydrocarbon. This may suggest that the reactivity of an LPA unit in an LPA mimic could match to the reactivity of the parent hydrocarbon. Hence, the stability of the LPA mimic could largely depend on the stability of the parent hydrocarbon. In fact, considering the enhancement in the total aromaticity of the LPA mimic due to the utilization of N-lone pairs in π-conjugation, the overall stability of the system could be predicted to be higher than the parent hydrocarbon. Thus, the MESP features strongly suggest the existence of stable LPA mimics containing N-heterocycles.

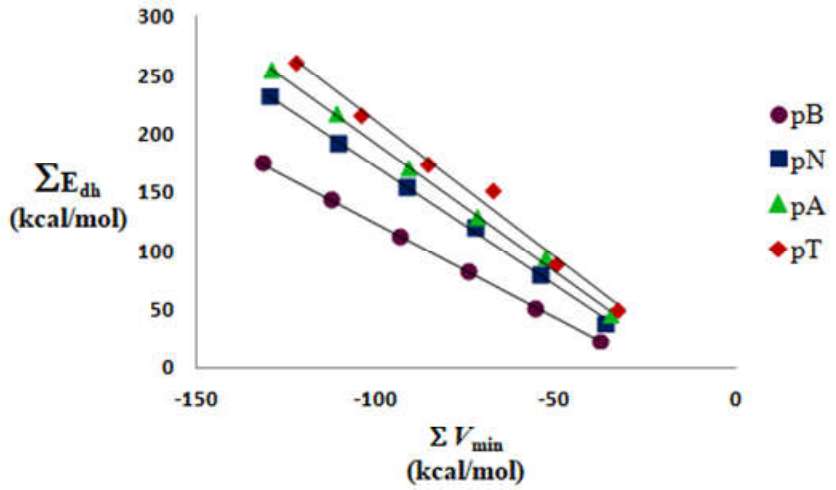


**Figure 2.11.** Correlation between $V_{min}$ and $\sum E_{dh}$ for pB, pN, pA, and pT series.

Calculations including the HF exchange are done using M06 and M06-2X methods for the substantiation of the results obtained by M06L method which has no HF exchange included in the formulation. The $V_{min}$ values on every LPA parts for a representative set of pN series is given in Table 2.19 and Table 2.20. As the HF exchange percentage increases the trends are same as that of M06L method but the values increases which is illustrated in the Figure 2.12. From the figure it is clear that for both methods including HF exchange, the correlation lies in the same line indicating that the systems follow same trends with the inclusion of HF exchange, when compared to the M06L method which has 0% HF exchange. For M06 method the increase in the magnitude is very less compared to the M06L method, 0.05 to 0.09 % only. For the values obtained after M062X method the increase is approximately 11% for all the systems.

**Table 2.19.** $V_{min}$ (kcal/mol) on LPA part using M06/6-311++G(d,p) method

| | $V_{min}$ on the LPA unit from left to right | | | | | | | $\Sigma V_{min}$ |
|---|---|---|---|---|---|---|---|---|
| System | 1 | 2 | 3 | 4 | 5 | 6 | 7 | |
| | | | | **M06** | | | | |
| $pN_1$ | -18.42 | -18.42 | | | | | | -36.85 |
| $pN_2$ | -19.88 | -15.16 | -19.88 | | | | | -54.92 |
| $pN_3$ | -20.41 | -16.38 | -16.38 | -20.41 | | | | -73.57 |
| $pN_4$ | -20.78 | -17.01 | -17.37 | -17.01 | -20.78 | | | -92.95 |
| $pN_5$ | -20.81 | -17.23 | -17.85 | -17.85 | -17.23 | -20.81 | | -111.80 |
| $pN_6$ | -20.85 | -17.41 | -18.20 | -18.39 | -18.20 | -17.41 | -20.85 | -131.30 |

**Table 2.20.** $V_{min}$ (kcal/mol) on LPA part using M06-2X/6-311++G(d,p) method.

| | $V_{min}$ on the LPA unit from left to right | | | | | | | $\Sigma V_{min}$ |
|---|---|---|---|---|---|---|---|---|
| System | 1 | 2 | 3 | 4 | 5 | 6 | 7 | |
| | | | | **M062X** | | | | |
| $pN_1$ | -20.34 | -20.34 | | | | | | -40.68 |
| $pN_2$ | -21.66 | -17.52 | -21.66 | | | | | -60.83 |
| $pN_3$ | -22.14 | -18.59 | -18.59 | -22.14 | | | | -81.48 |
| $pN_4$ | -22.40 | -19.01 | -19.52 | -19.01 | -22.40 | | | -102.30 |
| $pN_5$ | -22.48 | -19.40 | -20.12 | -20.12 | -19.40 | -22.48 | | -124.00 |
| $pN_6$ | -22.45 | -19.48 | -20.33 | -20.58 | -20.33 | -19.48 | -22.45 | -145.10 |

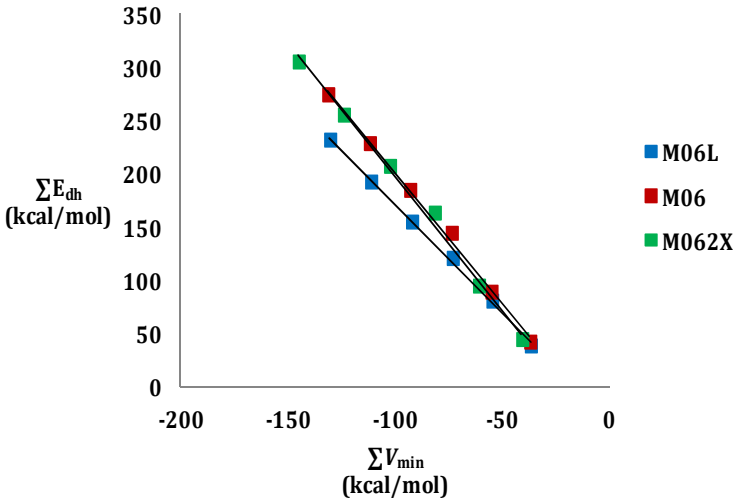


**Figure 2.12**. Correlation between $\sum V_{min}$ and $\sum E_{dh}$ for pN series of molecules at M06 and M062X methods.

## 2.4.6. Frontier Molecular Orbitals of LPA Mimics

HOMO-LUMO gap is closely related to number of resonant sextets in the molecule.[102] High kinetic stability is a direct consequence of large HOMO-LUMO gap ($E_{LUMO-HOMO}$) since addition of electrons to high lying LUMO ($E_{LUMO}$) and extraction of electrons from high lying HOMO ($E_{HOMO}$) is energetically unfavourable.[103-108]

A graph that plots the HOMO and LUMO energies along the Y-axis against the number of dihydropyrazine rings in every set of molecules in X-axis is drawn (Figure 2.13 – 2.16). The magnitude of $E_{HOMO}$ decreases with number of annulating acene units. Unlike $E_{LUMO}$, the gradual increase in the $E_{HOMO}$ is clearly visible in all the figures. The interesting phenomena is that for pB series this change is more

prominent, while in the case of other higher acene annulated LPA mimics, the change becomes less and less prominent. The figure clearly shows that that there is only a slight decrease in the $E_{LUMO}$ with the chain length increase, which appears like there is no substantial change in LUMO. As the size of the acene that is being annulated increases the magnitude of the $E_{LUMO}$ energy also decreases. This decrease together with the small decrease when number of annulated units increases are the main reasons for the $E_{LUMO-HOMO}$ tuning as we progress from smaller to longer LPA mimics, since the reduction in band gap is not supported by the energy lowering of the HOMO.

**Table 2.21**. HOMO, LUMO energies and HOMO-LUMO energy gap for LPA mimics.

| System | $E_{HOMO}$ (eV) | $E_{LUMO}$ (eV) | $E_{LUMO-HOMO}$ (eV) | System | $E_{HOMO}$ (eV) | $E_{LUMO}$ (eV) | $E_{LUMO-HOMO}$ (eV) |
|---|---|---|---|---|---|---|---|
| B | -6.44 | -0.95 | 5.49 | A | -5.04 | -2.49 | 2.55 |
| $pB_1$ | -4.15 | -0.94 | 3.21 | $pA_1$ | -4.55 | -2.44 | 2.11 |
| $pB_2$ | -3.61 | -0.93 | 2.69 | $pA_2$ | -4.34 | -2.40 | 1.93 |
| $pB_3$ | -3.40 | -0.91 | 2.50 | $pA_3$ | -4.17 | -2.38 | 1.80 |
| $pB_4$ | -3.28 | -0.89 | 2.39 | $pA_4$ | -4.08 | -2.36 | 1.73 |
| $pB_5$ | -3.21 | -0.88 | 2.33 | $pA_5$ | -4.02 | -2.35 | 1.68 |
| $pB_6$ | -3.17 | -0.87 | 2.30 | $pA_6$ | -3.99 | -2.34 | 1.65 |
| N | -5.56 | -1.88 | 3.68 | T | -4.69 | -2.89 | 1.80 |
| $pN_1$ | -4.43 | -1.81 | 2.62 | $pT_1$ | -4.32 | -2.84 | 1.47 |
| $pN_2$ | -3.96 | -1.77 | 2.19 | $pT_2$ | -4.16 | -2.81 | 1.35 |
| $pN_3$ | -3.75 | -1.74 | 2.01 | $pT_3$ | -4.08 | -2.79 | 1.29 |
| $pN_4$ | -3.62 | -1.71 | 1.92 | $pT_4$ | -4.03 | -2.77 | 1.26 |
| $pN_5$ | -3.55 | -1.69 | 1.86 | $pT_5$ | -4.00 | -2.76 | 1.24 |
| $pN_6$ | -3.49 | -1.67 | 1.82 | $pT_6$ | -3.98 | -2.75 | 1.22 |

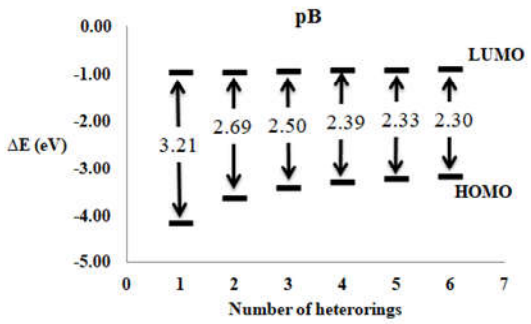


**Figure 2.13**. HOMO-LUMO energy gap modulation in pB series LPA mimics.

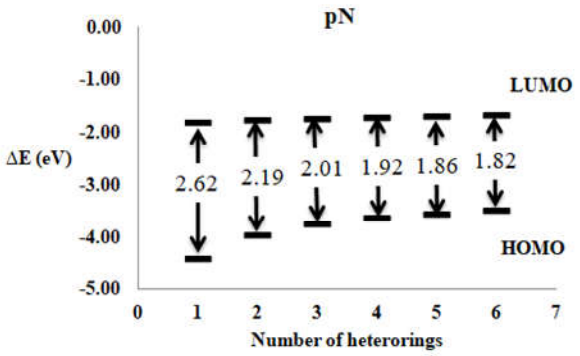


**Figure 2.14**. HOMO-LUMO energy gap modulation in pN series of LPA mimics.

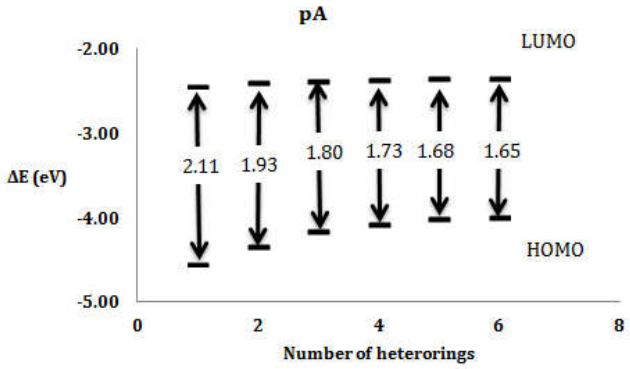


**Figure 2.15**. HOMO-LUMO energy gap modulation in pA series of LPA mimics.

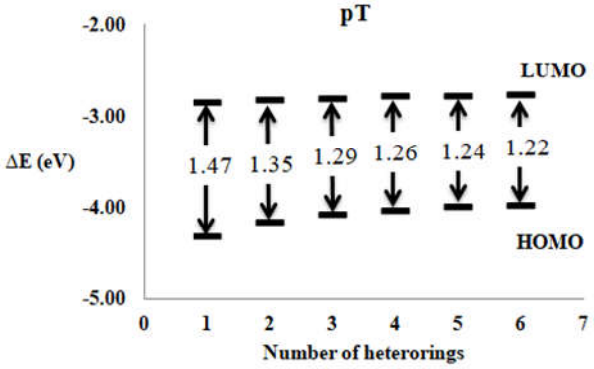


**Figure 2.16**. HOMO-LUMO energy gap modulation in pT series of LPA mimics.

The FMO energies and the gap between them for all the systems are given in Table 2.21. Compared to LPA, all the corresponding LPA mimics show significantly higher $E_{HOMO}$ and slightly higher $E_{LUMO}$ (Table 2.21). For instance, in the case of LPA mimics composed of anthracene moieties, *viz*. $pA_1$ - $pA_6$, $E_{HOMO}$ is in the range -4.55 to -3.99 eV which is higher than $E_{HOMO}$ of anthracene (-5.04 eV) while their $E_{LUMO}$ falls in a narrow range -2.44 to -2.34 eV is close to ε1 -2.49 eV observed for anthracene. Since only the $E_{HOMO}$ energy showed significant increase with respect to the length of the LPA mimic, a steady decease in $E_{LUMO-HOMO}$ with increase in size of

the molecule is observed in all the systems. In fact, going from $pB_1$ to $pT_6$, $E_{LUMO-HOMO}$ modulation can be achieved from 3.21 eV to 1.22 eV and suggests that excellent band gap tuning using dihydropyrazine annulated linear polyacenes can be achieved for solar cell applications.

The HOMO and LUMO pictures given for the representative cases $pA_2$ and $pT_2$ (Figure 2.17) show that HOMO is formed by the delocalization of N-lone pairs in to the $B_{1g}$ symmetric π-orbital for former and $A_u$ symmetric π-orbital for the latter whereas LUMO localized on to the LPA core shows features very similar to the $B_{3u}$ symmetric LUMO of anthracene and $B_{1g}$ symmetric LUMO of tetracene (under $D_{2h}$ molecular symmetry).

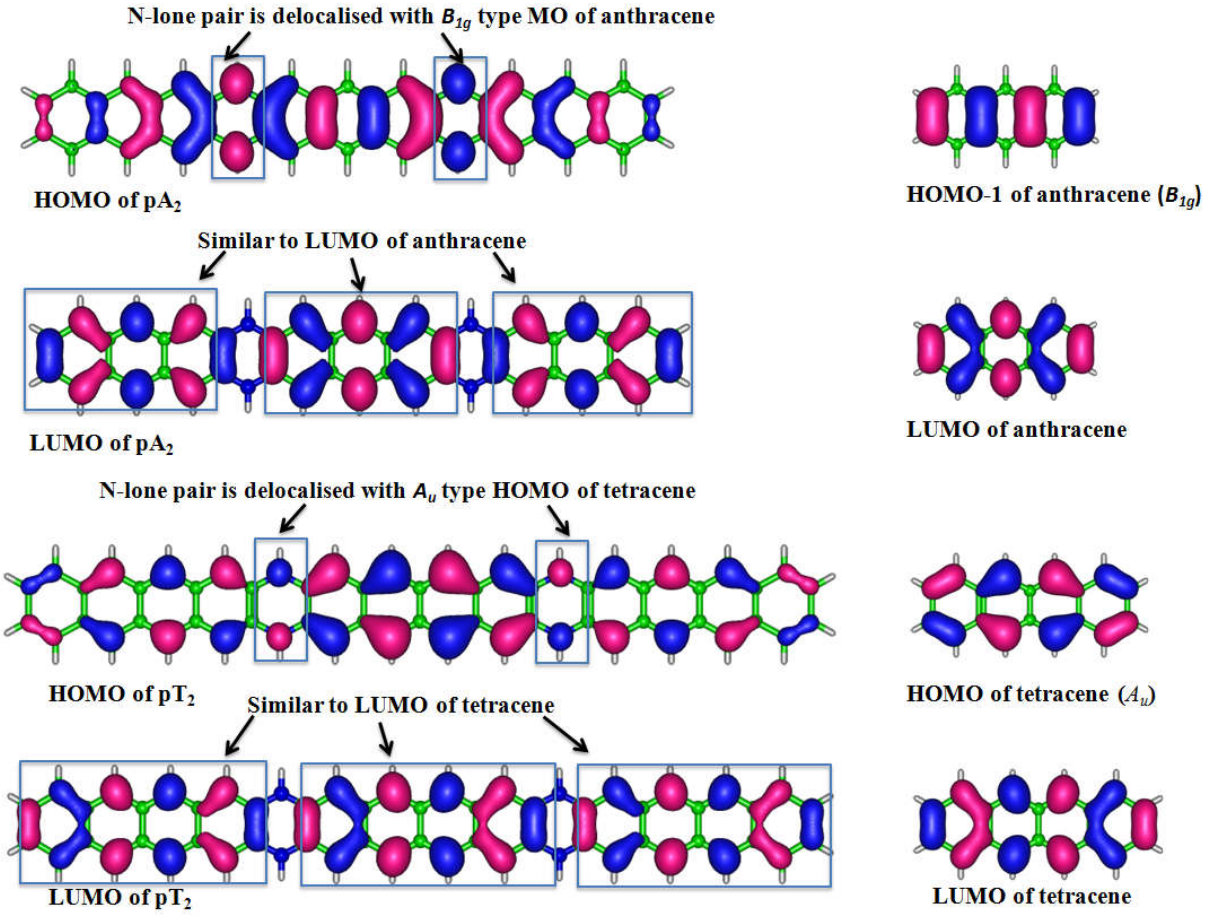


**Figure 2.17**. HOMO and LUMO orbitals of $pA_2$ and $pT_2$ with similar kind of MO's of anthracene and tetracene.

In fact, in every molecule, two sets of π-MOs are observed, *viz*. one characteristic of the LPA moiety, localized exclusively on them and devoid of any contributions from the N-lone pairs and the other consisting of the contributions of N-lone pairs. The delocalization of N-lone pairs in HOMO is observed for all the LPA

mimics and the energy of HOMO is influenced by the number of N-centres in the molecule whereas LUMO energy is independent of the N-centres. For all the systems MO shows similar characteristics features as mentioned above, proving electronic level similarity of LPA mimics with the LPAs composing them.

### 2.4.7. Singlet-triplet Energy Gap

Lowest singlet (S1) and triplet (T1) state energies and structures corresponding to every set of systems are done using time-dependent DFT optimisation. By plotting the number of dihydropyrazine moieties against the $\Delta E_{T1\text{-}S0}$ the trend of the decrease in the energy gap is visualised for every set of molecule (Figure 2.18).

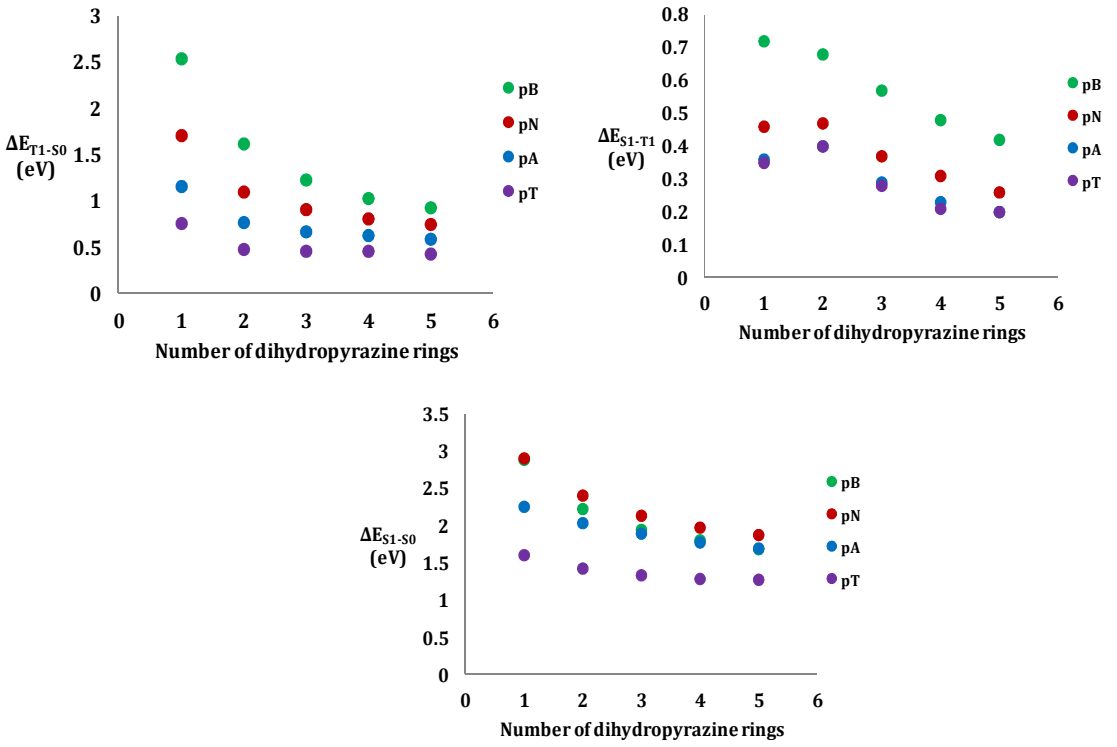


**Figure 2.18.**Plots showing trends in $\Delta E_{T1\text{-}S0}$ , $\Delta E_{S1\text{-}T1}$ & $\Delta E_{S1\text{-}S0}$ with size of system.

The emission process is the vertical S1→S0 transition; thereby the energy gap ($E_{S1}$-$E_{S0}$) is a direct measure of the emission lifetime. Delayed S1 to S0 de-excitation accounts for the fluorescence and the energy difference can be directly related to the fluorescence lifetime also. $\Delta E_{T1\text{-}S0}$ corresponds to the phosphorescence phenomena, and is directly related to the phosphorescence lifetime of the molecule, which has a direct relation with the photo-stability of the molecule. Whereas $\Delta E_{T1\text{-}S1}$ corresponds to the intersystem crossing (ISC) phenomena, which is a nonradiative form of relaxation having the slowest rate of all the transitions. The efficiency of ISC

can be improved by reducing the energy gap between the singlet and triplet excited states.[109] Spin-orbit coupling is directly related to the intersystem crossing. The rate of intersystem crossing largely affects the conversion efficiency of a solar cell.[110, 111] Phosphorescence is a manifestation of intersystem crossing where the relaxation from the excited triplet state to the singlet ground state happens occurs. Optical gap of a system is predicted by the energy of lowest singlet excited state, and energy ordering of T1 with respect to S1 is very important factor that determines the reverse intersystem crossing (RISC) which in turn is a determining factor of efficiency of electroluminescence.[112]

For pB and pN series the trend is clearly decreasing in nature, but for pA and pT seires even though the size increase is more than that of the former cases the change in the energy gap is not very significant. Thereby the plot corresponding to these series appears as a straight line. The energy gap between first singlet excited state and first triplet excited state ($\Delta E_{S1\text{-}T1}$) is plotted against the number of hetero-rings present in every set of molecules to give the plot (Figure 2.18) describing the decrease of the energy gap as the size of the molecular system is increased. Very small S1-T1 gap is observed experimentally and theoretically for conjugated systems. The difference in energy between S1 and T1 ($\Delta E_{S1\text{-}T1}$), T1 and S0 ($\Delta E_{T1\text{-}S0}$) and S1 and S0 ($\Delta E_{S1\text{-}S0}$)are calculated which are given in Table 2.22.

**Table 2.22.** Energy difference between singlet and triplet levels in eV.

| System | $\Delta E_{T1\text{-}S0}$ (eV) | $\Delta E_{S1\text{-}T1}$ (eV) | $\Delta E_{S1\text{-}S0}$ (eV) | System | $\Delta E_{T1\text{-}S0}$ (eV) | $\Delta E_{S1\text{-}T1}$ (eV) | $\Delta E_{S1\text{-}S0}$ (eV) |
|---|---|---|---|---|---|---|---|
| $pB_1$ | 2.26 | 0.63 | 2.89 | $pA_1$ | 1.53 | 0.73 | 2.26 |
| $pB_2$ | 1.74 | 0.49 | 2.23 | $pA_2$ | 1.49 | 0.55 | 2.04 |
| $pB_3$ | 1.56 | 0.39 | 1.95 | $pA_3$ | 1.49 | 0.41 | 1.90 |
| $pB_4$ | 1.47 | 0.34 | 1.81 | $pA_4$ | 1.49 | 0.29 | 1.78 |
| $pB_5$ | 1.40 | 0.29 | 1.69 | $pA_5$ | 1.49 | 0.21 | 1.70 |
| $pN_1$ | 2.31 | 0.60 | 2.91 | $pT_1$ | 0.94 | 0.67 | 1.61 |
| $pN_2$ | 1.99 | 0.42 | 2.41 | $pT_2$ | 0.92 | 0.51 | 1.43 |
| $pN_3$ | 1.85 | 0.29 | 2.14 | $pT_3$ | 0.93 | 0.41 | 1.34 |
| $pN_4$ | 1.78 | 0.20 | 1.98 | $pT_4$ | 0.94 | 0.35 | 1.29 |
| $pN_5$ | 1.74 | 0.14 | 1.88 | $pT_5$ | 0.94 | 0.34 | 1.28 |

The role of number and type of the heteroring is important in the tuning of the energy gap, as evident from the fact that for systems having same number of rings the excited energy gap is different. For example, $pB_2$ and $pN_1$ systems have 5 rings in them and the values $\Delta E_{T1\text{-}S0}$ and $\Delta E_{S1\text{-}T1}$ values are 1.74 eV and 0.49 eV for $pB_2$ and 2.31 eV and 0.60 eV for $pN_1$ systems. The emission lifetime can be accessed by the understanding of S1-S0 bandgap. The effective tuning in the values is illustrated using the Figure 2.18. The gradual decrease in the energy gap as the size increases is evident here.

## 2.4.8. Absorption Spectra

The theoretical absorption maxima values having maximum oscillator strength ($\lambda_{max}$) of all the molecules are given in Table 2.23 and the spectral features of all the systems are portrayed in Figure 2.19-2.22. Figure 2.19 represents the absorption spectra of all the molecules of pB series, whereas Figure 2.20, Figure 2.21 and Figure 2.22 are absorption spectra of all the molecules of pN, pA and pT series respectively.

**Table 2.23**. Absorption maxima values ($\lambda_{max}$) of LPA mimics.

| System | $\lambda_{max}$ (nm) | system | $\lambda_{max}$ (nm) | system | $\lambda_{max}$ (nm) | system | $\lambda_{max}$ (nm) |
|---|---|---|---|---|---|---|---|
| $pB_1$ | 242 | $pN_1$ | 296 | $pA_1$ | 342 | $pT_1$ | 381 |
| $pB_2$ | 388 | $pN_2$ | 330 | $pA_2$ | 376 | $pT_2$ | 413 |
| $pB_3$ | 427 | $pN_3$ | 564 | $pA_3$ | 638 | $pT_3$ | 706 |
| $pB_4$ | 441 | $pN_4$ | 605 | $pA_4$ | 681 | $pT_4$ | 645 |
| $pB_5$ | 458 | $pN_5$ | 636 | $pA_5$ | 619 | $pT_5$ | 684 |
| $pB_6$ | 464 | $pN_6$ | 659 | $pA_6$ | 650 | $pT_6$ | 715 |

For every system, as the size of the molecule increases, $\lambda_{max}$ shows significant red shift along with increase in the number of minor peaks in the spectrum. Analysing the absorption spectra of all the systems in pB series reveals that the $\lambda_{max}$ varies from 242 nm for $pB_1$ to 464 nm for $pB_5$. for $pB_1$ series the $\lambda_{max}$ having maximum oscillator strength is at 242 nm whereas the $\lambda_{max}$ at longest wavelength is at 338 nm. For $pB_2$ system the $\lambda_{max}$ values are at 388 and 409 nm. For $pB_3$ the in addition to the most prominent $\lambda_{max}$ at 427 nm, there are a set of $\lambda_{max}$ at 350, 360 and 446 nm. $pB_4$ system has $\lambda_{max}$ at 380, 441 and 465nm, whereas $pB_5$ system has $\lambda_{max}$ at 425, 458 and 475 nm. The longest system in the series $pB_6$ has $\lambda_{max}$ at 440,

464 and 475 nm. In the series $pB_1$ and $pB_2$ shows absorption in the UV region, while the other higher molecules in the series shows most of the absorption in the visible region of electromagnetic spectrum. One of the peculiarities of the systems is that the number of rings constituting does not have a profound effect on the value of absorption maxima. For example consider $pA_4$ and $pT_3$ both consisting of 19 rings, the values of $\lambda_{max}$ are 681 nm and 706 nm respectively. Similarly $pN_4$ and $pT_2$ are made up of 14 rings have $\lambda_{max}$ values at 605 nm and 413 nm respectively.

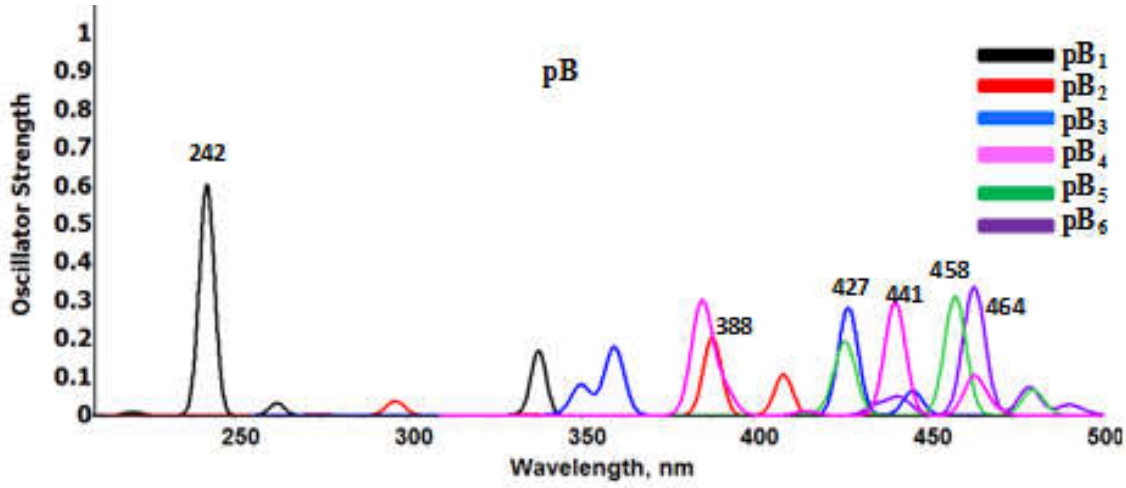


**Figure 2.19**. Absorption spectra of pB series at M06L/6-311++G(d,p) level of theory.

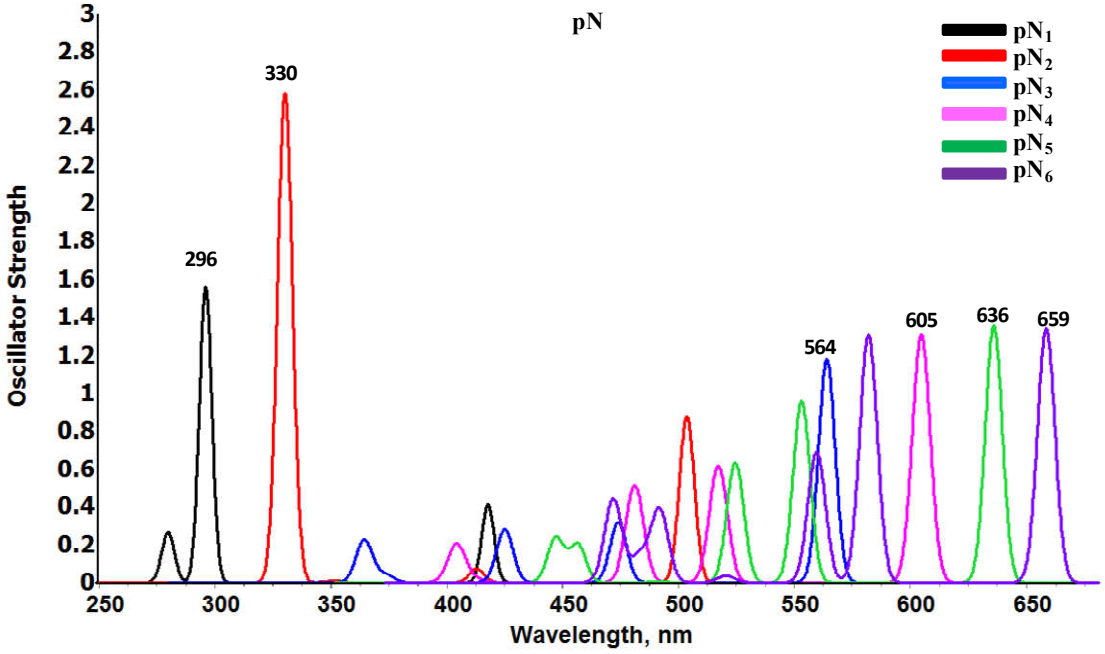


**Figure 2.20** Absorption spectra of pN series at M06L/6-311++G(d,p) level of theory.

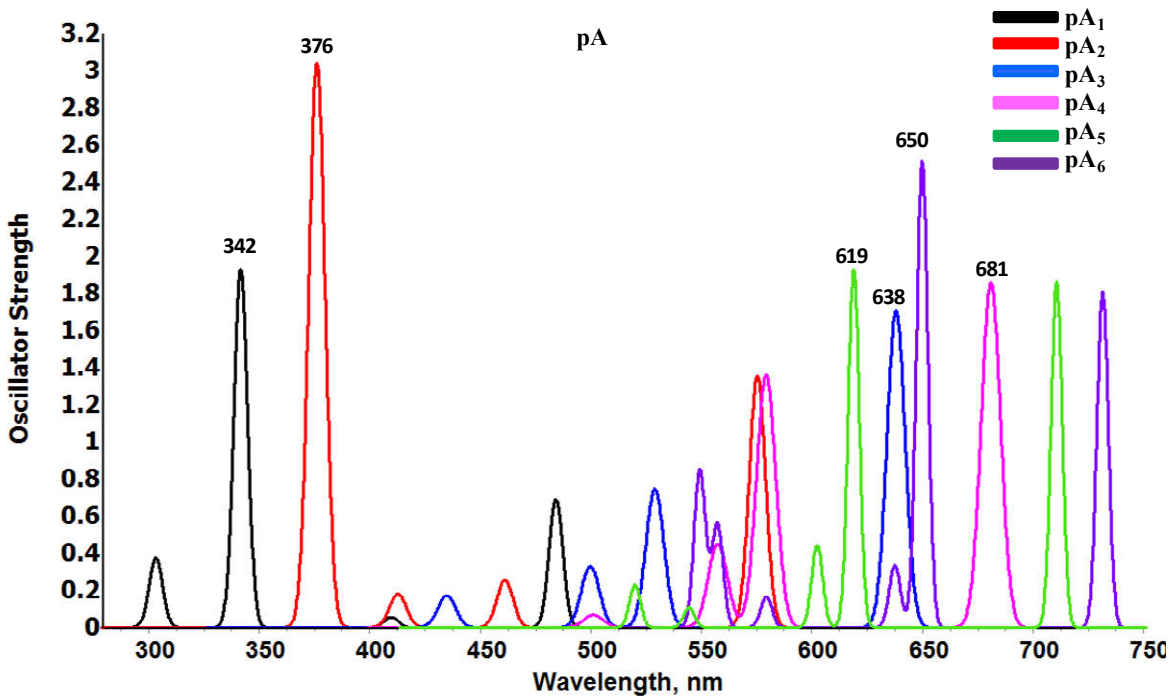


**Figure 2.2**1 Absorption spectra of pA series at M06L/6-311++G(d,p) level of theory.

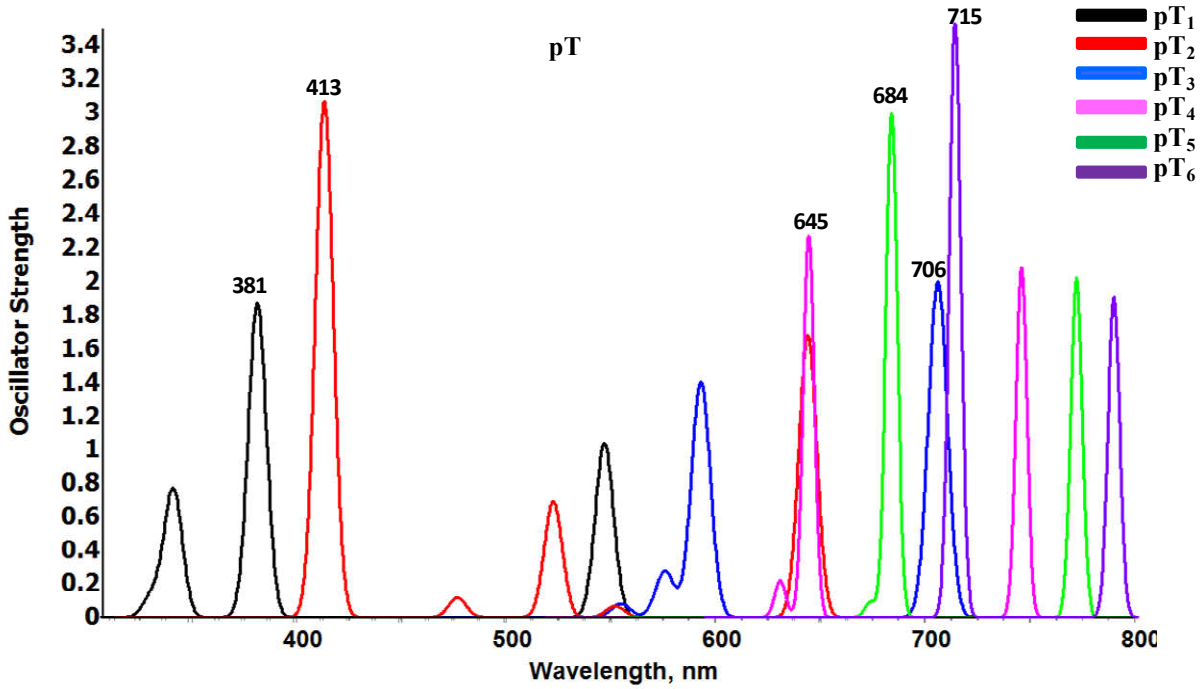


**Figure 2.22**. Absorption spectra of pT series at M06L/6-311++G(d,p) level of theory.

For pN series, $\lambda_{max}$ variation is from 296 to 659 nm. $pN_1$ system has absorption maxima having maximum oscillator strength at 296 nm and another one towards the red region at 417 nm. For $pN_2$ system the $\lambda_{max}$ values are at 330 and 504 nm. For $pN_3$ system the most prominent $\lambda_{max}$ appears at 564 nm, with a bunch of $\lambda_{max}$ at 364,

425 and 474 nm. $pN_4$ system has $\lambda_{max}$ at wavelengths 404, 481, 517 and 605 nm, whereas $pN_5$ system has prominent $\lambda_{max}$ at wavelengths 447, 457, 525, 553 and 636 nm. The most red shifted absorption is observed for the system $pN_6$ which has $\lambda_{max}$ at 659 nm, together with weak absorption at the wavelengths 472, 492, 560 and 582 nm. In the case of pN series like pB series first two members are showing absorption in the UV region and the other systems in the visible region.

For pA series, the change in $\lambda_{max}$ is from 303 nm to 731 nm. $pA_1$ system has absorption maxima having maximum oscillator strength at 342 nm and absorption in the blue shifted region at 303 nm and a red shifted one at 484 nm. For $pA_2$ system the $\lambda_{max}$ values are at 376 and 575 nm. For $pA_3$ system the most prominent $\lambda_{max}$ appears at 638 nm, with a set of $\lambda_{max}$ at 434, 500, and 529 nm. $pA_4$ system has $\lambda_{max}$ at wavelengths 501, 557, 579 and 681 nm, in which the most prominent one having the maximum oscillator strength is at wavelength 681 nm. $pA_5$ system has prominent $\lambda_{max}$ at wavelengths 520, 544, 602, 619 and 711 nm. The most red shifted absorption is observed for the system $pA_6$ which has $\lambda_{max}$ at 731nm, together with absorptions at the wavelengths 557, 579, 637, 650 nm, with the strongest absorption at 650 nm. Majority of the pA systems show absorption in the visible region while except $pA_1$ and $pA_2$, which shows absorption in the UV region.

In pT series, $pT_1$ and $pT_5$ show the lowest 341 nm and the highest 789 nm values for $\lambda_{max}$. $pT_1$ system has absorption maxima having maximum oscillator strength at 381 nm and absorption in the blue shifted region at 341 nm and a red shifted one at 547 nm. For $pT_2$ system the $\lambda_{max}$ values are at 413, 523 and 644 nm. For $pT_3$ system the most prominent $\lambda_{max}$ appears at 706 nm, together with absorptions at 575 and 592 nm. $pT_4$ system has $\lambda_{max}$ at wavelengths 631, 645 and 746 nm, whereas $pT_5$ system has prominent $\lambda_{max}$ at wavelengths 684 and 772 nm. The most red shifter absorption is observed for the system $pT_6$ which has $\lambda_{max}$ at 789 nm, and the strongest absorption at 715 nm. As the size of the system increases the number of $\lambda_{max}$ is decreasing in this series. Taking the example of $pT_5$ and $pT_6$, both having only two absorption maxima values in the theoretical spectra calculated the above statement is validated. In the case of pT series only $pT_1$ shows absorption in the UV region, while all others absorbs in the visible region. Theoretical tuning of the $\lambda_{max}$ values can be realised by the change in number of systems annulated which is very much beneficial in the engineering of dye-sensitized solar cells.[113]

**Table 2.23.** Light harvesting efficiency (LHE) of all LPA mimics.

| System | LHE | System | LHE | System | LHE | System | LHE |
|---|---|---|---|---|---|---|---|
| $pB_1$ | 0.748 | $pN_1$ | 0.972 | $pA_1$ | 0.988 | $pT_1$ | 0.986 |
| $pB_2$ | 0.375 | $pN_2$ | 0.997 | $pA_2$ | 0.999 | $pT_2$ | 0.999 |
| $pB_3$ | 0.477 | $pN_3$ | 0.934 | $pA_3$ | 0.981 | $pT_3$ | 0.990 |
| $pB_4$ | 0.495 | $pN_4$ | 0.952 | $pA_4$ | 0.986 | $pT_4$ | 0.995 |
| $pB_5$ | 0.511 | $pN_5$ | 0.956 | $pA_5$ | 0.989 | $pT_5$ | 0.999 |
| $pB_6$ | 0.561 | $pN_6$ | 0.955 | $pA_6$ | 0.998 | $pT_6$ | 1.000 |

Light harvesting efficiency (LHE) for a material is the maximum attainable efficiency for light absorption, which can be theoretically predicted from the electronic spectral data. LHE of a material is closely related to the magnitude of oscillator strength *(f)* as larger the oscillator strength, larger the light harvesting efficiency,[114-116] which is evident from the equation, LHE = $1\text{-}10^{-f}$. The LHE of all the system analysed is given in Table 2.22. Very high LHE of the order of 0.9 is observed for almost all systems in pN, pA and pT series. For pB series comparatively lower values are obtained. For pB series the lowest LHE of 0.375 is shown by $pB_2$ and maximum of 0.748 is exhibited by $pB_1$. Of all the systems analysed, the maximum LHE of 1.000 is exhibited by the longest system $pT_6$. These values infer that the size and the length of the LPA used are influencing the LHE, since same number of rings containing systems shows different LHE values. For example $pB_2$ and $pN_1$ systems having 5 rings in them show significantly varied LHE values of 0.375 and 0.972 respectively.

## 2.5. Conclusions

Density functional theory calculations at M06L/6-311++G(d,p) level have been carried out on 24 dihydropyrazine annulated linear polyacene systems to reveal their aromaticity, electronic character, UV spectra, HOMO-LUMO energy gap and singlet-triplet energy gap. The LPA mimics composed of benzene units ($pB_1$ – $pB_6$) are non-planar while those composed of naphthalene ($pN_1$ – $pN_6$), anthracene ($pA_1$ – $pA_6$) and tetracene ($pT_1$ – $pT_6$) units are planar. In pB series, mixing of N-lone pairs

with the π-system of benzene core is ineffective due to the core retaining six-π electron delocalization while the decrease in the net π-electron content of the higher acene cores promotes strong delocalization of N-lone pairs with the π-electrons of carbons rings, leading to planar structures. All the molecules showed strong multidimensional character of aromaticity such as energetic stabilization, bond length equalization, and magnetic properties. The dehydrogenation energy ($E_{dh}$) computed for each of the N-heterocycle of an LPA mimic provided a simple and effective way to assess the thermodynamic stability of the molecule due to aromaticity. The aromatic stabilization is enhanced in larger LPA mimics due to enhancement in the involvement of N-lone pairs in π-electron conjugation. This has been verified by the analysis of molecular electrostatic potential (MESP) features as this property showed improvements in electron rich character of the core hydrocarbon units at the expense of the N-lone pairs. The absorption spectra of the studied systems show the possibility of tuning the $\lambda_{max}$ values which is an advantage to the optoelectronic industry. As the size of the systems increases, $\lambda_{max}$ value gets more and more red shifted as expected. As the size of LPA mimic increased, the HOMO energy increased with concomitant decrease in LUMO energy resulting substantial reduction in HOMO-LUMO energy gap. The light harvesting efficiency of most of the designed systems is very high, which makes them good candidates for solar applications also. Moreover, a gradual decrease in the singlet-triplet energy gap ($\Delta E_{ST}$) proportional to the size of the LPA mimics is observed. In short, by adjusting the length of LPA unit as well as by choosing the appropriate number of dihydropyrazine rings for annulation, an LPA mimic showing the desired band gap and $\Delta E_{ST}$ gap can be designed for potential applications in the fabrication of efficient optoelectronic devices, as the calculated light harvesting efficiency of designed systems are high.

The dihydropyrazine systems $pB_1$[67, 117] and $pN_1$[57] are known in the literature while higher analogues or higher acene based systems are yet to be synthesised. As mentioned before, benzene core could be unattractive for making planar structures while for a higher acene such as tetracene, even with one annulation of the N-heterocycle can yield a planar, aromatic structure with nine rings. We hope that the theoretical predictions provided in this work may inspire the synthetic chemists to

explore the rich possibilities of higher LPA mimics, including the derivatization of the N-centres for improving the solubility requirements.

## 2.6. References


1. R. Firouzi and M. Zahedi, *J. Mol. Struct.:THEOCHEM*, **2008**, 862, 7-15.
2. J. E. Anthony, *Chem. Rev.*, **2006**, 106, 5028-5048.
3. T. Yamabe, S. Yata and S. Wang, *Synt. Met.*, **2003**, 137, 949-951.
4. T. Strassner, A. Weitz, J. Rose, F. Wudl and K. N. Houk, *Chem. Phys. Lett.*, **2000**, 321, 459-462.
5. J. E. Anthony, *Angew. Chem. Int. Ed.*, **2008**, 47, 452-483.
6. G. Brocks, J. van den Brink and A. F. Morpurgo, *Phys. Rev. Lett.*, **2004**, 93, 146405.
7. W.-Q. Deng and W. A. Goddard, *J. Phys. Chem. B*, **2004**, 108, 8614-8621.
8. Y. C. Cheng, R. J. Silbey, D. A. da Silva Filho, J. P. Calbert, J. Cornil and J. L. Brédas, *J. Chem. Phys.*, **2003**, 118, 3764-3774.
9. D. Biermann and W. Schmidt, *J. Am. Chem. Soc.*, **1980**, 102, 3163-3173.
10. C. Tönshoff and H. F. Bettinger, *Angew. Chem. Int. Ed.*, **2010**, 49, 4125-4128.
11. R. Mondal, B. K. Shah and D. C. Neckers, *J. Am. Chem. Soc.*, **2006**, 128, 9612-9613.
12. E. Clar, *Polycyclic hydrocarbons Vol. 1&2*, Academic Press, London, 1964.
13. E. Clar, *The Aromatic Sextet*, Wiley, New York, 1972.
14. M. Solà, *Front. Chem.*, **2013**, 1, 1-8.
15. M. Randić, *Chem. Rev.*, **2003**, 103, 3449-3606.
16. K. P. Vijayalakshmi and C. H. Suresh, *New J. Chem.*, **2010**, 34, 2132-2138.
17. S. R. Gadre and R. N. Shirsat, *Electrostatics of Atoms and Molecules*, Univesities Press, Hyderabad, 2000.
18. P. Bultinck, M. Rafat, R. Ponec, B. Van Gheluwe, R. Carbó-Dorca and P. Popelier, *J. Phys. Chem. A*, **2006**, 110, 7642-7648.
19. A. R. Katritzky, K. Jug and D. C. Oniciu, *Chem. Rev.*, **2001**, 101, 1421-1450.
20. F. Feixas, E. Matito, J. Poater and M. Sola, *Chem. Soc. Rev.*, **2015**, 44, 6434-6451.
21. S. K. Pandey, D. Manogaran, S. Manogaran and H. F. Schaefer, *J. Phys. Chem. A*, **2016**, 120, 2894-2901.

22. K. Jug and A. M. Köster, *J. Phys. Org. Chem.*, **1991**, 4, 163-169.
23. A. R. Katritzky, P. Barczynski, G. Musumarra, D. Pisano and M. Szafran, *J. Am. Chem. Soc.*, **1989**, 111, 7-15.
24. M. K. Cyrañski, T. M. Krygowski, A. R. Katritzky and P. v. R. Schleyer, *J. Org. Chem.*, **2002**, 67, 1333-1338.
25. M. Alonso and B. Herradón, *Chem. Eur. J.*, **2007**, 13, 3913-3923.
26. A. Stanger, *Chem. Commun.*, **2009**, 1939-1947.
27. P. Lazzeretti, *Phys. Chem. Chem. Phys.*, **2004**, 6, 217-223.
28. S. Motomura, M. Nakano, H. Fukui, K. Yoneda, T. Kubo, R. Carion and B. Champagne, *Phys. Chem. Chem. Phys.*, **2011**, 13, 20575-20583.
29. M. Kaipio, M. Patzschke, H. Fliegl, F. Pichierri and D. Sundholm, *J. Phys. Chem. A*, **2012**, 116, 10257-10268.
30. G. Monaco and R. Zanasi, *J. Phys. Chem. A*, **2014**, 118, 1673-1683.
31. P. O. Dral, M. Kivala and T. Clark, *J. Org. Chem.*, **2013**, 78, 1894-1902.
32. M. Winkler and K. N. Houk, *J. Am. Chem. Soc.*, **2007**, 129, 1805-1815.
33. A. L. Appleton, S. M. Brombosz, S. Barlow, J. S. Sears, J.-L. Bredas, S. R. Marder and U. H. F. Bunz, *Nat. Commun.*, **2010**, 1, 1-6.
34. Q. Miao, *Synlett*, **2012**, 2012, 326-336.
35. O. Tverskoy, F. Rominger, A. Peters, H.-J. Himmel and U. H. F. Bunz, *Angew. Chem. Int. Ed.*, **2011**, 50, 3557-3560.
36. J. U. Engelhart, B. D. Lindner, O. Tverskoy, F. Rominger and U. H. F. Bunz, *Org. Lett.*, **2012**, 14, 1008-1011.
37. B. D. Lindner, J. U. Engelhart, M. Märken, O. Tverskoy, A. L. Appleton, F. Rominger, K. I. Hardcastle, M. Enders and U. H. F. Bunz, *Chem. Eur. J.*, **2012**, 18, 4627-4633.
38. U. H. F. Bunz and J. U. Engelhart, *Chem. Eur. J.*, **2016**, 4680-4689.
39. C.-L. Song, C.-B. Ma, F. Yang, W.-J. Zeng, H.-L. Zhang and X. Gong, *Org. Lett.*, **2011**, 13, 2880-2883.
40. K. Goto, R. Yamaguchi, S. Hiroto, H. Ueno, T. Kawai and H. Shinokubo, *Angew. Chem. Int. Ed.*, **2012**, 51, 10333-10336.
41. K. Seth, S. Raha Roy and A. K. Chakraborti, *Chem. Commun.*, **2016**, 52, 922-925.
42. J. K. Laha, K. S. S. Tummalapalli and A. Gupta, *Org. Lett.*, **2014**, 16, 4392-4395.

43. Z. Wróbel, K. Stachowska and A. Kwast, *Eur. J. Org. Chem.*, **2014**, 2014, 7721-7725.
44. L. Yu, X. Zhou, D. Wu and H. Xiang, *J. Organomet. Chem.*, **2012**, 705, 75-78.
45. F. Wudl, P. A. Koutentis, A. Weitz, Bin Ma, T. Strassner, K. N. Houk and S. I. Khan, *Pure Appl. Chem.*, **1999**, 71, 295-302.
46. M. Altarawneh and B. Z. Dlugogorski, *Environ. Sci. Technol.*, **2015**, 49, 2215-2221.
47. O. Hinsberg, *Liebigs Ann.*, **1901**, 319, 257-286.
48. G. R. Clemo and H. McIlwain, *J. Chem. Soc.*, **1934**, 1991-1993.
49. U. H. F. Bunz, *Chem. Eur. J.*, **2009**, 15, 6780-6789.
50. H. Alvaro Galué, O. Pirali and J. Oomens, *Astron. Astrophys.*, **2010**, 517, A15.
51. Q. Miao, T.-Q. Nguyen, T. Someya, G. B. Blanchet and C. Nuckolls, *J. Am. Chem. Soc.*, **2003**, 125, 10284-10287.
52. Q. Miao, *Adv. Mater.*, **2014**, 26, 5541-5549.
53. K. E. Maly, *Cryst. Growth Des.*, **2011**, 11, 5628-5633.
54. Y. Sun, Y. Liu and D. Zhu, *J. Mater. Chem.*, **2005**, 15, 53-65.
55. C. An, X. Guo and M. Baumgarten, *Cryst. Growth Des.*, **2015**, 15, 5240-5245.
56. A. H. Endres, M. Schaffroth, F. Paulus, H. Reiss, H. Wadepohl, F. Rominger, R. Krämer and U. H. F. Bunz, *J. Am. Chem. Soc.*, **2016**, 138, 1792-1795.
57. Q. Tang, D. Zhang, S. Wang, N. Ke, J. Xu, J. C. Yu and Q. Miao, *Chem. Mater.*, **2009**, 21, 1400-1405.
58. S.-Z. Weng, P. Shukla, M.-Y. Kuo, Y.-C. Chang, H.-S. Sheu, I. Chao and Y.-T. Tao, *ACS Appl. Mater. Interfaces*, **2009**, 1, 2071-2079.
59. M. M. Islam, S. Pola and Y.-T. Tao, *Chem. Commun.*, **2011**, 47, 6356-6358.
60. X. Wang and K.-C. Lau, *J. Phys. Chem. C*, **2012**, 116, 22749-22758.
61. C. Li, W. Jiang, X. Zhu and Z. Wang, *Asian J. Org. Chem.*, **2014**, 3, 114-117.
62. M. Karim and Y. Jahng, *Molecules*, **2016**, 21, 407.
63. G. Westphal, *Z. Phys. Chem.*, **1969**, 9, 339-339.
64. S.-J. Chen and F. W. Fowler, *J. Org. Chem.*, **1970**, 35, 3987-3989.
65. G. B. Schuster, S. P. Schmidt and B. G. Dixon, *J. Phys. Chem.*, **1980**, 84, 1841-1843.
66. F. W. Fowler and S.-J. Chen, *J. Org. Chem.*, **1971**, 36, 4025-4028.

67. K. V. Subba Rao, B. Srinivas, A. R. Prasad and M. Subrahmanyam, *Chem. Commun.*, **2000**, 1533-1534.
68. K. Oshima, T. Ohmura and M. Suginome, *Chem. Commun.*, **2012**, 48, 8571-8573.
69. R. R. Schmidt, M. Dimmler and P. Hemmerich, *Ber.*, **1976**, 109, 2395-2404.
70. M. Märken, D. Lindner Benjamin, L. Appleton Anthony, F. Rominger and U. H. F. Bunz, *Pure Appl. Chem.*, **2014**, 86, 483-488.
71. H. Choi, X. Yang, G. W. Mitchell, C. P. Collier, F. Wudl and J. R. Heath, *J. Phys. Chem. B*, **2002**, 106, 1833-1839.
72. J. U. Engelhart, F. Paulus, M. Schaffroth, V. Vasilenko, O. Tverskoy, F. Rominger and U. H. F. Bunz, *J. Org. Chem.*, **2016**, 81, 1198-1205.
73. Y. Zhao and D. G. Truhlar, *Acc. Chem. Res.*, **2008**, 41, 157-167.
74. Y. Zhao and D. G. Truhlar, *Theor. Chem. Acc.*, **2008**, 120, 215-247.
75. G. W. T. M. J. Frisch, H. B. Schlegel, G. E. Scuseria,, J. R. C. M. A. Robb, G. Scalmani, V. Barone, B. Mennucci,, H. N. G. A. Petersson, M. Caricato, X. Li, H. P. Hratchian,, J. B. A. F. Izmaylov, G. Zheng, J. L. Sonnenberg, M. Hada,, K. T. M. Ehara, R. Fukuda, J. Hasegawa, M. Ishida, T. Nakajima,, O. K. Y. Honda, H. Nakai, T. Vreven, J. A. Montgomery, Jr.,, F. O. J. E. Peralta, M. Bearpark, J. J. Heyd, E. Brothers,, V. N. S. K. N. Kudin, T. Keith, R. Kobayashi, J. Normand,, A. R. K. Raghavachari, J. C. Burant, S. S. Iyengar, J. Tomasi,, N. R. M. Cossi, J. M. Millam, M. Klene, J. E. Knox, J. B. Cross,, C. A. V. Bakken, J. Jaramillo, R. Gomperts, R. E. Stratmann,, A. J. A. O. Yazyev, R. Cammi, C. Pomelli, J. W. Ochterski,, K. M. R. L. Martin, V. G. Zakrzewski, G. A. Voth,, J. J. D. P. Salvador, S. Dapprich, A. D. Daniels,, J. B. F. O. Farkas, J. V. Ortiz, J. Cioslowski, and and D. J. Fox *Gaussian 09, Revision D.01,*; Gaussian Inc.: Wallingford CT, 2013
76. P. v. R. Schleyer, C. Maerker, A. Dransfeld, H. Jiao and N. J. R. v. E. Hommes, *J. Am. Chem. Soc.*, **1996**, 118, 6317-6318.
77. J. Kruszewski and T. M. Krygowski, *Tetrahedron Lett.*, **1972**, 13, 3839-3842.
78. E. Runge and E. K. U. Gross, *Phys. Rev. Lett.*, **1984**, 52, 997-1000.
79. M. E. CASIDA, in *Recent Advances in Density Functional Methods*, WORLD SCIENTIFIC, 2011, pp. 155-192.
80. M. Petersilka, U. J. Gossmann and E. K. U. Gross, *Phys. Rev. Lett.*, **1996**, 76, 1212-1215.

81. K. Burke, J. Werschnik and E. K. U. Gross, *J. Chem. Phys.*, **2005**, 123, 062206.
82. C. Van Caillie and R. D. Amos, *Chem. Phys. Lett.*, **1999**, 308, 249-255.
83. C. Van Caillie and R. D. Amos, *Chem. Phys. Lett.*, **2000**, 317, 159-164.
84. F. Furche and R. Ahlrichs, *J. Chem. Phys.*, **2002**, 117, 7433-7447.
85. D. Jacquemin, E. A. Perpète, G. Scalmani, M. J. Frisch, X. Assfeld, I. Ciofini and C. Adamo, *J. Chem. Phys.*, **2006**, 125, 164324.
86. K. Remya and C. H. Suresh, *J. Comput. Chem.*, **2013**, 34, 1341-1353.
87. K. Remya and C. H. Suresh, *Phys. Chem. Chem. Phys.*, **2015**, 17, 27035-27044.
88. K. Remya and C. H. Suresh, *RSC Adv.*, **2016**, 6, 44261-44271.
89. T. D. Della and C. H. Suresh, *Phys. Chem. Chem. Phys.*, **2016**, 18, 14588-14602.
90. U. H. F. Bunz, *Accounts of Chemical Research*, **2015**, 48, 1676-1686.
91. T. M. Krygowski, H. Szatylowicz, O. A. Stasyuk, J. Dominikowska and M. Palusiak, *Chem. Rev.*, **2014**, 114, 6383-6422.
92. Z. Chen, C. S. Wannere, C. Corminboeuf, R. Puchta and P. v. R. Schleyer, *Chem. Rev.*, **2005**, 105, 3842-3888.
93. J. I. Wu, I. Fernández and P. v. R. Schleyer, *J. Am. Chem. Soc.*, **2013**, 135, 315-321.
94. J. Poater, M. Solà, R. G. Viglione and R. Zanasi, *J. Org. Chem.*, **2004**, 69, 7537-7542.
95. F. Feixas, E. Matito, J. Poater and M. Solà, *J. Comput. Chem.*, **2008**, 29, 1543-1554.
96. G. Portella, J. Poater, J. M. Bofill, P. Alemany and M. Solà, *J. Org. Chem.*, **2005**, 70, 2509-2521.
97. G. Portella, J. Poater, J. M. Bofill, P. Alemany and M. Solà, *J. Org. Chem.*, **2005**, 70, 4560-4560.
98. J. Poater, J. M. Bofill, P. Alemany and M. Solà, *J. Org. Chem.*, **2006**, 71, 1700-1702.
99. S. Osuna, J. Poater, J. M. Bofill, P. Alemany and M. Solà, *Chem. Phys. Lett.*, **2006**, 428, 191-195.
100. C. H. Suresh and S. R. Gadre, *J. Org. Chem.*, **1999**, 64, 2505-2512.
101. C. H. Suresh and M. J. Ajitha, *J. Org. Chem.*, **2013**, 78, 3918-3924.
102. Y. Ruiz-Morales, *J. Phys. Chem. A*, **2002**, 106, 11283-11308.
103. M. Yoshida and J.-i. Aihara, *Phys. Chem. Chem. Phys.*, **1999**, 1, 227-230.

104. R. G. Parr and Z. Zhou, *Acc. Chem. Res.*, **1993**, 26, 256-258.
105. Z. Zhou, R. G. Parr and J. F. Garst, *Tetrahedron Lett.*, **1988**, 29, 4843-4846.
106. D. E. Manolopoulos, J. C. May and S. E. Down, *Chem. Phys. Lett.*, **1991**, 181, 105-111.
107. J.-i. Aihara, *J. Phys. Chem. A*, **1999**, 103, 7487-7495.
108. J.-i. Aihara, *Theor. Chem. Acc.*, **1999**, 102, 134-138.
109. S. Xu, Y. Yuan, X. Cai, C.-J. Zhang, F. Hu, J. Liang, G. Zhang, D. Zhang and B. Liu, *Chem. Sci.*, **2015**, 6, 5824-5830.
110. C. Risko, M. D. McGehee and J.-L. Bredas, *Chem. Sci.*, **2011**, 2, 1200-1218.
111. D. Veldman, C. J. Meskers Stefan and A. J. Janssen René, *Adv. Funct. Mater.*, **2009**, 19, 1939-1948.
112. S. Naskar and M. Das, *ACS Omega*, **2017**, 2, 1795-1803.
113. M. Li, L. Kou, L. Diao, Q. Zhang, Z. Li, Q. Wu, W. Lu and D. Pan, *J. Phys. Chem. A*, **2015**, 119, 3299-3309.
114. S. Ardo and G. J. Meyer, *Chem. Soc. Rev.*, **2009**, 38, 115-164.
115. G. M. Hasselman, D. F. Watson, J. R. Stromberg, D. F. Bocian, D. Holten, J. S. Lindsey and G. J. Meyer, *J. Phys. Chem. B*, **2006**, 110, 25430-25440.
116. C. Sun, Y. Li, P. Song and F. Ma, *Materials*, **2016**, 9, 813.
117. M. G. Voronkov, É. N. Deryagina and É. N. Sukhomazova, *Chem. Heterocycl. Compd.*, **1977**, 13, 217-217.

# Chapter 3

# 1,4-dihydro-1,4-azaborinine Annulated Linear Polyacenes

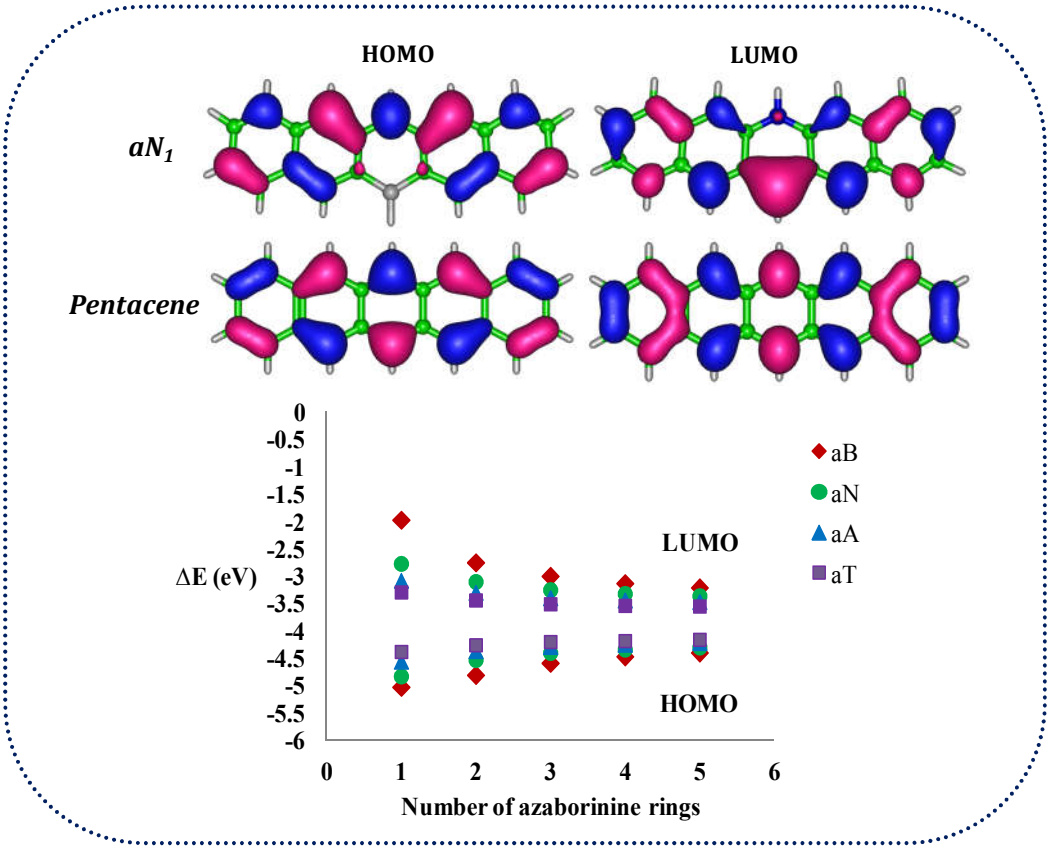

## *3.1. Abstract*

*Linear polyacene (LPA) mimics containing multiple heterocycles have been computationally designed by annulating 1,4-dihydro-1,4-azaborinine moieties to benzene ($aB_1$ - $aB_5$), naphthalene ($aN_1$ - $aN_5$), anthracene ($aA_1$ - $aA_5$) and tetracene ($aT_1$ - $aT_5$) cores. DFT studies conducted on them using M06L/6-311++G(d,p) method reveal a perfectly planar structure for all and suggest the utilization of nitrogen lone pairs for aromatic $\pi$-electron delocalization. The computed values of aromaticity indices such as HOMA, NICS, and dehydrogenation energy ($E_{dh}$) of heterocycles support strong aromatic character for each six-membered ring in the LPA mimics. On the basis of the minimum value of the molecular electrostatic potential ($V_{min}$) observed on each LPA unit in the LPA mimics, the extended delocalization of $\pi$-electrons is verified. The energetic parameter $E_{dh}$ showed strong linear correlation with HOMA, NICS and $V_{min}$ parameters, which strongly supports the multidimensional character of aromaticity in LPA mimics. The electronic property modification is shown by the theoretical absorption spectra data and singlet-triplet energy gap ($\Delta E_{ST}$). The band gap and $\Delta E_{ST}$ tunings are achieved for LPA mimics by selecting an appropriate number of azaborinine type units and the size of LPA core used for annulation. Quite high theoretical light harvesting efficiency of almost all the molecules reinforces the usefulness of such designed systems for solar applications.*

## 3.2. Introduction

Linear polyacenes are laterally fused benzenoid hydrocarbons[1] which can be considered as one atom thick nanowires. These class of molecules have least number of aromatic sextet per number of aromatic rings.[2] Acenes special features make them a very good candidate for electronic and optical applications. They have the least HOMO-LUMO gap comparing with other hydrocarbons consisting of same number of rings.[3, 4] Strong 2D interactions in the solid state and high charge mobility makes acenes beneficial in the nanotechnological applications.[3, 5, 6] The main drawback of using acenes for practical purposes is their declining stability as the length of chain increases, which is due to the phenomenon of aromatic dilution.[7, 8] Because of all these factors and olefin like reactivity, the syntheses and application of higher acenes beyond pentacene are very difficult.[9-11] The chemical unstability of higher acenes

paved the way for the designing of LPA mimics, which incorporates heteroatoms like nitrogen, sulphur or boron into the hexagonal rings without affecting the overall stability of the molecule.[12, 13] Nitrogen-rich oligoacenes are useful as organic semiconductors.[14] Very recently, a theoretical study on 1,4-dihydropyrazine annulated LPA systems has been done by us showed the effective use of N centers for band gap tuning in LPA mimics.[15] Boron anion is effectively demonstrated as a substitute for carbon in the case of 5-membered cyclopentadienyl rings.[16] Boron incorporated thiophene-based conjugated polymers have been synthesized.[17] Boron containing molecules have widespread applications in optoelectronic field because of the vacant $P_z$ orbital in them.[18] Boron and nitrogen together have an effective atomic mass of 12 which is equivalent to that of two carbon atoms, thereby making C=C and B-N as isoelectronic, isosteric and thereby similar.[12, 13] Therefore, polycyclic aromatic hydrocarbons having boron and nitrogen atoms embedded in their structural skeleton can be considered as LPA mimics. Yet because of the difference in electronegativity between boron and nitrogen, effective polarization will be different for such molecules compared to the LPAs. For instance, B,N-heteroacenes have been successfully demonstrated for their various properties namely in luminogens for detecting fluoride ions.[19] The aromaticity and electronic features of acenes and their BN analogues were investigated extensively theoretically also.[20]

Introducing boron and nitrogen in a benzene skeleton will lead to 3 isomers, *viz.* 1,2-dihydro-1,2-azaborinine, 1,3-dihydro-1,3-azaborinine and 1,4-dihydro-1,4-azaborinine wherein the heteroatoms occupy at the ortho, meta and para positions, respectively with respect to each other. Theoretical investigations on azaborinines started from 1998 onwards.[21] The pioneers in the area of synthesis of 1,2-azaborinine derivatives are Dewar and White in the 60s.[22-24] Many monocyclic and a few polycyclic 1,2-azaborinine derivatives have been synthesized afterward .[25-37] The first isolation and characterization of 1,2-dihydro-1,2-azaborinine were materialized only in 2009.[38] 1,3-dihydro-1,3-azaborinine was synthesized as an N-methyl, B-isopropyl amine derivative for the first time.[39] A number of benzo-fused examples for 1,4-dihydro-1,4-azaborinine is known in the literature.[40-46] In the case of LPA mimics made up of 1,2-dihydro-1,2-azaborinine and 1,3-dihydro-1,3-azaborinine units, more than one ring will share the B or N centers while in the case of 1,4-dihydro-1,4-azaborinine unit, the B and N centers are isolated within a single ring. Previously

Ghosh et al. have shown that more ring shared BN containing molecules are less aromatic than the less ring shared BN containing molecules.[47] In other words, 1,4-dihydro-1,4-azaborinine based LPA mimics are expected to have more aromatic character than other structures. The present study will focus only on LPA mimics composed of 1,4-azaborinine type units.

## 3.3. Computational Methods

Gaussian09 suite of programs at M06L/6-311++G(d,p) level of density functional theory (DFT) were used for optimising the geometry of all the molecules in the study.[48-50] The optimized structures were confirmed as energy minima by vibrational frequency analysis. A previous benchmark study by Remya and Suresh on a variety of non-covalent dimers using around 380 different DFT methods yielded M06L as the most reliable for geometry and interaction energy close to the CCSD(T) level accuracy. Recent studies conducted with M06L functional (the meta-GGA local functional with 0% Hartree-Fock (HF) exchange[51]) on a variety of systems have given reliable results in agreement with high accuracy *ab initio* methods and dispersion-corrected DFT methods.[52-54] The wavefunction generated at M06L/6-311++G(d,p) is used for molecular electrostatic potential (MESP) calculation. For all the molecules, aromaticity of each ring is quantified by computing the z component of the nucleus independent chemical shift at 1 Å above the ring center ($NICS_{zz}(1)$).[55] Using the procedure of Krygowski *et al*[56] harmonic oscillator model of aromaticity (HOMA) index is calculated for all the systems. Using time-dependent DFT techniques at the same level of theory, the absorption spectra of every set of molecules are calculated. The TD-DFT optimization is done to get the structure and energy for the first triplet (T1) and first singlet (S1) state of all the molecules analyzed, and the energy gap between the singlet and triplet energy are also calculated.

## 3.4. Results and Discussions

### 3.4.1. Design Strategy

The improvement of the Clar's sextet distribution in the LPA mimics is the driving force for the molecular design strategy.[8] Benzene has one π-electron per CC bond ($n_\pi$) and its conjugated cyclic π-electron system is often described as a perfect

aromatic sextet. For all polycyclic benzenoid hydrocarbons, number of π-electron per CC bond ($n_\pi$) is always less than 1 and it diminishes with increase in the size of an LPA molecule. For naphthalene, anthracene, tetracene, and pentacene, $n_\pi$ is 0.91, 0.88, 0.86 and 0.85, respectively. By fusing two LPA moieties through one -NH- unit and a –BH- unit, a higher LPA mimic can be designed. Every fusion point will represent a 1,4-dihydro-1,4-azaborinine unit. In our design, we consider a symmetric distribution of heteroatoms so that the fusion points will show connections to alternate BH and NH units (Figure 3.1). We use a notation that uses two letters and a number to represent the designed systems. The first notation is 'a' which represents 1,4-azaborinine-type character of the heterocycle while the second letter B, N, A or T represents the core hydrocarbon unit made up of benzene, naphthalene, anthracene or tetracene moieties, respectively. Further, the numbers 1, 2, 3, 4 and 5 represent the number of 1,4-azaborinine-type heterocycles in the molecule. For a system having 'n' 1,4-dihydro-1,4-azaborinine moieties, there will be 'n+1' benzene, naphthalene, anthracene or tetracene units present. For example, $aB_1$ is the 5,10-dihydrodibenzo[b,e][1,4]azaborinine molecule (Figure 3.1) which is made up of one 1,4-dihydro-1,4-azaborinine-type heterocycle and two benzene cores. Similarly $aN_2$ represents an LPA mimic made up of three naphthalene cores and two 1,4-dihydro-1,4-azaborinine type heterocycles. The dihydroazaborinine systems selected for this study are $aB_1$ – $aB_5$, $aN_1$ – $aN_5$, $aA_1$ – $aA_5$, $aT_1$ – $aT_5$.

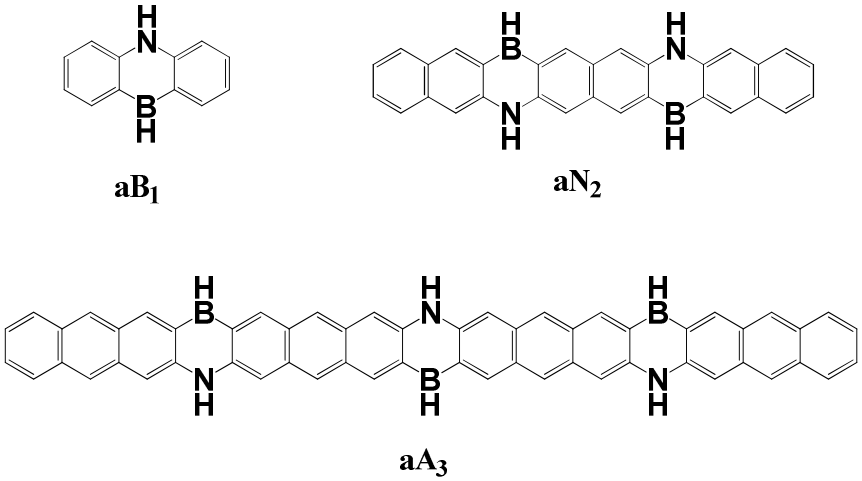


**Figure 3.1**. Representative structures of the molecules under study containing 1,4-azaborinine -type heterocycles.

Optimized structural parameter of a representative molecule $aN_1$ is shown in Figure 3.2. The entire sets of molecules show planar structure. Delocalization of the

lone pair electrons of N *via* the electron vacancy in B and the π-system of the carbon rings for aromatic π-conjugation is responsible for the perfect planar topology of all the systems under study.

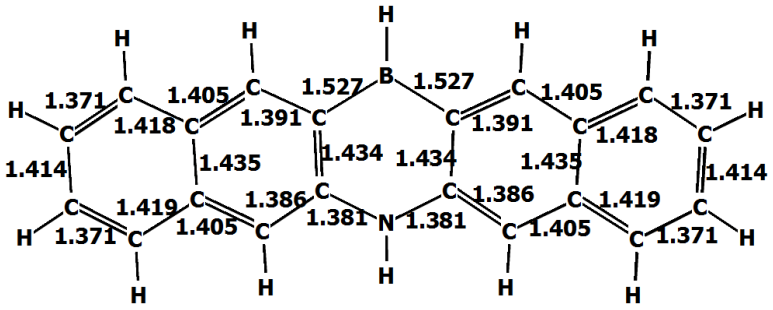


**Figure 3.2.** Optimized structure of $aN_1$ at M06L/6-311++G(d,p) level (all the bond lengths in Å).

In the molecules studied, boron with three formal satisfied valencies can account for only six electrons. In other words, boron is formally electron deficient by two electrons in the valence region. The two electron deficiency in boron center is compensated by lone pair electron donation from nitrogen. The nitrogen lone pair donation takes place through the π-electron bearing carbon centers. This is the reason for N-centers appearing in planar form. In other words, the N-lone pair is no longer a lone pair and it becomes part of the π-system. As a result, all the individual rings attain 6 π-electron count, the magic number for aromaticity.

## 3.4.2. Dehydrogenation Energy

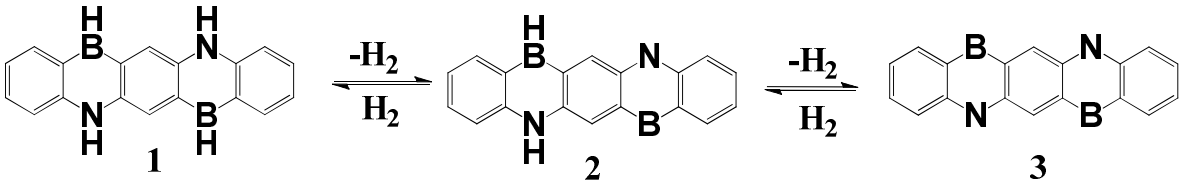


**Scheme 3.1**. Dehydrogenation of **1** to **2** and **2** to **3.**

In order to assess the thermodynamic stability of the systems ($aB_1$ – $aB_5$, $aN_1$ – $aN_5$, $aA_1$ – $aA_5$, $aT_1$ – $aT_5$), energy change associated with dehydrogenation of heterocentres is calculated. Dehydrogenation energy ($E_{dh}$) is calculated in a step-wise manner starting from the most peripheral heteroring (ring1) followed by the next neighboring ring (ring2) and so on until the last one to get the fully dehydrogenated system. Scheme 3.1 illustrates this strategy for $aB_2$ system. The $E_{dh}$ values corresponding to every dehydrogenation step is shown in Table 3.1.

**Table 3.1.** Dehydrogenation energies ($\sum E_{dh}$) values in kcal/mol of LPA mimics. Dehydrogenated structures of $aA_5$ and $aT_5$ were omitted due to convergence problems in optimization.

| System | ring1 | ring2 | ring3 | ring4 | ring5 | $\sum E_{dh}$ (kcal/mol) |
|---|---|---|---|---|---|---|
| $aB_1$ | 74.2 | | | | | 74.2 |
| $aB_2$ | 75.8 | 76.3 | | | | 152.1 |
| $aB_3$ | 75.7 | 78.2 | 77.2 | | | 231.0 |
| $aB_4$ | 76.1 | 77.7 | 79.1 | 77.2 | | 310.0 |
| $aB_5$ | 75.8 | 77.9 | 78.7 | 79.2 | 77.4 | 389.1 |
| $aN_1$ | 80.5 | | | | | 80.5 |
| $aN_2$ | 80.3 | 82.6 | | | | 162.8 |
| $aN_3$ | 80.4 | 82.4 | 82.8 | | | 245.5 |
| $aN_4$ | 80.4 | 82.2 | 82.8 | 82.8 | | 328.2 |
| $aN_5$ | 80.3 | 82.5 | 82.4 | 82.8 | 82.8 | 410.9 |
| $aA_1$ | 84.1 | | | | | 84.1 |
| $aA_2$ | 83.7 | 85.6 | | | | 169.3 |
| $aA_3$ | 83.8 | 85.1 | 81.9 | | | 250.8 |
| $aA_4$ | 83.7 | 85.1 | 85.3 | 77.5 | | 331.3 |
| $aT_1$ | 86.3 | | | | | 86.3 |
| $aT_2$ | 85.4 | 87.3 | | | | 172.6 |
| $aT_3$ | 85.9 | 86.6 | 77.5 | | | 250.0 |
| $aT_4$ | 85.7 | 86.9 | 76.6 | 83.9 | | 333.1 |

The dehydrogenation of a heterocycle is highly endothermic in nature with the lowest value of 74.2 kcal/mol observed for $aB_1$. In general, $E_{dh}$ of a heteroring increases with increase in the size of the annulation unit, *viz*. benzene, naphthalene, anthracene, and tetracene. This indicates that BH and NH hetero center connection is more stabilizing for a larger LPA unit. In the case of dihydropyrazine annulated LPA mimics described in a previous paper[15], average $E_{dh}$ for a ring is found to be 38.8 kcal/mol whereas in the present azaborinine incorporated systems, the average $E_{dh}$ 81.2 kcal/mol is very high meaning that the 1,4-dihydro-1,4-azaborinine based LPA mimics are more stable than the dihydropyrazine based systems. The

total increase in the dehydrogenation energy ($\sum E_{dh}$) is directly related to the increase in the number and size of the LPA units.

### 3.4.3. Bond length Equalization and Aromatic Character

Aromaticity is a multidimensional phenomenon, involving structural, electronic, magnetic and energetic properties of the molecules.[57-67] The HOMA index, developed by Krygowski *et al.* is one of the geometry based methods to compare the aromaticity of a variety of organic molecules.[56, 68] HOMA can be calculated using the equation 3.1, where $\alpha$ is an empirical normalization constant (which is selected in such a way that HOMA is zero and one for non-aromatic and aromatic systems, respectively). The $\alpha$ values for CC, CN and CB bonds are 275.7, 93.5 and 138.06, respectively.[68-72] n is the total number of bonds; $R_{opt}$ and $R_i$ are optimal aromatic bond length and computed bond length, respectively. $R_{opt}$ for CC, CN, and CB bonds are 1.388, 1.334 and 1. 561 Å, respectively[47, 68-72]

$$HOMA = 1 - \frac{\alpha}{n}\sum_{i}^{n}(R_{opt} - R_i)^2 \qquad \text{Eq. 3.1}$$

For a perfect aromatic system, HOMA is 1 because of the evident bond length equalisation, and a HOMA value close to zero indicates non-aromatic character. The CC bond length of benzene (1.388 Å), is considered as the most optimum for an aromatic hydrocarbon. In the present study, the notations Aring1, Aring2 etc. are used to indicate the most peripheral to the interior symmetrically distinguishable azaborinine heterocycles. Similarly, notations Cring1, Cring2 etc are used to indicate the most peripheral to the interior carbon rings (Figure 3.3).

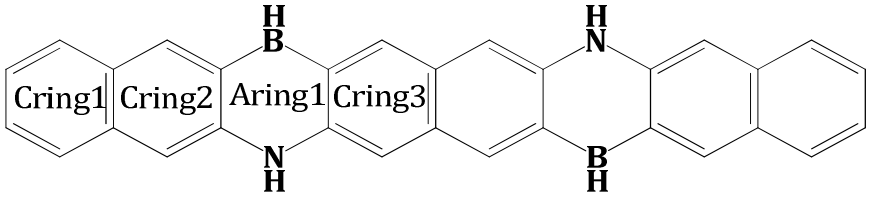


**$aN_2$**

**Figure 3.3**. Picture of $aN_2$ molecule with notations used to distinguish the rings.

The HOMA values for all the rings in the molecules of aB, aN, aA and aT series are given in Tables 3.2, 3.3, and 3.4, respectively. For aB series, HOMA is in the range 0.91 - 0.75, the maximum being 0.91 for the peripheral Cring1 of $aB_1$ and the minimum 0.75 for the Aring3 of $aB_5$. Compared to aB series, a gradual decrease in

HOMA is observed going from aN to aA to aT series as the HOMA range is 0.67 - 0.77, 0.60 - 0.72 and 0.59 - 0.66, respectively.

**Table 3.2.** HOMA index of aB series of LPA mimics.

| | $aB_1$ | $aB_2$ | $aB_3$ | $aB_4$ | $aB_5$ |
|---|---|---|---|---|---|
| Cring1 | 0.91 | 0.9 | 0.89 | 0.89 | 0.89 |
| Aring1 | 0.8 | 0.77 | 0.77 | 0.77 | 0.77 |
| Cring2 | | 0.87 | 0.86 | 0.86 | 0.86 |
| Aring2 | | | 0.75 | 0.75 | 0.75 |
| Cring3 | | | | 0.86 | 0.86 |
| Aring3 | | | | | 0.75 |
| ΣHOMA | 1.71 | 2.54 | 3.27 | 4.12 | 4.87 |

**Table 3.3**. HOMA index of aN series of LPA mimics.

| | $aN_1$ | $aN_2$ | $aN_3$ | $aN_4$ | $aN_5$ |
|---|---|---|---|---|---|
| Cring1 | 0.77 | 0.76 | 0.76 | 0.76 | 0.76 |
| Cring2 | 0.79 | 0.78 | 0.78 | 0.78 | 0.78 |
| Aring1 | 0.70 | 0.68 | 0.69 | 0.69 | 0.69 |
| Cring3 | | 0.75 | 0.75 | 0.75 | 0.75 |
| Cring4 | | | 0.75 | 0.75 | 0.75 |
| Aring2 | | | 0.67 | 0.67 | 0.67 |
| Cring5 | | | | 0.75 | 0.75 |
| Cring6 | | | | | 0.75 |
| Aring3 | | | | | 0.67 |
| ΣHOMA | 2.26 | 2.98 | 4.40 | 5.15 | 6.57 |

The hetero rings always show slightly smaller values of HOMA than the carbon rings. The lowest HOMA 0.59 is observed for Aring1 of $aT_5$, the largest molecule among the studied systems. The HOMA values of the molecules suggest that they all possess a substantial amount of aromatic character. In addition, the difference observed in the HOMA between carbon rings and heterorings is small which suggests the smooth distribution of π-electrons and aromatic character for the entire molecule.

**Table 3.4.** HOMA index of aA and aT series of LPA mimics.

| | $aA_1$ | $aA_2$ | $aA_3$ | $aA_4$ | $aA_5$ |
|---|---|---|---|---|---|
| Cring1 | 0.68 | 0.68 | 0.68 | 0.68 | 0.68 |
| Cring2 | 0.72 | 0.72 | 0.72 | 0.72 | 0.72 |
| Cring3 | 0.67 | 0.68 | 0.68 | 0.68 | 0.68 |
| Aring1 | 0.63 | 0.63 | 0.63 | 0.63 | 0.63 |
| Cring4 | | 0.67 | 0.67 | 0.66 | 0.66 |
| Cring5 | | 0.70 | 0.70 | 0.69 | 0.69 |
| Cring6 | | | 0.67 | 0.67 | 0.67 |
| Aring2 | | | 0.62 | 0.63 | 0.62 |
| Cring7 | | | | 0.67 | 0.67 |
| Cring8 | | | | 0.70 | 0.70 |
| Cring9 | | | | | 0.67 |
| Aring3 | | | | | 0.63 |
| ΣHOMA | 2.69 | 4.06 | 5.35 | 6.71 | 8.00 |
| | $aT_1$ | $aT_2$ | $aT_3$ | $aT_4$ | $aT_5$ |
| Cring1 | 0.63 | 0.63 | 0.63 | 0.63 | 0.63 |
| Cring2 | 0.66 | 0.66 | 0.66 | 0.66 | 0.66 |
| Cring3 | 0.65 | 0.64 | 0.65 | 0.65 | 0.65 |
| Cring4 | 0.61 | 0.62 | 0.62 | 0.61 | 0.62 |
| Aring1 | 0.60 | 0.59 | 0.60 | 0.59 | 0.60 |
| Cring5 | | 0.61 | 0.61 | 0.61 | 0.61 |
| Cring6 | | 0.64 | 0.64 | 0.64 | 0.64 |
| Cring7 | | | 0.64 | 0.64 | 0.64 |
| Cring8 | | | 0.62 | 0.62 | 0.62 |
| Aring2 | | | 0.60 | 0.60 | 0.60 |
| Cring9 | | | | 0.62 | 0.62 |
| Cring10 | | | | 0.64 | 0.64 |
| Cring11 | | | | | 0.64 |
| Cring12 | | | | | 0.61 |
| Aring3 | | | | | 0.60 |
| ΣHOMA | 3.15 | 4.39 | 6.25 | 7.50 | 9.36 |

The sum of HOMA indexes of all the rings in a molecule (∑HOMA) corresponding to every system studied is given in Table 3.5. ∑HOMA shows a strong linear correlation with $\sum E_{dh}$ for all the set of molecules (Figure 3.4) and indicates that dehydrogenation energy is proportional to the aromatic character of the molecule.

**Table 3.5.** ∑HOMA values of all LPA mimics.

| System | ΣHOMA | System | ΣHOMA | System | ΣHOMA | System | ΣHOMA |
|---|---|---|---|---|---|---|---|
| $aB_1$ | 1.71 | $aN_1$ | 2.26 | $aA_1$ | 2.69 | $aT_1$ | 3.15 |
| $aB_2$ | 2.54 | $aN_2$ | 2.98 | $aA_2$ | 4.06 | $aT_2$ | 4.39 |
| $aB_3$ | 3.27 | $aN_3$ | 4.40 | $aA_3$ | 5.35 | $aT_3$ | 6.25 |
| $aB_4$ | 4.12 | $aN_4$ | 5.15 | $aA_4$ | 6.71 | $aT_4$ | 7.50 |
| $aB_5$ | 4.87 | $aN_5$ | 6.57 | $aA_5$ | 8.00 | $aT_5$ | 9.36 |

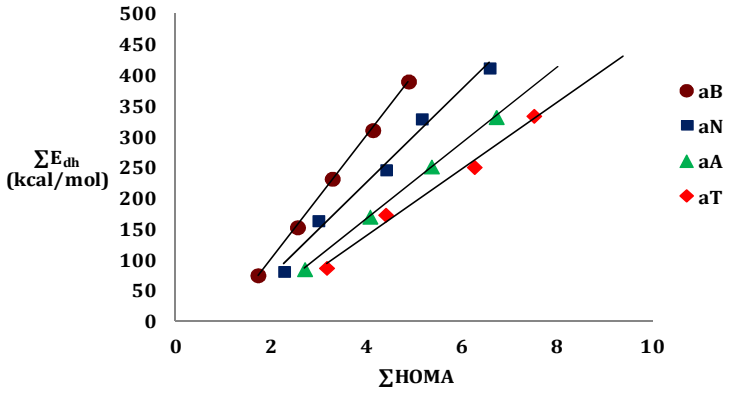


**Figure 3.4.** Correlation graph between ∑HOMA and $\sum E_{dh}$.

## 3.4.4. Nucleus Independent Chemical Shift (NICS) and Aromatic Character

Magnetic criteria of aromaticity can be quantified in terms of nucleus independent chemical shift (NICS) index as shown by Schleyer and co-workers.[73] Aromaticity of a system is indicated by negative NICS values, whereas positive NICS values are characteristics of antiaromatic systems. We have analyzed the z-component of NICS at 1 Å above the ring center ($NICS_{zz}(1)$). NICS would work best for comparing the aromaticity of a similar set of molecules and we will focus on the relative ordering of the NICS along the symmetrically distinguishable rings, starting from one at the terminal to the symmetrically distinguishable interior ring. Tables 3.6, 3.7 and 3.8 give the $NICS_{zz}(1)$ values of aB, aN, aA and aT series.

**Table 3.6**. $NICS_{zz}(1)$ values on symmetrically distinguishable rings in aB series .

| | $aB_1$ | $aB_2$ | $aB_3$ | $aB_4$ | $aB_5$ |
|---|---|---|---|---|---|
| Cring1 | -27.67 | -27.22 | -27.1 | -27.23 | -27.36 |
| Aring1 | -13.18 | -12.79 | -12.18 | -12.35 | -12.12 |
| Cring2 | | -29.6 | -28.82 | -28.73 | -28.6 |
| Aring2 | | | -12.92 | -12.7 | -12.46 |
| Cring3 | | | | -28.72 | -28.57 |
| Aring3 | | | | | -12.41 |
| $\Sigma NICS_{zz}(1)$ | -40.85 | -69.61 | -81.02 | -109.73 | -121.53 |

**Table 3.7**. $NICS_{zz}(1)$ values on symmetrically distinguishable rings in aN series.

| | $aN_1$ | $aN_2$ | $aN_3$ | $aN_4$ | $aN_5$ |
|---|---|---|---|---|---|
| Cring1 | -26.31 | -26.04 | -26.16 | -26.37 | -26.47 |
| Cring2 | -27.83 | -27.18 | -26.89 | -26.76 | -26.76 |
| Aring1 | -6.42 | -5.63 | -5.19 | -4.80 | -4.30 |
| Cring3 | | -27.44 | -26.96 | -26.85 | -26.47 |
| Cring4 | | | -27.48 | -27.41 | -27.65 |
| Aring2 | | | -5.72 | -5.58 | -5.33 |
| Cring5 | | | | -27.11 | -26.78 |
| Cring6 | | | | | -27.26 |
| Aring3 | | | | | -5.56 |
| $\Sigma NICS_{zz}(1)$ | -60.57 | -86.30 | -118.4 | -144.86 | -176.58 |

The $NICS_{zz}(1)$ values of benzene, naphthalene, Cring1 of anthracene and Cring1 of tetracene are -17.30, -28.65, -26.32 and -23.95 ppm respectively and that of Cring2 of anthracene and Cring2 of tetracene are -34.11 and -33.85, respectively. This gives a false impression that benzene is the least aromatic and the inner rings of anthracene and tetracene are the most aromatic. It is known that the coupling between induced magnetic fields from adjacent rings affects the NICS measure.[74-77] In all the aB, aN, and aA series of molecules, the Crings, as well as the heterorings, show significant negative $NICS_{zz}(1)$ indicating aromatic character for the whole molecule. aT series is an exception to this trend wherein the heterorings exhibit a small positive $NICS_{zz}(1)$ indicating the development of antiaromatic character. The values are in the range of 0.37 to 2.99, which is substantially small when compared to the negative $NICS_{zz}(1)$ values of carbons rings.

**Table 3.8**. $NICS_{zz}(1)$ values on symmetrically distinguishable rings in aA & aT series.

| | $aA_1$ | $aA_2$ | $aA_3$ | $aA_4$ | $aA_5$ |
|---|---|---|---|---|---|
| Cring1 | -24.78 | -24.25 | -24.10 | -23.12 | -22.62 |
| Cring2 | -30.79 | -30.13 | -29.80 | -30.07 | -29.75 |
| Cring3 | -24.32 | -24.38 | -24.33 | -25.38 | -26.14 |
| Aring1 | -1.40 | -1.15 | -1.32 | -0.58 | -0.28 |
| Cring4 | | -23.73 | -23.20 | -22.60 | -22.08 |
| Cring5 | | -30.44 | -30.32 | -30.18 | -30.01 |
| Cring6 | | | -23.92 | -24.38 | -24.98 |
| Aring2 | | | -1.07 | -0.70 | -0.32 |
| Cring7 | | | | -23.52 | -23.15 |
| Cring8 | | | | -30.05 | -30.04 |
| Cring9 | | | | | -23.88 |
| Aring3 | | | | | -1.13 |
| $\Sigma NICS_{zz}(1)$ | -81.29 | -134.10 | -158.07 | -210.60 | -234.40 |
| | $aT_1$ | $aT_2$ | $aT_3$ | $aT_4$ | $aT_5$ |
| Cring1 | -22.99 | -23.55 | -22.30 | -22.39 | -22.33 |
| Cring2 | -31.20 | -30.74 | -30.21 | -29.59 | -29.25 |
| Cring3 | -31.03 | -30.76 | -30.53 | -30.71 | -30.49 |
| Cring4 | -20.75 | -20.60 | -20.63 | -20.73 | -20.59 |
| Aring1 | 1.80 | 0.37 | 1.21 | 2.99 | 2.14 |
| Cring5 | | -20.72 | -20.20 | -20.18 | -19.79 |
| Cring6 | | -30.25 | -29.74 | -29.48 | -29.46 |
| Cring7 | | | -29.96 | -30.03 | -30.22 |
| Cring8 | | | -20.54 | -20.65 | -20.80 |
| Aring2 | | | 1.52 | 1.32 | 1.36 |
| Cring9 | | | | -20.34 | -20.21 |
| Cring10 | | | | -29.78 | -29.67 |
| Cring11 | | | | | -29.81 |
| Cring12 | | | | | -20.55 |
| Aring3 | | | | | 1.50 |
| $\Sigma NICS_{zz}(1)$ | -104.20 | -156.20 | -201.40 | -249.60 | -298.15 |

For carbon rings, the range of $NICS_{zz}(1)$ values for aB, aN, aA and aT series are (-27.10 to -29.60), (-26.04 to -27.83), (-22.08 to -30.79) and (-20.21 to -31.20) respectively. The most negative value being -31.20 for Cring2 in $aT_1$ and the least negative value -20.21 for Cring9 of $aT_5$. For all the series, the terminal Arings are slightly less aromatic than the interior ones.

The sum of $NICS_{zz}(1)$ values ($\sum NICS_{zz}(1)$)on all the rings in a system is considered as a global aromaticity parameter, which is given in Table 3.9. The absolute values of this quantity increases as size increases indicative of the increase in aromaticity with number of constituting rings. Strong linear correlation is observed between $\sum NICS_{zz}(1)$ and $\sum E_{dh}$ for all the set of molecules (Figure 3.5) which again confirms the direct relationship between geometrical parameter of aromaticity and dehydrogenation energy an energetic aroamticity parameter. The slopes which is highest for aB and decreases as the size of acene is increasing is indicative of the fact that the magnetic effects on aroamticity is maximum for aB sereis and the efect decreases as thesize of acene increases.

**Table 3.9**. $\sum NICS_{zz}(1)$ for all the systems.

| System | $\Sigma NICS_{zz}(1)$ (ppm) | System | $\Sigma NICS_{zz}(1)$ (ppm) | System | $\Sigma NICS_{zz}(1)$ (ppm) | System | $\Sigma NICS_{zz}(1)$ (ppm) |
|---|---|---|---|---|---|---|---|
| $aB_1$ | -40.85 | $aN_1$ | -60.57 | $aA_1$ | -81.29 | $aT_1$ | -104.20 |
| $aB_2$ | -69.61 | $aN_2$ | -86.30 | $aA_2$ | -134.10 | $aT_2$ | -156.20 |
| $aB_3$ | -81.02 | $aN_3$ | -118.40 | $aA_3$ | -158.07 | $aT_3$ | -201.40 |
| $aB_4$ | -109.73 | $aN_4$ | -144.86 | $aA_4$ | -210.60 | $aT_4$ | -249.60 |
| $aB_5$ | -121.53 | $aN_5$ | -176.58 | $aA_5$ | -234.40 | $aT_5$ | -298.15 |

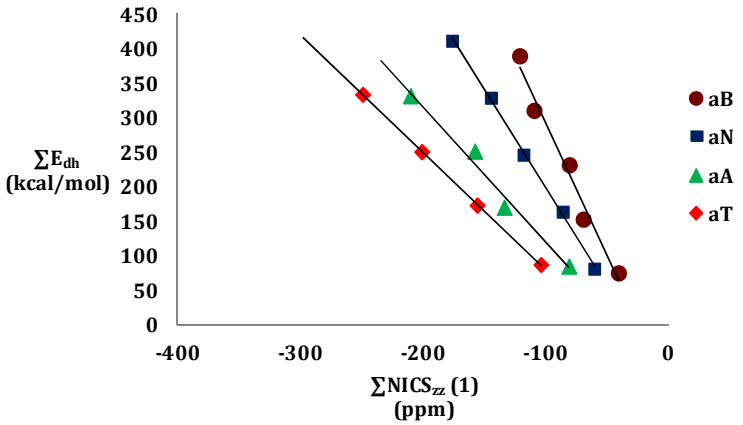


**Figure 3.5.** Correlation graph between $\Sigma NICS_{zz}(1)$ and $\sum E_{dh}$.

### 3.4.4. Molecular Electrostatic Potential (MESP) and Electron Delocalization

The most negative valued molecular electrostatic potential position in a molecule is termed $V_{min}$. Understanding the electron localization and delocalization characteristics of the molecules can be done by this quantification of electron region.[78, 79] The $V_{min}$ values on the LPA unit of all the molecules are shown in Table 3.10. along with sum of $V_{min}$ values ($\sum V_{min}$).

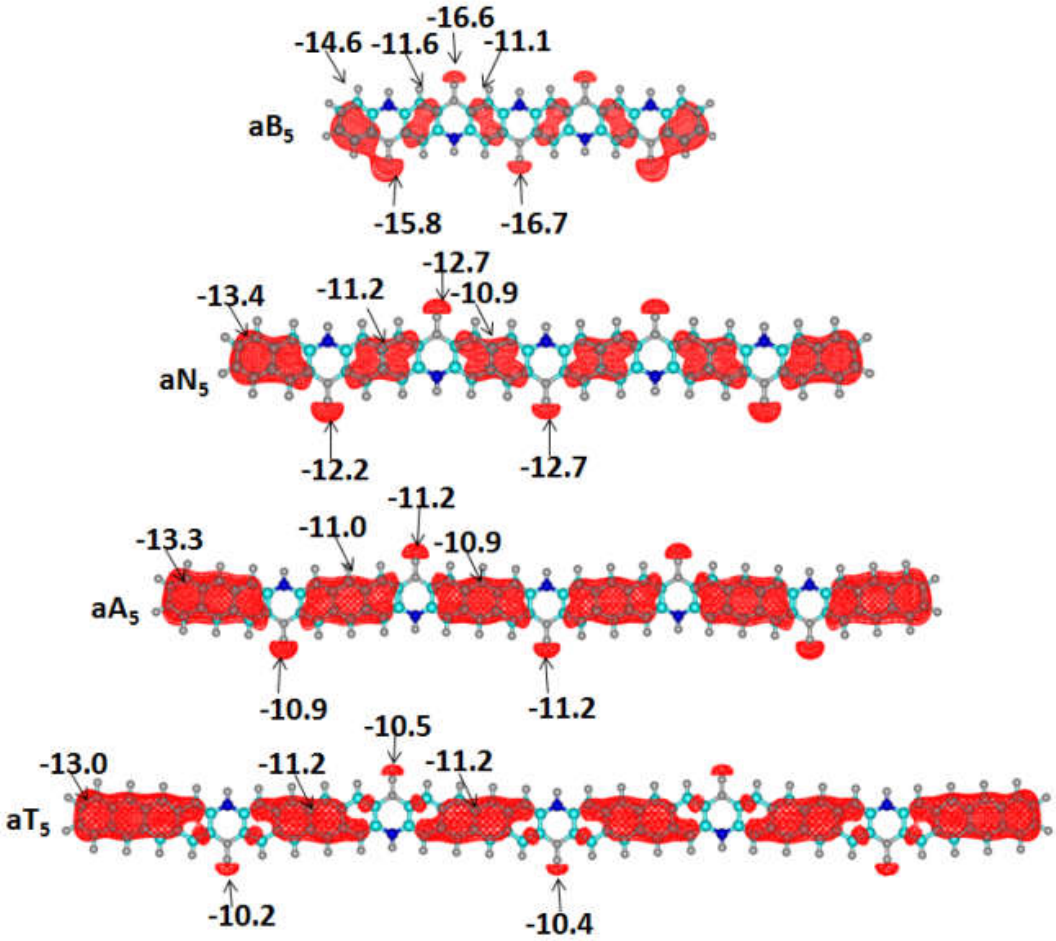


**Figure 3.6**. Plots of MESP isosurface (-8 kcal mol$^{-1}$) for $aB_5$ ,$aN_5$ ,$aA_5$ and $aT_5$ with MESP minimum in kcal mol$^{-1}$.

The $V_{min}$ values fall in the range of -10.9 to -15.0 kcal/mol for the LPA unit. In every case, except the most exterior LPA unit, $V_{min}$ is significantly less negative than the parent hydrocarbon. The azaborinine rings show $V_{min}$ in the range -16.8 to -10.1 kcal/mol at the hydrogen atom of the B-H bond. These values are significantly less negative than the $V_{min}$ value -6.1 kcal/mol observed for the B-H bond of $BH_3$ which support the extended delocalization of nitrogen lone pair in LPA mimics. Unlike the

previously reported dihydropyrazine annulated molecules,[15] $V_{min}$ of azaborinine annulated systems show only minor variation in the values, particularly for the interior LPA units.

**Table 3.10.** $V_{min}$ values of hydrocarbon part of LPA mimics in kcal/mol.

| LPA Mimics | $V_{min}$ on the LPA unit from left to right (kcal/mol) | | | | | | Σ $V_{min}$ (kcal/mol) |
|---|---|---|---|---|---|---|---|
| | 1 | 2 | 3 | 4 | 5 | 6 | |
| $aB_1$ | -15.0 | -15.0 | | | | | -30.0 |
| $aB_2$ | -14.8 | -11.7 | -14.8 | | | | -41.2 |
| $aB_3$ | -14.8 | -11.7 | -11.7 | -14.8 | | | -53.0 |
| $aB_4$ | -14.7 | -11.7 | -11.2 | -11.7 | -14.7 | | -64.0 |
| $aB_5$ | -14.6 | -11.6 | -11.1 | -11.1 | -11.6 | -14.6 | -74.6 |
| $aN_1$ | -13.8 | -13.8 | | | | | -27.7 |
| $aN_2$ | -13.7 | -11.4 | -13.7 | | | | -38.8 |
| $aN_3$ | -13.5 | -11.3 | -11.3 | -13.5 | | | -49.6 |
| $aN_4$ | -13.6 | -11.3 | -11 | -11.3 | -13.6 | | -60.9 |
| $aN_5$ | -13.4 | -11.2 | -10.9 | -10.9 | -11.2 | -13.4 | -71.2 |
| $aA_1$ | -13.5 | -13.5 | | | | | -27.0 |
| $aA_2$ | -13.3 | -10.9 | -13.3 | | | | -37.5 |
| $aA_3$ | -13.4 | -11.0 | -11.0 | -13.4 | | | -48.6 |
| $aA_4$ | -13.3 | -11.0 | -10.9 | -11.0 | -13.3 | | -59.6 |
| $aA_5$ | -13.3 | -11.0 | -10.9 | -10.9 | -11.0 | -13.3 | -70.4 |
| $aT_1$ | -13.3 | -13.3 | | | | | -26.6 |
| $aT_2$ | -13.2 | -11.3 | -13.2 | | | | -37.7 |
| $aT_3$ | -13.1 | -11.3 | -11.3 | -13.1 | | | -48.9 |
| $aT_4$ | -13.1 | -11.2 | -11.2 | -11.2 | -13.1 | | -60.0 |
| $aT_5$ | -13.0 | -11.2 | -11.2 | -11.2 | -11.2 | -13.0 | -70.8 |

$V_{min}$ has been already established as a tool for understanding the Clar's aromatic sextet theory in polycyclic aromatic hydrocarbons and other systems that are similar in structure.[80-82] The relative electron rich character of π-region in a molecule can be compared by the pinpointing of the $V_{min}$ in the total electron cloud of the molecule observed. The electron-rich character in aromatic systems increases with increase in the number of annulated rings as evident from the $V_{min}$ values of

benzene, naphthalene, anthracene, and tetracene which are -15.06, -14.24, -13.94 and -13.74 kcal/mol respectively. The MESP distribution for a set of representative systems (the longest molecule in every series) is shown in Figure 3.6. It shows that every LPA core unit in the molecule can be characterized by a $V_{min}$ value. A $V_{min}$ also appears near the hydrogen atom of each of the B-H bonds, which can be attributed to the electron donation from nitrogen centres to the boron centres.

Strong linear correlation is observed between $\sum V_{min}$ and $\sum E_{dh}$ for all series of molecules (Figure 3.7). The slopes of individual lines are only slightly varied indicating that the delocalization of the π-electrons in all these LPA mimics is very similar. The utilization of nitrogen lone pair for electron delocalization is very effective in all LPA mimics, which is directly related to the energetic stabilization of the molecule.

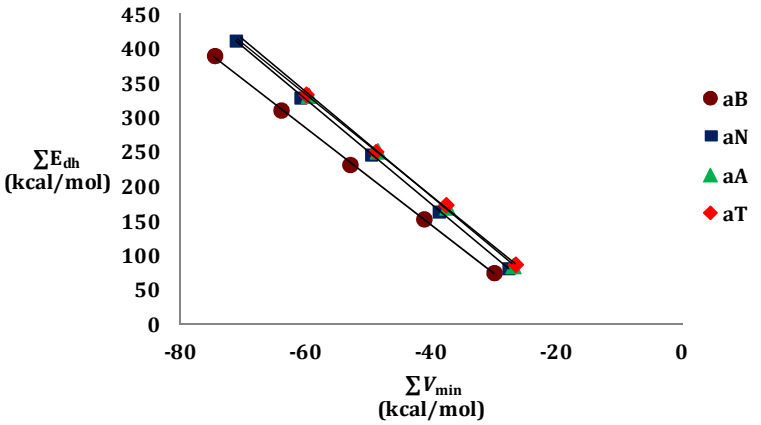


**Figure 3.7**. Correlation graph between $\Sigma V_{min}$ and $\sum E_{dh}$.

### 3.4.4.1. Natural Population Analysis on pN Series

For the substantiation of the use of $V_{min}$ as a measure of electron delocalization, we have done an NPA analysis on a set of representative aN series. The NPA charge δ1, δ2, δ3 and δ4 for B, N, H attached to boron and H attached to nitrogen are given in the Table 3.11. The trends in the variation of NPA charge are very similar for all these atoms where correlating any two quantities will give correlation coefficient ~0.999. Similar is the result with summation of NPA charges (Table 3.12). Further, NPA charge shows strong linear correlation with $V_{min}$ on the BH unit (Figure 3.8). This again confirms that $V_{min}$ is useful for the analysis of the charge localization/delocalization features.

**Table 3.11.** NPA charges on aN series of molecules.

| System | δ1(a.u.) | δ2 (a.u.) | δ3(a.u.) | δ4(a.u.) |
|---|---|---|---|---|
| $aN_1$ | 0.53587 | -0.54048 | -0.08903 | 0.37818 |
| $aN_2$ | 0.53791 | -0.54568 | -0.08985 | 0.37847 |
| | 0.53791 | -0.54568 | -0.08985 | 0.37847 |
| $aN_3$ | 0.53921 | -0.54516 | -0.08953 | 0.37859 |
| | 0.53896 | -0.54523 | -0.08957 | 0.37858 |
| | 0.53957 | -0.59868 | -0.09048 | 0.37577 |
| $aN_4$ | 0.54083 | -0.54651 | -0.09102 | 0.37839 |
| | 0.54021 | -0.59881 | -0.09039 | 0.37578 |
| | 0.53960 | -0.59981 | -0.09052 | 0.37554 |
| | 0.53815 | -0.54582 | -0.08978 | 0.37840 |
| $aN_5$ | 0.53911 | -0.54518 | -0.08957 | 0.37860 |
| | 0.53989 | -0.59880 | -0.09048 | 0.37570 |
| | 0.54241 | -0.54817 | -0.09028 | 0.37867 |
| | 0.53989 | -0.59880 | -0.09048 | 0.37570 |
| | 0.53911 | -0.54518 | -0.08957 | 0.37860 |

**Table 3.12**. The sum of NPA charges on boron, nitrogen, boron proton and nitrogen proton, and the sum of $V_{min}$ values of the boron attached proton of aN series.

| System | $\sum\delta1$ (a.u.) | $\sum\delta2$ (a.u.) | $\sum\delta3$ (a.u.) | $\sum\delta4$ (a.u.) | $\sum V_{min}$ (kcal/mol) |
|---|---|---|---|---|---|
| $aN_1$ | 0.53587 | -0.54048 | -0.08903 | 0.37818 | -12.2992 |
| $aN_2$ | 1.07582 | -1.09136 | -0.17970 | 0.75694 | -22.6782 |
| $aN_3$ | 1.61774 | -1.68907 | -0.26958 | 1.13294 | -33.0196 |
| $aN_4$ | 2.15879 | -2.29095 | -0.36171 | 1.50811 | -43.5743 |
| $aN_5$ | 2.70041 | -2.83613 | -0.45038 | 1.88727 | -53.3007 |

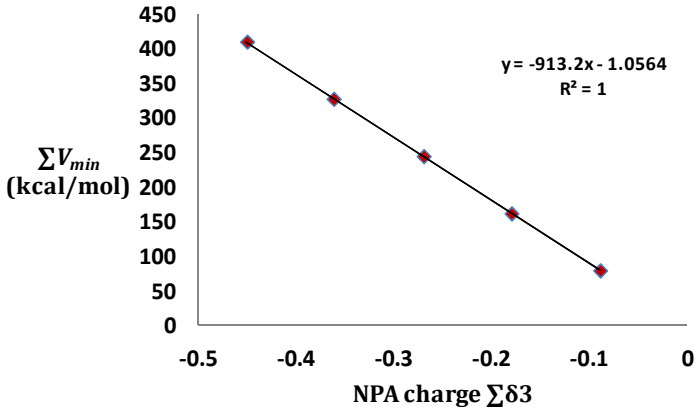


**Figure 3.8**. Correlation between NPA charge on B-H hydrogen and $\sum V_{\min}$.

## 3.4.5. Frontier Molecular Orbitals

The absorption spectra details reveal that fine-tuning of the HOMO-LUMO band gap is taking place in the LPA mimics with respect to increase in the number of rings in the system. The HOMO energy ($E_{HOMO}$), LUMO energy ($E_{LUMO}$), and HOMO-LUMO energy gap ($E_{LUMO\text{-}HOMO}$) are presented in Table 3.13. The ordered triplet ($E_{HOMO}$, $E_{LUMO}$, $E_{LUMO\text{-}HOMO}$) for benzene, naphthalene, anthracene and tetracene are (-6.44, -0.95, 5.49), (-5.56, -1.88, 3.68), (-5.04, -2.49, 2.55) and (-4.69, -2.89, 1.80) eV, respectively. Compared to polyacenes, a significant reduction in the magnitude of $E_{HOMO}$ and $E_{LUMO\text{-}HOMO}$ is observed for the azaborinine annulated LPA mimics whereas a significant increase in the absolute $E_{LUMO}$ value of LPA mimics indicates the stabilization of LUMO level. For instance, ($E_{HOMO}$, $E_{LUMO}$, $E_{LUMO\text{-}HOMO}$) observed for $aB_5$, $aN_5$, $aA_5$ and $aT_5$ are respectively (-4.40, -3.21, 1.19), (-4.30, -3.36, 0.94), (-4.22, -3.47, 0.75) and (-4.16, -3.55, 0.61). The reduction in $E_{LUMO\text{-}HOMO}$ is proportional to the length of the molecule and suggests that higher LPA mimics are better suited for optoelectronic applications. All these reductions and increase are observed in the absolute value of $E_{HOMO}$, $E_{LUMO}$ and $E_{LUMO\text{-}HOMO}$ values. $aN_3$, $aA_2$ and $aT_1$ systems showing $E_{LUMO\text{-}HOMO}$ close to 1.1 eV are particularly attractive for possible usage in solar energy trapping. A steady decrease in the $E_{LUMO\text{-}HOMO}$ with respect to the size of the acene is evident and suggests that large LPA systems are attractive for HOMO-LUMO energy modulation for photonic applications and the limiting factor is the unstable character of the higher derivatives.

**Table 3.13**. HOMO, LUMO energies and HOMO-LUMO gap for LPA mimics.

| System | $E_{HOMO}$ (eV) | $E_{LUMO}$ (eV) | $E_{LUMO-HOMO}$ (eV) | System | $E_{HOMO}$ (eV) | $E_{LUMO}$ (eV) | $E_{LUMO-HOMO}$ (eV) |
|---|---|---|---|---|---|---|---|
| B | -6.44 | -0.95 | 5.49 | A | -5.04 | -2.49 | 2.55 |
| $aB_1$ | -5.03 | -1.97 | 3.06 | $aA_1$ | -4.56 | -3.08 | 1.48 |
| $aB_2$ | -4.81 | -2.75 | 2.06 | $aA_2$ | -4.37 | -3.30 | 1.07 |
| $aB_3$ | -4.59 | -3.00 | 1.59 | $aA_3$ | -4.29 | -3.40 | 0.89 |
| $aB_4$ | -4.47 | -3.13 | 1.34 | $aA_4$ | -4.25 | -3.44 | 0.80 |
| $aB_5$ | -4.40 | -3.21 | 1.19 | $aA_5$ | -4.22 | -3.47 | 0.75 |
| N | -5.56 | -1.88 | 3.68 | T | -4.69 | -2.89 | 1.80 |
| $aN_1$ | -4.83 | -2.77 | 2.06 | $aT_1$ | -4.38 | -3.29 | 1.09 |
| $aN_2$ | -4.53 | -3.1 | 1.43 | $aT_2$ | -4.26 | -3.44 | 0.82 |
| $aN_3$ | -4.40 | -3.25 | 1.16 | $aT_3$ | -4.2 | -3.51 | 0.70 |
| $aN_4$ | -4.34 | -3.32 | 1.02 | $aT_4$ | -4.18 | -3.54 | 0.64 |
| $aN_5$ | -4.30 | -3.36 | 0.94 | $aT_5$ | -4.16 | -3.55 | 0.61 |

The HOMO-LUMO energy tuning for aB, aN, aA and aT series are projected in Figure 3.9, Figure 3.10, Figure 3.11 and Figure 3.12 respectively. The gradual decrease in the gap with an increase in length is evident in all the figures. A very low HOMO-LUMO gap is possible by increasing the length of the whole molecule which is evident from the values in Table 3.13.

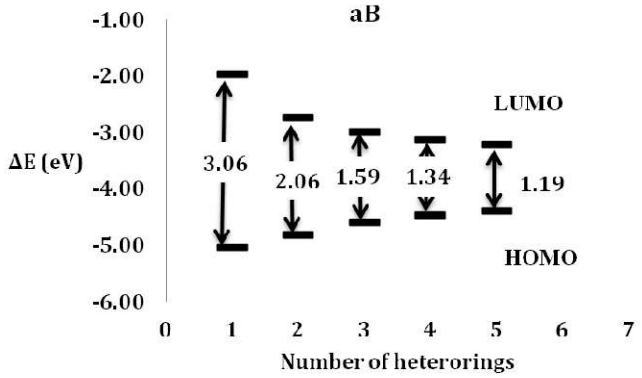


**Figure 3.9**. HOMO-LUMO gaps for aB series of LPA mimics.

The systems have same number of rings in them have almost similar energy gap, for example $aB_2$ and $aN_1$ systems have five rings in their structure and the HOMO-LUMO gap is 2.06 eV for both the systems. All the systems made up of same number of rings does not follow this property for example consider the case of 11

ring containing $aN_3$ and $aA_2$, the HOMO-LUMO gaps are 1.16 eV and 1.07 eV respectively, similarly for 14 ring containing $aN_4$ and $aT_2$, the valuesa are 1.02 eV and 0.82 eV respectlively. This difference in value is increases as the size of the acene annulated increases, which is evident from the values discussed. The change in both HOMO and LUMO energy is similar for all the systems leading to the tapering effect in the HOMO-LUMO band gap. Form 3.06 eV for $aB_1$, 0.61 eV for $aT_5$, the effective tuning is possible by changing the number and size of acene parts that are being connected by the azaborinine heterocycle.

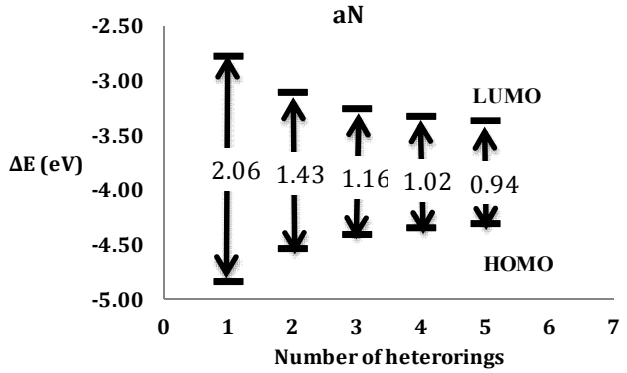


**Figure 3.10**. HOMO-LUMO gaps for aN series of LPA mimics.

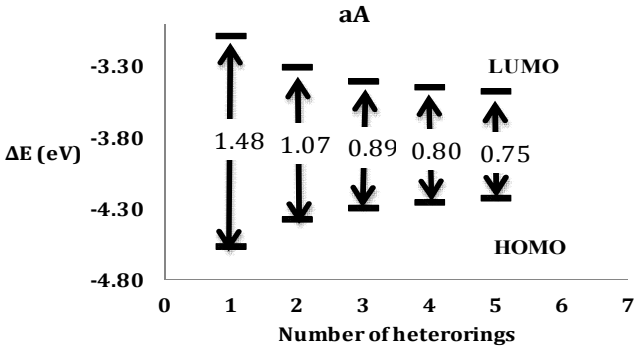


**Figure 3.11**. HOMO-LUMO gaps for aA series of LPA mimics.

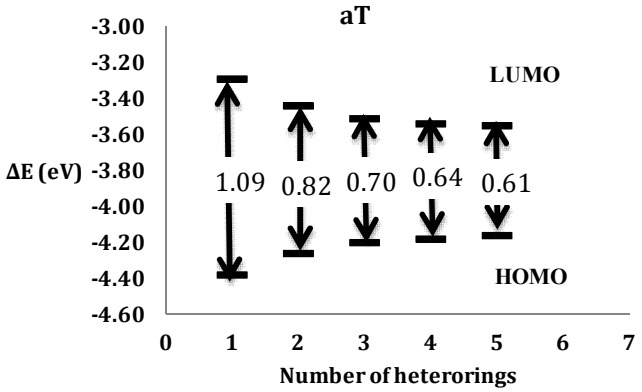


**Figure 3.12**. HOMO-LUMO energy gaps for aT series of LPA mimics.

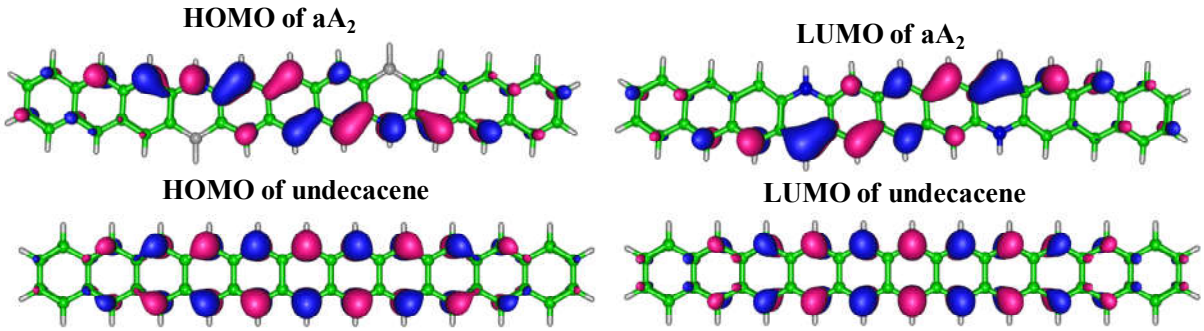


**Figure 3.13**. HOMO and LUMO of $aA_2$ and corresponding LPA (undecacene).

The frontier molecular orbitals of a representative system $aA_2$ and its corresponding 11 ring containing LPA undecacene is given in Figure 3.13. It is clear from the picture that the HOMO and LUMO are structurally similar for both the systems, other than the effect of concentration change the heteroatoms positions at LPA mimic.

## 3.4.6. Singlet-Triplet Energy Gap

First triplet (T1) and first singlet (S1) excited state geometries of all the molecules were calculated using the TD-DFT method. The gap between the energy states corresponding to intersystem crossing ($\Delta E_{S1\text{-}T1}$) phosphorescence ($\Delta E_{T1\text{-}S0}$) and emission ($\Delta E_{S1\text{-}S0}$) are given in Table 3.14.

**Table 3.14.** Energy gaps $\Delta E_{T1\text{-}S0}$, $\Delta E_{S1\text{-}T1}$ and $\Delta E_{S1\text{-}S0}$ in eV of all LPA mimics.

| System | $\Delta E_{S1\text{-}T1}$ (eV) | $\Delta E_{T1\text{-}S0}$ (eV) | $\Delta E_{S1\text{-}S0}$ (eV) | System | $\Delta E_{T1\text{-}S0}$ (eV) | $\Delta E_{S1\text{-}S0}$ (eV) | $\Delta E_{S1\text{-}T1}$ (eV) |
|---|---|---|---|---|---|---|---|
| $aB_1$ | 0.72 | 2.54 | 3.26 | $aA_1$ | 0.36 | 1.16 | 1.53 |
| $aB_2$ | 0.68 | 1.62 | 2.31 | $aA_2$ | 0.40 | 0.77 | 1.17 |
| $aB_3$ | 0.57 | 1.23 | 1.80 | $aA_3$ | 0.29 | 0.67 | 0.96 |
| $aB_4$ | 0.48 | 1.03 | 1.52 | $aA_4$ | 0.23 | 0.63 | 0.86 |
| $aB_5$ | 0.42 | 0.93 | 1.35 | $aA_5$ | 0.20 | 0.60 | 0.80 |
| $aN_1$ | 0.46 | 1.71 | 2.17 | $aT_1$ | 0.35 | 0.76 | 1.11 |
| $aN_2$ | 0.47 | 1.10 | 1.57 | $aT_2$ | 0.40 | 0.48 | 0.88 |
| $aN_3$ | 0.37 | 0.91 | 1.28 | $aT_3$ | 0.28 | 0.46 | 0.74 |
| $aN_4$ | 0.31 | 0.81 | 1.12 | $aT_4$ | 0.21 | 0.46 | 0.67 |
| $aN_5$ | 0.26 | 0.75 | 1.02 | $aT_5$ | 0.20 | 0.43 | 0.63 |

$\Delta E_{ST}$ corresponding to the phosphorescence band gap steadily decreases with increase in the number of aromatic hydrocarbon unit as well as an increase in the

number of Crings. The data in Table 3.14 indicates that as the size of the molecule or the number of six-membered annulated rings in the molecule increases, $\Delta E_{ST}$ decreases in all series. The reduction in $\Delta E_{ST}$ is beneficial for improving the intersystem crossing (ISC) efficiency[83], phosphorescence quantum yield[83] and thermally activated delayed fluorescence of a molecule.[84-86]

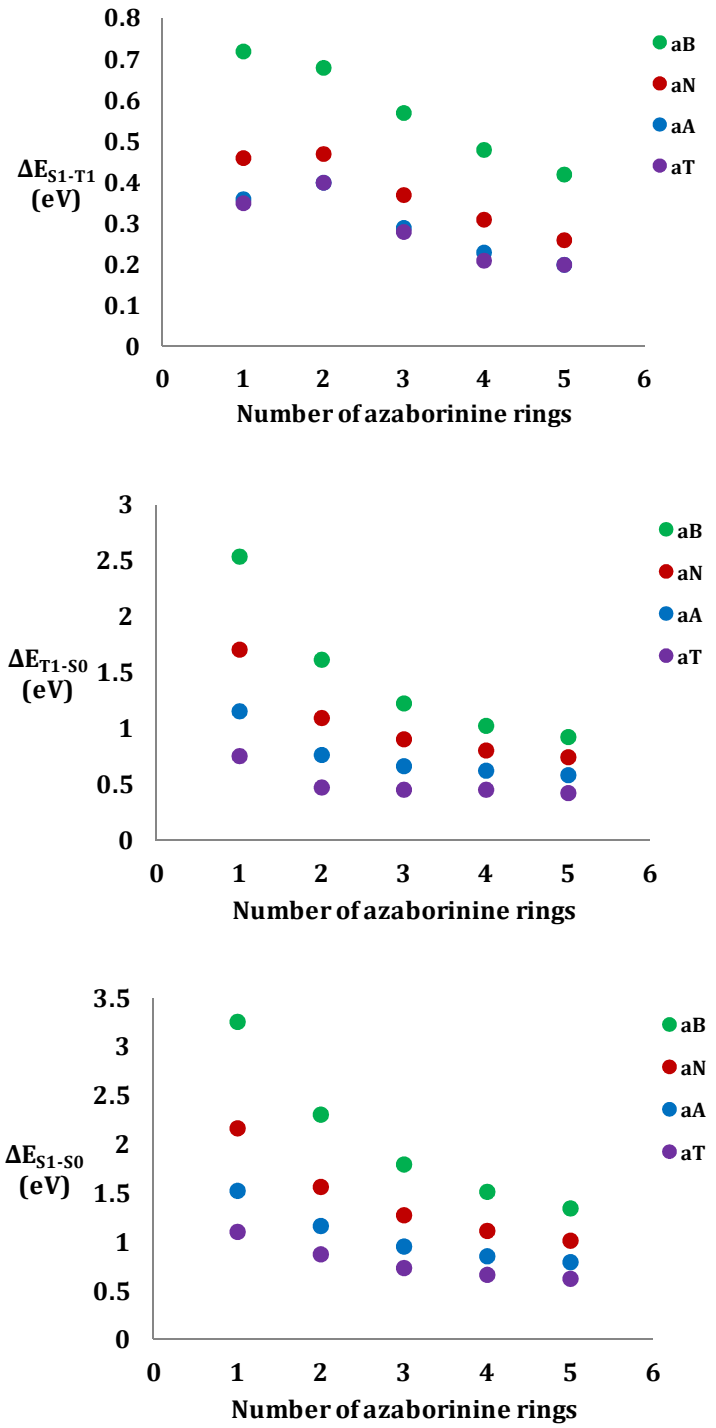


**Figure. 3.14**. Plots showing trends in $\Delta E_{T1\text{-}S0}$ , $\Delta E_{S1\text{-}T1}$ and $\Delta E_{S1\text{-}S0}$ with size of LPA mimic.

Plotting the energy gap against the number of azaborinine rings being used for annulation, a pictorial representation of the trends in the decrease is obtained. Such plots are given in Figure 3.14. For the plot corresponding to the phosphorescence and emission phenomena, this decrease is very evident, but for the intersystem crossing corresponding plot, there is slight variation in the trend. For this set of calculations the energy gap for the second member for aN, aA and aT series the energy value is higher than that of the first system. This difference is clearly visible in the graph plotted.

### 3.4.7. Absorption Spectra

The theoretical absorption maxima values ($\lambda_{max}$) having the highest oscillator frequency of all the molecules are given in Table 3.15 and the spectral features of all the systems are portrayed in Figure 3.15 to 3.18.

**Table 3.15.** Absorption maxima values ($\lambda_{max}$) of LPA mimics.

| System | $\lambda_{max}$ (nm) | system | $\lambda_{max}$ (nm) | system | $\lambda_{max}$ (nm) | System | $\lambda_{max}$ (nm) |
|---|---|---|---|---|---|---|---|
| $aB_1$ | 243 | $aN_1$ | 298 | $aA_1$ | 330 | $aT_1$ | 373 |
| $aB_2$ | 294 | $aN_2$ | 334 | $aA_2$ | 378 | $aT_2$ | 838 |
| $aB_3$ | 332 | $aN_3$ | 370 | $aA_3$ | 686 | $aT_3$ | 905 |
| $aB_4$ | 355 | $aN_4$ | 511 | $aA_4$ | 686 | $aT_4$ | 905 |
| $aB_5$ | 371 | $aN_5$ | 523 | $aA_5$ | 702 | $aT_5$ | 965 |

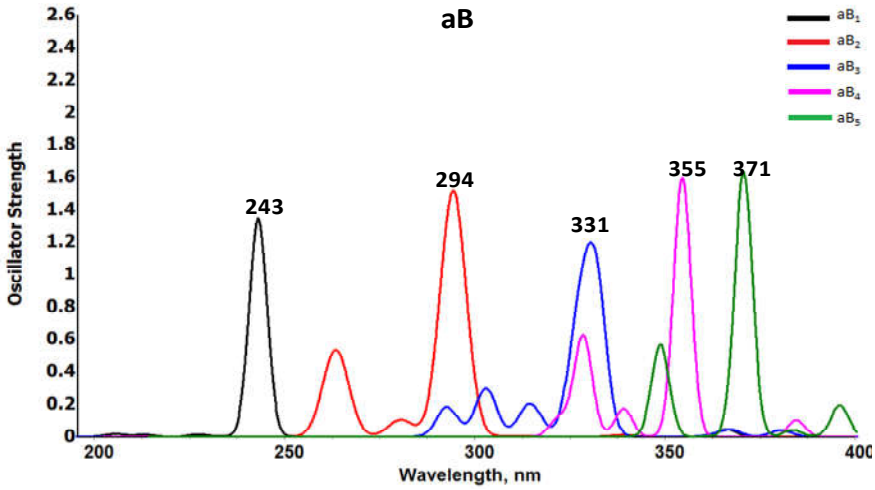


**Figure 3.15**. Absorption spectra of aB series at M06L/6-311++G(d,p) level of theory.

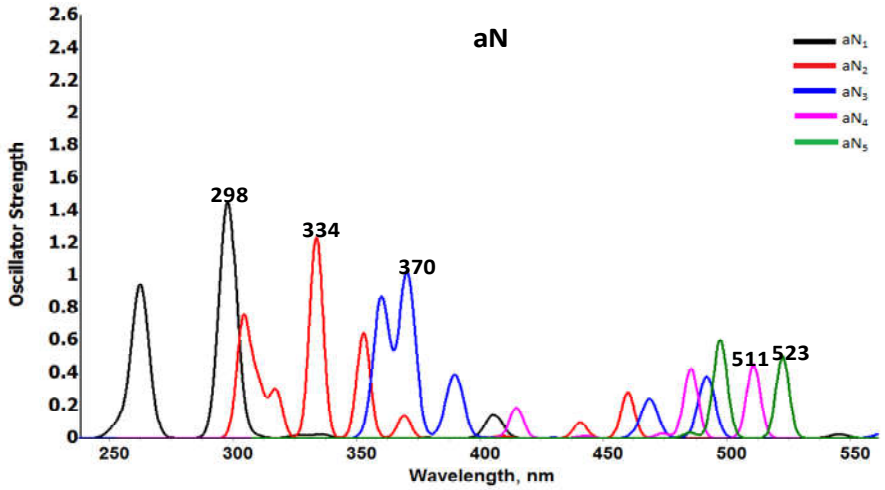


**Figure 3.16**. Absorption spectra of aN series at M06L/6-311++G(d,p) level of theory.

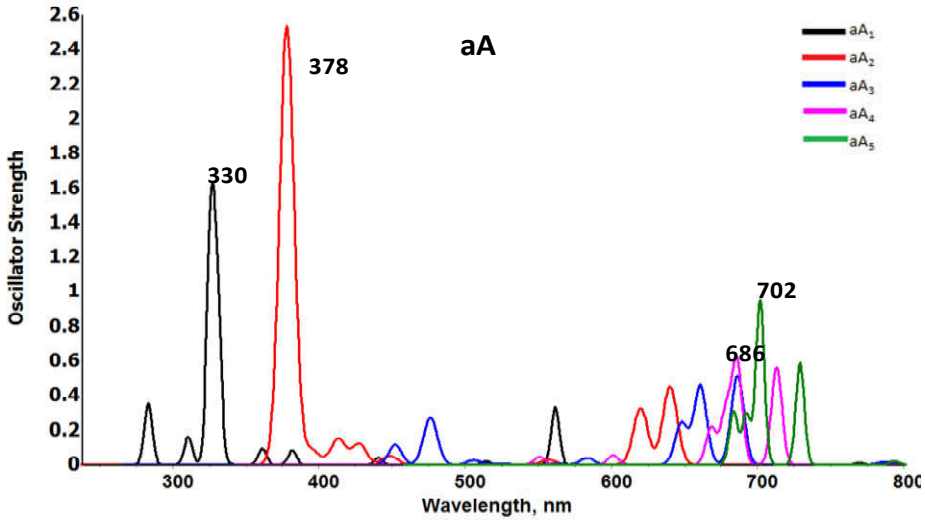


**Figure 3.17**. Absorption spectra of aA series at M06L/6-311++G(d,p) level of theory.

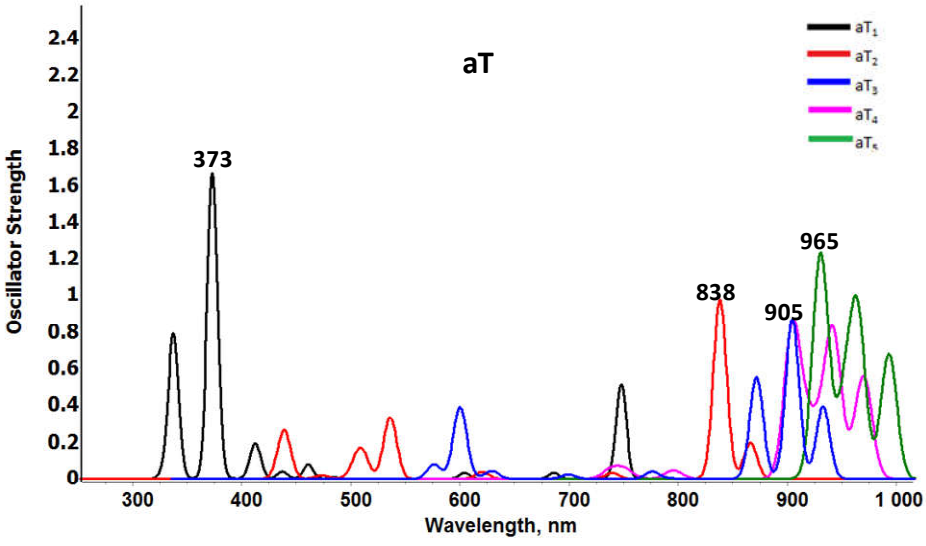


**Figure 3.18**. Absorption spectra of aT series at M06L/6-311++G(d,p) level of theory.

For every system, as the size of the molecule increases, $\lambda_{max}$ shows significant red shift along with an increase in the number of minor peaks in the spectrum. For molecules showing the same number of rings, $\lambda_{max}$ show similar values. For example, $aB_5$ and $aN_3$ have 11 rings and their respective $\lambda_{max}$ are 371 and 370 nm. Similarly, $aB_3$ and $aA_1$ have seven rings and their $\lambda_{max}$ are 332 and 330 nm, respectively.For aB series, $\lambda_{max}$ varies from 243 nm for $aB_1$ to 371 nm for $aB_5$. $aB_1$ has a single $\lambda_{max}$ which is at 243 nm, and when coming to $aB_2$ in addition to the strongest one at 294, another $\lambda_{max}$ is observed around 260 nm. For $aB_3$ system in addition to the main absorption corresponding to HOMO-LUMO transition, weak absorption around the range of 290-310 nm is observed. Similarly for $aB_4$ and $aB_5$ there is weak absorption around 330 nm and 350 nm respectively. For aN series, $\lambda_{max}$ variation is from 298 to 523 nm. $aN_1$ system has the most prominent $\lambda_{max}$ at 298 nm in addition to absorption in the range of 260 nm. For $aN_2$ in addition to the $\lambda_{max}$ at 334nm, weak absorption bands are observed around 300 nm and 350 nm. In the case of $aN_3$ absorption bands are observed around 360 nm and 390 nm. For $aN_4$ and $aN_5$, most of the absorption maxima are centred in the range of 480 to 530 nm. For aA series, the change in $\lambda_{max}$ is from 330 nm to 702 nm. The prominent maxima are marked in the Figure 3.17. For $aA_2$ system a set of weak absorption maxima are seen around 600- 660 nm, whereas the maximum strength $\lambda_{max}$ is at 378 nm. For $aA_3$, $aA_4$ and $aA_5$, all the absorption peaks are observed in the 650-740 nm range. The most prominent $\lambda_{max}$ for $aA_3$ and $aA_4$ are at the same wavelength of 686 nm. For $aA_5$ which has the highest valued absorption maxima at around 720 nm, the prominent one is at 702 nm. In aT series, $aT_1$ has the most prominent $\lambda_{max}$ at 373 nm while a comparatively weak absorption around 330 nm. For $aT_2$ system there is absorption maxima in the region between 410 – 540 nm, in addition to the most prominent one at 838 nm. All the systems other than $aT_1$ has most of the absorption around 800 – 1000 nm, which lies in the infrared region in the electromagnetic spectrum. $aT_3$ and $aT_4$ has the most prominent $\lambda_{max}$ at the same wavelength of 905 nm, quite analogous to that of aA series. $aT_5$ has absorption maxima in the most red shifted region when all the systems in the series is considered, from 965 nm to almost 1000 nm. The aB series clearly show absorption in the UV region while aN series show peaks in the visible region only for $aN_4$ and $aN_5$, the systems containing 14 and 17 rings, respectively. Majority of the aA systems show absorption in the visible region while except $aT_1$, all

systems in aT series absorbs mainly in the infra-red region. By theoretically tuning the $\lambda_{max}$ value the use of LPA mimic in dye-sensitized solar cells can be engineered.[87]

The theoretical calculation of light harvesting efficiency (LHE) of systems is found out, using the equation, $LHE = 1 - 10^{-f}$, where $f$ represents the oscillator strength corresponding to the absorption maxima. The value for all the LPA analogues is given in Table 3.16. From the table it is clear that for most of the systems high LHE is attained when the size is small. When the length of the whole system is increasing the efficiency with which the light harvesting process occurs is decreasing.

**Table 3.16.** Light harvesting efficiency (LHE) of all LPA mimics.

| System | LHE | System | LHE | System | LHE | System | LHE |
|---|---|---|---|---|---|---|---|
| $aB_1$ | 0.955 | $aN_1$ | 0.964 | $aA_1$ | 0.883 | $aT_1$ | 0.979 |
| $aB_2$ | 0.945 | $aN_2$ | 0.942 | $aA_2$ | 0.954 | $aT_2$ | 0.894 |
| $aB_3$ | 0.895 | $aN_3$ | 0.900 | $aA_3$ | 0.693 | $aT_3$ | 0.866 |
| $aB_4$ | 0.975 | $aN_4$ | 0.646 | $aA_4$ | 0.746 | $aT_4$ | 0.857 |
| $aB_5$ | 0.977 | $aN_5$ | 0.682 | $aA_5$ | 0.744 | $aT_5$ | 0.868 |

## 3.5. Conclusions

The design and study of long chain linear polyacene analogues containing heteroatoms in the acene structural skeleton (LPA mimics) are important due to potential applications of such molecules in optoelectronic devices. Herein, DFT calculations at M06L/6-311++G(d,p) level have been carried out on several 1,4-azaborinine annulated LPA mimics to reveal their stability, aromaticity, electronic character, HOMO-LUMO energy gap, and singlet-triplet energy gap. The isoelectronic nature of BN with CC makes this type of a molecule a proper analogue for LPA. The LPA mimics consist of 3 - 29 six-membered rings and is built with benzene ($aB_1$ - $aB_5$), naphthalene ($aN_1$ - $aN_5$), anthracene ($aA_1$ - $aA_5$) and tetracene ($aT_1$ - $aT_5$) core annulated to 1,4-dihydro-1,4-azaborinine units. Studying the nature of aromaticity, thermodynamic stability, HOMO-LUMO energy gap, singlet-triplet energy gap along with the molecular electrostatic potential characteristics is useful for assessing their application potential as structural components in optoelectronic devices. The dehydrogenation energy ($E_{dh}$) of the heterocycles of the LPA mimics is used as an energetic parameter to assess the thermodynamic stability. The large positive values

of $E_{dh}$ indicated stability of these molecules in the hydrogenated form. All of them showed strong multidimensional character of aromaticity such as energetic stabilization, bond length equalization, and magnetic properties. Further, the electron delocalization in LPA mimics is assessed in terms of MESP features. The localization of the negative MESP around the H atom connected to boron indicated the donation of nitrogen lone pair for extended π-conjugation in the molecule. The individual hydrocarbon moieties in the LPA mimics largely retained the electron-rich character of the parent hydrocarbon.

As the size of LPA mimics increased, the HOMO energy increased with a concomitant decrease in LUMO energy resulting in a substantial reduction in HOMO-LUMO energy gap. Moreover, a gradual decrease in the singlet-triplet energy gap ($\Delta E_{ST}$) proportional to the size of the LPA mimics is observed. In short, by adjusting the length of LPA unit as well as by choosing the appropriate number of azaborinine rings for annulation, an LPA mimic showing the desired band gap and $\Delta E_{ST}$ gap can be designed for potential applications in the fabrication of efficient optoelectronic devices. The absorption features which are important criteria in solar photovoltaics, can also be controlled by the change in constituting number and length of systems, which is also effectively shown by simulation of absorption spectra. The absorption maxima of the designed systems cover the wide range of ultraviolet, visible and infrared regions. High theoretical light harvesting efficiency for most of the systems reinforces the application potential of 1,4-dihydro-1,4-azaborinine systems in the optoelectronic and solar industries.

## 3.6. References


1. J. M. André, B. Champagne, E. A. Perpète and M. Guillaume, *Int. J. Quantum Chem.*, **2001**, 84, 607-616.
2. Y. Ruiz-Morales, *J. Phys. Chem. A*, **2002**, 106, 11283-11308.
3. J. E. Anthony, *Angew. Chem. Int. Ed.*, **2008**, 47, 452-483.
4. G. Brocks, J. van den Brink and A. F. Morpurgo, *Phys. Rev. Lett.*, **2004**, 93, 146405.
5. W.-Q. Deng and W. A. Goddard, *J. Phys. Chem. B*, **2004**, 108, 8614-8621.
6. Y. C. Cheng, R. J. Silbey, D. A. da Silva Filho, J. P. Calbert, J. Cornil and J. L. Brédas, *J. Chem. Phys.*, **2003**, 118, 3764-3774.

7. E. Clar, *Polycyclic hydrocarbons Vol. 1&2*, Academic Press, London, 1964.

8. E. Clar, *The Aromatic Sextet*, Wiley, New York, 1972.

9. R. Mondal, B. K. Shah and D. C. Neckers, *J. Am. Chem. Soc.*, **2006**, 128, 9612-9613.

10. D. Biermann and W. Schmidt, *J. Am. Chem. Soc.*, **1980**, 102, 3163-3173.

11. C. Tönshoff and H. F. Bettinger, *Angew. Chem. Int. Ed.*, **2010**, 49, 4125-4128.

12. M. J. D. Bosdet and W. E. Piers, *Can. J. Chem.*, **2009**, 87, 8-29.

13. Z. Liu and T. B. Marder, *Angew. Chem. Int. Ed.*, **2008**, 47, 242-244.

14. M. Winkler and K. N. Houk, *J. Am. Chem. Soc.*, **2007**, 129, 1805-1815.

15. R. Rakhi and C. H. Suresh, *Phys. Chem. Chem. Phys.*, **2016**, 18, 24631-24641.

16. A. J. Ashe, *Organometallics*, **2009**, 28, 4236-4248.

17. L. G. Mercier, W. E. Piers, R. W. Harrington and W. Clegg, *Organometallics*, **2013**, 32, 6820-6826.

18. Z. M. Hudson and S. Wang, *Dalton Trans.*, **2011**, 40, 7805-7816.

19. J. Zhou, R. Z. Tang, X. Y. Wang, W. Z. Zhang, X. D. Zhuang and F. Zhang, *J. Mater. Chem. C*, **2016**, 4, 1159-1164.

20. A. K. Phukan, R. P. Kalagi, S. R. Gadre and E. D. Jemmis, *Inorg. Chem.*, **2004**, 43, 5824-5832.

21. R. J. Doerksen and A. J. Thakkar, *J. Phys. Chem. A*, **1998**, 102, 4679-4686.

22. M. J. S. Dewar, V. P. Kubba and R. Pettit, *J. Chem. Soc.*, **1958**, 3073-3076.

23. G. C. Culling, M. J. S. Dewar and P. A. Marr, *J. Am. Chem. Soc.*, **1964**, 86, 1125-1127.

24. D. G. White, *J. Am. Chem. Soc.*, **1963**, 85, 3634-3636.

25. M. Lepeltier, O. Lukoyanova, A. Jacobson, S. Jeeva and D. F. Perepichka, *Chem. Commun.*, **2010**, 46, 7007-7009.

26. T. Taniguchi and S. Yamaguchi, *Organometallics*, **2010**, 29, 5732-5735.

27. A. J. Ashe, X. D. Fang, X. G. Fang and J. W. Kampf, *Organometallics*, **2001**, 20, 5413-5418.

28. X. D. Fang, A. J. Ashe and J. W. Kampf, *Abstr. Pap. Am. Chem. S.*, **2001**, 222, U603-U603.

29. J. Pan, J. W. Kampf and A. J. Ashe Iii, *J. Organomet. Chem.*, **2009**, 694, 1036-1040.

30. J. Pan, J. W. Kampf and A. J. Ashe, *Organometallics*, **2009**, 28, 506-511.

31. A. N. Lamm, E. B. Garner, D. A. Dixon and S. Y. Liu, *Angew. Chem. Int. Ed.*, **2011**, 50, 8157-8160.

32. S. A. Brough, A. N. Lamm, S. Y. Liu and H. F. Bettinger, *Angew. Chem. Int. Ed.*, **2012**, 51, 10880-10883.

33. P. G. Campbell, E. R. Abbey, D. Neiner, D. J. Grant, D. A. Dixon and S.-Y. Liu, *J. Am. Chem. Soc.*, **2010**, 132, 18048-18050.

34. C. Tanjaroon, A. Daly, A. J. V. Marwitz, S. Y. Liu and S. Kukolich, *J. Chem. Phys.*, **2009**, 131.

35. A. J. V. Marwitz, S. P. McClintock, L. N. Zakharov and S.-Y. Liu, *Chem. Commun.*, **2010**, 46, 779-781.

36. A. J. V. Marwitz, J. T. Jenkins, L. N. Zakharov and S. Y. Liu, *Angew. Chem. Int. Ed.*, **2010**, 49, 7444-7447.

37. A. N. Lamm and S.-Y. Liu, *Mol. Biosyst.*, **2009**, 5, 1303-1305.

38. A. J. V. Marwitz, M. H. Matus, L. N. Zakharov, D. A. Dixon and S.-Y. Liu, *Angew. Chem. Int. Ed.*, **2009**, 48, 973-977.

39. S. M. Xu, L. N. Zakharov and S. Y. Liu, *J. Am. Chem. Soc.*, **2011**, 133, 20152-20155.

40. P. M. Maitlis, *J. Chem. Soc.*, **1961**, 425-429.

41. M. Kranz, F. Hampel and T. Clark, *J. Chem. Soc. Chem. Commun.*, **1992**, 1247-1248.

42. T. Agou, H. Arai and T. Kawashima, *Chem. Lett.*, **2010**, 39, 612-613.

43. T. Agou, T. Kojima, J. Kobayashi and T. Kawashima, *Org. Lett.*, **2009**, 11, 3534-3537.

44. T. Agou, M. Sekine, J. Kobayashi and T. Kawashima, *Chem. Eur. J.*, **2009**, 15, 5056-5062.

45. T. Agou, T. Kojima, J. Kobayashi and T. Kawashima, *Org. Lett.*, **2009**, 11, 3534-3537.

46. X. Liu, Y. Zhang, B. Li, L. N. Zakharov, M. Vasiliu, D. A. Dixon and S.-Y. Liu, *Angew. Chem. Int. Ed.*, **2016**, 128, 8473-8477.

47. D. Ghosh, G. Periyasamy and S. K. Pati, *Phys. Chem. Chem. Phys.*, **2011**, 13, 20627-20636.

48. Y. Zhao and D. G. Truhlar, *Acc. Chem. Res.*, **2008**, 41, 157-167.

49. Y. Zhao and D. G. Truhlar, *Theor. Chem. Acc.*, **2008**, 120, 215-247.

50. G. W. T. M. J. Frisch, H. B. Schlegel, G. E. Scuseria,, J. R. C. M. A. Robb, G. Scalmani, V. Barone, B. Mennucci,, H. N. G. A. Petersson, M. Caricato, X. Li, H. P. Hratchian,, J. B. A. F. Izmaylov, G. Zheng, J. L. Sonnenberg, M. Hada,, K. T. M. Ehara, R. Fukuda, J. Hasegawa, M. Ishida, T. Nakajima,, O. K. Y. Honda, H. Nakai, T. Vreven, J. A. Montgomery, Jr.,, F. O. J. E. Peralta, M. Bearpark, J. J. Heyd, E. Brothers,, V. N. S. K. N. Kudin, T. Keith, R. Kobayashi, J. Normand,, A. R. K. Raghavachari, J. C. Burant, S. S. Iyengar, J. Tomasi,, N. R. M. Cossi, J. M. Millam, M. Klene, J. E. Knox, J. B. Cross,, C. A. V. Bakken, J. Jaramillo, R. Gomperts, R. E. Stratmann,, A. J. A. O. Yazyev, R. Cammi, C. Pomelli, J. W. Ochterski,, K. M. R. L. Martin, V. G. Zakrzewski, G. A. Voth,, J. J. D. P. Salvador, S. Dapprich, A. D. Daniels,, J. B. F. O. Farkas, J. V. Ortiz, J. Cioslowski, and and D. J. Fox *Gaussian 09, Revision D.01,*; Gaussian Inc.: Wallingford CT, 2013

51. K. Remya and C. H. Suresh, *J. Comput. Chem.*, **2013**, 34, 1341-1353.

52. K. Remya and C. H. Suresh, *Phys. Chem. Chem. Phys.*, **2015**, 17, 27035-27044.

53. K. Remya and C. H. Suresh, *RSC Adv.*, **2016**, 6, 44261-44271.

54. T. D. Della and C. H. Suresh, *Phys. Chem. Chem. Phys.*, **2016**, 18, 14588-14602.

55. P. v. R. Schleyer, C. Maerker, A. Dransfeld, H. Jiao and N. J. R. v. E. Hommes, *J. Am. Chem. Soc.*, **1996**, 118, 6317-6318.

56. J. Kruszewski and T. M. Krygowski, *Tetrahedron Lett.*, **1972**, 13, 3839-3842.

57. A. R. Katritzky, K. Jug and D. C. Oniciu, *Chem. Rev.*, **2001**, 101, 1421-1450.

58. F. Feixas, E. Matito, J. Poater and M. Sola, *Chem. Soc. Rev.*, **2015**, 44, 6434-6451.

59. S. K. Pandey, D. Manogaran, S. Manogaran and H. F. Schaefer, *J. Phys. Chem. A*, **2016**, 120, 2894-2901.

60. K. Jug and A. M. Köster, *J. Phys. Org. Chem.*, **1991**, 4, 163-169.

61. A. R. Katritzky, P. Barczynski, G. Musumarra, D. Pisano and M. Szafran, *J. Am. Chem. Soc.*, **1989**, 111, 7-15.

62. M. K. Cyrañski, T. M. Krygowski, A. R. Katritzky and P. v. R. Schleyer, *J. Org. Chem.*, **2002**, 67, 1333-1338.

63. M. Alonso and B. Herradón, *Chem. Eur. J.*, **2007**, 13, 3913-3923.

64. A. Stanger, *Chem. Commun.*, **2009**, 1939-1947.

65. P. Bultinck, S. Fias and R. Ponec, *Chem. Eur. J.*, **2006**, 12, 8813-8818.

66. P. Bultinck, *Faraday Discuss.* , **2007**, 135, 347-365.

67. Z. Badri and C. Foroutan-Nejad, *Phys. Chem. Chem. Phys.*, **2016**, 18, 11693-11699.

68. T. M. Krygowski, H. Szatylowicz, O. A. Stasyuk, J. Dominikowska and M. Palusiak, *Chem. Rev.*, **2014**, 114, 6383-6422.

69. T. M. Krygowski, *J. Chem. Inf. Comput. Sci.*, **1993**, 33, 70-78.

70. T. M. Krygowski and M. K. Cyrański, *Chem. Rev.*, **2001**, 101, 1385-1420.

71. M. K. Cyrański, *Chem. Rev.*, **2005**, 105, 3773-3811.

72. C. P. Frizzo and M. A. P. Martins, *Struct. Chem.*, **2012**, 23, 375-380.

73. P. v. R. Schleyer, C. Maerker, A. Dransfeld, H. Jiao and N. J. R. v. E. Hommes, *J. Am. Chem. Soc.*, **1996**, 118, 6317-6318.

74. J. I. Wu, I. Fernández and P. v. R. Schleyer, *J. Am. Chem. Soc.*, **2013**, 135, 315-321.

75. P. Lazzeretti, *Phys. Chem. Chem. Phys.*, **2004**, 6, 217-223.

76. Z. Chen, C. S. Wannere, C. Corminboeuf, R. Puchta and P. v. R. Schleyer, *Chem. Rev.*, **2005**, 105, 3842-3888.

77. J. Poater, M. Solà, R. G. Viglione and R. Zanasi, *J. Org. Chem.*, **2004**, 69, 7537-7542.

78. S. R. Gadre, S. V. Bapat, K. Sundararajan and I. H. Shrivastava, *Chem. Phys. Lett.*, **1990**, 175, 307-312.

79. S. R. Gadre, S. A. Kulkarni and I. H. Shrivastava, *J. Chem. Phys.*, **1992**, 96, 5253-5260.

80. K. P. Vijayalakshmi and C. H. Suresh, *New J. Chem.*, **2010**, 34, 2132-2138.

81. C. H. Suresh and S. R. Gadre, *J. Org. Chem.*, **1999**, 64, 2505-2512.

82. C. H. Suresh and M. J. Ajitha, *J. Org. Chem.*, **2013**, 78, 3918-3924.

83. S. Xu, Y. Yuan, X. Cai, C.-J. Zhang, F. Hu, J. Liang, G. Zhang, D. Zhang and B. Liu, *Chem. Sci.*, **2015**, 6, 5824-5830.

84. D. R. Lee, J. M. Choi, C. W. Lee and J. Y. Lee, *ACS Appl. Mater. Interfaces*, **2016**, 8, 23190-23196.

85. S. Wu, M. Aonuma, Q. Zhang, S. Huang, T. Nakagawa, K. Kuwabara and C. Adachi, *J. Mater. Chem. C*, **2014**, 2, 421-424.

86. Q. Zhang, J. Li, K. Shizu, S. Huang, S. Hirata, H. Miyazaki and C. Adachi, *J. Am. Chem. Soc.*, **2012**, 134, 14706-14709.

87. M. Li, L. Kou, L. Diao, Q. Zhang, Z. Li, Q. Wu, W. Lu and D. Pan, *J. Phys. Chem. A*, **2015**, 119, 3299-3309.

# Chapter 4

# Polycyclic Aromatic Hydrocarbons of Various Size and Shapes

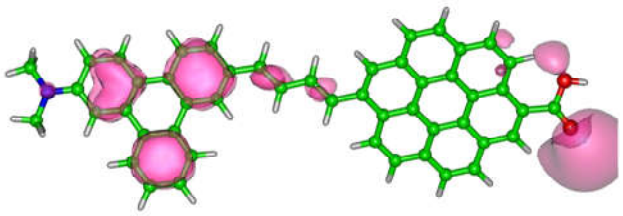

**MESP features showing localization of electron density to one PAH part**

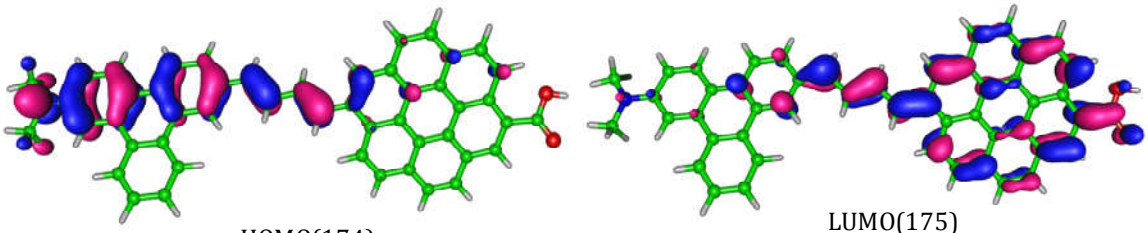

HOMO(174) LUMO(175)

**Molecular orbital features showing efficient PAH-π-PAH system (FMOs localized to differnt PAH parts)**

## *4.1. Abstract*

*Polycyclic aromatic hydrocarbons (PAH) can be considered as graphene nanoflakes in which the edges are hydrogenated. The optical and electronic properties are widely studied for graphene flakes. We have analyzed six different types of PAH molecules which are classified based on the shape of the system. Both zigzag and armchair-edged circular, parallelogram, armchair-edged triangular and rectangular PAHs are analyzed theoretically using M06L/6-31+G(d) level of density functional theory. A total number of 24 systems (4 from each set) are analyzed in the present study. Molecular electrostatic potential analysis of all the molecules is done to visualize the electronic nature of the systems, together with the time-dependent DFT analysis for the absorption spectral analysis. From MESP isosurface, the Clar's sextet like electronic arrangement in armchair-edged systems is evident, whereas the zigzag-edged ones have electron isosurface localization towards the edges of systems. The TD-DFT analysis casts the light upon the absorption features of these systems, which followed linear trends for most of the armchair-edged systems with respect to the number of π-electron in the system. The frontier molecular orbital analysis of every system is also done for the picturization of molecular orbitals which is very much beneficial in analyzing the respective reactivity. The different electronic features on variously shaped PAH systems led to the design of PAH-π-spacer-PAH systems which are made by connecting two differently shaped PAH systems via a conjugated diene. In these systems, one of the PAH moiety showed slightly higher electron density (Donor) than the other (Acceptor). The entire systems behaved weakly as a donor-π-acceptor system (D-π-A). With the introduction of electron donating functional group ($NMe_2$) on one PAH and electron withdrawing group (COOH) on the other PAH, the PAH-π-spacer-PAH system behaved as a strong D-π-A system. The MESP features, FMO distribution and absorption spectra features corroborated these finding. Among the different shapes studied, the rectangular shaped PAH moiety showed the most efficient tuning of HOMO-LUMO gap with respect to the size of the system.*

## 4.2. Introduction

The field of molecular materials flourished after the isolation of graphene by Nobel Prize winners Geim and Novoselov[1] even though the pioneering theoretical

work was done by P. Wallace in the year 1947.[2] By definition, Graphene is a polycyclic aromatic hydrocarbon (PAH) which is a flat monolayer of $sp^2$ carbon atoms packed into a two dimensional π-conjugated systems[3-5] having exceptional electronic, thermal and mechanical properties.[1, 6] Despite being one atom thick, graphene can be optically visualised.[7, 8] Together with this visibility, other remarkable optical properties like hot luminescence, saturable absorption, and broadband applicability renders graphene an ideal photonic and optoelectronic material.[9-17] It can be termed as the mother of most of the carbon allotropes, like fullerene, carbon nanotubes, and graphite. Graphene can be wrapped up after the introduction of pentagons on the hexagonal lattice to form fullerenes, it can be stalked one sheet above another to form graphite and if a graphene sheet is rolled then carbon nanotubes are made.

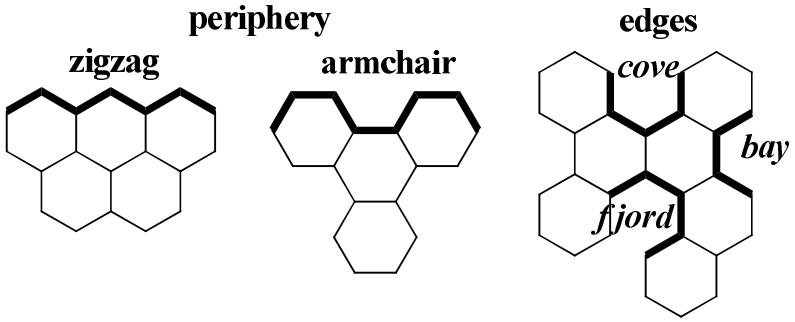


**Figure 4.1.** Different types of periphery and edges in PAHs.

Large flakes of graphene in which every ring are different from the othebr are termed nanographene,[3, 18-23] the properties of which are largely influenced by the size and edge shape.[24-26] As the size of the PAH increases, the number of isomers possible also increases[27]. Graphene nanoflakes are stable than carbon nanotubes of similar size, but less stable than the corresponding fullerenes. In addition, large flakes have almost zero bandgap whereas small ones are semiconductors or insulators. Graphene nanoflakes tend to show new and unexpected electronic, optical, vibrational and magnetic properties based on the size and geometry. [24, 25, 28-33]. For example, triphenylene and tetracene are made of four aromatic rings, the absorption maximum of former is at 265 nm and the same for latter is 471 nm, a much higher value. In addition, triphenylene is quite stable against oxidation whereas tetracene is easily oxidized. Two types of periphery (zigzag and armchair) and three types of edges (the bay, the cove and the fjord) are observed for PAHs,

(Figure 4.1).[24] PAHs with armchair periphery are more resonance stabilized compared to those with the zigzag periphery, making zigzag ones more reactive so that larger PAHs with zigzag periphery is instantaneously converted to quinine in the air.[24 29] It is already proven that the HOMO-LUMO band gap engineering can be done by changing the size and the shape of graphene nanoflakes.[34]

From optoelectronics to energy storage, every field can be benefitted by the use of graphene.[22, 35-37] Some of the applications of graphene are, as a support to study samples in transmission electron microscope (TEM),[38-40] as conducting transparent coating for solar cells and liquid crystal displays,[41, 42] as field-effect transistors (FETs) for high frequency applications,[43, 44] and as composite materials.[45] Extremely high charge carrier mobility makes graphene exceptionally promising material in nanoelectronics,[23] but the use of it in native form is difficult in FETs because of the zero band gap.[46]

Large PAHs are present naturally, but graphene nanoflakes are very difficult to synthesis and are not found in naturally.[47] Syntheses of nanoflakes are done,[48-51] but the growth and nucleation trends are yet to be understood. Both top-down[36, 52-55] and bottom-up[49, 56] approaches are adopted for synthesis. Extensive theoretical research on graphene nanoflakes have been done by various groups.[57-62] The sustainability, biocompatibility and tunable electronic and structural properties of carbon nano-materials support their role as charge-transfer systems.[63-67]

## 4.3. Computational Methods

All the molecules are optimised using Gaussian 16 suit of programs[68] using ground state DFT method M06L, with basis set 6-31+G(d). The optimised geometries are confirmed as energy minima by vibrational frequency analysis. For the absorption spectra calculation, time-dependent DFT (TD-DFT) calculation at the same level of theory is done on the optimised geometry.

## 4.4. Results and Discussion

### 4.4.1. Structure and MESP Features

#### 4.4.1.1. PAH systems: Structure

PAHs can be considered as graphene sheets that have been cut into different shapes and the terminal carbon valance is satisfied by hydrogen atoms. The major

differentiation in PAHs is based on the shape of the edges, both zigzag and armchair edged PAHs are observed in nature. Considering this in mind, we have categorized the PAHs into six groups. Those groups are circularly shaped PAHs which are again divided into armchair and zigzag edged. Similarly, parallelogram-shaped PAHs are also designed in both armchair and zigzag edged forms. Armchair edged triangular shaped PAH is the next set of molecules. Zigzag edged triangular ones are not included in the study due to the requirement of odd number of C-H bonds to complete the triangular shape. Such a system will have one unpaired electron and exist as free radicals in nature, which tend to have different properties than other systems being investigated. In addition to these five groups, rectangular shaped PAHs are also designed. Designating this group as totally zigzag or armchair edged was not possible for a closed shell structure. In such molecules, if one side is zigzag edged, the adjacent edge will be always armchair edged. Hence, this set is named hybrid-set.

In every set of molecules, 4 systems are analysed in the present study, which are designated as $X_yN$, *where* $X$ = *C, T, P* or *R* denoting circular, triangular, parallelogram and rectangular respectively. y = *z, a or h* standing for zigzag morphology, armchair morphology and hybrid morphology respectively. The notation *N* is used as a serial number (*1-4*) for the smallest to the largest system studied in each category. A representative molecule from each category is given in Figure 4.2. All the molecules show planar geometry as expected.

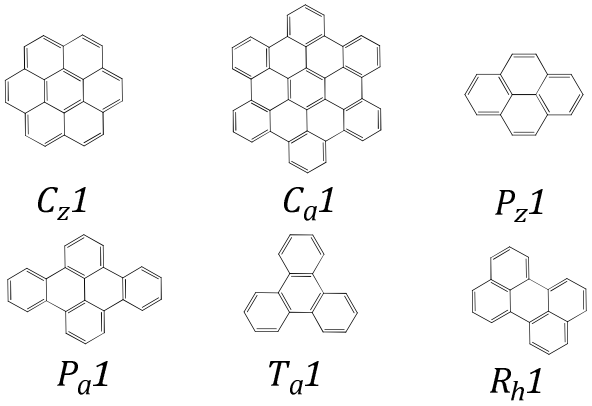


**Figure 4.2.** Representative set of PAH molecules under study

For the PAH systems, the number of π-electrons and number of π-electrons per CC bonds ($n_\pi$) is calculated and is given in Table 4.1, $n_\pi$ can be used as a simple measure to assess the π-electron density in every molecule. In every category, $n_\pi$ is

bound to decrease as the size of the system increases because the number of CC bonds monotonically increases. The $C_xN$ systems show the lowest $n_\pi$ value.

**Table 4.1.** The number of π- electrons and ratio of number of π electrons to the total number of bonds ($n_\pi$) in PAH systems.

| System | No. of π-ē | $n_\pi$ | System | No. of π-ē | $n_\pi$ | System | No. of π-ē | $n_\pi$ |
|---|---|---|---|---|---|---|---|---|
| $C_z1$ | 24 | 0.800 | $P_z1$ | 16 | 0.842 | $T_a1$ | 18 | 0.857 |
| $C_z2$ | 54 | 0.750 | $P_z2$ | 30 | 0.789 | $T_a2$ | 36 | 0.800 |
| $C_z3$ | 96 | 0.727 | $P_z3$ | 48 | 0.762 | $T_a3$ | 60 | 0.769 |
| $C_z4$ | 150 | 0.714 | $P_z4$ | 70 | 0.745 | $T_a4$ | 90 | 0.750 |
| $C_a1$ | 42 | 0.778 | $P_a1$ | 24 | 0.828 | $R_h1$ | 20 | 0.833 |
| $C_a2$ | 72 | 0.750 | $P_a2$ | 54 | 0.771 | $R_h2$ | 42 | 0.778 |
| $C_a3$ | 132 | 0.733 | $P_a3$ | 96 | 0.744 | $R_h3$ | 74 | 0.771 |
| $C_a4$ | 184 | 0.713 | $P_a4$ | 152 | 0.738 | $R_h4$ | 110 | 0.733 |

### 4.4.1.2. PAH Systems: MESP Analysis

To understand the electronic characteristics of every PAH systems, the most negative valued MESP ($V_{min}$) position in the molecules is determined.[69, 70] MESP has been successfully demonstrated as an effective tool in studying PAH and other related systems, especially to interpret Clar's aromatic sextet theory.[71-73] Figure 4.3. shows MESP features of a representative set of systems (the smallest member in every category). The black dot in the MESP isosurface denotes the deepest $V_{min}$ and their values are given in Table 4.2. A gradual decrease in the absolute value of the $V_{min}$ is observed with increase in the size of the PAH which indicates the diminishing electron richness due to enhancement in electron delocalization.

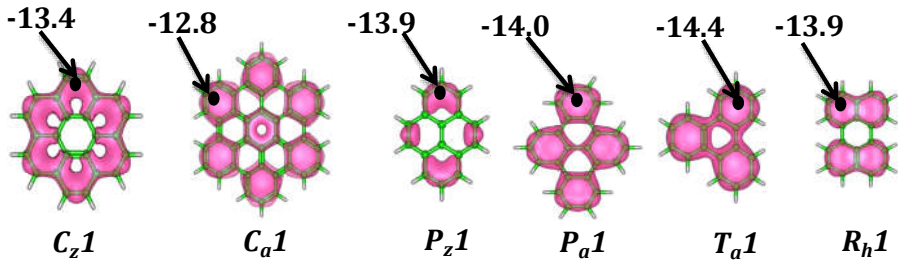


**Figure 4.3.** MESP features on smallest PAH system in all categories.

A plot between $n_\pi$ values and the corresponding $V_{min}$ values are given in Figure 4.4. The first plot gives the correlation for $C_zN$, $C_aN$ and $T_aN$ categories whereas the second pictures gives the same for $P_zN$, $P_aN$ and $R_hN$ systems. Good linear correlations are obtained for all the systems indicating that in a series, the π-

electronic features gradually decrease with increase in the size of the molecule (increase in number of π-electrons). The circular shaped systems show the highest rate of decrease in π-electron density while the rectangular $R_h$N systems display the lowest.

**Table 4.2**. $V_{min}$ values on all the PAH systems in kcal/mol

| System | $V_{min}$ values in kcal/mol | | | | | |
|---|---|---|---|---|---|---|
| | $C_zN$ | $C_aN$ | $P_zN$ | $P_aN$ | $T_aN$ | $R_hN$ |
| *N=1* | -13.4 | -12.8 | -13.9 | -14.0 | -14.4 | -13.9 |
| *N=2* | -12.5 | -11.9 | -13.1 | -13.0 | -13.5 | -13.4 |
| *N=3* | -11.8 | -11.7 | -12.4 | -12.3 | -12.9 | -13.0 |
| *N=4* | -11.0 | -11.3 | -11.9 | -12.1 | -12.6 | -12.7 |

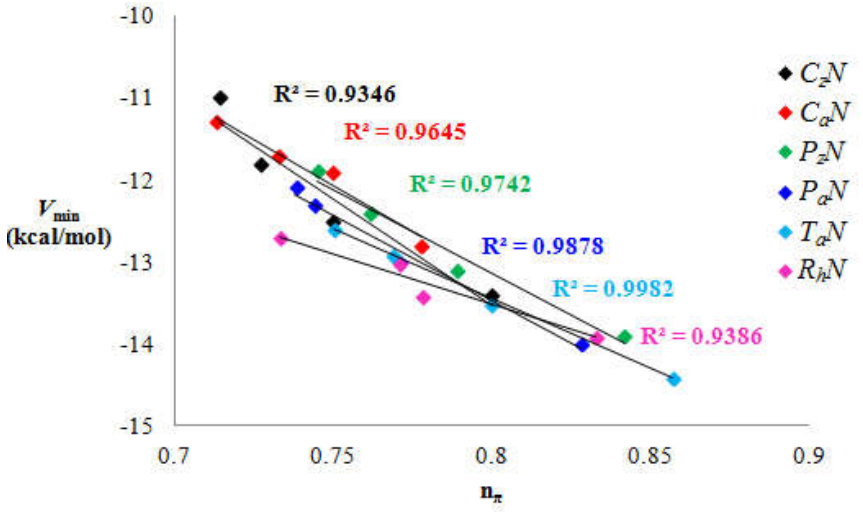


**Figure 4.4.** Graph plotting $n_\pi$ values and $V_{min}$ values on all the PAH systems.

Figure 4.5 and Figure 4.6 represents the MESP isosurface on every zigzag ($C_zN$) and armchair edged ($C_aN$) circular PAHs respectively. For $C_zN$ the electron localization can be observed in the peripheral rings in all the structures as evident from the $V_{min}$ values at the outermost rings. In the case of $C_aN$ systems, the bay region aromatic rings show the most negative $V_{min}$. In $C_aN$ systems, the Clar's aromatic sextet retention is easily visualised (Figure 4.7) while for the $C_zN$ ones Clar's sextet features of hexagons cannot be distinguished. In $C_zN$, the electron cloud as seen in MESP is localised strongly towards the outermost rings. This trend indicates that the armchair edged ones are more stabilised by aromaticity than the zigzag edged ones.

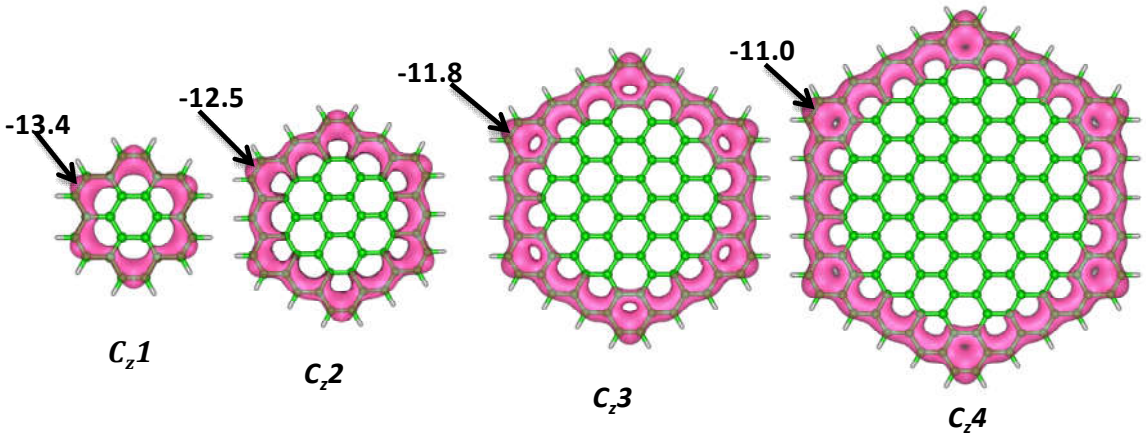


**Figure 4.5.** MESP isosurface at -7.5 kcal/mol of $C_zN$ series of molecules with $V_{min}$ marked in kcal/mol.

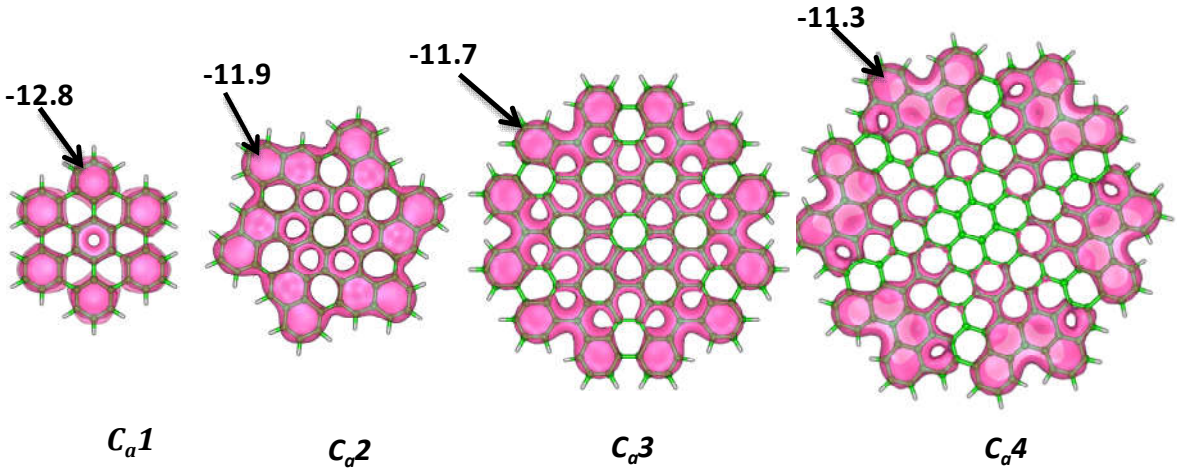


**Figure 4.6.** MESP isosurface at -8 kcal/mol of and $C_aN$ series of molecules with $V_{min}$ marked in kcal/mol.

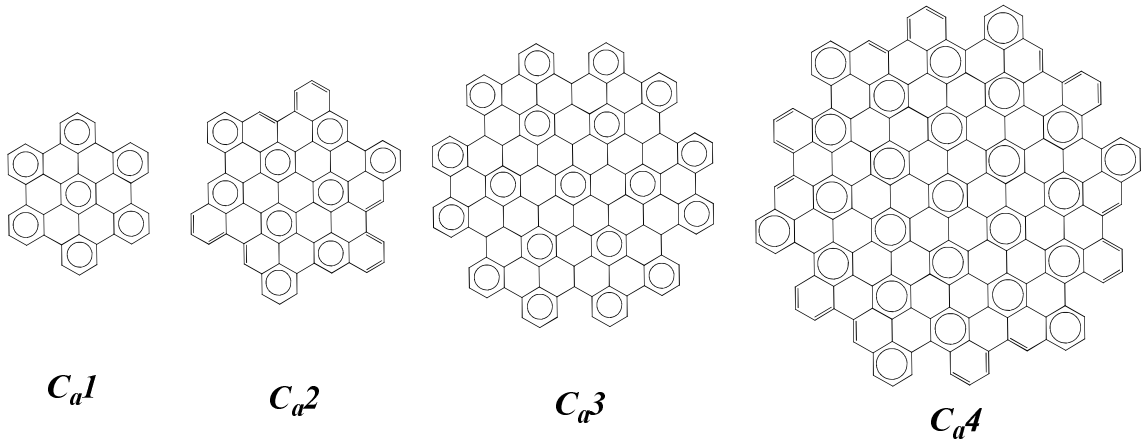


**Figure 4.7.** Clar's structure representation of $C_aN$ series of PAH

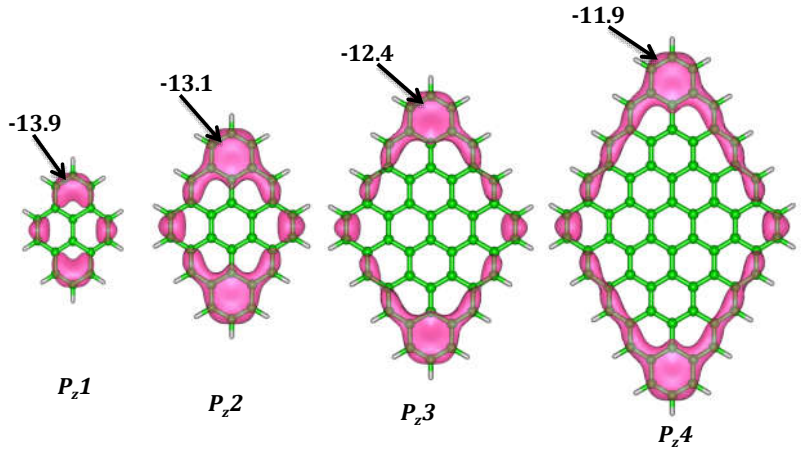


**Figure 4.8.** MESP isosurface at -8 kcal/mol of and $P_zN$ series of molecules with $V_{\min}$ marked in kcal/mol.

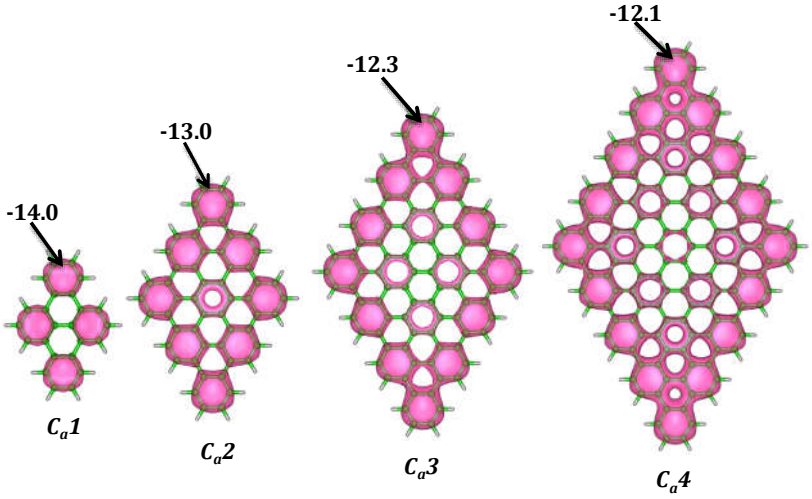


**Figure 4.9.** MESP isosurface at -8 kcal/mol of and $P_aN$ series of molecules with $V_{\min}$ marked in kcal/mol.

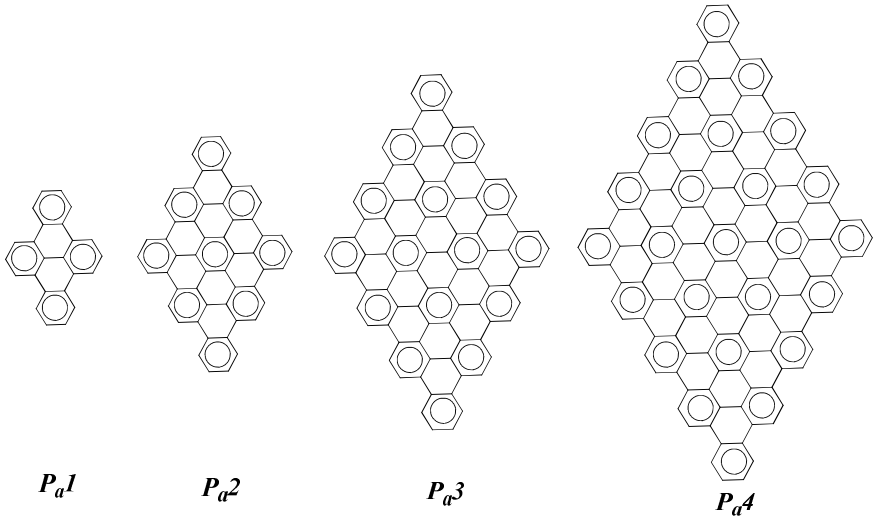


**Figure 4.10.** Clar's structure representation of $P_aN$ series of PAH

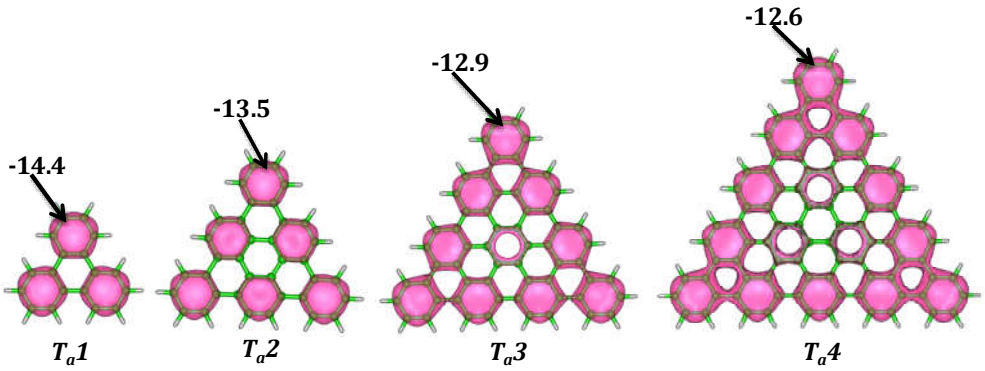


**Figure 4.11.** MESP isosurface at -8 kcal/mol of *TaN* series of molecules with $V_{min}$ marked in kcal/mol.

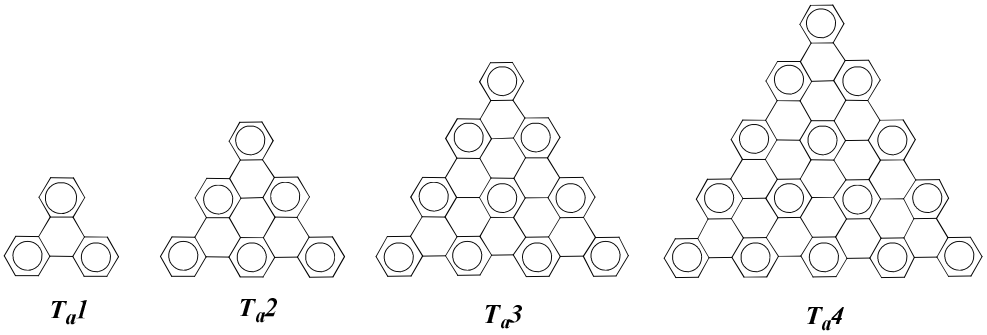


**Figure 4.12.** Clar's structure representations of $T_aN$ PAH systems

The MESP features of $R_hN$ PAHs are given in Figure 4.13. The $V_{min}$ is observed at the corner rings in every systems. For these systems, the constituting individual acene parts *viz.* naphthalene, anthracene, tetracene and pentacene can be visualised from the topology of MESP.

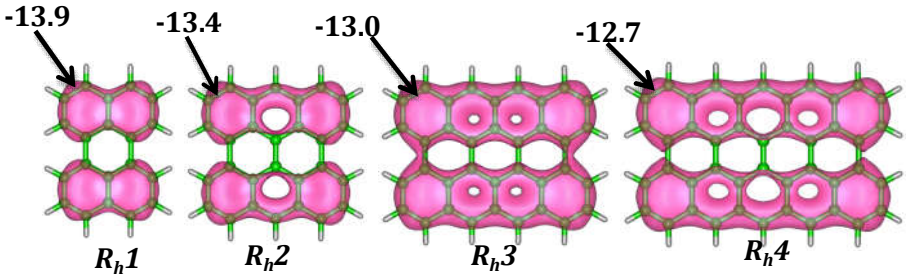


**Figure 4.13**. MESP isosurface at -8 kcal/mol of *RhN* series of molecules with $V_{min}$ marked in kcal/mol.

Figure 4.8 represents the MESP features of $P_zN$ and Figure 4.9 shows the same of $P_aN$ systems. The $V_{min}$ values of all the systems are marked and the corresponding value is given in the picture. The peripheral localisation of the electron cloud is clearly visible in the MESP picture for $P_zN$ systems, whereas for the $P_aN$ ones, MESP features are clearly expressed as Clar's sextets (Figure 4.10). For

$P_zN$ systems most terminal rings having three C-H bonds are the ones which show the most negative MESP features and for $P_aN$ type PAHs the $V_{min}$ values are observed at the terminal rings having four C-H bonds. `

Figure 4.11 gives the pictorial representation of MESP isosurface on every $T_aN$ PAH systems. The peculiarity of armchair edged systems, as mentioned for $C_aN$ and $P_aN$ type PAHs are retained in the $T_aN$ systems also. The visualisation of Clar's sextet is evident by comparing with the Clar's structure for all $T_aN$ given in Figure 4.12. In this case the $V_{\min}$ values are observed at the corner rings of every structure, the magnitude of which gradually diminishes as the size increases.

### 4.4.1.3. PAH-π-PAH Type Systems: Structure

Only the first member from each category of molecules ($C_z1$, $C_a1$, $P_z1$, $P_a1$, $T_a1$ and $R_h1$) is selected to design the PAH-π-spacer-PAH system (PAH-π-PAH). The selected π-spacer is *t*-butadiene moiety. These systems thus designed are named as $C_z1$-$C_a1$, $C_z1$-$P_z1$, $P_a1$-$C_z1$, $T_a1$-$C_z1$, $C_z1$-$R_h1$, $P_z1$-$C_a1$, $P_a1$-$C_a1$, $T_a1$-$C_a1$, $R_h1$-$C_a1$, $P_a1$-$P_z1$, $T_a1$-$P_z1$, $P_z1$-$R_h1$, $T_a1$-$P_a1$, $P_a1$-$R_h1$, *and* $T_a1$-$R_h1$. Naming is done in such a manner so that the PAH system having the highest $V_{\min}$ value is given first, followed by the second PAH moiety name. The most electron rich carbon of the PAH systems as seen in MESP topography (the carbon that appears nearest to the $V_{\min}$ point) are selected to join the spacer butadiene moiety. Most of the designed systems possess perfect planar structures and in cases $R_h1$-$C_a1$, $C_z1$-$C_a1$, $C_z1$-$P_z1$, $P_a1$-$C_z1$, $T_a1$-$C_z1$, and $C_z1$-$R_h1$.

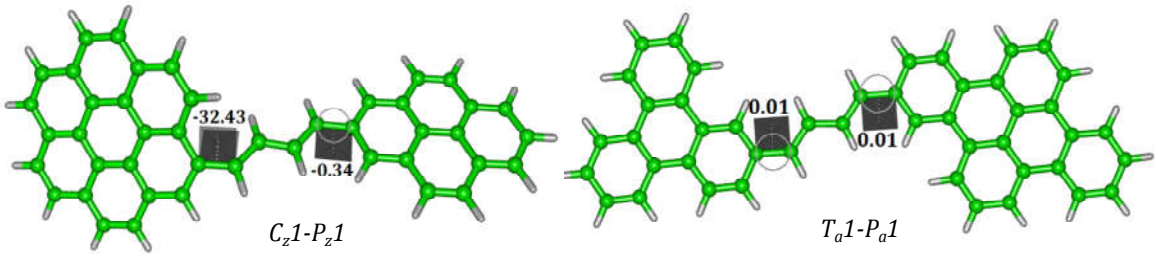


**Figure 4.14.** Optimised geometry of non-planar ($C_z1$-$P_z1$) and planar ($T_a1$-$P_a1$) systems (dihedral angle is marked in both the structures).

All the $C_z1$ connected systems are non-planar. Slight amount of non-planarity occurs which is measured in terms of the largest twist angle between the conjugated diene and the PAH moieties. A representative set of one planar system and a non-planar one is shown in Figure 4.14. The dihedral angles made by both PAH parts with the diene are marked in the figure; a dihedral angle of -32.43 is

visible between the $C_z1$ part and the rest of the system showing the deviation from the molecular plane.

#### 4.4.1.4. PAH-π-PAH Type Systems: MESP Analysis

These systems have been analysed for their electronic features using the tool of molecular electrostatic potential and the $V_{min}$ values on both the PAH systems are given in Table 4.3. In the table the name notations are color coded; the PAH moiety showing more electron rich character than the other is given in red color (donor moiety) while the other (acceptor moiety) is shown in blue color. $V_{min}$D represents the $V_{min}$ of donor moiety whereas $V_{min}$A represents the same for acceptor moiety and $V_{min}$S is for the $V_{min}$ value of spacer unit (butadiene moiety) used.

**Table 4.3**. $V_{min}$ values in kcal/mol on different parts of designed PAH-π-PAH systems.

| System | $V_{min}$D (kcal/mol) | $V_{min}$S (kcal/mol) | $V_{min}$A (kcal/mol) |
|---|---|---|---|
| $C_z1$-$C_a1$ | -12.8 | -13.6 | -12.4 |
| $C_z1$-$P_z1$ | -13.4 | -14.3 | -13.3 |
| $P_a1$-$C_z1$ | -13.5 | -13.9 | -13.0 |
| $T_a1$-$C_z1$ | -13.7 | -14.0 | -13.2 |
| $C_z1$-$R_h1$ | -13.3 | -13.8 | -13.0 |
| $P_z1$-$C_a1$ | -13.0 | -13.6 | -12.6 |
| $P_a1$-$C_a1$ | -13.4 | -13.3 | -12.5 |
| $T_a1$-$C_a1$ | -13.5 | -13.6 | -12.4 |
| $R_h1$-$C_a1$ | -13.2 | -13.8 | -12.5 |
| $P_a1$-$P_z1$ | -13.7 | -14.0 | -13.2 |
| $T_a1$-$P_z1$ | -13.8 | -14.3 | -13.2 |
| $P_z1$-$R_h1$ | -13.6 | -14.7 | -13.4 |
| $T_a1$-$P_a1$ | -13.7 | -13.7 | -13.6 |
| $P_a1$-$R_h1$ | -13.5 | -13.8 | -13.2 |
| $T_a1$-$R_h1$ | -13.7 | -13.9 | -13.4 |

The PAH moieties connected have different values of MESP minima independent of the shape of these systems. The $V_{min}$ values of the individual PAH

parts shows lesser values when compared with the PAH systems that we have earlier discussed. For example consider $T_a1$-$C_a1$ system, in which $T_a1$ part has a $V_{min}$ of -13.5 kcal/mol, while the free $T_a1$ system has a $V_{min}$ value of -14.4 cal/mol. Similarly the PAH system $C_a1$ has $V_{min}$ value of -12.8 kcal/mol, which is changed to a lesser value of -12.4 kcal/mol, when it is part of the designed system.

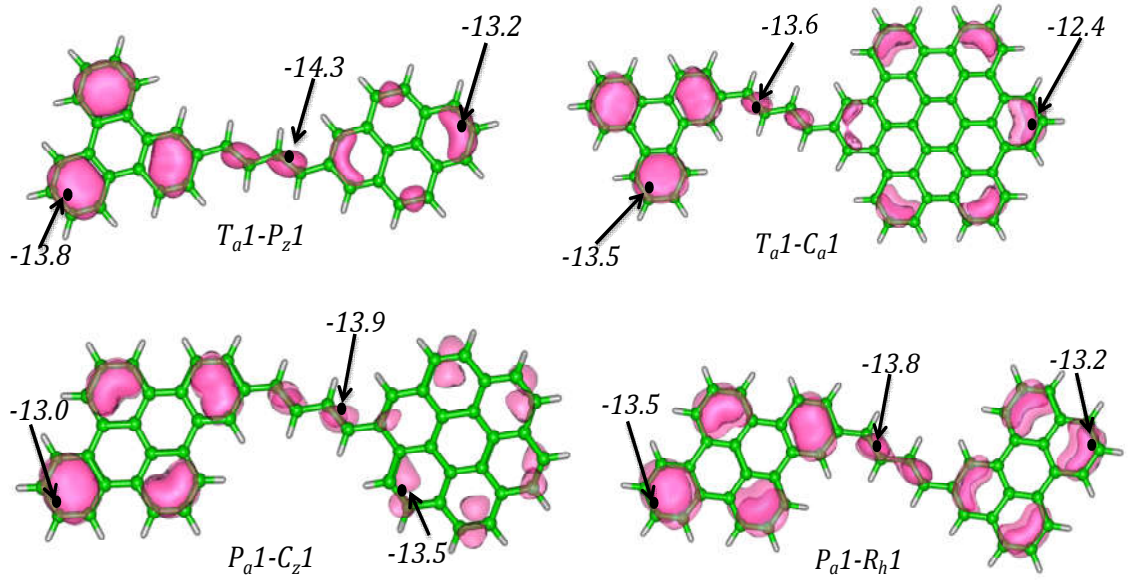


**Figure 4.15.** MESP isosurface at -11.0 kcal/mol on a representative set of systems ($V_{min}$ positions are marked by the black dot).

In these designed systems $T_a1$-$C_a1$ system has the highest difference of 1.1 kcal/mol in the $V_{min}$ values between the two PAH connected via the diene. This difference indicates that the electron cloud localization in one of the PAH part is very much possible and evident for the designed systems. The system $C_z1$-$P_z1$ has the least difference of 0.1 kcal/mol between the $V_{min}$ of the two PAH parts. From the values it is clear that even though the electronic distribution is different on PAH parts connected by the diene, that difference is not very prominent. The spacer part is having the highest $V_{min}$ value ranging from -13.3 to -14.7 kcal/mol, when the whole system is considered. This indicates the electron density is maximum for the butadiene spacer instead of the PAH parts, which leaded to the idea of introducing electron withdrawing and donating functional groups to the opposite ends of the system. This strategy could improve the electronic feature of the system to the extent of the localization of the electron density to one of the PAH moiety so that the

system resembles a true donor-π-acceptor (D-π-A) system having different electron densities on different parts.

### 4.4.1.5. Functionalised PAH-π-PAH Type Systems: Structure

The D-π-A character is very weak in PAH-π-PAH systems. Hence to force more significant electronic rearrangement on the PAH moieties, an electron withdrawing group COOH and electron releasing group $NMe_2$ are selected for connecting to the different PAH ends of the system. We have considered 7 PAH-π-PAH systems which showed the difference 0.5 kcal/mol between the $V_{min}$ values of the constituting PAH parts, to design the corresponding functionalised PAH-π-PAH (*f*_PAH-π-PAH). These systems in abbreviated names are *f*_$P_a1$-$C_z1$, *f*_$T_a1$-$C_z1$, *f*_$P_a1$-$C_a1$, *f*_$T_a1$-$C_a1$, *f*_ $R_h1$-$C_a1$, *f*_$P_a1$-$P_z1$ and *f*_$T_a1$-$P_z1$ where *f* denotes the functionalization. The geometrical characteristics of planarity of PAH-π-PAH are retained in the functionalised systems. The optimised geometries of two designed functionalised PAH-π-PAH systems (*f*_$T_a1$-$C_z1$ and *f*_$R_h1$-$C_a1$) are given in Figure 4.16.

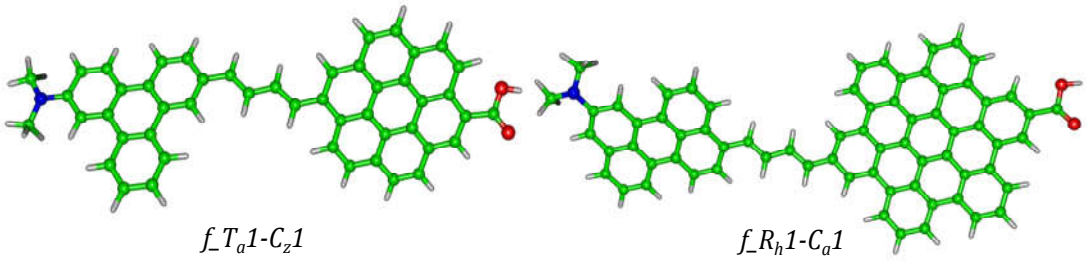


**Figure 4.16.** Optimised geometry of representative functionalized systems at M06L/6-31+G(d) level.

### 4.4.1.6. Functionalised PAH-π-PAH Systems: MESP Analysis

As expected the MESP topography is significantly modified when the system is functionlised using electron donating and withdrawing groups. The visual representation is obtained by the plot of MESP for the functionalised system (Figure 4.17). In both the figures the isosurface (in pink color) is plotted at the constant value of -10 kcal/mol and the position of the $V_{min}$ is marked using a black dot. From the values it is clear that the electron density on the donor PAH part is enhanced significantly compared to the non-functionalised systems. For example, the $V_{min}$D on $P_a1$-$C_a1$ is -13.4 kcal/mol, which is enhanced to a more negative -16.1 kcal/mol in *f*_$P_a1$-$C_a1$. It is also observed that in the acceptor part of PAH, the electron density shows only a moderate variation when functionalised, and for example, the $V_{min}$A on

$P_a1$-$C_a1$ of -12.5 kcal/mol is reduced to -12.0 kcal/mol for the functionalised *f_*$P_a1$-$C_a$-*1* system. Exceptions are *f_*$P_a1$-$C_z1$ *and f_*$T_a1$-$C_z1$ where the electron rich character of the donor site shows a more negative $V_{min}$ than the PAH-π-PAH system. The MESP features confirm the fact that the functionalised systems are more like a true D-π-A system.

**Table 4.4**. $V_{min}$ values on different parts of the functionalised PAH-π-PAH systems

| System | $V_{min}$D (kcal/mol) | $V_{min}$S (kcal/mol) | $V_{min}$A (kcal/mol) |
|---|---|---|---|
| *f_*$P_a1$-$C_z1$ | -16.2 | -13.8 | -14.4 |
| *f_*$T_a1$-$C_z1$ | -15.6 | -15.4 | -13.7 |
| *f_*$P_a1$-$C_a1$ | -16.1 | -13.8 | -12.0 |
| *f_*$T_a1$-$C_a1$ | -15.9 | -15.7 | -12.3 |
| *f_*$R_h1$-$C_a1$ | -16.4 | -14.0 | -11.9 |
| *f_*$P_a1$-$P_z1$ | -16.0 | -13.5 | -11.3 |
| *f_*$T_a1$-$P_z1$ | -15.5 | -15.2 | -12.2 |

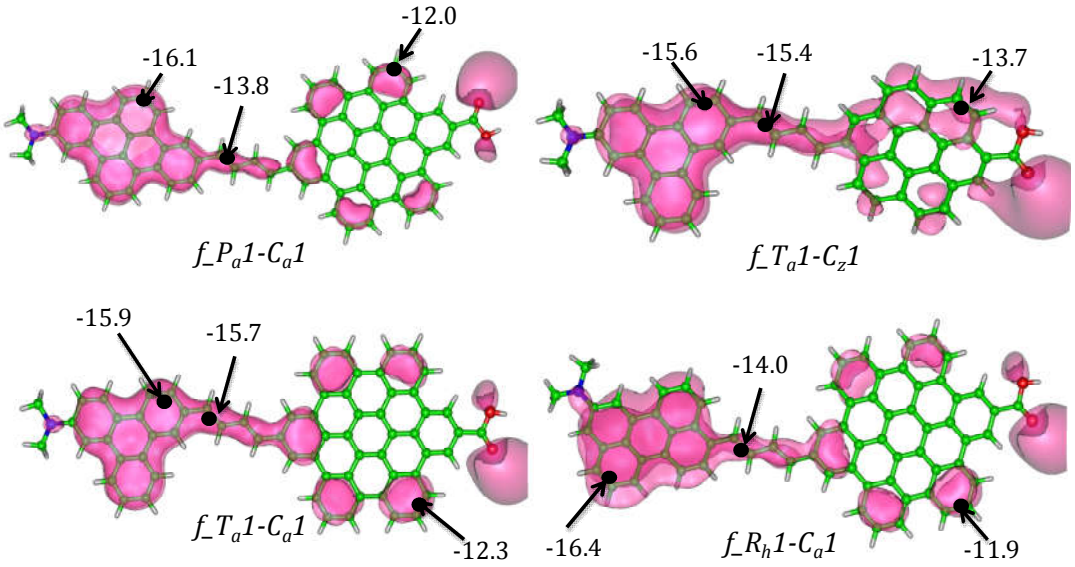


**Figure 4.17.** MESP features on a representative set of the functionalised PAH-π-PAH type systems with MESP isosurface at 10 kcal/mol and $V_{min}$ marked.

## 4.4.2. Molecular Orbital Analysis

### 4.4.2.1. PAH systems

The frontier orbitals of all the systems are generated and a representative set including all the series are given in Figure 4.19.

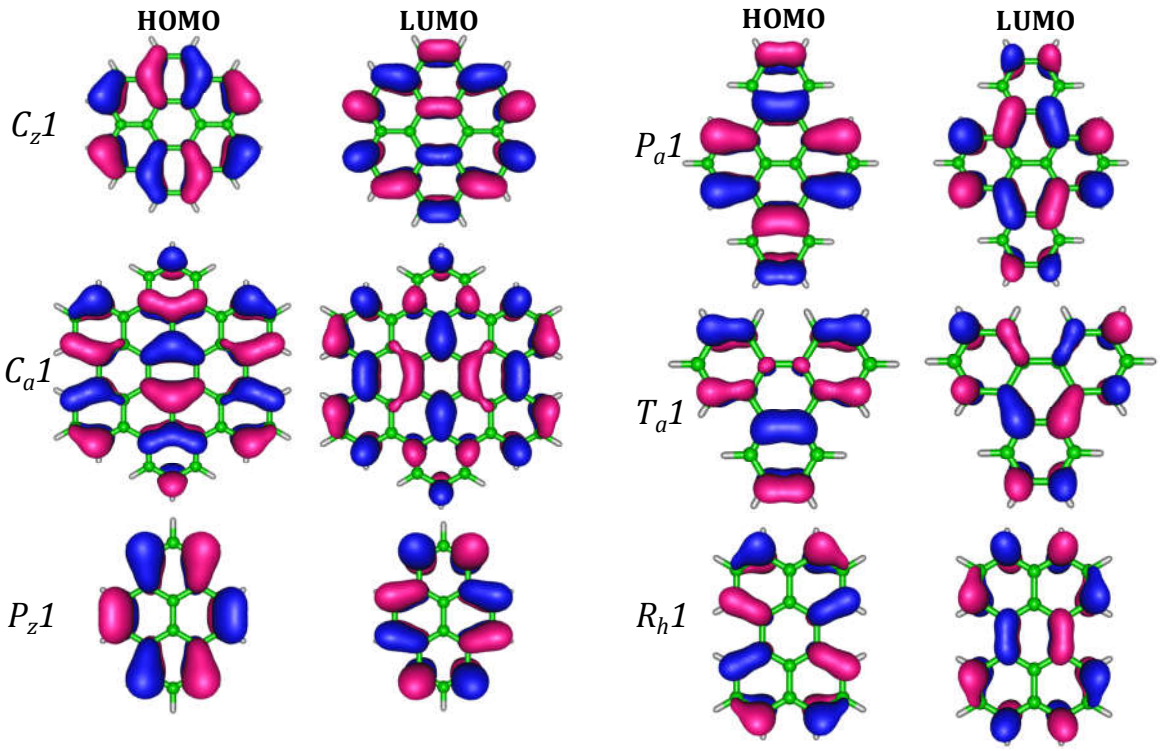


**Figure 4.18.** HOMO and LUMO of representative PAH systems

The retention of pattern and type of molecular orbital distribution is present in a series irrespective of the size change. By changing the size and shape, the HOMO-LUMO gap can be engineered.[34] The HOMO energy ($E_{HOMO}$), LUMO energy ($E_{LUMO}$) and the corresponding HOMO-LUMO gap ($E_{LUMO-HOMO}$) of every system are given in Table 4.5. The gradual tuning with increase in number of rings is observed while analysing the values in a series. The shape of the system and periphery characteristics influences the $E_{LUMO-HOMO}$ greatly. Taking examples of $C_a4$ having 73 rings, $P_a4$ consisting of 57 rings, and $R_h4$ made up of 14 rings, it is observed that the HOMO-LUMO band gaps are 0.88, 1.30 and 0.14 eV respectively. This proves that it is the shape of the PAH system that plays the most crucial part in determining the electronic features of systems. The peculiarity of $R_hN$ type systems is very evident from these values as for very less number of rings, they exhibit very low HOMO-LUMO band gap than other shaped structures. For $R_h1$ having 5 rings and $C_z2$ having 19 rings, both having a band gap of 2.05 eV.

The total number of π-electrons per total number of bonds ($n_\pi$) is one parameter that can be used as a simple gauge to understand the relative π-electron density in PAH systems. When the $E_{LUMO-HOMO}$ is plotted against this parameter the plot obtained is given in Figure 4.18. From the figure it is clear that $C_zN$, $C_aN$, $P_zN$ and

$P_aN$ systems show a similar trend in the change in $E_{LUMO-HOMO}$ values, whereas the trends in the same for $T_aN$ and $R_hN$ systems are significantly varied compared to the former. In $T_aN$ and $R_hN$ PAH systems, the $E_{LUMO-HOMO}$ reduction is very high even for systems having less number of π-electrons.

**Table 4.5.** HOMO, LUMO energies and HOMO-LUMO gap of PAH systems in eV

| System | $E_{HOMO}$ | $E_{LUMO}$ | $E_{LUMO-HOMO}$ | System | $E_{HOMO}$ | $E_{LUMO}$ | $E_{LUMO-HOMO}$ |
|---|---|---|---|---|---|---|---|
| $C_z1$ | -5.19 | -2.11 | 3.09 | $P_z1$ | -5.05 | -2.22 | 2.83 |
| $C_z2$ | -4.75 | -2.70 | 2.05 | $P_z2$ | -4.42 | -2.99 | 1.43 |
| $C_z3$ | -4.51 | -3.05 | 1.46 | $P_z3$ | -4.11 | -3.42 | 0.69 |
| $C_z4$ | -4.36 | -3.29 | 1.07 | $P_z4$ | -3.96 | -3.64 | 0.31 |
| $C_a1$ | -5.00 | -2.34 | 2.65 | $P_a1$ | -5.22 | -2.08 | 3.14 |
| $C_a2$ | -4.58 | -2.90 | 1.68 | $P_a2$ | -4.77 | -2.62 | 2.15 |
| $C_a3$ | -4.51 | -3.13 | 1.38 | $P_a3$ | -4.54 | -2.91 | 1.63 |
| $C_a4$ | -4.28 | -3.39 | 0.88 | $P_a4$ | -4.40 | -3.10 | 1.30 |
| $R_h1$ | -4.69 | -2.64 | 2.05 | $T_a1$ | -5.54 | -1.72 | 3.82 |
| $R_h2$ | -4.20 | -3.19 | 1.01 | $T_a2$ | -5.12 | -2.21 | 2.91 |
| $R_h3$ | -3.94 | -3.51 | 0.43 | $T_a3$ | -4.87 | -2.52 | 2.35 |
| $R_h4$ | -3.83 | -3.69 | 0.14 | $T_a4$ | -4.70 | -2.73 | 1.96 |

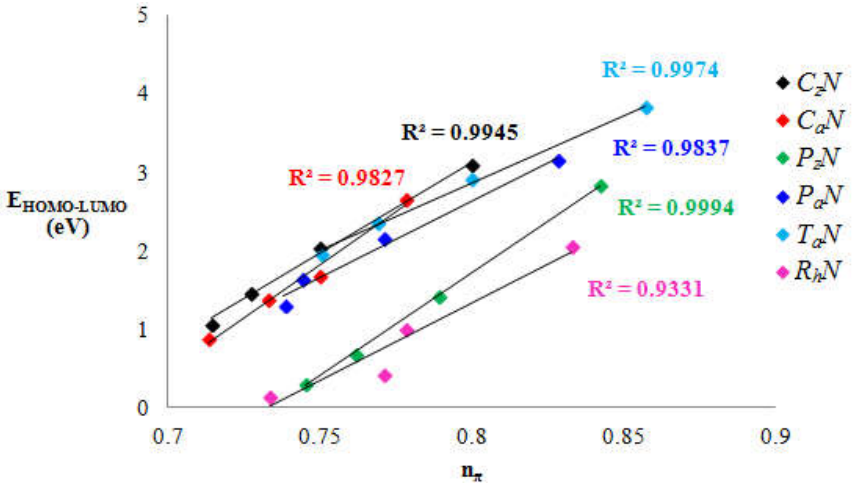


**Figure 4.19.** Graphs plotting $E_{LUMO-HOMO}$ and $n_\pi$ values on all the PAH systems.

### 4.4.2.2. PAH-π-PAH Systems

For these systems, the energies $E_{HOMO}$, $E_{LUMO}$ and $E_{LUMO-HOMO}$ are given in Table 4.6. For all the systems the $E_{LUMO-HOMO}$ is in the range of 1.60 to 2.31 eV. The peculiarity of $R_hN$ systems in lowering the energy gap is reflected in the designed

systems. For example the D-π-A systems which have $R_h1$ as structural component has the lowest $E_{LUMO-HOMO}$ values (1.60 eV for $R_h1$-$C_a1$ and 1.61 eV for $C_z1$-$R_h1$). For systems having $R_h1$ part the $E_{LUMO-HOMO}$ value is below 2.00 eV. The highest band gap of 2.31 eV is observed for $T_a1$-$P_z1$ system.

**Table 4.6.**HOMO, LUMO energy and HOMO-LUMO gap for PAH-π-PAH systems in eV

| System | $E_{HOMO}$ | $E_{LUMO}$ | $E_{LUMO-HOMO}$ |
|---|---|---|---|
| $C_z1$-$C_a1$ | -4.77 | -2.71 | 2.05 |
| $C_z1$-$P_z1$ | -4.82 | -2.58 | 2.24 |
| $P_a1$-$C_z1$ | -4.78 | -2.70 | 2.08 |
| $T_a1$-$C_z1$ | -4.79 | -2.68 | 2.12 |
| $C_z1$-$R_h1$ | -4.52 | -2.91 | 1.61 |
| $P_z1$-$C_a1$ | -4.82 | -2.65 | 2.17 |
| $P_a1$-$C_a1$ | -4.78 | -2.70 | 2.08 |
| $T_a1$-$C_a1$ | -4.79 | -2.70 | 2.10 |
| $R_h1$-$C_a1$ | -4.53 | -2.93 | 1.60 |
| $P_a1$-$P_z1$ | -4.87 | -2.62 | 2.25 |
| $T_a1$-$P_z1$ | -4.88 | -2.57 | 2.31 |
| $P_z1$-$R_h1$ | -4.52 | -2.87 | 1.65 |
| $T_a1$-$P_a1$ | -4.83 | -2.67 | 2.16 |
| $P_a1$-$R_h1$ | -4.69 | -2.74 | 1.95 |
| $T_a1$-$R_h1$ | -4.66 | -2.80 | 1.86 |

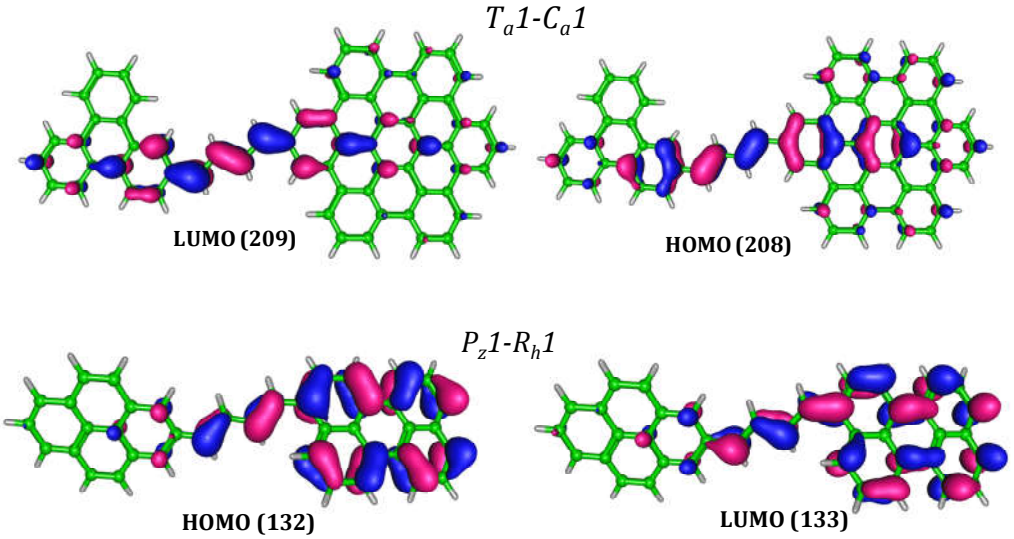


**Figure 4.20**. Frontier molecular orbitals of $T_a1$-$C_a1$ and $P_z1$-$R_h1$ system.

The visualisation of HOMO and LUMO of a representative $T_a1$-$C_a1$ system is given in Figure 4.20. The localisation of HOMO and LUMO towards one of the PAH part is visualised. In all the cases, the connecting diene has a clear influence on the MO population. One of the peculiarities of systems containing $R_h1$ is that the HOMO and LUMO distribution is mostly localised in the $R_h1$ part in all the cases (A representative case of $P_z1$-$R_h1$ system is given in Figure 4.20). A clear demarcation between the donor and acceptor part of these molecules is not emerged from the HOMO and LUMO analysis.

### 4.4.2.3. Functionalised PAH-π-PAH Systems

The functionalised systems have low $E_{LUMO\text{-}HOMO}$ in comparison with the pure hydrocarbons, PAH-π-PAH system. The values for frontier molecular energies and the HOMO-LUMO band gap are given in Table 4.7. As evident, the enhancement of molecular orbital distribution is visible in the pictorial representation of HOMO and LUMO(Figure4.21).

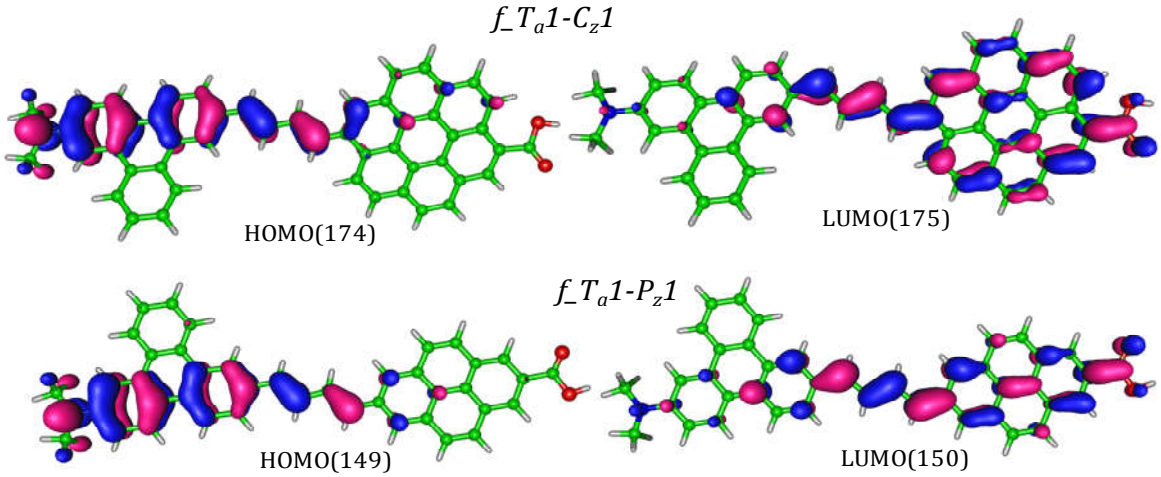


**Figure 4.21.** Frontier molecular orbitals of modified $f\_T_a1$-$C_z1$ and $f\_T_a1$-$P_z1$ systems.

The HOMO is localised in the PAH region connected to the electron donating group, and LUMO is localised towards the PAH which has direct connection with the electron withdrawing acid group. In the functionalised systems, lowering of $E_{HOMO}$ is observed for all the cases. For example $E_{HOMO}$ is -4.65 eV for $f\_P_a1$-$C_z1$ which is lower than that of $P_a1$-$C_z1$ ($E_{HOMO}$ -4.78 eV). For $f\_R_h1$-$C_a1$, $E_{LUMO}$ is -2.90 eV which is slightly lower in energy than the -2.93 eV, $E_{LUMO}$ for $R_h1$-$C_a$. $E_{LUMO}$ is enhanced in all the cases except $f\_R_h1$-$C_a$. Consider $f\_P_a1$-$C_z1$, in which $E_{LUMO}$ is -2.79 eV higher in magnitude than that for $P_a1$-$C_z1$, which is -2.70 eV. The data clearly shows that the HOMO-LUMO tuning is very efficient for $R_hN$ systems.

**Table 4.7.** HOMO, LUMO energies and HOMO-LUMO gap for functionalised PAH-π-PAH type systems in eV

| System | $E_{HOMO}$ | $E_{LUMO}$ | $E_{LUMO-HOMO}$ |
|---|---|---|---|
| *f_Pa1-Cz1* | -4.65 | -2.79 | 1.86 |
| *f_Ta1-Cz1* | -4.54 | -2.70 | 1.84 |
| *f_Pa1-Ca1* | -4.66 | -2.76 | 1.90 |
| *f_Ta1-Ca1* | -4.54 | -2.71 | 1.83 |
| *f_Rh1-Ca1* | -4.41 | -2.90 | 1.51 |
| *f_Pa1-Pz1* | -4.66 | -2.72 | 1.94 |
| *f_Ta1-Pz1* | -4.57 | -2.61 | 1.96 |

## 4.4.3. Optical Properties

The optical properties of all the PAH systems are calculated using the time-dependent density functional theory (TD-DFT). The absorption parameters are of prime interest since the applicability of designed systems in solar and organic electronics is determined mainly by the absorption of energy and the associated changes in the systems. The properties calculated are absorption maxima values, oscillator strength (*f*), the theoretically calculated light harvesting efficiency (LHE), the vertical absorption energy corresponding to the absorption, and the prominent molecular orbital contribution corresponding to the transition. The photo-absorption ability of differently shaped PAH systems can be accessed by the theoretical absorption spectra calculation. Tuning of the absorption maxima values ($\lambda_{max}$) can be attained by changing the number of rings around the core of every system analysed. From the absorption maxima values, it is evident that the geometry and the periphery characteristics hold the major role in determining the $\lambda_{max}$ values rather than the number of rings. Detailed analysis of these properties in different classes is described in the following sub-sections.

### 4.4.3.1. PAH Systems

The optical properties that are calculated using time-dependent density functional theory for both *CzN* and *CaN* is given in Table 4.8. The absorption spectra with all the $\lambda_{max}$ values for all the circularly shaped PAH is given in Figures 4.22 and 4.23. As the size of the system increases, there is a clear red shift in the $\lambda_{max}$ values compared to the smaller systems.

**Table 4.8.** Optical data of $C_zN$ and $C_aN$ PAH systems

| System | $\lambda_{max}$ (nm) | Oscillator strength *(f)* | LHE | Excitation energy (eV) | MO contribution (%) | |
|---|---|---|---|---|---|---|
| $C_z1$ | 317 | 0.562 | 0.726 | 3.07 | HOMO→ LUMO | 44 |
| $C_z2$ | 469 | 0.747 | 0.821 | 2.04 | HOMO→ LUMO | 32 |
| $C_z3$ | 648 | 0.864 | 0.863 | 1.45 | HOMO→ LUMO | 46 |
| $C_z4$ | 865 | 0.901 | 0.875 | 1.07 | HOMO→ LUMO | 46 |
| $C_a1$ | 397 | 0.520 | 0.698 | 2.65 | HOMO→ LUMO | 46 |
| $C_a2$ | 619 | 0.477 | 0.666 | 1.68 | HOMO→ LUMO | 39 |
| $C_a3$ | 754 | 0.742 | 0.819 | 1.39 | HOMO→LUMO | 48 |
| $C_a4$ | 1122 | 0.714 | 0.807 | 0.88 | HOMO→LUMO | 5 |

For $C_zN$ series of molecules, most of the absorption is in the UV and visible region, making them effective in the solar energy trapping applications. The light harvesting efficiency for the PAH systems increases as the number of rings increases. As evident from the Table 4.8, the energy requirement for the vertical excitation declines with the size enhancement. For the absorption process, the prominent molecular orbitals participation is from the frontier MOs with high percentage contributions in the range of 32 – 48 %, only exception being the $C_4N$ having HOMO→LUMO percentage contribution of 5% only. The absorption spectra of all the systems in $C_zN$ series is illustrated in Figure 4.22. For all the systems single $\lambda_{max}$ values are observed with an exception of system $C_z4$, for which a week absorption in the region around 600 nm is present. For a comparison with experimentally available absorption data, the value 300 nm in the case of $C_z1$ (coronene) is matched with the calculated value at M06L/6-31+G(d) level 317 nm[74] (Figure 4.22). For $C_z2$, the $\lambda_{max}$ is at 469 nm, whereas for $C_z3$, it is at 648. For the largest system studied in the series is $C_z4$, which has an $\lambda_{max}$ at 865 nm together with weak absorption in the region of 600- 640 nm. The absorption spectral illustration is given for the $C_aN$ series in Figure 4.23. $C_a1$ system has $\lambda_{max}$ at 397 nm with very weak absorption at 341 nm. For comparison, the experimental $\lambda_{max}$ for hexabenzocoronene ($C_a1$) is centred around 350nm.[75] $C_a2$ has $\lambda_{max}$ at 619 nm and 413nm. $C_a3$ system has $\lambda_{max}$ at 754 and 552 nm, whereas the largest system analysed $C_a4$ has $\lambda_{max}$ at 1122 nm and 764 nm. In the series, all systems other than $C_a4$ has absorption in the UV-Vis region whereas the last one absorbs mainly in the infrared region.

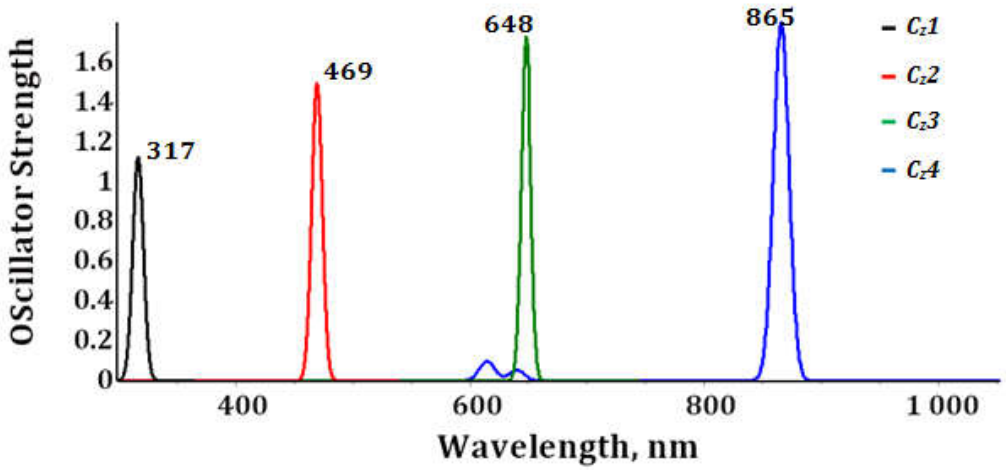


**Figure 4.22.** Absorption spectra of $C_zN$ systems at M06L/6-31+G(d,p) level of theory

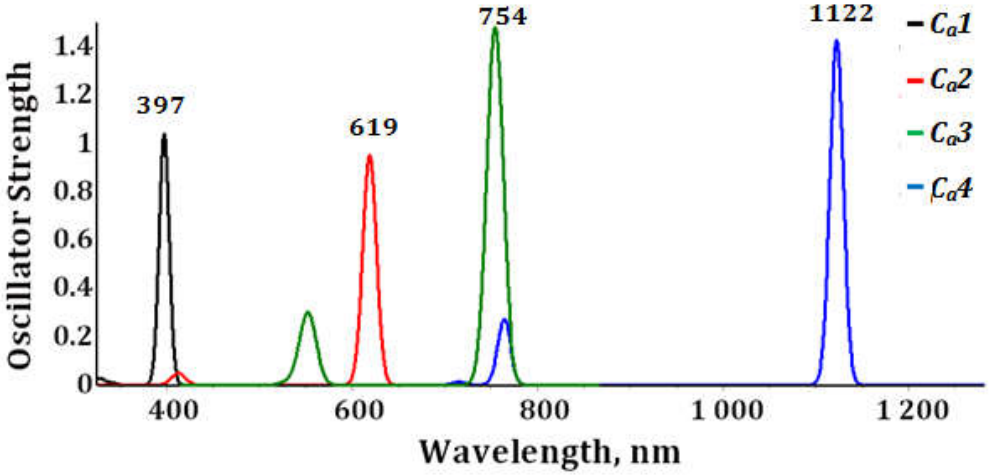


**Figure 4.23.**Absorption spectra of $C_aN$ systems at M06L/6-31+G(d,p) level of theory

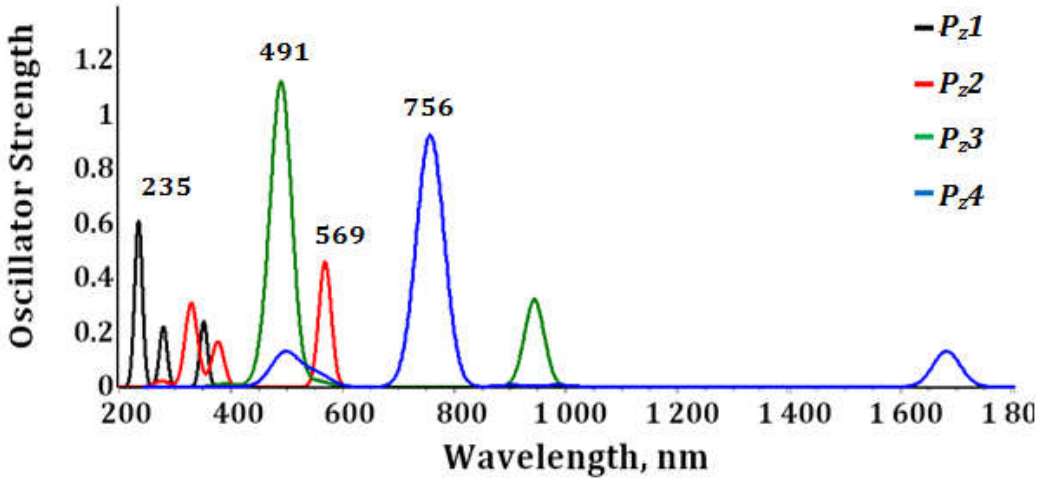


**Figure 4.24.** Absorption spectra of $P_zN$ systems at M06L/6-31+G(d,p) level of theory

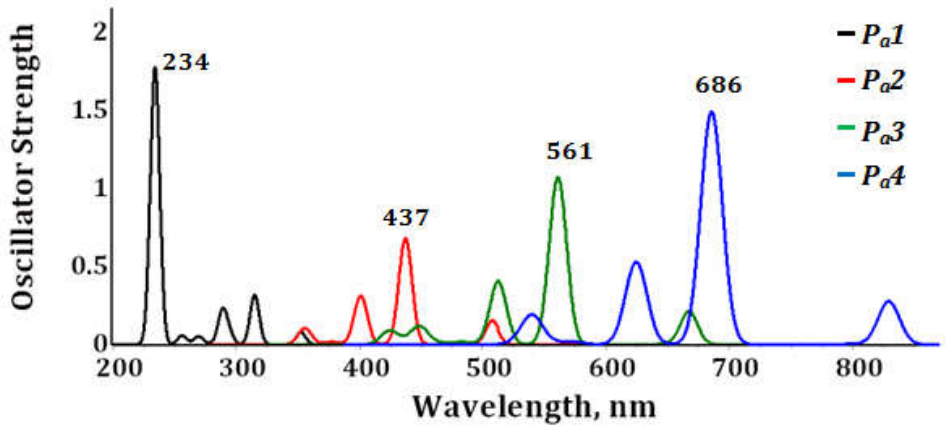


**Figure 4.25.**Absorption spectra of $P_aN$ systems at M06L/6-31+G(d,p) level of theory

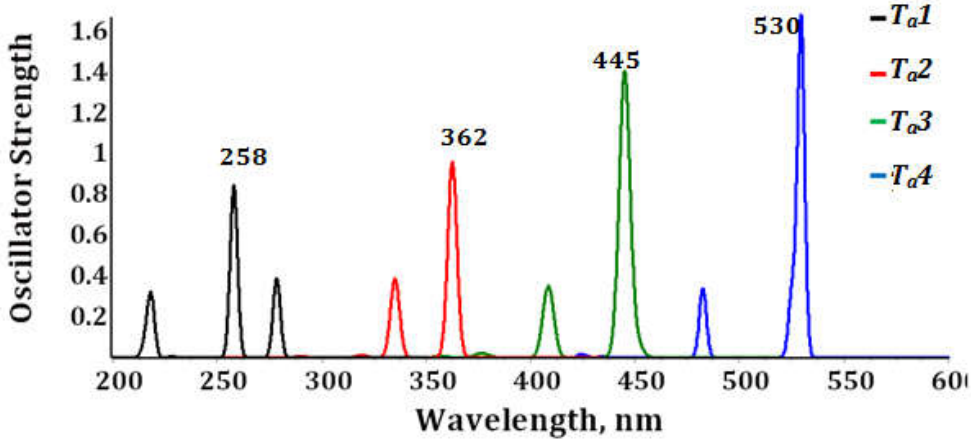


**Figure 4.26.**Absorption spectra of $T_aN$ systems at M06L/6-31+G(d,p) level of theory

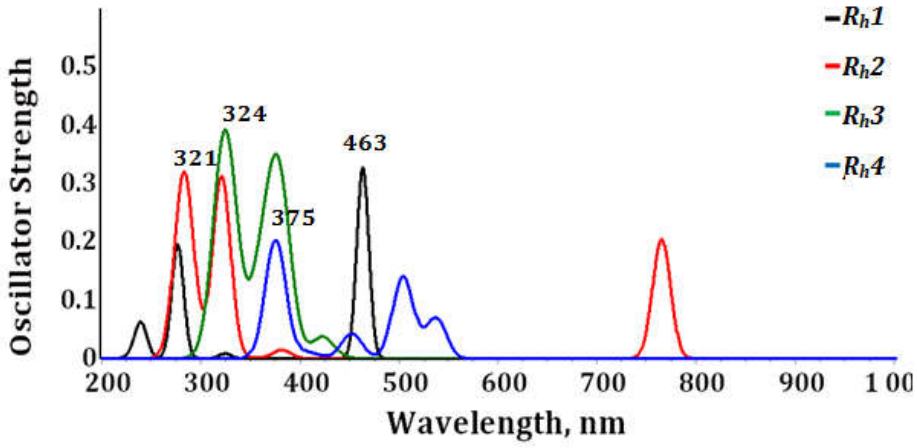


**Figure 4.27.**Absorption spectra of $R_hN$ systems at M06L/6-31+G(d,p) level of theory

For both $P_zN$ and $P_aN$ systems, the optical properties obtained after the TD-DFT calculations are tabulated in Table 4.9. The gradual increase in the $\lambda_{max}$ values is visible in both the set of series. Most prominent $\lambda_{max}$ are tabulated whereas other weak absorptions are described in text. The self repeating patterns are visible in all

the four systems analysed. The $\lambda_{max}$ is observed at the highest wavelength together with weak absorption in the blue region compared to the prominent one.

**Table 4.9.** Optical data of $P_zN$ and $P_aN$ PAH systems

| System | $\lambda_{max}$ (nm) | Oscillator strength (*f*) | LHE | Excitation energy (eV) | MO contribution (%) | |
|---|---|---|---|---|---|---|
| $P_z1$ | 235 | 0.610 | 0.755 | 3.53 | HOMO-1→LUMO+1 | 79 |
| $P_z2$ | 569 | 0.460 | 0.653 | 2.18 | HOMO→LUMO | 95 |
| $P_z3$ | 491 | 1.079 | 0.917 | 1.29 | HOMO-1→LUMO+1 | 77 |
| $P_z4$ | 756 | 0.926 | 0.881 | 0.66 | HOMO-1→LUMO+1 | 67 |
| $P_a1$ | 234 | 1.726 | 0.981 | 3.48 | HOMO-2→LUMO+3 | 52 |
| $P_a2$ | 437 | 0.681 | 0.792 | 2.44 | HOMO→LUMO+1 | 50 |
| $P_a3$ | 561 | 1.073 | 0.916 | 1.86 | HOMO→LUMO+1 | 50 |
| $P_a4$ | 686 | 1.495 | 0.968 | 1.49 | HOMO→LUMO+1 | 50 |

The absorption spectra for $P_zN$ and $P_aN$ are given in Figure 4.24 and 4.25 respectively. The number of rings has profound effect on the value of absorption and a linear dependence is visible for both the systems. Most of the systems have high light harvesting efficiency in the range from 0.755 to 0.981. The highest percentage of molecular orbital contribution together with the type of transition corresponding to the strongest absorption are also tabulated. For $P_zN$ series other than $P_z2$, all others have $\lambda_{max}$ resulting from the HOMO-1 to LUMO+1 transition with orbital contribution around 67-79 %. For $P_z2$ system the most prominent is HOMO to LUMO transition with orbital contribution of 95 %. For $P_aN$ series, except for $P_a1$, all other systems have $\lambda_{max}$ corresponding to HOMO to LUMO+1 with 50% orbital contribution, whereas for $P_a1$, inner MO's participation is high and the transition is corresponding to the HOMO-2 to LUMO+3 with contribution of 51%. The narrowing of vertical excitation energy, inferring the ease of vertical absorption as the size of the system increases is evident from the values.

$P_z1$ system which is pyrene molecule has an experimental $\lambda_{max}$ around 250 nm,[76] for which the theoretical value obtained is 235 nm. Other than this strongest absorption the system absorbs weakly in the wavelengths 352 nm and 279 nm. For $P_z2$ system, $\lambda_{max}$ values are at 329, 377 and 569 nm. $P_z3$ system absorbs strongly in the 491 nm and weakly in the 945 nm. The largest system $P_z4$ absorbs strongly in the wavelength 756 nm, and weak absorption peaks are also observed at 495 and 1680 nm. For all the systems in $P_aN$ series, the fine structure of the absorption

spectra is retained as evident from the Figure 4.25. Predominantly four sets of $\lambda_{max}$ can be visualised for all the systems. *$P_a1$* system has $\lambda_{max}$ at 234, 289 and 315 nm. For *$P_a2$*, the strongest absorption occurs at 437 nm and it absorbs in the wavelengths 355, 401 and 508 nm. For *$P_a3$* system, $\lambda_{max}$ values are at 668, 561, 512 and 449 nm. *$P_a4$* system absorbs strongly in the 686 nm and weakly in the regions of wavelength 829, 625 and 540 nm.

The optical properties obtained after the TD-DFT calculations for *$T_aN$* and *$R_hN$* PAH systems are given in Table 4.10. The gradual increase in the $\lambda_{max}$ values is visible in both the set of series. Most prominent $\lambda_{max}$ are tabulated.

**Table 4.10.** Optical data of *$T_aN$* and *$R_hN$* shaped PAH systems

| System | $\lambda_{max}$ (nm) | Oscillator strength *(f)* | LHE | Excitation energy (eV) | MO contribution (%) | |
|---|---|---|---|---|---|---|
| *$T_a1$* | 258 | 0.423 | 0.622 | 3.81 | HOMO-2→LUMO | 51 |
| *$T_a2$* | 362 | 0.480 | 0.669 | 2.91 | HOMO→LUMO | 41 |
| *$T_a3$* | 445 | 0.702 | 0.802 | 2.34 | HOMO→LUMO+1 | 41 |
| *$T_a4$* | 530 | 0.838 | 0.855 | 1.96 | HOMO→LUMO+1 | 39 |
| *$R_h1$* | 463 | 0.327 | 0.529 | 2.68 | HOMO→LUMO | 98 |
| *$R_h2$* | 321 | 0.311 | 0.512 | 1.08 | HOMO→LUMO+5 | 52 |
| *$R_h3$* | 324 | 0.381 | 0.584 | 0.96 | HOMO→LUMO+7 | 61 |
| *$R_h4$* | 375 | 0.201 | 0.370 | 0.49 | HOMO→LUMO+5 | 40 |

The absorption spectral features for all are illustrated in Figure 4.26 and 4.27. *$T_aN$* systems have LHE in the range of 0.6 to 0.8. For *$R_hN$* systems, the LHE is the lowest for all the different types of system analysed. From the analysis of vertical excitation energy, it is evident that the rectangular systems have very low value and are easily excited via absorption of radiation. Although, the transitions other than the HOMO-LUMO can give rise to absorption maxima values of different strengths, the one corresponding to HOMO-LUMO will be at the longest wavelength and need not be the most prominent one.

Triphenylene which is denoted as *$T_a1$*, has the reported experimental $\lambda_{max}$ in the region of 250 nm.[77] This value is in agreement with the calculated value of 258 nm that we have obtained. *$T_a1$* have $\lambda_{max}$ 278 and 218 nm other than the most prominent one. *$T_a2$* system has $\lambda_{max}$ at 362 nm and 335 nm. For *$T_a3$*, the strongest absorption corresponding to the HOMO→ LUMO+1 transition is at 451 nm, with a weak absorption at 409 nm. In the case of *$T_a4$*, the transition corresponding to

HOMO → LUMO+1 yields $\lambda_{max}$ at 530 nm together with a weak absorption in the region of 483 nm. The calculated TD-DFT absorption spectra of all the systems in the *$R_hN$* series are given in Figure 4.27 (Full spectra is not given for the clarity of absorption peaks). Perylene molecule which is denoted as *$R_h1$* in has an experimental $\lambda_{max}$ of approximately 430 nm in methanol[78] which is very close to the theoretical value of 446 nm that we have calculated. *$R_h1$* has $\lambda_{max}$ at 229, 277 and 463 nm. *$R_h2$* has mainly three $\lambda_{max}$ which lie at wavelengths 284, 321 and 765 nm. For *$R_h3$* systems, $\lambda_{max}$ are observed at 324 and 380 and 1297 nm. For the largest studied stystem *$R_h4$*, $\lambda_{max}$ are observed at 375, 504 and 2505 nm.

The effect of periphery structure on the absorption is clearly visible in these values. Even though *$R_h4$* system has only 14 rings in them which is much less compared to other larger systems that are studied, the $\lambda_{max}$ values which are quite high (for example $\lambda_{max}$ at 1297 nm for *$R_h3$* anf 2505 nm for *$R_h4$*) corresponding to even IR region in electromagnetic spectrum is obtained. The extensive conjuation together with the structural effects makes the very low energy gap between MOs resulting in such a high $\lambda_{max}$ value.

### 4.4.3.2. PAH-π-PAH Systems

Table 4.11 and Table 4.12 give the optical features of designed PAH-π-PAH systems. The absorption maxima values in the range of 433 nm to 630 nm are possible for these systems. The highest $\lambda_{max}$ is observed for the *$R_h1$-$C_a1$* system which is at 630 nm and the least $\lambda_{max}$ of 433 nm is for *$T_a1$-$P_z1$* system. The absorption in the visible region of solar spectrum is attained for all the systems, which can be highly beneficial in solar applications. In all the systems, the most prominent peak having the highest oscillator strength is the absorption corresponding to HOMO → LUMO transition and consequently the most red shifted $\lambda_{max}$. A set of $\lambda_{max}$ having lower wavelength absorption are present in all the systems indicative of the extended π-conjugation. The oscillator strength of all the designed PAH-π-PAH systems ranges from of 0.8 to 1.95. Oscillator strength being a direct measure of the LHE, the changes in the formers values are reflected in the LHE of all the systems. And consequently the theoretical LHE of all the systems gets enhanced and is in the range of 0.80 – 0.99. The *$T_a1$-$P_z1$* system has maximum LHE of 0.989 with the oscillator strength of 1.957, and the least efficient in light harvesting is *$P_a1$-*

$R_h1$ system with a LHE of 0.802 and oscillator strength 0.703. Vertical excitation energies of all the designed systems are in the range of 2.0 – 2.6 eV. Systems having high LHE and low excitation energy are idea for the photonic applications.

**Table 4.11.** Optical data for PAH-π-PAH type systems: Set I

| System | $\lambda_{max}$ (nm) | MO contribution (%) | | Oscillator strength ($f$) | LHE | Excitation energy (eV) |
|---|---|---|---|---|---|---|
| $C_z1$-$C_a1$ | 542 | HOMO→LUMO | 87 | 1.218 | 0.940 | 2.29 |
| | 463 | HOMO→LUMO+3 | 30 | | | |
| | 409 | HOMO-1→LUMO+1 | 29 | | | |
| | 403 | HOMO-1→LUMO+2 | 35 | | | |
| $C_z1$-$P_z1$ | 475 | HOMO→LUMO | 72 | 1.006 | 0.901 | 2.54 |
| | 460 | HOMO→LUMO+1 | 50 | | | |
| | 382 | HOMO-2→LUMO+2 | 30 | | | |
| | 358 | HOMO-1→LUMO+1 | 56 | | | |
| $P_a1$-$C_z1$ | 506 | HOMO→LUMO | 90 | 1.543 | 0.971 | 2.45 |
| | 396 | HOMO-4→LUMO | 27 | | | |
| | 360 | HOMO-5→LUMO | 34 | | | |
| $T_a1$-$C_z1$ | 495 | HOMO→LUMO | 92 | 1.478 | 0.967 | 2.50 |
| | 391 | HOMO→LUMO+3 | 26 | | | |
| | 375 | HOMO-4→LUMO | 72 | | | |
| | 335 | HOMO-2→LUMO+2 | 16 | | | |
| $C_z1$-$R_h1$ | 610 | HOMO→LUMO | 90 | 1.357 | 0.956 | 2.03 |
| | 421 | HOMO-1→LUMO+1 | 72 | | | |
| | 394 | HOMO-3→LUMO | 35 | | | |
| | 363 | HOMO→LUMO+6 | 30 | | | |
| $P_z1$-$C_a1$ | 518 | HOMO→LUMO | 79 | 0.821 | 0.849 | 2.39 |
| | 440 | HOMO-1→LUMO+3 | 41 | | | |
| | 437 | HOMO-1→LUMO+1 | 30 | | | |
| | 391 | HOMO-1→LUMO+4 | 25 | | | |
| $P_a1$-$C_a1$ | 532 | HOMO→LUMO | 85 | 1.101 | 0.921 | 2.33 |
| | 460 | HOMO-2→LUMO | 18 | | | |
| | 430 | HOMO-1→LUMO+1 | 27 | | | |
| | 412 | HOMO→LUMO | 3 | | | |

**Table 4.12.** Optical data for PAH-π-PAH type systems: Set II

| System | $\lambda_{max}$ (nm) | MO contribution (%) | | Oscillator strength (*f*) | LHE | Excitation energy (eV) |
|---|---|---|---|---|---|---|
| *$T_a1$-$C_a1$* | 529 | HOMO→LUMO | 85 | 1.010 | 0.902 | 2.34 |
| | 446 | HOMO-1→LUMO+1 | 41 | | | |
| | 409 | HOMO-2→LUMO+3 | 26 | | | |
| | 393 | HOMO→LUMO+5 | 23 | | | |
| *$R_h1$-$C_a1$* | 630 | HOMO→LUMO | 82 | 1.413 | 0.961 | 1.97 |
| | 423 | HOMO-2→LUMO+2 | 44 | | | |
| *$P_a1$-$P_z1$* | 467 | HOMO→LUMO | 61 | 0.928 | 0.882 | 2.53 |
| | 453 | HOMO→LUMO+1 | 56 | | | |
| | 442 | HOMO→LUMO+2 | 42 | | | |
| | 408 | HOMO-3→LUMO | 65 | | | |
| | 349 | HOMO-2→LUMO+2 | 22 | | | |
| *$T_a1$-$P_z1$* | 451 | HOMO→LUMO+1 | 41 | 1.957 | 0.989 | 2.57 |
| | 433 | HOMO→LUMO | 67 | | | |
| | 354 | HOMO-4→LUMO | 42 | | | |
| *$P_z1$-$R_h1$* | 578 | HOMO→LUMO | 95 | 1.317 | 0.952 | 2.14 |
| | 360 | HOMO→LUMO+4 | 29 | | | |
| *$T_a1$-$P_a1$* | 480 | HOMO→LUMO | 79 | 1.495 | 0.968 | 2.58 |
| | 454 | HOMO-1→LUMO | 52 | | | |
| *$P_a1$-$R_h1$* | 478 | HOMO-1→LUMO | 30 | 0.703 | 0.802 | 2.20 |
| | 454 | HOMO-2→LUMO | 46 | | | |
| | 421 | HOMO-1→LUMO+2 | 41 | | | |
| | 391 | HOMO-3→LUMO+1 | 50 | | | |
| *$T_a1$-$R_h1$* | 468 | HOMO→LUMO+1 | 50 | 1.189 | 0.935 | 2.18 |
| | 414 | HOMO-1→LUMO+1 | 63 | | | |

For all the systems other than *$T_a1$-$R_h1$* and *$P_a1$-$R_h1$*, the HOMO→LUMO orbital contribution towards the absorption is in the range of 62 - 92 %. The most prominent MO transition is HOMO to LUMO for all the PAH-π-PAH systems.

### 4.4.3.3. Functionalised PAH-π-PAH Systems

The introduction of functional groups on the designed PAH-π-PAH systems is done, so that there is improvement in the electronic features and also for the ease for processability in optoelectronic device applications.

**Table 4.13**. Optical data of all the functionalised PAH-π-PAH type systems

| System | $\lambda_{max}$ (nm) | MO contribution (%) | | Oscillator strength(*f*) | LHE | Excitation energy (eV) |
|---|---|---|---|---|---|---|
| *f_P$_a$1-C$_z$1* | 546 | HOMO-1→LUMO | 75 | 0.836 | 0.854 | 1.92 |
| | 528 | HOMO →LUMO+3 | 70 | | | |
| | 450 | HOMO-2→LUMO+2 | 30 | | | |
| *f_T$_a$1-C$_z$1* | 626 | HOMO→LUMO | 87 | 0.695 | 0.798 | 1.98 |
| | 503 | HOMO→LUMO+1 | 76 | | | |
| | 482 | HOMO-1→LUMO | 81 | | | |
| | 384 | HOMO-5→LUMO | 36 | | | |
| | 355 | HOMO-4→LUMO-1 | 60 | | | |
| *f_P$_a$1-C$_a$1* | 546 | HOMO-1→LUMO | 75 | 0.836 | 0.854 | 1.92 |
| | 528 | HOMO-1→LUMO+3 | 70 | | | |
| | 450 | HOMO-2→LUMO-1 | 30 | | | |
| | 425 | HOMO-4→LUMO-1 | 69 | | | |
| *f_T$_a$1-C$_a$1* | 634 | HOMO→LUMO | 90 | 0.887 | 0.870 | 1.96 |
| | 510 | HOMO-1→LUMO | 67 | | | |
| | 496 | HOMO→LUMO+3 | 63 | | | |
| | 456 | HOMO-3→LUMO | 39 | | | |
| *f_R$_h$1-C$_a$1* | 708 | HOMO→LUMO | 67 | 0.580 | 0.737 | 1.75 |
| | 603 | HOMO→LUMO+1 | 50 | | | |
| | 589 | HOMO→LUMO+3 | 72 | | | |
| | 421 | HOMO-3→LUMO+2 | 20 | | | |
| *f_P$_a$1-P$_z$1* | 552 | HOMO-1→LUMO | 55 | 1.011 | 0.903 | 1.88 |
| | 537 | HOMO→LUMO+1 | 60 | | | |
| | 469 | HOMO-1→LUMO+1 | 55 | | | |
| | 390 | HOMO→LUMO+5 | 31 | | | |
| | 382 | HOMO-6→LUMO | 44 | | | |
| *f_T$_a$1-P$_z$1* | 570 | HOMO→LUMO | 81 | 0.809 | 0.845 | 2.18 |
| | 429 | HOMO-1→LUMO | 32 | | | |
| | 421 | HOMO-3→LUMO | 53 | | | |
| | 411 | HOMO-2→LUMO+1 | 46 | | | |
| | 367 | HOMO-1→LUMO+2 | 43 | | | |

All the optical data that have been analysed is tabulated in Table 4.13. Introduction of functional groups shifts the absorption maxima to more red-shifted region as evident from the values. Light harvesting efficiency of all the systems are reduced when functionalization is done of PAH-π-PAH systems, with an exceptional case of *f_Pa1-Pz1*, where the LHE is enhanced to 0.903 from that of *Pa1-Pz1* which is 0.882. The vertical excitation energy is increased for all the systems after the introduction of electron withdrawing and electron donating groups. Changes of 0.22 to 0.65 eV is observed from that of PAH- π-PAH systems. The maximum change is observed for f*_Pa1-Pz1*, which has excitation energy of 1.88 eV whereas the same for *Pa1-Pz1* system is 2.53 eV. The prominent effect due to the introduction of electron donating and electron accepting groups in D-π-A type system on the optical properties are the following. Absorption shifts significantly to red region, for example *Ta1-Ca1* has $\lambda_{max}$ at 529 nm, whereas *f_Ta1-Ca1* has it at 634 nm. The strongest absorption corresponds to HOMO→ LUMO for the functionalised systems, whereas for PAH-π-PAH prototype the strongest absorption does not always correspond to HOMO-LUMO transition.

## 4.5. Conclusions

The design and study of polycyclic aromatic hydrocarbons (PAH) or nanographenes or graphene nanoflakes has significance in the photo sciences and photonics fields due to the excellent photonic and optoelectronic properties exhibited by them. Here several PAH systems are designed by changing the number of constituting rings, the shape of periphery and the geometry of the whole molecule. Hexagonal, parallelogram, triangular and rectangular shaped PAH's have been designed and studied. DFT calculations at M06L/6-31+G(d) level have been carried out on the PAH systems to theoretically analyse the absorption properties together with electronic properties. In all the molecules, the frontier molecular orbitals analysis is carried out for the better understanding of reactivity and electronic features. In all the different shaped PAH's, there is direct increase in the absorption maxima with increase in number of carbon atoms. This phenomenon is obvious because as the number of carbon atoms increases there is extending of conjugation in the structure, which shifts the absorption maxima to greater wavelengths. As conjugation increases, the HOMO-LUMO gap gets shortened, thus

less energy is required to cause the electronic transitions. As a result of which, the corresponding wavelength gets enhanced. One important feature that was observed is the dependence of shape and periphery geometry on the optical and electronic features of PAH systems. For molecules that are composed of same number of benzene rings, the electronic structure, features, and optical properties are distinctly different. As a direct result for PAHs having same number of carbon atoms, the electron density can be different if their shape is differed. This paved the design and studies on D-π-A type systems connecting two PAH units via a conjugated π-system. The theoretical calculations on 15 such designed systems are done, which enhanced the possibility of developing D-π-A system as the PAH moieties showed different electronic features compared to each other. However, the donor-acceptor type feature is mildly present in the designed PAH-π-PAH systems and a quantification of the electronic feature is done with the help of $V_{\min}$ values, which were different on different parts of the same system. Introduction of electron donating and withdrawing groups on such designed systems is done for further enhancement of electronic and optical features to improve the donor-acceptor character. The frontier molecular orbital analysis also reinforced the difference in the observed electronic features. The functionalization results in the minor lowering of the light harvesting efficiency and excitation energy for all the analysed systems.

Armchair edged PAH system are found to be more resonance stabilised, which is supported by the Clar's aromatic sextet like MESP isosurface arrangement in the entire structure. For zigzag periphery systems, the electron cloud is localised more towards the edges and these classes of systems might be very useful for donor-acceptor type electronic applications. Rectangular shaped PAH systems having both armchair and zigzag edges in same molecule are electronically very dense which has a characteristic of very low HOMO-LUMO gap even when number of rings constituting is less. This effect is verified by comparing with other systems of much higher number of constituting rings. In summary, the theoretical study on PAH, PAH-π-PAH and *f*_PAH-π-PAH systems provide new insight on the design and development of efficient light harvesting molecules that are derived from graphene nanoflakes of different sizes and shapes.

## 4.6. References


1. K. S. Novoselov, A. K. Geim, S. V. Morozov, D. Jiang, Y. Zhang, S. V. Dubonos, I. V. Grigorieva and A. A. Firsov, *Science*, **2004**, 306, 666.
2. P. R. Wallace, *Phys. Rev.*, **1947**, 71, 622-634.
3. M. D. Watson, A. Fechtenkötter and K. Müllen, *Chem. Rev.*, **2001**, 101, 1267-1300.
4. W. Pisula, X. Feng and K. Müllen, *Chem. Mater.*, **2011**, 23, 554-567.
5. A. K. Geim and A. H. MacDonald, *Phys. Today*, **2007**, 60, 35-41.
6. K. S. Novoselov, *Angew. Chem. Int. Ed.*, **2011**, 50, 6986-7002.
7. C. Casiraghi, A. Hartschuh, E. Lidorikis, H. Qian, H. Harutyunyan, T. Gokus, K. S. Novoselov and A. C. Ferrari, *Nano Lett.*, **2007**, 7, 2711-2717.
8. P. Blake, E. W. Hill, A. H. C. Neto, K. S. Novoselov, D. Jiang, R. Yang, T. J. Booth and A. K. Geim, *Appl. Phys. Lett.*, **2007**, 91, 063124.
9. R. R. Nair, P. Blake, A. N. Grigorenko, K. S. Novoselov, T. J. Booth, T. Stauber, N. M. R. Peres and A. K. Geim, *Science*, **2008**, 320, 1308.
10. T. Hasan, Z. Sun, F. Wang, F. Bonaccorso, P. H. Tan, A. G. Rozhin and A. C. Ferrari, *Adv. Mater.*, **2009**, 21, 3874-3899.
11. Z. Sun, T. Hasan, F. Torrisi, D. Popa, G. Privitera, F. Wang, F. Bonaccorso, D. M. Basko and A. C. Ferrari, *ACS Nano*, **2010**, 4, 803-810.
12. R. J. Stöhr, R. Kolesov, J. Pflaum and J. Wrachtrup, *Phys. Rev. B*, **2010**, 82, 121408.
13. T. Gokus, R. R. Nair, A. Bonetti, M. Böhmler, A. Lombardo, K. S. Novoselov, A. K. Geim, A. C. Ferrari and A. Hartschuh, *ACS Nano*, **2009**, 3, 3963-3968.
14. G. Eda, Y.-Y. Lin, C. Mattevi, H. Yamaguchi, H.-A. Chen, I. S. Chen, C.-W. Chen and M. Chhowalla, *Adv. Mater.*, **2010**, 22, 505-509.
15. X. Sun, Z. Liu, K. Welsher, J. T. Robinson, A. Goodwin, S. Zaric and H. Dai, *Nano Res.*, **2008**, 1, 203-212.
16. Z. Luo, P. M. Vora, E. J. Mele, A. T. C. Johnson and J. M. Kikkawa, *Appl. Phys. Lett.*, **2009**, 94, 111909.
17. F. Bonaccorso, Z. Sun, T. Hasan and A. C. Ferrari, *Nat. Photon.*, **2010**, 4, 611-622.
18. A. K. Geim and K. S. Novoselov, *Nat. Mater.*, **2007**, 6, 183-191.

19. I. Snook and A. Barnard, in *Physics and Applications of Graphene - Theory.*, ed. S. Mikhailov, InTech., Rijeka, Croatia, 2011, pp. 277-302.
20. S. Müller and K. Müllen, *Phil. Trans. R. Soc. A*, **2007**, 365, 1453-1472.
21. A. S. Barnard and I. K. Snook, *Modelling Simul. Mater. Sci. Eng.*, **2011**, 19, 054001.
22. J. Wu, W. Pisula and K. Müllen, *Chem. Rev.*, **2007**, 107, 718-747.
23. A. Narita, X.-Y. Wang, X. Feng and K. Mullen, *Chem. Soc. Rev.*, **2015**, 44, 6616-6643.
24. R. Rieger and K. Müllen, *J. Phys. Org. Chem.*, **2010**, 23, 315-325.
25. S. Kim, S. W. Hwang, M.-K. Kim, D. Y. Shin, D. H. Shin, C. O. Kim, S. B. Yang, J. H. Park, E. Hwang, S.-H. Choi, G. Ko, S. Sim, C. Sone, H. J. Choi, S. Bae and B. H. Hong, *ACS Nano*, **2012**, 6, 8203-8208.
26. M. Bacon, S. J. Bradley and T. Nann, *Part. Part. Syst. Charact.*, **2014**, 31, 415-428.
27. K. Siegmann and K. Sattler, *J. Chem. Phys.*, **2000**, 112, 698-709.
28. A. D. Güçlü and P. Hawrylak, *Phys. Rev. B*, **2013**, 87, 035425.
29. A. Kuc, T. Heine and G. Seifert, *Phys. Rev. B*, **2010**, 81, 085430.
30. D. P. Kosimov, A. A. Dzhurakhalov and F. M. Peeters, *Phys. Rev. B*, **2010**, 81, 195414.
31. R. Alessandra, Charles W. Bauschlicher, Jr., B. Christiaan, G. G. M. T. Alexander and J. A. Louis, *Astrophys. J.*, **2012**, 754, 75.
32. P. Lu, Z. Zhang, C. H. Woo and W. Guo, *J. Phys. Chem. C*, **2012**, 116, 626-631.
33. S. Hongqing, S. B. Amanda and K. S. Ian, *Nanotechnology*, **2012**, 23, 065707.
34. B. Mandal, S. Sarkar and P. Sarkar, *J. Nanopart. Res.*, **2012**, 14, 1317.
35. M. C. Lemme, T. J. Echtermeyer, M. Baus and H. Kurz, *IEEE Electron Device Lett.*, **2007**, 28, 282-284.
36. M. Y. Han, B. Özyilmaz, Y. Zhang and P. Kim, *Phys. Rev. Lett.*, **2007**, 98, 206805.
37. Y. M. Lin, C. Dimitrakopoulos, K. A. Jenkins, D. B. Farmer, H. Y. Chiu, A. Grill and P. Avouris, *Science*, **2010**, 327, 662.
38. R. S. Pantelic, J. C. Meyer, U. Kaiser, W. Baumeister and J. M. Plitzko, *J. Struct. Biol.*, **2010**, 170, 152-156.

39. N. R. Wilson, P. A. Pandey, R. Beanland, R. J. Young, I. A. Kinloch, L. Gong, Z. Liu, K. Suenaga, J. P. Rourke, S. J. York and J. Sloan, *ACS Nano*, **2009**, 3, 2547-2556.
40. R. R. Nair, P. Blake, J. R. Blake, R. Zan, S. Anissimova, U. Bangert, A. P. Golovanov, S. V. Morozov, A. K. Geim, K. S. Novoselov and T. Latychevskaia, *Appl. Phys. Lett.*, **2010**, 97, 153102.
41. P. Blake, P. D. Brimicombe, R. R. Nair, T. J. Booth, D. Jiang, F. Schedin, L. A. Ponomarenko, S. V. Morozov, H. F. Gleeson, E. W. Hill, A. K. Geim and K. S. Novoselov, *Nano Lett.*, **2008**, 8, 1704-1708.
42. X. Wang, L. Zhi and K. Müllen, *Nano Lett.*, **2008**, 8, 323-327.
43. J. S. Moon, D. Curtis, M. Hu, D. Wong, C. McGuire, P. M. Campbell, G. Jernigan, J. L. Tedesco, B. VanMil, R. Myers-Ward, C. Eddy and D. K. Gaskill, *IEEE Electron Device Lett.*, **2009**, 30, 650-652.
44. Y.-M. Lin, K. A. Jenkins, A. Valdes-Garcia, J. P. Small, D. B. Farmer and P. Avouris, *Nano Lett.*, **2009**, 9, 422-426.
45. L. Gong, I. A. Kinloch, R. J. Young, I. Riaz, R. Jalil and K. S. Novoselov, *Adv. Mater.*, **2010**, 22, 2694-2697.
46. F. Schwierz, *Nat. Nano.*, **2010**, 5, 487-496.
47. N. Wohner, P. Lam and K. Sattler, *Carbon*, **2014**, 67, 721-735.
48. A. L. Vázquez de Parga, F. Calleja, B. Borca, M. C. G. Passeggi, J. J. Hinarejos, F. Guinea and R. Miranda, *Phys. Rev. Lett.*, **2008**, 100, 056807.
49. D. Geng, B. Wu, Y. Guo, L. Huang, Y. Xue, J. Chen, G. Yu, L. Jiang, W. Hu and Y. Liu, *Proc. Nat. Acad. Sci. USA*, **2012**, 109, 7992-7996.
50. S. Helveg, C. Lopez-Cartes, J. Sehested, P. L. Hansen, B. S. Clausen, J. R. Rostrup-Nielsen, F. Abild-Pedersen and J. K. Norskov, *Nature*, **2004**, 427, 426-429.
51. P. Samorí, N. Severin, C. D. Simpson, K. Müllen and J. P. Rabe, *J. Am. Chem. Soc.*, **2002**, 124, 9454-9457.
52. U. Khan, A. O'Neill, H. Porwal, P. May, K. Nawaz and J. N. Coleman, *Carbon*, **2012**, 50, 470-475.
53. J. Güttinger, F. Molitor, C. Stampfer, S. Schnez, A. Jacobsen, S. Dröscher, T. Ihn and K. Ensslin, *Rep. Prog. Phys.*, **2012**, 75, 126502.

54. A. Barreiro, H. S. J. van der Zant and L. M. K. Vandersypen, *Nano Lett.*, **2012**, 12, 6096-6100.
55. J. Wang, K. K. Manga, Q. Bao and K. P. Loh, *J. Am. Chem. Soc.*, **2011**, 133, 8888-8891.
56. N. G. Shang, P. Papakonstantinou, M. McMullan, M. Chu, A. Stamboulis, A. Potenza, S. S. Dhesi and H. Marchetto, *Adv. Funct. Mater.*, **2008**, 18, 3506-3514.
57. T. Nakajima and K. Shintani, *J. Appl. Phys.*, **2009**, 106, 114305.
58. S. E. Stein and R. L. Brown, *J. Am. Chem. Soc.*, **1987**, 109, 3721-3729.
59. J. Akola, H. P. Heiskanen and M. Manninen, *Phys. Rev. B*, **2008**, 77, 193410.
60. A. T. Balaban, *Phys. Chem. Chem. Phys.*, **2011**, 13, 20649-20658.
61. M. Baldoni, A. Sgamellotti and F. Mercuri, *Chem. Phys. Lett.*, **2008**, 464, 202-207.
62. J. E. Graver, *Eur. J. Comb.*, **2007**, 28, 1115-1130.
63. V. Georgakilas, J. A. Perman, J. Tucek and R. Zboril, *Chem. Rev.*, **2015**, 115, 4744-4822.
64. J. Vilatela Juan and D. Eder, *ChemSusChem*, **2012**, 5, 456-478.
65. L. Yan, F. Zhao, S. Li, Z. Hu and Y. Zhao, *Nanoscale*, **2011**, 3, 362-382.
66. M.-M. Titirici, R. J. White, N. Brun, V. L. Budarin, D. S. Su, F. del Monte, J. H. Clark and M. J. MacLachlan, *Chem. Soc. Rev.*, **2015**, 44, 250-290.
67. V. Strauss, A. Roth, M. Sekita and Dirk M. Guldi, *Chem*, **2016**, 1, 531-556.
68. M. J. Frisch, G. W. Trucks, H. B. Schlegel, G. E. Scuseria, M. A. Robb, J. R. Cheeseman, G. Scalmani, V. Barone, G. A. Petersson, H. Nakatsuji, X. Li, M. Caricato, A. V. Marenich, J. Bloino, B. G. Janesko, R. Gomperts, B. Mennucci, H. P. Hratchian, J. V. Ortiz, A. F. Izmaylov, J. L. Sonnenberg, Williams, F. Ding, F. Lipparini, F. Egidi, J. Goings, B. Peng, A. Petrone, T. Henderson, D. Ranasinghe, V. G. Zakrzewski, J. Gao, N. Rega, G. Zheng, W. Liang, M. Hada, M. Ehara, K. Toyota, R. Fukuda, J. Hasegawa, M. Ishida, T. Nakajima, Y. Honda, O. Kitao, H. Nakai, T. Vreven, K. Throssell, J. A. Montgomery Jr., J. E. Peralta, F. Ogliaro, M. J. Bearpark, J. J. Heyd, E. N. Brothers, K. N. Kudin, V. N. Staroverov, T. A. Keith, R. Kobayashi, J. Normand, K. Raghavachari, A. P. Rendell, J. C. Burant, S. S. Iyengar, J. Tomasi, M. Cossi, J. M. Millam, M. Klene, C. Adamo, R. Cammi, J. W.

Ochterski, R. L. Martin, K. Morokuma, O. Farkas, J. B. Foresman and D. J. Fox *Gaussian 16 Rev. B.01* Wallingford, CT, 2016

69. S. R. Gadre, S. V. Bapat, K. Sundararajan and I. H. Shrivastava, *Chem. Phys. Lett.*, **1990**, 175, 307-312.
70. S. R. Gadre, S. A. Kulkarni and I. H. Shrivastava, *J. Chem. Phys.*, **1992**, 96, 5253-5260.
71. C. H. Suresh and S. R. Gadre, *J. Org. Chem.*, **1999**, 64, 2505-2512.
72. K. P. Vijayalakshmi and C. H. Suresh, *New J. Chem.*, **2010**, 34, 2132-2138.
73. C. H. Suresh and M. J. Ajitha, *J. Org. Chem.*, **2013**, 78, 3918-3924.
74. C. Wang, J. Wang, N. Wu, M. Xu, X. Yang, Y. Lu and L. Zang, *RSC Adv.*, **2017**, 7, 2382-2387.
75. J. M. Hughes, Y. Hernandez, D. Aherne, L. Doessel, K. Müllen, B. Moreton, T. W. White, C. Partridge, G. Costantini, A. Shmeliov, M. Shannon, V. Nicolosi and J. N. Coleman, *J. Am. Chem. Soc.*, **2012**, 134, 12168-12179.
76. G. Lu and G. Shi, *J. Electroanal. Chem.*, **2006**, 586, 154-160.
77. C. González-Piñuela, R. M. Alonso-Salces, A. Andrés, I. Ortiz and J. R. Viguri, *J. Chromatogr. A*, **2006**, 1129, 189-200.
78. Z. Mahmood and J. Zhao, *J. Org. Chem.*, **2016**, 81, 587-594.

# LIST OF PUBLICATIONS

## ARTICLES IN JOURNALS

1. Aromatization Energy and Strain Energy of Buckminsterfullerene from Homodesmotic Reactions: C. H. Suresh, T. L. Lincy, N. Mohan, and **R. Rakhi**, J. *Phys. Chem. A,* **2015,** 119, 25, 6683-6688.

2. A DFT study on dihydropyrazine annulated linear polyacenes: aromaticity, stability and HOMO–LUMO energy modulation: **R. Rakhi** and C. H. Suresh, *Phys. Chem. Chem. Phys.*, **2016**,18, 24631-24641.

3. A DFT study on 1,4-dihydro-1,4-azaborinine annulated linear polyacenes: Absorption spectra, singlet-triplet energy gap, aromaticity, and HOMO–LUMO energy modulation: **R. Rakhi** and C. H. Suresh*. J. Comput. Chem*. **2017**, 38, 2232–2240.

4. TD-DFT analysis of dihydropyrazine annulated polyacenes: First excited singlet-triplet states, energy gap and absorption spectra: **R. Rakhi** and C. H. Suresh (to be submitted)

5. Optoelectronic properties of polycyclic aromatic hydrocarbons of various shapes and size: A DFT study: **R. Rakhi** and C. H. Suresh (to be submitted)

## POSTERS PRESENTED IN ACADEMIC CONFERENCES

1. A poster presented entitled *"Theoretical studies on miniature graphene models: Effect of size and shape on electronic properties"*, on NANO INDIA 2013 during February 19-20, 2013 held at CSIR-NIIST, Thiruvananthapuram.

2. A poster presented entitled *"Linear Polyacenes Analogues: HOMO and LUMO Energy Level Modulation for Electronic Applications*" in the Theoretical Chemistry Symposium (TCS) 2014, during December 18-21, 2014, held at CSIR-NCL-Pune.